

Alma Mater Studiorum – Università di Bologna

DOTTORATO DI RICERCA IN

CHIMICA

Ciclo XXXIII

Settore Concorsuale: 03/C2

Settore Scientifico Disciplinare: CHIM/04

**SUPPORTED GOLD NANOPARTICLES FOR SUSTAINABLE CATALYTIC
APPLICATIONS**

Presentata da: Eleonora Monti

Coordinatore Dottorato

Prof. Domenica Tonelli

Supervisore

Prof. Fabrizio Cavani

Correlatori

Prof. Nikolaos Dimitratos

Prof. Stefania Albonetti

Dott. Tommaso Tabanelli

Esame finale anno 2021

A volte dimostra più forza una persona che insegue il suo sogno di una che lo afferra
Sogo Okita- Gintama, Volume 14

Abstract

Negli ultimi anni, l'utilizzo delle biomasse come fonte alternativa per la produzione di energia e di prodotti di interesse industriale è stato caratterizzato da una costante crescita, anche in risposta alla richiesta da parte dell'opinione pubblica, di soluzioni ai problemi legati all'utilizzo delle fonti fossili e all'inquinamento da esse causate. In particolare, le biomasse lignocellulosiche sono quelle maggiormente studiate grazie alla grande varietà di applicazioni che le diverse parti della lignocellulosa offrono, a partire da lignina, emicellulosa e cellulosa. Proprio l'utilizzo di queste ultime due parti, ci permette di ottenere molteplici molecole di interesse industriale, come ad esempio l'acido glucarico, l'acido furandicarbossilico o l'acido adipico. Per fare tali sintesi, diversi processi sono stati studiati per ciascuna reazione, tra cui l'utilizzo di catalizzatori eterogenei; per le reazioni di ossidazione, i catalizzatori più studiati sono nanoparticelle di metalli nobili come oro, platino, palladio supportati su diversi materiali. Per questo motivo, il seguente lavoro di tesi si è suddiviso in due parti:

- La prima parte focalizzata sullo studio dei catalizzatori, in particolare nanoparticelle di oro supportate su carbone attivo. Il metodo utilizzato per la preparazione dei catalizzatori è stato la sol-immobilization, il quale ci ha permesso di cambiare facilmente alcuni parametri di sintesi, come quantità di stabilizzante o tipologia di polimero, e di studiare sistematicamente l'influenza di tali cambiamenti sulle proprietà del materiale finale.
- La seconda parte invece incentrata sull'applicazione di tali materiali ad alcune reazioni di interesse industriale. In particolare, le reazioni investigate sono:
 - Ossidazione di Glucosio ad Acido Glucarico;
 - Riduzione del 4-Nitrofenolo a 4-Amminofenolo;
 - Ossidazione dell'HMF a FDCA;
 - Ossidazione del 1,6-esandiolo ad acido adipico;
 - Condensazione ed esterificazione ossidativa di Furfurale.

Per la prima parte si è deciso di investigare tre differenti tipi di polimeri come agenti stabilizzanti: il polivinil alcol (PVA), polivinil pirrolidone (PVP) e il polietilenglicole (PEG). Inizialmente si è deciso di variare il rapporto in massa stabilizzante: Au (Pol:Au 0, 0.3, 0.6, 1.2, 2.4) per valutare quale effetto produce sulle nanoparticelle prodotte. Tramite tecniche UV-VIS sulla soluzione colloidale, XRD e TEM su catalizzatori finiti, si sono potuti osservare tre andamenti differenti: il PVA in maggiori quantità favorisce la formazione di nanoparticelle più piccole e ben distribuite; l'aumentare del PVP

invece sembra causare un aumento nelle dimensioni, mentre il PEG ha un andamento intermedio: inizialmente le dimensioni diminuiscono, ma per valori maggiori di 1.2 la dimensione ritorna ad aumentare. Nel confronto tra i tre polimeri, il PVA sembra lo stabilizzante più efficace in termini di dimensioni, forse per la doppia natura di stabilizzante elettrosterico. Inoltre le analisi XPS ci hanno permesso di determinare la quantità di oro disponibile sulla superficie (Au on surface) e il rapporto Au/C sulla superficie, i quali ci danno un'indicazione di quanta fase attiva è esposta per la reazione. Dai dati ottenuti si può vedere che l'aumento di PVA permette la formazione di piccole nanoparticelle, ma copre la superficie dell'oro, riducendo la superficie di metallo disponibile. Varie tecniche di lavaggio o di trattamento termico sul catalizzatore sono state valutate per rimuovere parzialmente lo stabilizzante senza alterare in maniera significativa le dimensioni nanoparticellare. Aumento di dimensioni e di stabilizzante PVP fa diminuire il rapporto Au/C sulla superficie dell'oro. Una volta investigate le proprietà dei diversi materiali, questi sono stati testati per le reazioni sopra descritte. Per ciascuna reazione si è investigato inizialmente come i principali parametri di reazione come tempo, temperatura, quantità di base vanno a influire sulla reazione, a seguito si è valutato le varie serie di catalizzatori. Per la serie Au/AC PVP si è visto come per tutte le reazioni provate, Au/AC PVP0.3 sia quello che dà maggiori rese nel prodotto desiderato, in quanto è il catalizzatore con nanoparticelle più piccole e maggiore superficie disponibile. La serie Au/AC PVA dà risultati differenti: per alcune reazioni come l'ossidazione dell'HMF, la condensazione ossidativa della furfurale e la riduzione del 4-nitrofenolo sembrano dipendere dalla dimensione delle nanoparticelle e non dal rapporto Au/C sulla superficie misurata, perciò Au/AC PVA2.4 è quello con risultati migliori in termini di resa nel prodotto. Le condizioni di reazione potrebbero influenzare però questo ultimo dato: la temperatura/lungo tempo per HMF/furfurale o la presenza di NaBH_4 per la riduzione di 4NP potrebbe rimuovere parzialmente lo stabilizzante. Altre reazioni come l'ossidazione del glucosio o l'ossidazione dell'HDO sembrano invece dipendere dalla quantità di oro presente sulla superficie e il catalizzatore migliore diventa Au/AC PVA0.6. Sicuramente ulteriori test sono necessari per capire in modo più approfondito quali aspetti del catalizzatore vanno a influire sulla reazione, ma i risultati riportati sicuramente possono essere una buona base di partenza per capire meglio come strutturare i catalizzatori futuri.

Table of contents

1. Chapter 1-Introduction	4
1.1 Green chemistry	4
1.2 Nanoparticle: a tiny world full of possibility.....	9
1.2.1 Introduction	9
1.2.2 Impregnation.....	11
1.2.3 Deposition-precipitation	11
1.2.4 Anion adsorption.....	12
1.2.5 Vapor synthesis	13
1.2.6 Sol-immobilization	13
1.2.7 Effect of different stabilizing agents	16
1.3 Glucose oxidation to glucaric acid.....	17
1.3.1 The importance of glucaric acid	17
1.3.2 Chemical methods to produce glucaric acid	20
1.3.3 The importance of the catalytic performance of the supported monometallic nanoparticles.....	22
1.4 Catalytic reduction of 4-Nitrophenol to 4-aminophenol	28
1.5 5-hydroxymethylfurfural oxidation to 2,5-furan dicarboxylic acid.....	31
1.6 Furfural oxidation.....	35
1.6.1 Furfural esterification.....	37
1.6.2 Furfural condensation	39
1.7 1,6 hexanediol oxidation to adipic acid.....	41
2 Chapter 2-Scope	50
3 Chapter 3-Experimental section	52
3.1 Materials.....	52
3.1.1 Catalyst preparation.....	52
3.1.2 Glucose oxidation.....	52
3.1.3 4-Nitrophenol reduction	52
3.1.4 HMF oxidation	52
3.1.5 Furfural oxidation.....	53
3.1.6 1,6 Hexanediol oxidation.....	53
3.2 Synthesis of the catalysts	53
3.2.1 Preparation Method A	53
3.2.2 Preparation Methods B-C-D	54
3.3 UV-VIS spectroscopy.....	57
3.4 XRD.....	58
3.5 TEM	60
3.6 X-ray photoelectron spectroscopy (XPS)	61
3.7 Analytical procedures and protocols.....	62
3.7.1 Glucose oxidation.....	62
3.7.2 4-Nitrophenol reduction	68
3.7.3 HMF oxidation	72
3.7.4 Furfural oxidative condensation	74
3.7.5 1,6 hexanediol (HDO) oxidation	78

4 Chapter 4- Supported gold catalysts: effect of preparation methods.....	81
4.1 Preparation Method: Old (Method A) VS New method (Method D).....	81
4.2 Preparation Method: Au/AC-PVA series.....	84
4.3 Preparation Method: Effect of heat treatment and washing step on the Au NPs	99
4.4 Preparation Method: Choice of stabilizer, PVA vs PVP and PEG	105
5 Chapter 5-Glucose Catalytic oxidation of glucose to glucaric acid	120
5.1 Glucose oxidation: Preliminary study.....	120
5.2 Glucose oxidation: Screening of Au/AC PVA series	126
5.3 Glucose oxidation: Effect of heat treatment vs washing to conversion and yield.....	130
5.4 Glucose oxidation: Catalytic performance of Au/ACPVA- Au/ACPVP- Au/ACPEG.....	134
6 Chapter 6-4-Nitrophenol reduction.....	141
6.1 4-Nitrophenol reduction: Effect of substrate adsorption on the support.....	141
6.2 4-Nitrophenol reduction: Optimization of reaction setup.....	143
6.3 4-Nitrophenol reduction: Screening of the catalysts.....	146
7 Chapter 7-Furan compounds oxidation.....	156
7.1 Hydroxymethylfurfural.....	156
oxidation	156
7.1.1 HMF oxidation: Effect of the reaction time to conversion and yield	156
7.1.2 HMF oxidation: Screening of the catalysts.....	158
7.2 Furfural oxidative condensation-esterification	164
7.2.1 Furfural oxidation: Effect of the reaction time to conversion and yield	165
7.2.2 Furfural oxidation: Screening of the catalysts.....	167
7.2.3 Furfural oxidation: Effect of reaction temperature.....	174
8 Chapter 8-Conclusions and Future work	185
8.1 Catalytic oxidation of 1,6-hexanediol.....	187
8.1.1 Oxidation of 1,6-hexanediol: Effect of reaction time	188
8.1.2 Oxidation of 1,6-hexanediol: Screening of the catalysts.....	189
8.1.3 Oxidation of 1,6-hexanediol: Effect of base for Au/AC PVA series	192

Full Name	Abbreviation
<i>Glucose</i>	Glu
<i>Glucaric Acid</i>	GA
<i>Adipic Acid</i>	AA
<i>Nanoparticles</i>	NPs
<i>Polyvinil alcohol</i>	PVA
<i>Polyvynil pirrolidone</i>	PVP
<i>Polyethylene glycole</i>	PEG
<i>1,6 hexanediol</i>	HDO
<i>6-hydroxihexanoic acid</i>	HHC
<i>Hydroxymethylfurfural</i>	HMF
<i>4-Nitrophenol</i>	4-NP
<i>2,5-furan dicarboxylic acid</i>	FDCA
<i>5-hydroxymethyl-2-furancarboxylic acid</i>	HMFCA
<i>2,5-diformylfuran</i>	DFF
<i>5-formyl-2-furancarboxylic</i>	FFCA
<i>6-hydroxyhexanal</i>	HH
<i>6-oxohexanoic acid</i>	OH
<i>Furfural</i>	Fur
<i>Ethyl furoate</i>	EtFur
<i>Furan-2-acrolein</i>	Fur2Ac
<i>Activated carbon</i>	AC
<i>Heat treatment</i>	HT
<i>X-ray diffraction</i>	XRD
<i>Transmission electron microscopy</i>	TEM
<i>X-ray photoelectron spectroscopy</i>	XPS

1. Chapter 1-Introduction

1.1 Green chemistry

The concept of green chemistry or sustainable chemistry found its origin in the XX century when the realization of the dangers of the chemicals produced in society starts to be evident. One of the first publications and actions reported were from the publication of *Silent Spring*¹ by Rachel Carson (1962), who set the agenda for the protection of the environment with her book or the creation of a new organization. From then on, gradually, politics got involved, resulting in the foundation of the US Environmental Protection Agency (US EPA) in 1970 by President Nixon.² Thereafter, the cooperation between this organization and different countries increased and the green chemistry philosophy started to be delineated; this consists of a combination of several chemical concepts, a conceptual framework that can be used in the design of chemical processes achieving environmental and economic goals by way of preventing pollution. This includes for instance ambient reaction conditions, renewable feedstocks, and minimization of reaction steps. All these notions can be summarized in two main concepts: the first one is Atom Economy, and, the other one is catalysis, which is a “fundamental area of investigation”. All these ideas acquire a formulation in the “12 principles of green chemistry” developed by Paul Anastas and John Warner in 1998.³ Here are reported all the 12 principles:

1. *Prevention*: it is better to prevent waste than to treat or clean up waste after it is formed.
2. *Atom Economy*: synthetic methods should be designed to maximize the incorporation of all materials used in the process into the final product.
3. *Less Hazardous Chemical Syntheses*: wherever practicable, synthetic methodologies should be designed to use and generate substances that possess little or no toxicity to human health and the environment.
4. *Designing Safer Chemical*: chemical products should be designed to preserve the efficacy of function while reducing toxicity.
5. *Safer Solvents and Auxiliaries*: the use of auxiliary substances (e.g. solvents, separation agents, etc.) should be made unnecessary wherever possible and innocuous when used.
6. *Design for Energy Efficiency*: energy requirements should be recognized for their environmental and economic impacts and should be minimized. Synthetic methods should be conducted at ambient temperature and pressure.

7. *Use of Renewable Feedstocks*: a raw material of feedstock should be renewable rather than depleting wherever technically and economically practicable.
8. *Reduce Derivatives*: Unnecessary derivatization (blocking group, protection/deprotection, temporary modification of physical/chemical processes) should be avoided whenever possible.
9. *Catalysis*: catalytic reagents (as selective as possible) are superior to stoichiometric reagents.
10. *Design for Degradation*: chemical products should be designed so that at the end of their function they do not persist in the environment and break down into innocuous degradation products.
11. *Real-time analysis for Pollution Prevention*: analytical methodologies need to be further developed to allow for real-time, in process monitoring and control before the formation of hazardous substances.
12. *Inherently Safer for Accident Prevention*: substances and the form of a substance used in a chemical process should be chosen to minimize the potential for chemical accidents, including releases, explosions, and fire.

After the postulation of these principles, a significant growth in the volume and scope of green chemistry-related research in terms of publications, patents and development of new and sustainable chemical processes was observed. Tomorrow's chemical products should be designed to preserve the efficacy of function while reducing or eliminating hazards (including physical, global, and toxicological hazards).

This was driven by numerous national and, to a lesser extent, trans-national initiatives to fund the area and by the growing appreciation of the value of green chemistry at all stages in the lifecycle from "cradle to grave", how it is showed in the scheme reported below (Figure1.1).⁴

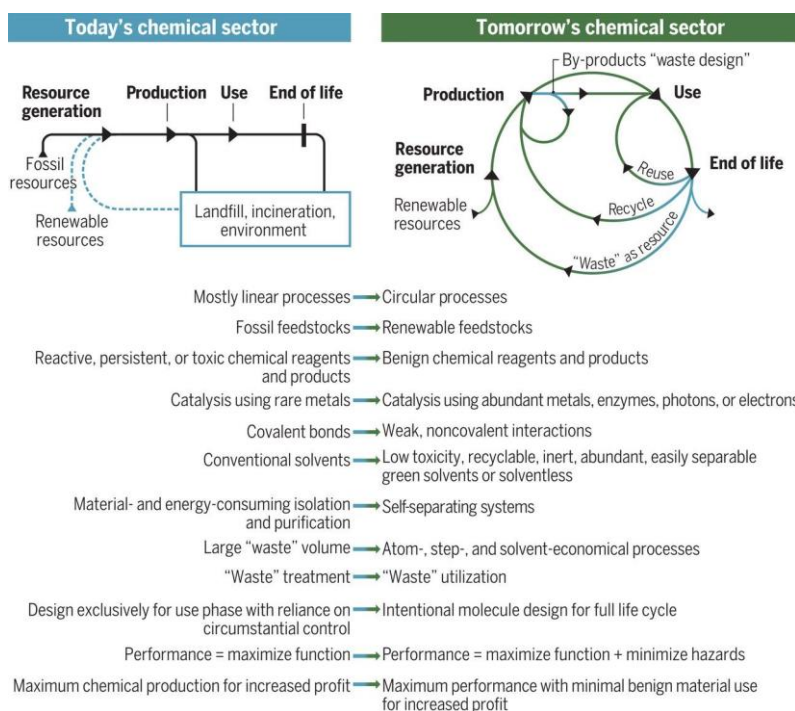


Figure 1.1: Comparison between old chemistry industry set up and the new one⁵

Starting from a renewable resource, like biomass material, instead of fossil material, is one of the most efficient ways for industry to make the transition over green systems. In particular lignocellulosic biomass is composed of three main parts:

- ☒ Lignin: it represents 15-25% of the plant mass and for this reason, it is one of the main vegetal components. It can be found in cell walls, and plays a role as a structural element in the plant. It is a three-dimensional biopolymer with a complex structure, composed of phenol derivatives like p-coumaryl alcohol, caniferyl alcohol, and sinapyl alcohol.⁶
- ☒ Hemicellulose: it composes 23-32% of the plant and it is a saccharide with an irregular composition. It is made of several monosaccharides, like hexose, pentose, and desoxihexose, and for this reason, hemicellulose has an amorphous structure.⁷
- ☒ Cellulose: it is 38-50% of the plant and it is a polysaccharide made of glucose molecules bonded to each other with glycosidic bonds. The regularity of the structure and these kinds of bonds leads to the formation of a crystalline structure.

The graph reported from Kamm in 2004 (Figure 1.2) illustrates all the kinds of product and building block molecules that can be produced starting from the 3 three-part of the lignocellulosic biomasses.⁸

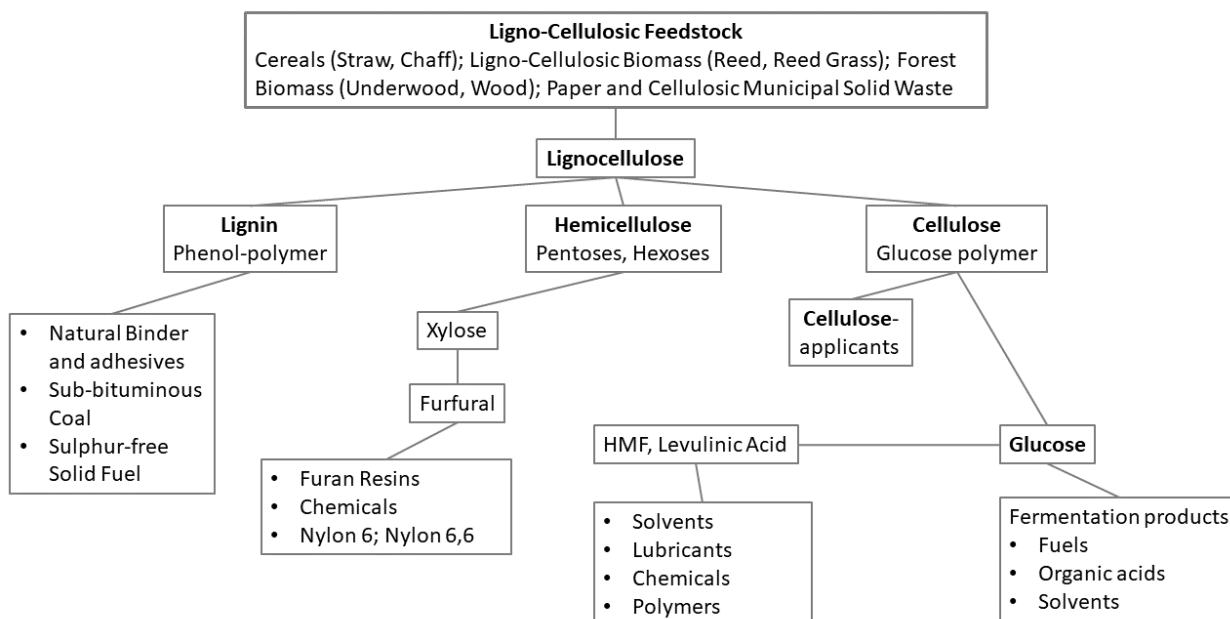


Figure 1.2: Product and application of lignocellulosic biorefinery

From Figure 1.2 it can be noticed that glucose plays an important role in the production of other molecules. Industrially glucose can be synthesized from the hydrolysis of many carbohydrates, including sucrose, maltose, cellulose, starch, and glycogen and it occurs the influence of dilute acid or, more commonly, under that of enzymes. Both ways cause the creation of a variety of mixtures of glucose and intermediates that can be characterized by a DE number. DE stands for Dextrose Equivalent. The analytical procedure measures reducing end groups and attach a DE of 100 to pure glucose (glucose = dextrose) and a DE of 0 to pure starch and usually enzyme process leads to higher DE.⁹

However, following all these guidelines, it is evident how the new sustainable processes have to be economically competitive in comparison with the old ones; in this way, the transition from the old process to the new one would be faster and easier. For this reason, it is very appealing a report produced by the Pacific Northwest National Laboratory (PNNL) and the National Renewable Energy Laboratory (NREL), where the top 12 added-value chemicals in 2004 were reported. The final selection of 12 building blocks began with a list of more than 300 candidates that can be produced from removable resources. However, not all these molecules show the same appealing and the shorter list of potential candidates was selected using an iterative review process based on the petrochemical model of building blocks, chemical data, known market data, properties, the

performance of the potential candidates. Here it was reported the final candidates derivate from sugar (Table1.1).¹⁰

1,4 diacids (succinic, fumaric and malic)
2,5 furan dicarboxylic acid
3 hydroxy propionic acid
aspartic acid
glucaric acid
glutamic acid
itaconic acid
levulinic acid
3-hydroxybutyrolactone
Glycerol
Sorbitol
xylitol/arabinitol

Table 1.1: List of top 12 added-value chemicals

1.2 Nanoparticle: a tiny world full of possibility

1.2.1 Introduction

Noble metals are promising candidates to act as heterogeneous catalysts for the oxidation of alcohols and aldehydes.¹¹ However, these materials are more active if the size of the particles is nanometric (this may also induce new properties) and this is why nanoparticle starts to dominate on the bulk one. By creating nanometer-scale structures, it is possible to control the fundamental properties of materials, such as their melting temperature, magnetic properties, charge capacity, and even their colours, without changing the chemical composition. Making use of this potential will lead to new, high-performance products and technologies that were not possible before. This is also why several ways to produce it were developed over time (Figure 1.3).

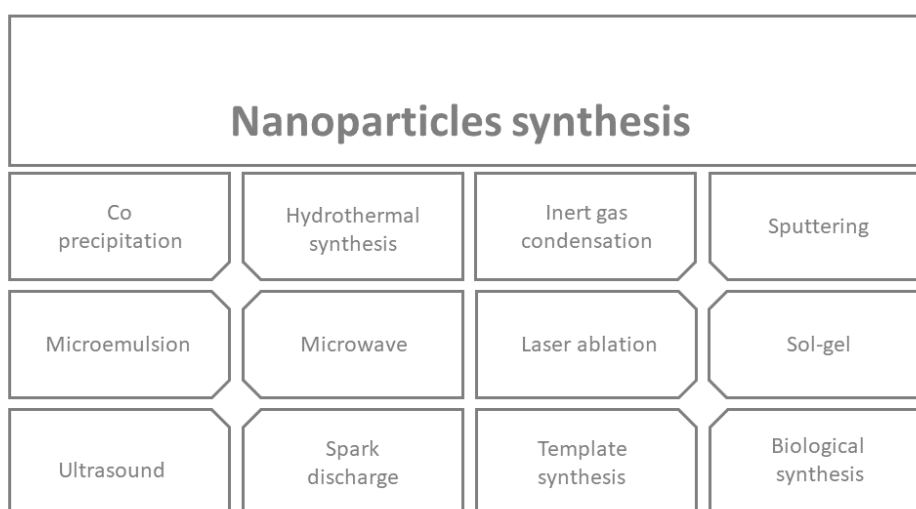


Figure 1.3: Several approaches for nanoparticles synthesis¹²

There are two main different approaches to produce metal nanoparticles (Figure 1.4)¹³:

- *Top-down*: begin with a pattern generated on a larger scale, then reduced to the nanoscale.
- *Bottom-up*: start with atoms or molecules and build up to nanostructures.

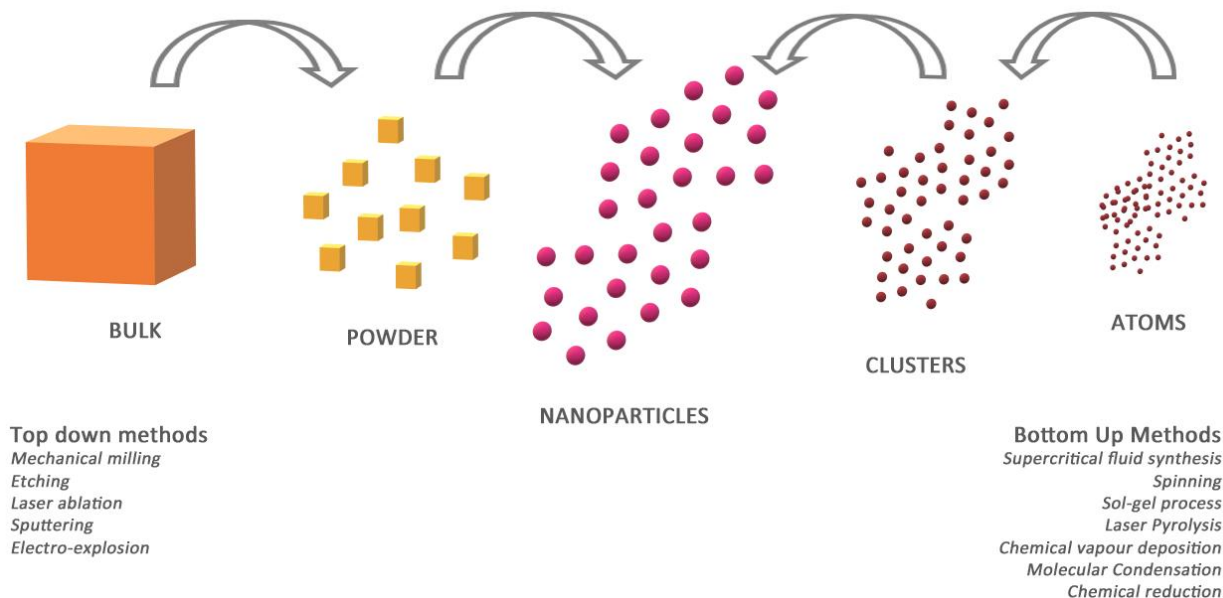


Figure 1.4: Schematic scheme of the Top down and Bottom up approaches

There are different methods which follow the first guideline, like the lithography, the focused ion-beam machining, the milling, the sputtering or the chemical etching; however these methodologies show some drawbacks, like they are expensive and slow to manufacture and not suitable for large scale production. For this reason, this first approach was not discussed in this work.

Nevertheless, the bottom-up approaches are more appealing for the research and industry field. One of the first methods used was molecular condensation. In this technique, the material is vaporized using thermal evaporation sources, in a controlled atmosphere. In gas evaporation, a high residual gas pressure causes the formation of ultrafine particles (100 nm) by gas phase collision. The ultrafine particles are formed by the collision of evaporated atoms with residual gas molecules. However, this method shows some drawbacks, like the long time necessary for this process, and different preparation methods were developed, like the physical or chemical vapor deposition, chemical reduction, or sol gel process. The bottom up approach permits also the combination of nanoparticle formation with a further step of immobilization on support. This could bring to several advantages: the use of heterogeneous catalyst, easier to separate from the bulk in comparison to a homogeneous species, the possibility to combine the proprieties of the support with the proprieties of the nanoparticles, and the higher stability. The main method to produce supported nanoparticles with bottom up approaches are the impregnation method, the precipitation-deposition, the sol-immobilization, the anion adsorption, the vapour synthesis. In the following part there will be explained the main method and their advantages and drawbacks.

1.2.2 Impregnation

Among the many methods to prepare supported metal catalysts, impregnation is the simplest and most widespread method used (an example is reported in Figure 1.5). It consists of the dispersion of the metallic precursor in an aqueous solution on a support, followed by drying and calcination phases. Using an amount of the precursor solution above the pore volume of the support, yielding a thin slurry is termed wet impregnation (WI). Limiting the solution amount to just fill the pore volume is called dry or incipient wetness impregnation (DI or IWI). Various metal oxides can be used as a support. The advantages are that there is no need to adjust the pH and that it is a relatively simple and inexpensive method. However, the major weakness of the impregnation method is the lack of size control of metal particles except when the porous substrate has a narrow pore size distribution.¹⁴

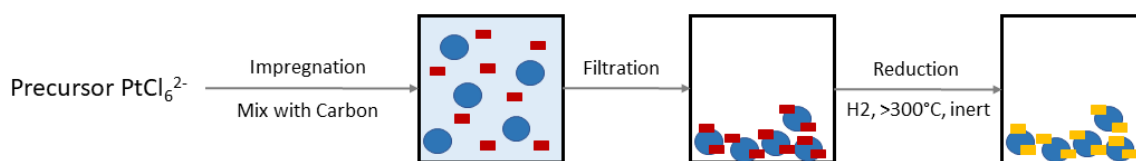


Figure 1.5: Schematic illustration of impregnation method to synthesize supported platinum nanoparticles¹⁵

1.2.3 Deposition-precipitation

The deposition-precipitation (DP) method involves the conversion of a highly soluble metal salt precursor into a less-soluble substance that precipitates only on the support and not in solution.¹⁶ Typically, this process is achieved by a change in solution pH, addition of a precipitation agent, addition of a reducing agent, or change in the concentration of a complexation agent. Two main conditions that must be fulfilled to make sure that the precipitation occurs only on the support instead of in solution: (i) strong interaction between the soluble metal precursor and the surface of the support and (ii) controlled concentrations of the precursor in solution to avoid spontaneous precipitation. Usually, in the presence of a support, the solubility limit shifts to a lower concentration compared to the solubility limit in solution to help deposition on the support. This technique consists of stirring the support powder in a solution containing the metal precursor, a hydroxide, or a hydrated oxide. By adding a precipitating agent as a base, the precursor of the metal becomes insoluble by increasing the pH and precipitates on the support (Figure 1.6). The pH is an important

parameter that can influence the character of the nanoparticles formed, like the dimension or the gold metal loading. For instance, there are reported studies carried on the preparation of Au/TiO₂ that correlate the NP size with the pH of the solution: the resulting mean gold particle size varies differently with pH. Particles are large (around 10 nm) when the preparation is performed below the support point of zero charge (PZC), but the size decreases when pH increases above the PZC. The trend is not just influenced by the pH, but also by the support used. If for the TiO₂ the development of the gold loading versus pH looks like a volcano curve with a maximum at the PZC of titania, the Al₂O₃ rather shows an S-type shape. Though, it was seen that the catalysts prepared in this method possess poor control of metal distribution and surface composition.¹⁷

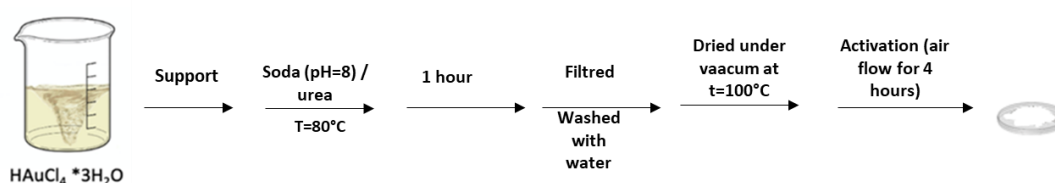


Figure 1.6: Example of deposition-precipitation synthetic method

1.2.4 Anion adsorption

In this synthetic method particular importance is given to the isoelectric point (IEP) of the support. In particular, it was seen that if the pH of the solution is lower than the IEP of the oxide, the surface of the oxide is positively charged (OH²⁺ groups), adsorbing the anions from the solution on it. Conversely, if the pH of the solution is higher, the cations are absorbed on the oxide surface, negatively charged (O⁻ groups). Depending on the precursor used, different adsorption on the support may occur: for example for gold, in the case of HAuCl₄ there is anionic adsorption; instead with Au(CH₃)(NH₂)₂ there is cationic adsorption.¹⁸ As a result, oxides with IEP ≈ 7 such as TiO₂, CeO₂, ZrO₂ produce highly active catalysts while acidic support such as SiO₂ (IEP = 1-2) will usually be inactive. Pitchon and co-workers designed a method called direct anionic exchange, adding alumina (IEP=8-9) in a solution of HAuCl₄ (Figure 1.7).¹⁹ They observed an increase in pH over time when the solution and the support are in contact. For a concentration of HAuCl₄, 1.44×10⁻³ M, an increase in pH from 2.9 to 3.7. At this pH the gold species in solution are [AuCl₃OH]⁻ and [AuCl₂(OH)₂]⁻. The latter is the one that leads to the formation of the complex and the increase in pH, due to the loss of a proton which reacts with the OH⁻ groups of Al₂O₃, leading to the formation of OH₂ on the

support surface. With this method, after washing with water and calcination, They discovered that there is not a great mass loss of gold (~2 wt%), but the nanoparticles are quite large (10-20 nm).

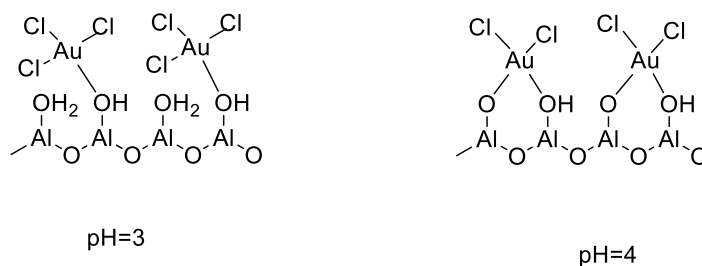


Figure 1.7: Mechanism of interaction of the gold complex with the alumina surface according to the pH

1.2.5 Vapor synthesis

The vapor synthesis methods can be chemical or physical. Physical methods include PVD (physical vapor deposition) and atomic and molecular condensation. The PVD method is based on the transition from the vapor to the solid-state. By heating, a saturated vapor of the metal is obtained, which then, rapidly cooled, settles on the substrate. By varying the reaction conditions (substrate, heating method, etc.) a product with different properties is obtained. On the other hand, atomic or molecular condensation starts by heating a solid material under vacuum; the flow of vaporized and atomized matter obtained is sent to a chamber containing a gas, inert or reactive. Then there is a rapid cooling of the metal atoms, caused by their collision with the gas molecules, which leads to the formation of metal nanoparticles. If the gas is oxygen, an oxide is formed. Among the chemical methods, there is the CVD (chemical vapor deposition): it is similar to the PVD, but the product is obtained by a chemical reaction in the vapor phase or on the substrate. These methods usually use organometal complex or halide composites and allow them to obtain a high purity, but they are expensive and industrious. With the CVD the particle distribution that is generally obtained is quite wide and quite big; Clair Ka Tze Chew. reports in her thesis different range and the smallest one obtained is 10-40nm.²⁰

1.2.6 Sol-immobilization

Nanoparticles can be obtained in water by sol-immobilization. In this technique, the metal precursor is reduced and the nanoparticles formed are stabilized by the presence of a surfactant or stabilizing agent leading to a colloidal solution. Afterward, support is added, like Figure 1.8 shows. Sol

immobilization has proved significant advantages given the obtaining of a more uniform and narrow distribution of nanoparticles in the surface of the support.

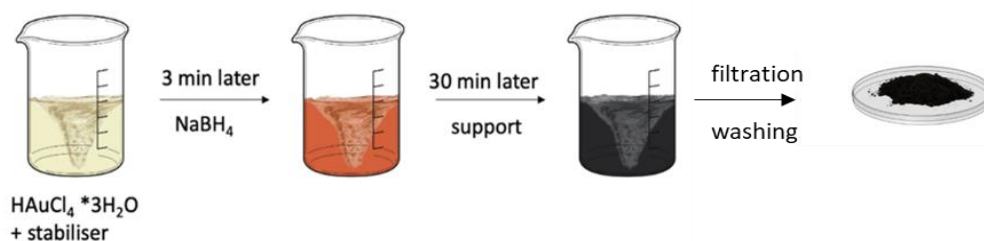


Figure 1.8: Example of schematic procedure of sol immobilization for supported gold nanoparticles

The amount of reducing agent used strongly influences the size of the nanoparticles. High concentrations of reducing agent lead to the formation of a greater number of nuclei, and consequently to smaller nanoparticles. In the aqueous phase also, the pH has a great influence. In the synthesis of gold nanoparticles, the addition of a base such as NaOH enhances the power of the reducing agent leading to the formation of smaller nanoparticles. In addition to the concentration, the type of reducing agent also has great effects on the morphology of the nanoparticles. One of the most widely used reducing agent is sodium borohydride (NaBH₄), although sodium citrate,²¹ ascorbic acid, and alcohols are used as well.²² Polte et co-workers²³ studied the formation mechanism using a static mixer in continuous flow analysis with small-angle X-ray scattering (SXAS). First, there is a rapid reduction of the precursor with the formation of the first nuclei (primary particles) of gold, in less than 200 ms; subsequently, there is the growth of the nuclei due to the coalescence together with a corresponding decrease in the number of particles. It is necessary to add a stabilizing agent to block the growth.

Hence nanoparticles are thermodynamically unstable in solution, the protective agent has a fundamental role, avoiding the sintering of nanoparticles (Figure 1.9). There are three types of stabilization: the electrostatic stabilization, where anions and cations from the starting materials that remain in solution interact with the nanoparticles forming an electrical double layer that avoids aggregation; the steric stabilization, thanks to the adsorption of large molecules; the electrostatic stabilization, which combines both steric and electrostatic effects. Some examples of polymer stabilizers are the PVA (polyvinyl alcohol) and PVP (polyvinyl pyrrolidone) which are commonly used because it is non-toxic and soluble in many polar solvents. Moreover, the PVP possesses an N group that interacts with the gold, donating electrons to the noble metal. Part of the PVP adsorbs on the

NP surface, while the other part dissolves freely in the suspension, creating a second protective shell. Both concentrations are important for controlling the NP size.²⁴

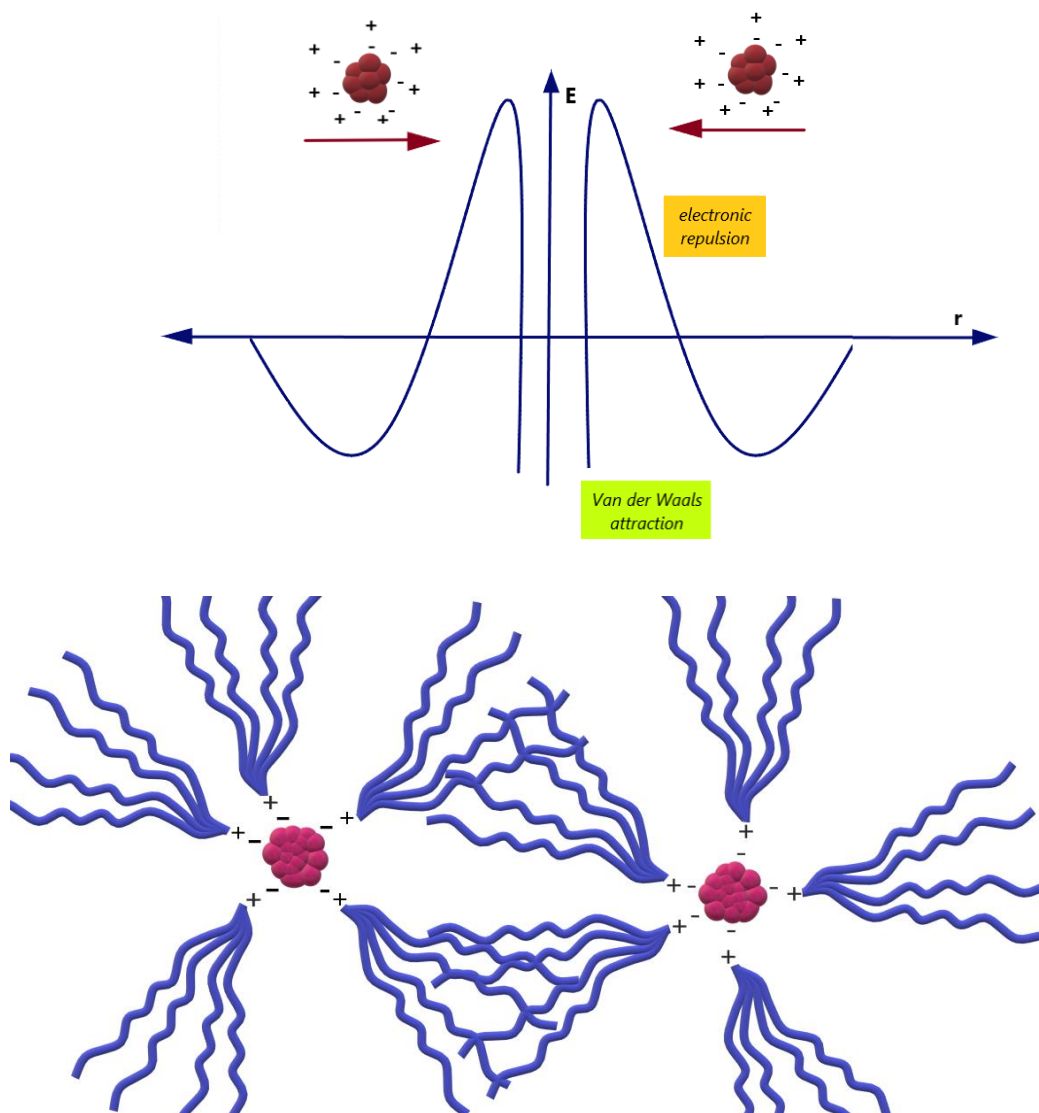


Figure 1.9: Stabilization of metal nanoparticles

A recent study has compared three stabilizers (PVA, PVP, and THPC): it shows that the colloidal method with PVA allows obtaining the best catalyst compared to the deposition-precipitation method.²⁵ This study also highlighted that a PVA/Au 3:1 ratio must not be exceeded, to avoid total immobilization of the NPs; in fact the stability of the colloids is proportional to the PVA concentration, so the anchoring of gold could become more difficult.²⁶

1.2.7 Effect of different stabilizing agents

It was stated that the stabilizing agent is necessary for the formation of small metal nanoparticles, with small mean metal nanoparticle size, narrow particle distribution, and good dispersion of the synthesized metal nanoparticles on the chosen support. However, it was demonstrated in the previous part that PVA has the drawback to block active sites on the particles of the catalyst and therefore, reducing the catalytic activity. Polyvinyl alcohol acts like an electro steric stabilizer, which means that uses steric and electronic repulsion, so it acts like a strong stabilizing agent. The use of different stabilizers, where the molecular weight, the nature of the polymer, and the introduction of a heteroatom like N, could affect not only the final morphology of the synthesized nanoparticles, but also to permit access on the active sites, and also affect the electronic properties of the metal nanoparticle by donation of electrons, like in the case of PVP.²⁷ Therefore we have chosen the following polymers (showed in Figure 1.10) to study the effect of the nature of the polymer as a stabilizer (PVP and PEG), and we discuss the chemical nature of these polymers in the following paragraph.

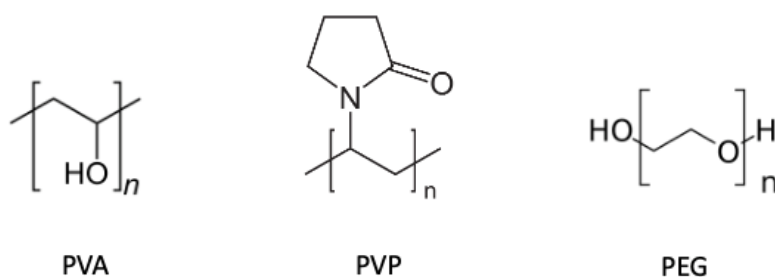


Figure 1.10: Chemical structure of the polymers PVA, PVP, and PEG

The three polymers have a very different chemical structure, as can be seen in Figure 1.10, which causes them to stabilize and interact with Au nanoparticles in different ways. Regarding PVA (polyvinyl alcohol) it is known that the interaction with gold nanoparticles happens mainly by the -OH groups and is not particularly strong, i.e. no covalent bonds are formed. PVA is also known to allow the synthesis of colloidal nanoparticles of small (2-3 nm) size.²⁸ PEG (polyethylene glycol is also known as PEO, polyethylene oxide) weakly interacts with Au nanoparticles and its main function is to give a steric stabilization.²⁹ On the contrary, PVP (polyvinyl pyrrolidone) is known to be an electron donor and through its C=O group and N group on the pyrrolidone residue, it can interact with Au nanoparticles.³⁰ It's preferential binding to Au (111) facet was also exploited to control the morphological growth of Au NPs.³¹ It was shown in a range of reactions to the positive role of

increasing catalytic activity by using functional Au nanoparticles by using PVP as the chosen stabilizer.³²

1.3 Glucose oxidation to glucaric acid

1.3.1 The importance of glucaric acid

As we have already presented in the previous section, some chemicals to be used as building block are more interesting than others for the potential use and application in the field of green chemistry. In this work, it was decided to focus on one of these molecules: glucaric acid.

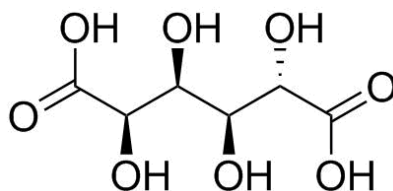


Figure 1.11: Glucaric acid molecular structure

Glucaric acid (Figure 1.11), also called saccharic acid, is a C6 molecule and it is a member of a much larger family of materials known as oxidized sugars. These substances have a significant market and applications that could have increase over time.

The principal key applications of glucaric acid are food ingredients, detergents, corrosion inhibitors, and de-icing chemicals, as the diagram in Figure 1.12 reports. In particular, the demand for the product in detergent manufacturing has witnessed a boost due to the ban on the use of phosphates, particularly in liquid detergents. Growing demand for biodegradable cleaners is also expected to have a positive impact on the glucaric acid market over the next eight years. The detergent industry was the largest consumer of this product followed by food, which accounted for 22% of the market revenue in 2016. Growing awareness about the importance of this product in maintaining current levels of essential nutrients has resulted in increased consumption in everyday meals, which has played a key role in driving its demand.

glucarate was administered in large doses.³⁵ Clinical trials on humans are still pending for outcomes, and preliminary results have not shown adverse effects to its use.

Thanks to the widespread application that glucaric acid and its derivatives could have, the global glucaric acid market size is very huge. It is reported that it was equal to USD 550.4 million in 2016 on account of increasing demand from detergents, soaps, food ingredients, corrosion inhibitors, and de-icing applications and this market is projected to grow at a CAGR of 8% during the forecast period shown in Figure 1.14 (2020-2025). In detail, the Asia Pacific region witnessed the highest demand for glucaric acid and its derivatives in 2016. This region is also expected to grow at the highest CAGR of 12% from 2017 to 2025. Growing demand for this product from the detergent and food industry, especially in emerging countries such as China and India, has propelled market growth over the next eight years. Most of the manufacturing of this product takes place in this region. China, India, and Taiwan are known to possess abundant raw material sources and cheaper labor, as compared to European and North American countries. Thus, major players including Rivertop and Rennovia have established manufacturing facilities in these emerging countries of Asia Pacific. North America held the second-largest share of 23% by revenue, in 2016. The sale market in this region is dominated by the U.S., which was the pioneer in introducing this product. Since it is an organic product, the use of glucaric acid in this country was encouraged by the governing bodies such as the Environmental Protection Agency (EPA), further incrementing its demand.

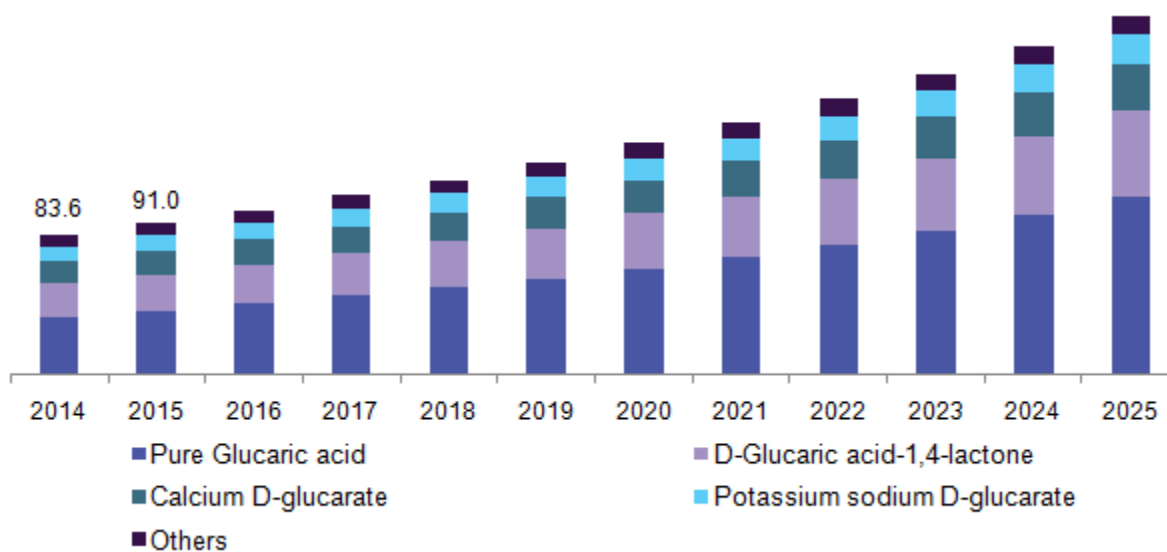


Figure 1.14: U.S. glucaric acid market revenue by product, 2014 - 2025 (USD Million)

The production of glucaric acid as a building block chemical is difficult. However, the value to the biorefinery of converting cheap glucose into glucaric acid arises from two features: 1) glucaric acid can serve as a starting point for the production of a wide range of products with applicability in high volume markets and 2) development of efficient processes for the production of glucaric acid will also apply to efficient oxidation of other inexpensive sugars studied in this evaluation, such as xylose or arabinose.³⁶

1.3.2 Chemical methods to produce glucaric acid

The synthetic preparation of D-glucaric acid dates back to a report of Sohst and Tollens (1888) who carried out the nitric acid oxidation of D-glucose to D-glucaric acid.³⁷



Figure 1.15: Glucose oxidation reaction using HNO₃ as oxidant agent

Indeed this method showed in Figure 1.15 is still attractive for commercialization because of its relative simplicity with nitric acid serving as both solvent and source of the oxidizing agent. A large number of studies were made starting from this process. For example, A. Dietz in 1945 has screened different catalysts and several ways to purify the salt obtained, finding that the best yields of potassium bisaccharate are obtained if it is precipitated by half acidification of dipotassium saccharate.

Moreover, the first commercial plant used a proprietary technology developed by Rivertop that consists of a one-pot oxidation process without NO_x release (modification of the conventional process).³⁸ Current methods for its production are based on this process and involve the chemical oxidation of D-glucose, frequently with nitric acid. Despite its commercial potential, large scale production of D-glucaric acid by nitric acid oxidation of D-glucose was hindered, primarily due to competing side reactions which result in low conversion to D-glucaric acid (<50% yield), the rapid and highly exothermic character of the oxidation and the hazardous reagent used. Therefore, research has moved through different and more sustainable ways to synthesize it.

TEMPO (2,2,6,6-Tetramethyl-1-piperidinyloxy) and its 4-acetamido derivatives are one of the first alternative used and commercially available nitroxide catalysts. The system TEMPO–NaBr–NaOCl

reported in Figure 1.16 is utilized in the high yield oxidation of unprotected mono- and polysaccharides. Thus, glucaric acid, isolated as its monopotassium or disodium salt, can be made under carefully controlled pH and temperature conditions from glucose in yields approaching 90%. Nonetheless, the drawbacks of this reaction are several such as i) the salts obtained require further purification to glucaric acid-generating large quantities of waste and ii) the oxidants used are expensive making this process less sustainable and environmentally benign.³⁹

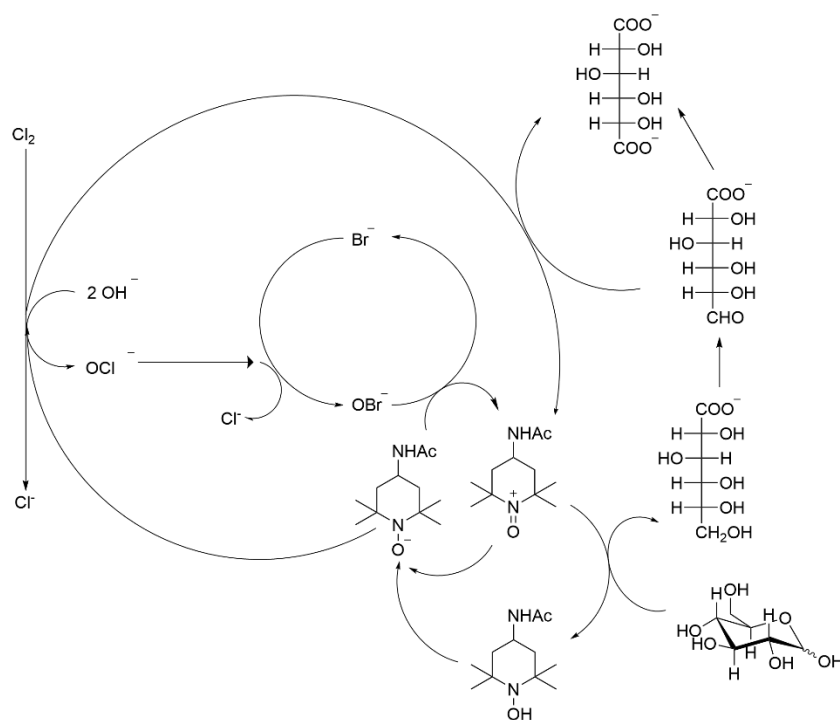


Figure 1.16: Glucose oxidation scheme using TEMPO system as catalyst

Another effective way is the utilization of enzymes to convert selectively the raw material to GA. For example, Yu Deng et al. have optimized the process using *E.coli* modified (coexpression of 3 genes obtained from *Saccharomyces cerevisiae*, *Pseudomonas syringae*) reducing the number of reaction steps and obtaining 5g/L of glucaric acid.⁴⁰ Moreover, Hui-Hui Su et al. have found an in vitro multi-enzyme cascade system for the production of GA from sucrose, without the addition of coenzyme or ATP and obtaining a yield GA of 75% (Figure 1.17).⁴¹

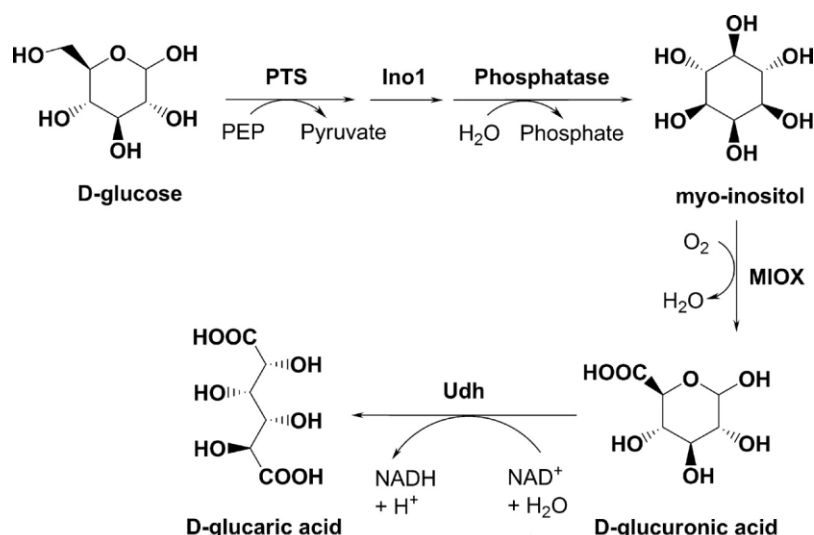


Figure 1.17: Reaction scheme of glucaric synthesis via enzymatic system

However, these two approaches have two main drawbacks: the homogeneous condition, which makes expensive and not easy the separation, and purification steps from the metabolite and the long reaction time (3 days for a GA yield of 17%); the heterogeneous catalyst utilization could be a suitable answer for these drawbacks. The following chapter will show the main promising class of material active in this oxidation: supported metal nanoparticles.

1.3.3 The importance of the catalytic performance of the supported monometallic nanoparticles

Gold, platinum, and palladium are noble metals widely investigated in the oxidation of alcohols and aldehydes. For this reason, numerous studies investigate Au, Pt, or Pd nanoparticles (NPs) for the oxidation of glucose to gluconic acid (the intermediate of the reaction, Figure 1.18) and glucaric acid providing a potential application in the last 15 years.

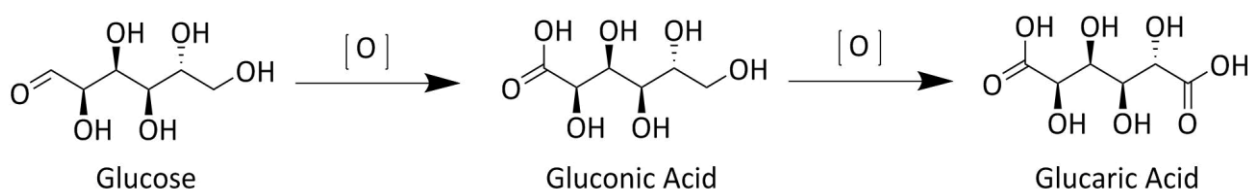


Figure 1.18: Schematic pathway for glucaric acid synthesis

Bimetallic nanoparticles composed of either two of these three metals have proven to be more efficient in comparison to the monometallic counterparts. In particular, bimetallic catalysts have often been shown to surpass their monometallic counterpart in terms of activity and selectivity. Traditionally, there were two reasons proposed for the enhanced performance of a bimetallic catalyst over each monometallic species. The first one is known as ensemble (structural) effects, which could affect the surface composition or the number of single-atom sites available. The other one is an electronic (ligand) effect; here it is presumed that the electronic properties of one element can be modified by the presence of another element and that this, in turn, can modify the chemisorption and reaction properties of adsorbates. Also for this reaction, monometallic catalysts have some drawbacks, like deactivation, leaching, and the use of a base (NaOH) for their activation. Some of these disadvantages could be avoided by combining two metals. The properties of bimetallic catalysts are meaningfully different from their monometallic analogues because of the “synergistic” effects between the two metals. Ferrando and coworkers⁴² have reported a range of effective structures that bimetallic catalysts could form, finding that there are different possible types of mixing patterns between the two metals and in Figure 1.19 are represent the main one.

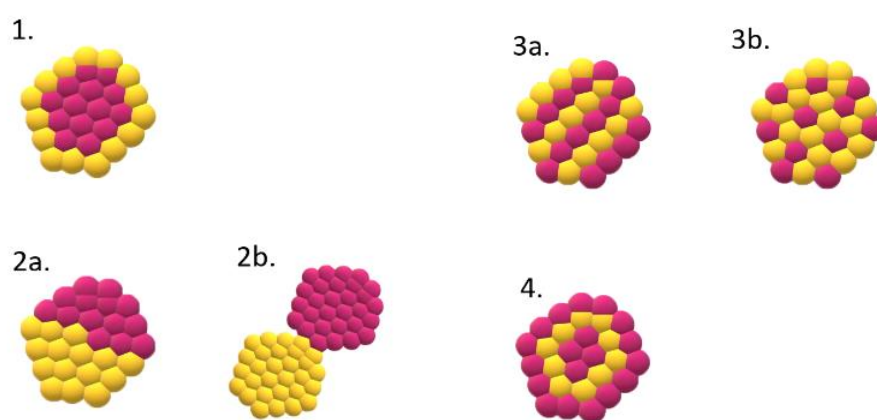


Figure 1.19: Possible bimetallic nanoparticles structure: 1) core–shell nanoparticle structures; 2) sub-cluster segregated nanoalloys; 3) homogeneously mixed alloys; 4) multi-shell nanoalloys

Nevertheless, monometallic nanoparticles of Au, Pt, and Pd are currently used in research to evaluate novel methods of preparation, the effect of size and shape, the effect of support and stability of the catalyst.

The first reaction step, which is the oxidation of glucose to gluconic acid, is a fast reaction step because the aldehyde group is easier to oxidize than an OH group. This is why in literature several works are using monometallic nanoparticles for the first step and here are reported some of the

main works dealing with it. Pt and Pd are known to exhibit the highest catalytic activities towards selective oxidation of carbohydrates but some of the fundamental issues on their catalytic properties for selective oxidation of glucose still need clarification. Pd and Pt are known to be easily oxidized; the formation of oxide on the surface could decrease the active sites and make the catalyst less active; however, the catalytic activity can be extended if the reaction is well controlled. Delidovich et al. used monometallic Pt and Pd nanoparticles supported on mesoporous graphite-like carbon. The preparation of the catalysts was carried out with two different procedures; in particular, the Pt/C were prepared using the impregnation method and Pd/C instead was prepared with the deposition-precipitation, controlling the dispersion with the reduction or calcination step. The glucose oxidation reaction was carried out in a batch reactor at 60°C and an O₂ flow for 7 hours, keeping constant the pH with NaOH solution (pH=8.8-9.2). It was found that Pd/C catalysts with an particle size of 3.2 nm provide a substantially higher selectivity to gluconic acid than Pt/C regardless of the smaller size of Pt nanoparticles (~1.1 nm). Also, a larger mean particle size (6 nm) seems to slightly increase the initial rate in contrast to the mean 3 nm size. It was suggested a higher tolerance of larger palladium particles towards the formation of strong surface Pd–O bonds leading to deactivation of the catalyst.⁴³ Therefore, particle size control is key for the catalytic performance, and therefore it is important to utilize preparation methods for the synthesis of nanoparticles with controlled particle size and in the metallic state. This is why Liang et al. investigated a new preparation method, producing Pd NPs by atomic layer deposition (ALD) over alumina as support in a fluidized bed reactor which allowed to control the quantity of precursor deposited and the dispersion. The ALD method permit to avoid the large amounts of solvent and precursor is required for the wet-chemical process, which is not environmentally friendly. With the Pd precursor dose time of 12 min, the Pd content can reach 0.9 wt% after 10 cycles of Pd ALD and 2.1 wt% after 20 cycles of Pd ALD. However, the Pd dispersion decreased from 72 to 36 % when the number of ALD cycles increased from 10 to 20. By TEM analysis, an mean particle size of Pd was estimated: ~3 nm in diameter for 0.9% wt Pd/Al₂O₃. In contrast to 2.1% wt Pd/ Pd/ Al₂O₃, there are two size distributions of Pd particles, one centered at ~3 nm and the other centered at ~4.5 nm. When the synthesized catalysts were tested in the glucose oxidation, 2.1% Pd/ Al₂O₃ shows a fast initial rate but after 360 min it reached a 66% conversion whilst 0.9% Pd/ Al₂O₃ reached 62% conversion. After 4 cycles, 2.1% Pd/ Al₂O₃ shows good stability and no leaching phenomena, a thing that confirms the strong metal-support interaction for the ALD-prepared Pd catalysts.⁴⁴ Hermans and his team worked with two different methods of synthesis (precipitation-reduction PR and urea-assisted sodium

formate deposition HD) to prepare Pd nanoparticles supported on carbon black, a non-porous material. They found that this optimal particle size of Pd for the reaction was 7 nm which was obtained by the PR method and treated at 573 K giving the highest yield of 50% to gluconic acid amongst all the prepared catalysts. Further analysis of the used catalyst by XPS showed an increase of O/Pd surface ratio above a stoichiometric Pd1:O1 ratio expected for the PdO oxide. TGA analysis did not indicate a loss of activity corresponding to carbohydrates as well the content of Pd remained constant concluding that the catalysts were deactivated by a gradual formation of oxygen layers on the Pd particles.⁴⁵ To avoid the overoxidation problem, the use of gold could be a good solution. Indeed, gold has demonstrated good resistance to overoxidation which makes it suitable for glucose oxidation in highly oxidant atmospheres, like high pressure of air and especially oxygen. Junying Zhang and Zhimin Li synthesized Au nanoclusters stabilized with PET (phenylethanethiolate) and immobilized on activated carbon via a simple impregnation method.⁴⁶ Au₂₅(PET)₁₈, Au₃₈(PET)₂₄, and Au₁₄₄(PET)₆₀ nanoclusters were analyzed by TEM showing mean particle sizes of 1.3, 1.5, and 1.9 nm, respectively. The XPS analysis results showed that the surface gold atoms covalently bond with the thiolate ligands and the Au was in a metallic state. Then, the nanoclusters were subject to an annealing process (120, 150, and 300°C for 1 h in air) to remove the thiolate cap. Au₂₅(PET)₁₈ treated at 120°C maintained the size intact but the Au₂₅(PET)₁₈ treated at 150 and 300°C increased their size to 3-7 and 8-15 nm, respectively. This was attributed mainly due to the weak interaction between the gold nanoclusters and activated carbon supports. After the nanoclusters were used in the aerobic oxidation of glucose to gluconic acid at 60°C, constant pH of 9.5 with NaOH, bubbling O₂ at atmospheric pressure. The nanoclusters treated at 300°C gave the worst catalytic performance with only 37% of glucose conversion in 60 min. In contrast to the catalyst treated at 120°C reached 94% conversion of glucose after 30 min of reaction (turnover frequency (TOF) is 0.76, 0.90, 0.37, and 0.096 s⁻¹ for the Au₂₅(PET)₁₈/AC, Au₂₅/AC-120, Au₂₅/AC-140, and Au₂₅/AC-300). This gives an insight into a size-activity relationship. When testing the fresh catalyst (without the final heat treatment process), the Au₁₄₄(PET)₆₀ gave the best results amongst them resulting in a 99% conversion of glucose at 141 min. Finally, to investigate the size-dependence of nanoclusters, the molar ratio of D-glucose to gold nanocluster largely raised and comparing the TOF obtained it can be seen that glucose conversion increased with the increasing core size and surface area of the gold nanoclusters (Au₂₅(PET)₁₈/AC < Au₃₈(PET)₂₄/AC < Au₁₄₄(PET)₆₀/AC).⁴⁷ Wojcieszak et al studied Au nanoparticles prepared by microemulsion with hydrous hydrazine as reductant, in the production of glucuronic acid (an intermediate of gluconic acid oxidation to glucaric acid). By TEM

analysis it was observed the mean size of the nanoparticles produced is 4 nm and XPS analysis confirm that hydrous hydrazine is capable to reduce completely gold in Au⁰. Au/CeO₂ was investigated in the oxidation of glucose, performed in aqueous solution at low temperature using O₂ as oxidant and without adding any base. The catalysts synthesized by the microemulsion method gave an 11% yield to glucuronic acid compared to 1% obtained with the catalyst prepared by sol immobilization Au(PVA)/CeO₂. They have found that the preparation method has a key role in the catalyst activity, in particular, hydrazine treatment permits to increase the basicity of the catalyst.⁴⁸ The pH of the reaction solution plays an important role in the stability of the catalyst. Megias-Sayago et al. studied the effect of recycling of gold-based catalysts in base-free conditions. The catalysts tested were prepared by sol immobilization, screening the amount of NaBH₄ in the reduction step. TEM analysis has shown that the higher ratio of reducing agent formed small nanoparticles, with a size of 4.8 nm against 8 nm, and more stable catalytic activity after 4 cycles (7.7 nm vs 20 nm). To evaluate the activity of this material, the reactions were carried out in a batch reactor bubbling oxygen at 40°C for 18h. All the catalysts give similar results and glucose conversion reached around 80% with a selectivity to gluconic acid of almost 100%. The catalyst was reused and the catalytic activity decays gradually after the 1st cycle. To regain the initial performance, the catalyst was treated with hot static air, water, or NaOH. The catalytic activity did not return to the initial performance as in the 1st cycle in any treatment. Gold is sensitive to strong absorption of aldehydes, ketones, enones, or compounds with β-dicarbonyl structure issued from highly oxygenated species. But the most important factor leading to the loss of activity is the leaching of gold (15% of initial gold) in the reaction medium which accounts for a 20% decrease in glucose conversion between the 1st cycle and 2nd cycle. This was attributed to the chelating effect of the main major product: gluconic acid, which is never neutralized in the reaction medium.⁴⁹ The presence of the base is critical for the long-term usage of catalyst. Zhang et al. studied the effect of several bases in Pd nanoparticles supported on cellulose, a material known to be resistant, widely available, and biodegradable. Pd nanoparticles, obtained by the impregnation method, show an mean size of 5nm; the XPS analysis confirmed the presence of metallic Pd, which was immobilized to the cellulose surface thanks to the hydroxyl group presence. This catalyst was tested in the oxidation of glucose to gluconic acid using different bases (pyridine, NaOH, Na₂CO₃, NaHCO₃, and Mg(OH)₂), bubbling O₂ at room temperature in a batch reactor. Na₂CO₃ and NaHCO₃ resulted in high selectivity (~90%) to gluconic acid while NaOH gave lower selectivity to gluconic acid (63%) but a complete conversion of glucose and with pyridine no conversion at all. NaOH is such a strong base that leads to the

isomerization or degradation of the glucose, in contrast to Na_2CO_3 and NaHCO_3 which are milder bases. The initial pH of the reaction solution with NaOH was 13, while those for Na_2CO_3 and NaHCO_3 were less than 9. Glucose started to decompose in a strongly alkaline solution at pH above 11, so there were many more side reactions for the glucose oxidation by the use of NaOH as an additive. Besides, the use of $\text{Mg}(\text{OH})_2$ as the additive also gives a high selectivity, but at a low glucose conversion and they attribute this thing to the fact that $\text{Mg}(\text{OH})_2$ is heterogeneous that cannot effectively contact the substrate. Using 0.5 eq Na_2CO_3 , 40 mg of catalyst at room temperature for 3h, Pd/cellulose was reused 5 times (previously washed thoroughly with water). The performance of the catalyst never decreased the gluconic acid yield maintaining 90% after five consecutive runs.⁵⁰ If for this first step of reaction there are several studies with monometallic nanoparticles, the synthesis of glucaric acid from glucose is a more difficult process and few works are published dealing with it, especially using only monometallic nanoparticles.

Jechan Lee et al. have tested several commercial catalysts, in particular, Pt on different supports, like SiO_2 , Al_2O_3 , and carbon. All the tests were carried out in a batch reactor at room temperature without pH control, using O_2 as an oxidant agent, screening different temperature, oxygen pressure, and glucose: Pt ratio. Pt/C is the catalyst that gave better results and good stability after 5 cycles, with a TOF of 879 h^{-1} against 195 h^{-1} , and 102 h^{-1} for Pt/ Al_2O_3 , and Pt/ SiO_2 respectively; after the chemisorption and physisorption characterization, they attribute the best performance to the high surface area of carbon. The screening of the different conditions underlines that the reactions under base-free and mild basic conditions give the best yield of glucaric acid compared to acidic and highly basic because the C–C bond cleavage of glucaric acid at basic pH results in low carbon chain carboxylic acids.⁵¹ Solmi et al. studied this reaction in more detail the reaction conditions (O_2 pressure, base concentration, the quantity of catalyst and alloying Au with Bi in NPs) and concluded the need for a basic environment (Glucose: NaOH molar ratio of 1:3) under milder conditions, lower reaction times and the possibility to carry out the reaction at higher metal molar ratios (Glucose: Me molar ratio of 500:1) compared to other studies regarding Pt-based catalysts. Studies were performed to have a better insight into the reaction mechanism.⁵² In 2005, Rossi and coworkers continued with the investigation and confirmed the formation of gluconate and hydrogen peroxide through a two-electron mechanism (Figure 1.20). The key point is represented by the electron-rich gold species, formed by the hydrated glucose anion with gold surface atoms, which is supposed to activate molecular oxygen by the nucleophilic attack. Assuming an efficient nucleophilic behaviour determined by the electronic properties of nanometric gold particles (< 10 nm). In the dioxogold

intermediate either Au^+-O_2^- or $\text{Au}^{2+}-\text{O}_2^{2-}$ couples can be formally considered as a bridge for the two-electron transfer from glucose to dioxygen.⁵³ Saliger et al. proposed recently the use of H_2O_2 as an oxidizing agent in glucose oxidation under alkaline conditions. They found that oxygen and hydrogen peroxide comprise the same rate-determining step leading to similar activation energies (48 kJ/mol for H_2O_2 and 47 kJ/mol for O_2 at 30-60°C range). It was assumed that O_2 formed by the decomposition of H_2O_2 is the effective oxidizing agent.⁵⁴

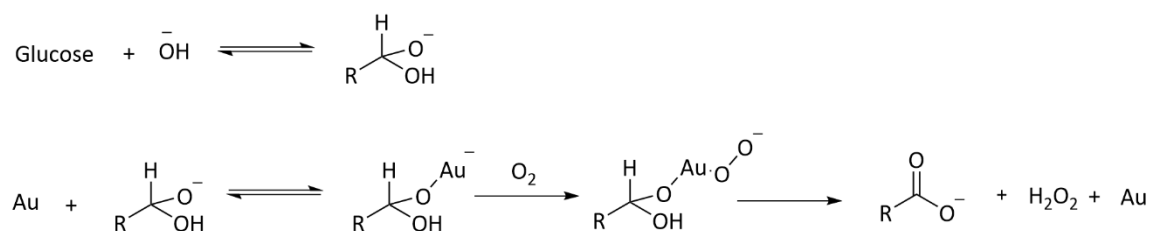


Figure 1.20: Proposed mechanism for alkali promoting effect in glucose oxidation and H_2O_2 formation as a reaction product

Also, alkaline pH results in an increase of heterogeneous catalyst activity due to the stabilization of the particle size and preventing metal leaching in the reaction medium. Acidic conditions increase the selectivity to gluconic acid but suppress enormously the oxidation reaction.⁵⁵ Efforts were made to avoid the use of basic conditions in the oxidative reaction because of the promoting effect of hydroxyl groups in the isomerization of glucose to fructose and mannose. Despite this effect, it was proved that OH groups on the surface of Au sites are required for a high yield of gluconic acid. Similar results were reported in base-free conditions but at much longer times (18 h).⁵⁶

1.4 Catalytic reduction of 4-Nitrophenol to 4-aminophenol

4-nitrophenol (4-NP) is a phenol derivative used in a wide range of chemical applications, such as fungicides, medicines, dyes, and leather manufacture.⁵⁷ In particular, it is reported that the formation of pesticides and dyes (fenitrothion and parathion are two examples) produce the 4-NP as an intermediate product and it is also used as an indicator and raw material for leather fungicide.^{58, 59} This is why the main routes of entry to the aquatic environment are through the industrial effluents of production plants and chemical firms where these compounds are used as intermediates or from agriculture treatments. However, it is well known 4-nitrophenol to be

carcinogenic and mutagenic and causes skin diseases.⁶⁰ Because of these two factors, it is important to remove 4-NP from wastewater, to ensure the environment and human health and safety. However, this process exhibits some limitations and challenges; physical, chemical, and biological treatments have to be used for this purpose.

The chemical catalytic route (Figure 1.21) could be one of the most promising ways; in particular, 4-NP reduction product, 4-aminophenol (4-AP), finds applications as a photographic developer of black and white films, corrosion inhibitor, drying agent, precursor for the manufacture of analgesic and antipyretic drugs, and is an important intermediate in the synthesis of paracetamol.

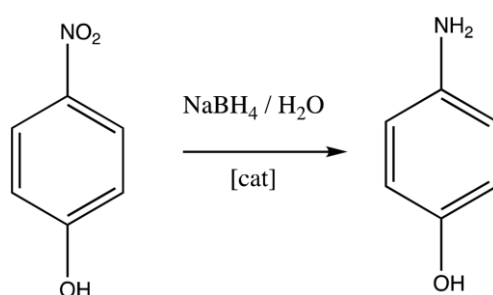


Figure 1.21: Catalytic reduction of 4-Nitrophenol scheme

For this reason, several works are reported in the literature and noble metals are frequently used in these systems, such as palladium^{61,62} platinum^{63,64} and gold-based systems.⁶⁵ For example, Jingwen Sun and coworkers had employed Palladium, in particular, they had synthesized palladium/graphene (Pd/G) nanocomposite by hydrothermal method. These materials exhibited higher activity and higher stability than the commercial Pd/C and this was attributed to the graphene sheets' strong dispersion effect for Pd nanoparticles and good adsorption ability for nitrobenzene derivatives via π - π stacking interactions.⁶⁶ Instead, Hugo Rodríguez Molina et al have tested gold nanoparticles supported on carbon. After an accurate investigation on the catalyst preparation, they have found that the mean particle size of the Au nanoparticles affects drastically the reaction rate and the experimental procedure, which facilitates the formation of smaller Au nanoparticles and demonstrated higher catalytic activity.⁶⁷

The mechanism of the reaction involving gold nanoparticles was investigated by several research groups. In particular, Ballauff and co-workers have shown that the kinetics of this model reaction can be treated in terms of the Langmuir–Hinshelwood model (Figure 1.22): both reactants adsorb on the surface of the supported metal particles during the reaction. The adsorption of both substrates is fast, and it is modeled in terms of an equilibrium process described by a Langmuir

isotherm. In the first step, the NaBH_4 is decomposed by hydrolysis, then the B(OH)_4^- and active hydrogen are formed; then, the active hydrogen is transferred to the nano-gold and adsorbed at the surface; finally, the H atom at the nano-gold surface reacts with 4-NP to yield the product 4-AP. Finally, the reaction product dissociates from the surface.⁶⁸

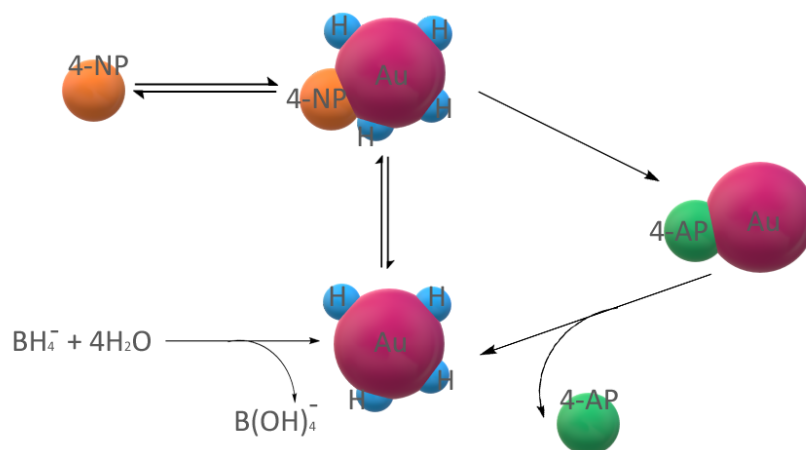


Figure 1.22: Proposed reaction mechanism for the catalytic 4-nitrophenol reduction using NaBH_4 as the reducing agent

It is clear how the surface of the metal and, therefore, the dimension of the nanoparticles, plays a key role in the activity of the catalysts. Tao Ma and co-workers have investigated the effect of Au particle size, by synthesizing and comparing Au nanoparticles with different particle size and shape, with a range of sizes between 4 nm to 140 nm for the Au nanoparticles. Two experimental methods were used for the catalyst preparation: a seeded growth method was applied for the synthesis of the smaller ones (4, 16, 40, and 80 nm), varying the ratio between seeds and metal ratio and a surfactant-free wet-chemistry method for the one with star-shape for the Au nanoparticles. With different methods and stabilizers, they were able to create Au nanospheres (Au-NPs) and nanostars (Au-NSs) (Figure 1.23). The catalytic test demonstrated that reaction proceeds nearly faster on Au-NSs than on Au-NPs. In their case, Au-NSs exhibited stronger catalytic activity than that of Au-NPs, which suggests that the corresponding surface area of metal nanoparticles influences the adsorption of the reactants and plays a dominant role in the reaction rate. The considerable enhancement in catalytic activity for the Au-NSs could probably be attributed to their higher surface area-to-volume ratio of multi-branched nanostructures.⁶⁹

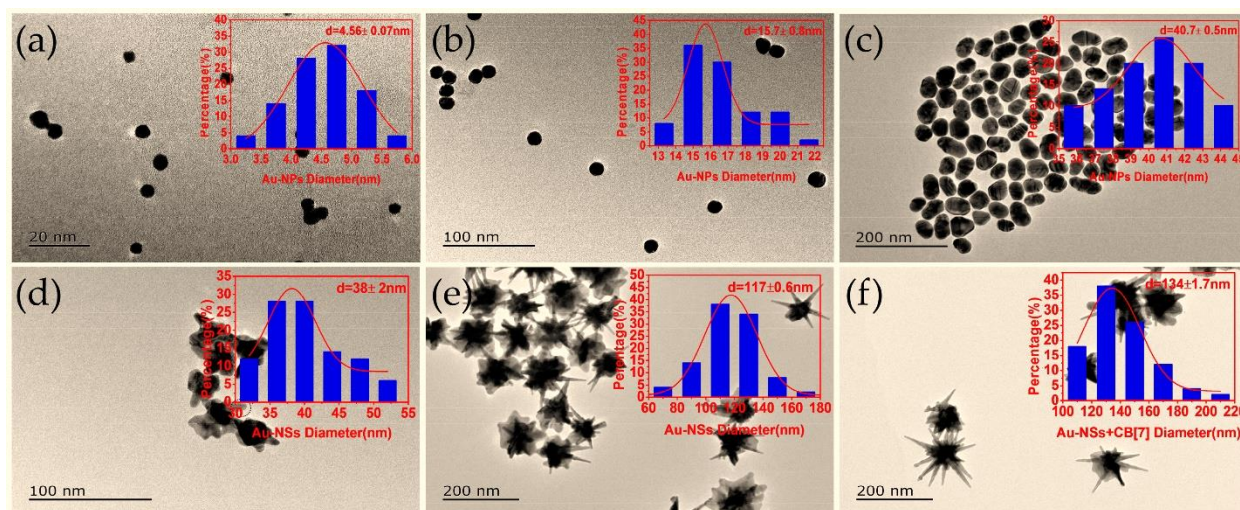


Figure 1.23: TEM analysis of synthesized gold nanoparticles in this work: (a) 4 nm gold nanospheres (Au-NPs); (b) 16 nm Au-NPs; (c) 40 nm Au-NPs; (d) 40 nm Au-NSs; (e) 117 nm Au-NSs; (f) 134 nm Au-NSs + CB[7] (cucurbit[7]uril)

Another important parameter is the stabilizing agent used during the catalyst preparation for the synthesis of colloidal nanoparticles. Siyam M. Ansar, Christopher L. Kitchens and co-workers, have investigated the catalytic activity of AuNP functionalized with HS-PEG ligands for the catalytic reduction of 4-nitrophenol, especially as a function of thiolated polyethylene glycol (HS-PEG) chain length and packing density. They have found that by increasing the HS-PEG chain length, the HS-PEG surface coverage on AuNPs decreasing (AuNP-SPEG1K has a packing density of 2.61 molecules/nm² vs AuNP-SPEG30K with 0.47 molecules/nm²). Thanks to absorption test, they concluded that the high packing density of HS-PEG1K creates well-ordered closed packing, which may cause a high diffusion barrier and/or leaves no space under the HS-PEG1K layer on AuNP surface to adsorb small molecules. This is why lower molecular weight showed lower catalytic activity and the rate constants for the AuNP-SPEG1K, AuNP-SPEG2K, AuNP-SPEG5K, AuNP-SPEG10K, and AuNP-SPEG30K are 0, 0.06, 0.15, 0.28, and 2.1 min⁻¹, respectively.⁷⁰

1.5 5-hydroxymethylfurfural oxidation to 2,5-furan dicarboxylic acid

The valorization and especially the oxidation of biomass derived molecules to aldehydes and carboxylic acids is an important topic to produce high-value molecules. For example, one of the most important biomass derived platform chemicals that can be found in the top 12 added value chemicals from biomass is the 2,5-furan dicarboxylic acid (FDCA, Figure 1.24).⁷¹

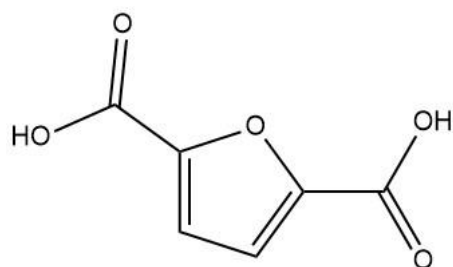


Figure 1.24: Chemical structure of 2,5 furan dicarboxylic acid

Its importance is due to the possibility to use it as a renewable substitute for terephthalate in the production of polyesters.⁷² It is also commonly employed as a precursor for the synthesis of bio-based polyesters and various other polymers: for instance, the biomass-derived polyester coating namely “2,5-furan dicarboxylic acid, isosorbide, succinic acid, 1,3-propanediol, and 1,5-pentanediol”⁷³ shows tunable properties and improved performance against common petrochemical-derived coatings.^{74, 75, 76, 77, 78} Applications of FDCA in the synthesis of several metal-organic frameworks (MOFs) have also been reported.^{79,80}

Several routes to FDCA were reported, but most of all proceeds via the catalytic oxidation of 5-hydroxymethylfurfural (HMF) with air or molecular oxygen over different catalysts. This is because HMF could be easily obtained via acid-catalyzed dehydration of fructose or glucose, so it represents a good green building block to involve.

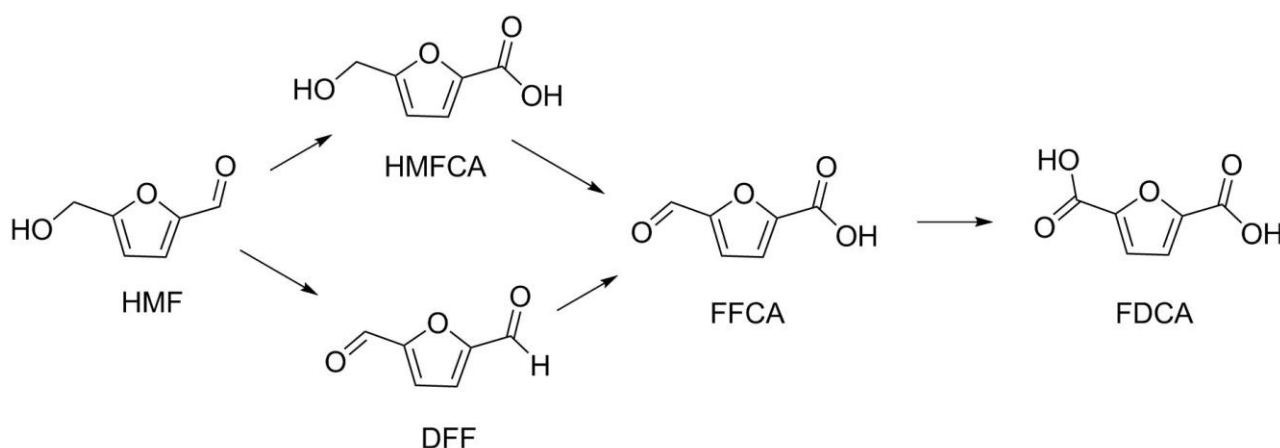


Figure 1.25: Reaction pathway for the HMF oxidation to FDCA

The oxidation pathway is shown in Figure 1.25 and the oxidation of HMF can proceed through two different partially oxidized intermediates: the 5-hydroxymethyl-2-furancarboxylic acid (HMFCFA) and 2,5-diformylfuran (DFF). Both intermediates subsequently oxidized to 5-formyl-2-furancarboxylic acid (FFCA) and finally, the oxidation of the aldehyde group fast lead to the formation of FDCA.⁸¹ To carry out this reaction, the homogeneous process involving acetic acid as solvent and Co-based catalyst⁸² was abandoned for the use of heterogeneous catalyst based on Au, Pd, and Pt nanoparticles.^{83,84,85} Among others, gold was commonly used in the form of gold nanoparticles (1-10 nm) because of its high resistance against oxide formation, which is believed to be one of the main causes of catalyst deactivation for other metals.

Davis et al. have investigated thoroughly the reaction mechanism of the HMF oxidation over supported gold catalysts.⁸⁶ From Figure 1.26 it can be seen that hydroxyls play an important role in HMF oxidation. OH⁻ ions catalyze the formation of geminal diols from aldehyde and water (Figure 1.26, steps 1 and 4). Furthermore, OH⁻ ions adsorbed on gold surface or at the gold-support interface abstract hydrogen from C-H and O-H groups of alcohol or geminal diol to yield carbonyl groups, respectively (Figure 1.26, steps 2, 3 and 5). While the formation of geminal diols can be catalyzed by OH⁻ in solution, dehydrogenation steps are catalyzed by hydroxyls adsorbed on the surface (or in the close vicinity) of gold, since electron density formed as a result of hydrogen abstraction is present on the gold nanoparticles. The electrons are then scavenged by oxygen to regenerate the hydroxyls (Figure 1.26, steps 2, 3 and 5, right side).

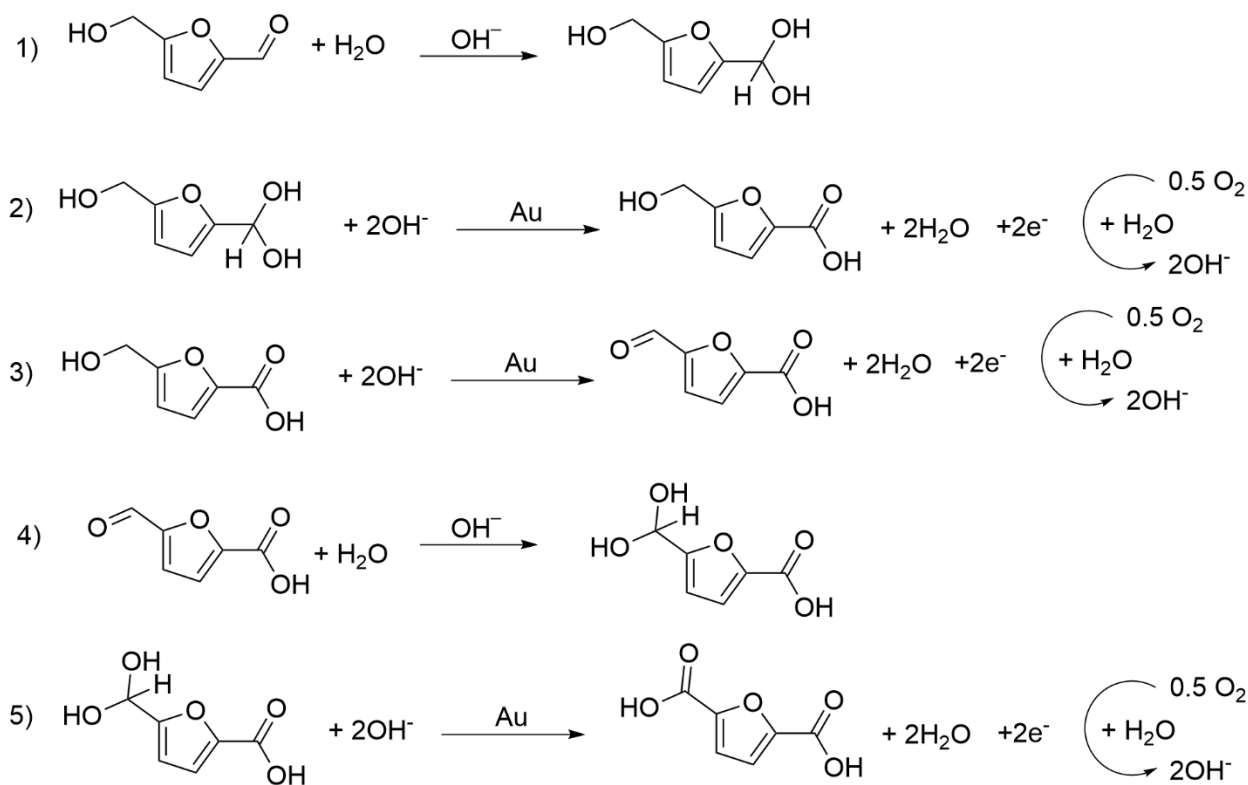


Figure 1.26: Mechanism for the HMF oxidation using gold and oxygen in the presence of a base (OH^-)

Another example was reported by Corma and co-workers that have used Au nanoparticles supported on various oxides such as ceria, titania, and carbon, working in mild reaction conditions (65°C) in an aqueous medium to obtain quantitative yields in FDCA in 8h reaction in an oxidizing atmosphere (O_2).⁸⁷ The comparison between the different support shows that CeO_2 and TiO_2 are the ones that show better catalytic performance, achieving 100% yield of FDCA after 8 h; instead, the use of Fe_2O_3 or activated char coal give yields below 80 mol% after 24 h reaction time. In particular, CeO_2 results as the best support and therefore, further studies were carried out to investigate the degradation side reactions. Substrate degradation is strongly diminished, and the catalyst life increased by performing the reaction in two temperature steps.

To avoid or to minimize the use of NaOH addition (strong alkaline conditions), basic supports like MgO or hydrotalcites have also been considered. However, the decrease of the pH during the reaction due to the formation of acid product could dissolve them in solution and details study were carried out to verify this hypothesis: for example, Bhushan N. Zope et al. have investigated the possibility to use a hydrotalcite Mg:Al as support for the gold NPs. To do that they measured the possible leaching of the hydrotalcite in a batch reactor, using a flow O_2 as oxidant agent, in base-free condition at 90°C . However, the ICP analysis shows that 70% of the Mg in the HT added to the

reactor was leached in the liquid phase.⁸⁸ Camila P. Ferraz and co-workers have tested the MgO as possible support: after they prepared Au/MgO by sol immobilization method, they have tested in a batch reactor at 110°C using 20 bar of air. Even if after 2 hours, this catalyst leads to 99% of HMF conversion, and 97% of FDCA selectivity, the leaching of the support was detected.⁸⁹

1.6 Furfural oxidation

Another reaction where these series of catalysts could have a nice application is the oxidation of furfural to furoic acid. Furfural is another molecule that could be easily obtained by the treatment of biomasses, for example from dehydration/dehydrocyclization reaction of C5 sugars like xylose and arabinose.⁹⁰ Starting from this molecule as the main building block chemical, a big range of important chemical products could be prepared, such as phenol-furfural-resins,⁹¹ or can be converted to furfuryl alcohol, tetrahydrofurfuryl alcohol, furan, tetrahydrofuran⁹² and other product like Figure 1.27 shows.

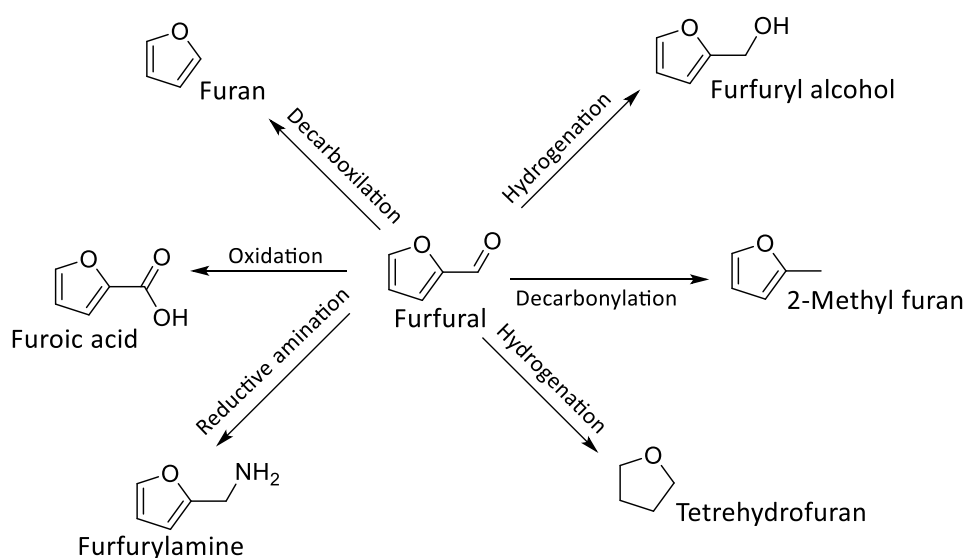


Figure 1.27: Scheme of possible furfural derivatives⁹³

One of them is furoic acid (FA), which can find different applications such bactericide and fungicide. It is also been considered an acceptable flavoring ingredient characterized as sweet, oily, herbaceous, and earthy.⁹⁴ 2-furoic acid may have an important role in the field of optic technology. 2-furoic acid is highly transparent in the 200–2000 nm, wavelength region, is stable up to 130°C, and

generally has low absorption in the UV, visible, and IR spectrums.⁹⁵ In optical and dielectric studies, 2-furoic acid crystals were shown to have decreasing dielectric constants with increasing frequencies. This could mean that the crystals may act as paraelectric in the temperature range before 45°C and ferroelectrics in temperature ranges after 45°C.⁹⁶ However, not so many studies were reported on the synthesis of furoic acid from furfural (It is more overspread the study dealing with the hydrogenation of furfural). Furoic acid is currently produced industrially via a Cannizzaro reaction with NaOH (Figure 1.28).

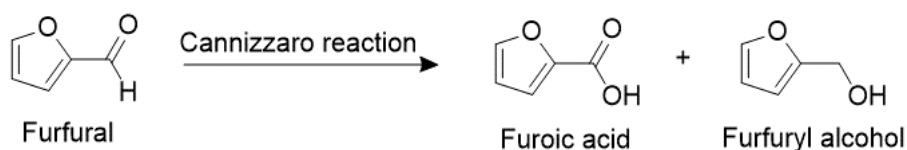


Figure 1.28: Cannizzaro reaction for the furfural

The application of a heterogeneous catalyst to improve the efficiency of this process was investigated and a number of interesting studies were reported. For instance, Sha and co-workers also showed that high selectivity to FA (92%) was obtainable in the presence of an Ag₂O/CuO catalyst.⁹⁷ Instead, Douthwaite and coworkers have tested a bimetallic catalyst AuPd/MgO and they have investigated how the base (NaOH) and the oxygen presence could influence the pathway of the reaction and avoid the polymerization reactions; in this way, they have achieved a furfural conversion of 88% with a FA yield of 84%.⁹⁸ However, if alcohol is used as solvent instead of water, this can be involved in the reaction, giving rise to cascade reactions. There are two possible reactions:

- oxidative esterification: this pathway leads to the formation of alkyl furoates, which possess interesting applications for flavors and fragrances, as well as in the fine chemical industry.
- oxidative condensation: it occurs only when the alcohol used to contain an H in alpha (for example methanol is selective for the preview pathway).

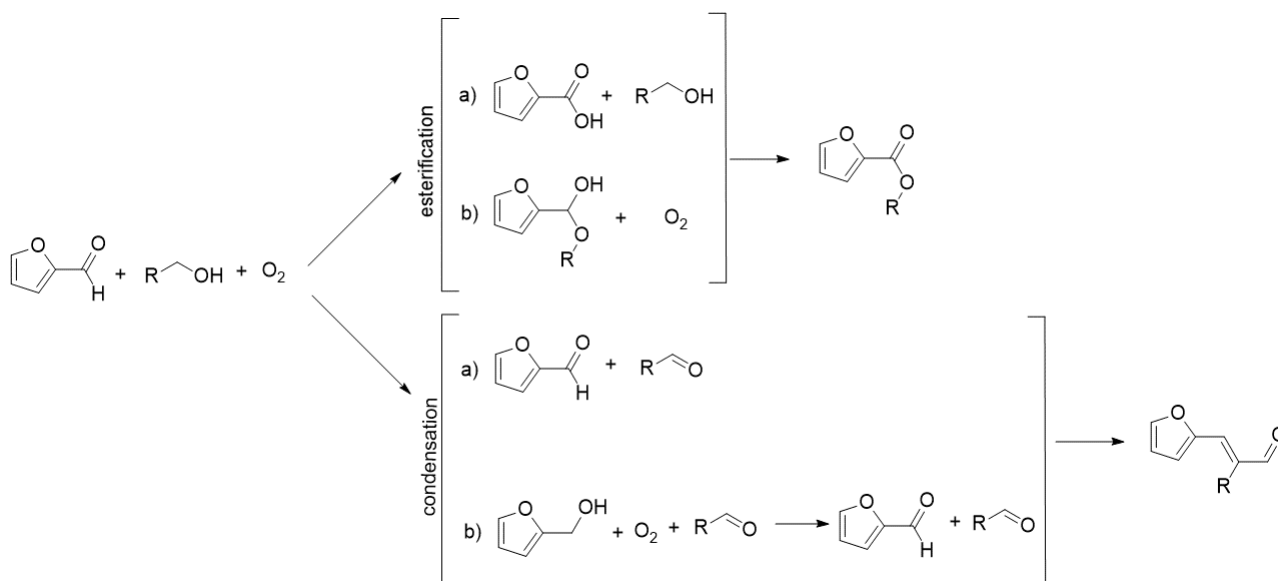


Figure 1.29: Mechanism for the oxidative esterification and oxidative condensation

As Figure 1.29 shows, if the alcohol used contains a H in alpha the condensation pathway and the esterification one is competitive reactions. Several parameters can influence the selectivity on the route followed in the oxidation process. Thus, the chain length is one of the parameters that affect: short-chain alcohols help the formation of oxidative condensation products, while alcohols with longer chains increase the esterification selectivity. These authors have pointed out that the selectivity towards oxidative condensation follows the next trend: ethanol = n-propanol > i-propanol > n-butanol > n-hexanol.⁹⁹ The nature of the support can also affect: weak acid sites favor condensation products, thus support acidity is favorite if this route is preferred. Besides, the promoting effect of the base is another important parameter influencing selectivity. These authors have established that an increase in basicity also favors the formation of oxidative condensation products.¹⁰⁰ However, this basicity must be carefully tuned, since too strong bases can cause uncontrolled polymerization.¹⁰¹ In the following part, it is reported the state of art for both pathways.

1.6.1 Furfural esterification

In literature, gold is the noble metal most used for this type of reaction and researchers have focused their study on the support investigation. For example, Maela Manzoli and coworkers have studied the performance of ZrO₂, TiO₂, and CeO₂ as support for Au NPs. The comparison between the catalyst prepared by sol-immobilization synthesis shows that Zirconia achieves the best results

in terms of conversion and selectivity a better Au NPs dispersion on the surface; the tests carried out in a batch reactor at 120°C using O₂ show a better conversion and selectivity compared to TiO₂ and CeO₂ (conversion of 82% vs 20% and 66% respectively and selectivity of 96% vs 91% and 69%). Although, this is not the only parameter that influences the reactivity; in fact, the presence of free OH groups on the surface, which bring about the formation of hydrogen-carbonate species, helps the reaction. In this way, it is explained why CeO₂ has worst catalytic performance than ZrO₂ and why TiO₂ maintains a high selectivity.¹⁰²

Also, Centi et al. confirmed the effectiveness of ZrO₂ as support for Au NPs for the esterification reaction. They made an overspread comparison between all the possible support. All the Au-based catalysts (the paper reported commercial samples and catalyst prepared by deposition-precipitation or photo-deposition) reported in Table 1.2 were tested in a batch reactor at different temperature using a pressure of air and Figure 1.30 confirm the good performance of ZrO₂ as support.¹⁰³

Id	Support	Pretreatment	Catalyst
A	Al ₂ O ₃	250	1 % Au/Al₂O₃
B	C	250	Au/C
C	CeO ₂	250	Au/CeO₂
D	CeO ₂ /Al ₂ O ₃	250	Au/CeO₂/Al₂O₃
E	CeO ₂ /ZrO ₂	250	1 % Au / CeO₂/ZrO₂
F	Co ₃ O ₄ /Al ₂ O ₃		Au /Co₃O₄/Al₂O₃ CALCINED
G	Fe ₂ O ₃	250	Au /Fe₂O₃
H	Fe ₂ O ₃ /Al ₂ O ₃	250	Au /Fe₂O₃/Al₂O₃
I	MgAl ₂ O ₄	250	Au /MgAl₂O₄
L	MnO ₂	250	1 % Au /MnO₂
M	MnO ₂ /Al ₂ O ₃	250	Au /MnO₂/Al₂O₃
N	MnO ₂ /Co ₃ O ₄ /Al ₂ O ₃	250	Au /MnO₂/Co₃O₄/Al₂O₃
O	TiO ₂	250	1 % Au /TiO₂ 100 % ANATASE
P	TiO ₂		Au /TiO₂ (P25) CALCINED
Q	ZrO ₂	250	1 % Au / ZrO₂
R	ZrO ₂ -TiO ₂		Au / ZrO₂-TiO₂ CALCINED
S	ZrO ₂ -TiO ₂	250	1 % Au / ZrO₂-TiO₂
T	ZrO ₂ -Y ₂ O ₃	250	Au / ZrO₂-Y₂O₃
U	ZrO ₂		Au / ZrO₂ CALCINED

Table 1.2: Au commercial catalysts used for the screening

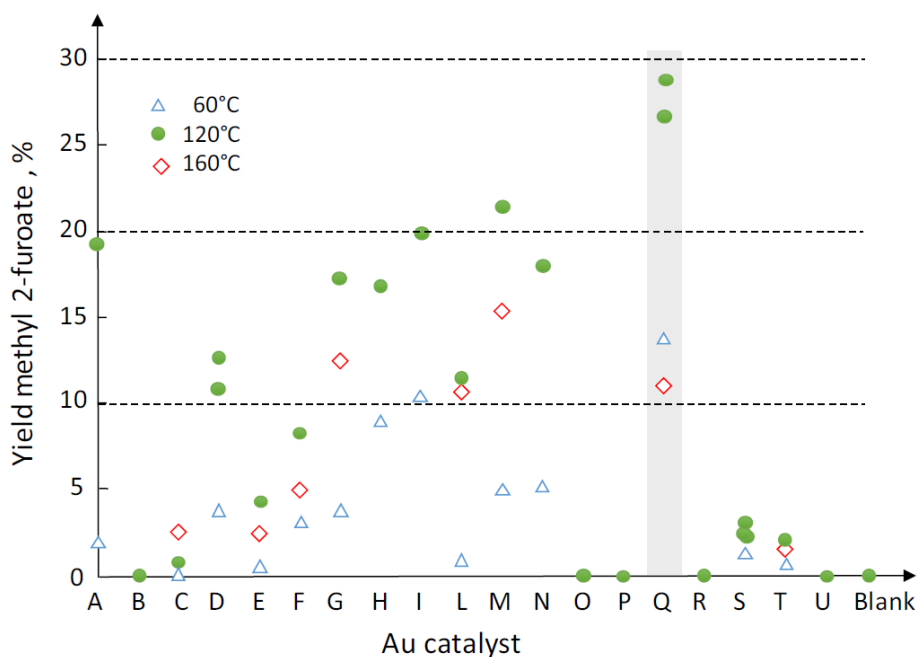


Figure 1.30: Methyl 2-furoate yield obtained from different gold-based catalysts (see Table 1.2) at three reaction temperatures

Because of the importance of the OH group on the support surface, the report of Camila P. Ferraz et al. presents the use of a basic oxide, such as MgO, as the chosen support. In particular, they have synthesized Au nanoparticles via sol-immobilization method, using as support MgO, CaO, SrO, BaO. There was no major difference dealing with the dimension of NPs obtained for every catalyst, and the TEM analysis shows an mean size around 4nm for the majority of the Au catalysts. All these catalysts were tested in a batch reactor at 110°C using air as oxidant agent and the results show that Au/MgO sample formed up to 95% methyl furoate (MF) yield, showing a fast reaction rate, and high catalytic performance for furfural: Au molar ratios between 50 and 300. Furthermore, this catalyst was stable during reusability, since both the selectivity and the activity were maintained after four consecutive cycles, with no trace of support or metal leaching. Tests were carried out also with other alcohols: ethanol, isopropanol, n-butanol, and isopentanol leading to the formation of the corresponding esters (ethyl-, isopropyl-, n-butyl, and isopentyl furoates) with high selectivity (>99%). Linear and branched esters were formed, but the long-chain linear alcohols resulted in higher yields, such as n-butyl furoate in 94% yield.¹⁰⁴

1.6.2 Furfural condensation

The alcohol more studied for this reaction is ethanol, because the product of the oxidative condensation, which is the furan-2-acrolein, could have a good application as a flavoring agent in

the food industry. Pt and Au are the common metals used for this reaction; Zonghui Liu and co-workers have synthesized several samples of Pt NPs supported on FeO_x -hydroxyapatite (FH), hydroxyapatite (H), Hydrotalcite (HT), Fe_3O_4 , Al_2O_3 and ZrO_2 ; Al_2O_3 . FH, and H are the supports that permit to have smaller nanoparticles, with an mean size between 5 and 8 nm by TEM analysis, quite different from 12nm for HT and 26nm for ZrO_2 . The catalytic tests in autoclave reactor at 140 °C under 0.3 MPa of O_2 , using K_2CO_3 as base and two different alcohols: ethanol and n-propanol. The catalysts which achieve higher conversion and selectivity are Pt/HT and Pt/ Al_2O_3 :

- Pt/FH
 - for ethanol: X furfural= 93.9%, Selectivity furan-2-acrolein=67.9%, Selectivity other= 32.1%
 - For propanol: X furfural= 90.1%,
Selectivity 3-(furan-2-yl)-2-methylacrylaldehyde=90.0 %, Selectivity Other=10.0 %
- Pt/ Al_2O_3
 - For ethanol: X furfural=97.1%, Selectivity furan-2-acrolein=68.6%, Selectivity Other=31.4 %.
 - For propanol X furfural=81.4%, Selectivity 3-(furan-2-yl)-2-methylacrylaldehyde =90.4 %, Selectivity Other=9.6 %.

They attributed these results to the combination of different characteristics: large surface area and pore volume, small and mean-size Pt nanoparticles and the presence of weak acid sites¹⁰⁵. Also, gold was tested on this type of support, and a range of catalysts ($\text{Au}/\text{Al}_2\text{O}_3$, Au/HTc , Au/CeO_2 , $\text{Au}/\text{Fe}_3\text{O}_4$, $\text{Au}/\text{Nb}_2\text{O}_5$) were prepared by deposition-precipitation. The results reported in Table 1.3 are obtained in a batch reactor at 0.3 MPa of O_2 , reaction time 4 h, temperature 130 °C, and for the same reason of Pt series, Al_2O_3 seems the best support tested.¹⁰⁶

Entry	Catalytic system	Conversion (%)	Selectivity (%)			
			1	2	3	Others
1	None (baseline)	9.4	0	0	>99%	0
2	Au/Fe ₃ O ₄	29.5	0	0	>99	0
3	Au/Fe ₃ O ₄ + K ₂ CO ₃	68.4	91.3	2.9	0	5.8
4	Fe ₃ O ₄ + K ₂ CO ₃	25.6	0	0	79.6	20.5
5	K ₂ CO ₃	21.2	0	0	0	100
6	Fe ₃ O ₄	23.2	0	0	0	100
7	Au/HTc + K ₂ CO ₃	78.0	81.0	5.4	0	13.6
8	Au/Co ₃ O ₄ + K ₂ CO ₃	80.1	83.2	2.7	0	14.0
9	Au/Al ₂ O ₃ + K ₂ CO ₃	84.9	80.1	4.9	0	15.0
10	Au/CeO ₂ + K ₂ CO ₃	97.3	54.9	17.7	0	27.4
11	Au/Nb ₂ O ₅ + K ₂ CO ₃	39.6	84.6	3.9	0	11.5

The compound 1 is furan-2-acrolein; the Compound 2 is ethyl furoate; the Compound 3 is 2-(diethoxymethyl) furan.

Table 1.3: Summary of the catalyst tested and the results obtained for a range of Au based catalysts

1.7 1,6 hexanediol oxidation to adipic acid

As it was already reported in the first chapter, glucaric acid could be potentially used as starting material for the production of adipic acid, well known as a monomer for the production of Nylon6,6. However, glucaric acid is not the only starting material that was taken into consideration for the synthesis of this molecule and literature reports other bio-derived building blocks, like the 1,6-hexanediol. 1,6-hexanediol (HDO) is a C6 containing two OH groups in the terminal part, a characteristic that makes it a possible monomer for the synthesis of polyester and polyurethane.¹⁰⁷ The most common synthetic route for HDO preparation involves the hydrogenation of adipic acid (made using petroleum sourcing) or its esters by various homogeneous or heterogeneous catalyst;¹⁰⁸ however, in the last years, new studies¹⁰⁸ were carried out to produce this alcohol starting from bio building blocks and this is the most promising process:

- the selective ring opening/hydrogenolysis of 2,5-tetrahydrofuran-2-methanol (synthesized from 2,5-hydroxymethylfurfural),¹⁰⁹
- the selective hydrogenolysis of intermediate tetrahydropyran-2-methanol,¹¹⁰ or its sequential dehydration/hydration/hydrogenation,¹¹¹
- hydrogenolysis of sorbitol,¹¹²

- hydrogenation of levoglucosenone ^{113,114}

Those research lines are very promising, however, nowadays the yields were still moderate (25%–40%) so it is necessary for further investigation. This possibility permits to use of the HDO as a green starting material for the production of Adipic acid (AA).

AA is usually synthesized starting from cyclohexane, from the distillation of petroleum, or the reduction of benzene; the cyclohexane passes through the first oxidation step (formation of KA oil, specifically a mixture of cyclohexanone/cyclohexanol) and the second one using an excess of nitric acid. The use of this process can be harmful to the environment leading to a huge impact on global warming. The most convenient way to upgrade AA to HDO is through a two-step process: the first consists of the AA esterification with methanol to form dimethyl adipate (DMA), then a second step is followed to hydrogenate the DMA into HDO.¹¹⁵ However, this process presents some drawbacks: distillation is required to remove water and side products to facilitate the slow and reversible esterification step. Another promising catalytic route is the oxidation of HDO with air or oxygen with a noble metal. For example, S. Ide and co-workers have tested a commercial 2.7 wt% Pt/C, which shows a yield of 85% AA in 0.35 M acetic acid at 100% conversion after 24 h of reaction at 70 °C under 10 bar O₂, using a molar substrate/metal ratio of 100.¹¹⁶ Moreover, they have tested the nature of support and metal-support interaction, by testing Pd nanoparticles supported on boron nitrate (BN), SiO₂, TiO₂ and Al₂O₃. The preparation method used was the incipient wet impregnation, a method that permits to obtain metal nanoparticles with a dimension of 1.6-1.8nm (except for BN and Al₂O₃). The reaction trend was collected in the same catalytic system, but with a different molar ratio substrate:metal (500:1 instead 100:1) at different reaction times; for all the catalysts were observed a plateau in the HDO conversion, and the hypothesis given was the possible leaching of the noble metal. However, neither the leaching of Pt into solution nor the sintering of Pt nanoparticles was significant enough to account for the observed Pt deactivation, while it was the over-oxidation of the Pt catalyst by treatment with O₂ before the reaction decreased the initial oxidation rate.¹¹⁷

As it has already been seen that the use of gold avoids the over-oxidation problem seen before. This is why Tianfu Wang et al. have preferred the use of Au/C as the preferred catalyst for testing. The catalyst was prepared by sol immobilization and an mean Au particle size of 5nm were achieved. A semi-discontinue reactor was employed and at 70°C oxidation of a 0.1M HDO in a 1M NaOH aqueous solution over Au/C catalyst gave a 97% sodium adipate yield.¹¹⁸

-
- ¹ American Chemical Society National Historic Chemical Landmarks. Rachel Carson's Silent Spring. <http://www.acs.org/content/acs/en/education/whatischemistry/landmarks/rachel-carson-silent-spring.html>
- ² R. Farrah, Origins of the EPA, *The Guardian*, **1992**
- ³ P. T. Anastas, J. C. Warner, Green Chemistry: Theory and Practice, *Oxford University Press: New York*, **1998**, 3
- ⁴ P. T. Anastas, E. S. Beach, Changing the Course of Chemistry, *ACS Symposium Series*, **2009**, 1011, 1, 1-18
- ⁵ J. B. Zimmerman, P. T. Anastas, H. C. Erythropel, W. Leitne, Designing for a green chemistry future, *Science*, **2020**, 367, 6476, 397-400
- ⁶ W.G. Glasser, S.Sarkanen, Lignin Properties and Materials, *ACS Symposium Series*, 1992, 397.
- ⁷ <https://it.wikipedia.org/wiki/Emicellulosa>
- ⁸ B. Kamm, P. Gruber, M. Kamm, Biorefineries – Industrial Processes and Products, *Weinheim: Wiley-VCH*, **2006**.
- ⁹ International Starch Institute, <http://www.starch.dk/isi/glucose/tmggluc.htm>
- ¹⁰ T. Werpy, G. Petersen, Top Value Added Chemicals from Biomass: Volume I -- Results of Screening for Potential Candidates from Sugars and Synthesis Gas, *US Department of Energy*, **2004**
- ¹¹ I. Gandarias, P. J. Miedziak, E. Nowicka, M. Douthwaite, D. J. Morgan, G. J. Hutchings, S. H. Taylor, Selective Oxidation of n-Butanol Using Gold-Palladium Supported Nanoparticles Under Base-Free Conditions, *ChemSusChem*, **2015**, 8(3), 473-480
- ¹² A. Vasudeo Rane, K. Kanny, V.K. Abitha, S. Thoma, Synthesis of Inorganic Nanomaterials, *Micro and Nano Technologies* **2018**, 121-139
- ¹³ K. Habiba, V.I. Makarov, B.R. Weiner, G. Morell, Fabrication of Nanomaterials by Pulsed Laser Synthesis, *Manufacturing Nanostructures*, **2014**, 263-92 (9).
- ¹⁴ K. J. Kim, H. G. Ahn, Complete oxidation of toluene over bimetallic Pt–Au catalysts supported on ZnO/Al₂O₃. *Applied Catalysis B: Environmental*, **2009**, 91(1-2), 308-318
- ¹⁵ K. Y. Chan, J. Ding, J. Ren, S. Cheng, K. Y. Tsang, Supported mixed metal nanoparticles as electrocatalysts in low temperature fuel cells, *J. Mater. Chem.*, **2004**, 14, 505-516
- ¹⁶ M. Signoreto, F. Menegazzo, A. Di Michele, E. Fioriniello, Effects of Support and Synthetic Procedure for Sol-Immobilized Au Nanoparticles, *Catalysts*, **2016**, 6(6), 87
- ¹⁷ L. Prati, A. Villa, Gold Catalysis, *Jenny Stanford Publishing*, **2015**
- ¹⁸ S. Ivanova, C. Petit, V. Pitchon, A new preparation method for the formation of gold nanoparticles on an oxide support, *Applied Catalysis A: General*, **2004**, 267(1-2), 191-201.
- ¹⁹ S. Ivanova, V. Pitchon, C. Petit, Application of the direct exchange method in the preparation of gold catalysts supported on different oxide materials, *Journal of Molecular Catalysis A: Chemical*, **2006**, 256(1-2), 278-283.
- ²⁰ P.C. Sercel, W.A. Saunders, H.A. Atwater, K.J. Vahala, Vapor phase synthesis of crystalline nanometer-scale GaAs clusters, *Appl. Phys. Lett.*, **1992**, 61, 696-698
- ²¹ Z. Khan, T. Singh, J. I. Hussain, A. A. Hashmi, Au (III)–CTAB reduction by ascorbic acid: Preparation and characterization of gold nanoparticles, *Colloids and Surfaces B: Biointerfaces*, **2013**, 104, 11-17
- ²² M. S. Álvarez Cerimedo, L. G. Baronio, C. E. Hoppe, M. A. Ayude, The Effect of Poly (vinylpyrrolidone)(PVP) on the Au Catalyzed Reduction of p-nitrophenol: The Fundamental Role of NaBH₄, *ChemistrySelect*, **2019**, 4(2), 608-616.

-
- ²³J. Polte, R. Erler, A. F. Thunemann, S. Sokolov, T. T. Ahner, K. Rademann, R. Kraehnert, Nucleation and growth of gold nanoparticles studied via in situ small angle X-ray scattering at millisecond time resolution, *ACS nano*, **2010**, 4(2), 1076-1082.
- ²⁴ C.E. Hoppe, M. Lazzari, I. Blanco, M.A. Lopez-Quintela, One-step synthesis of gold and silver hydrosols using poly(N-vinyl-2-pyrrolidone) as a reducing agent, *Langmuir*, **2006**, 22, 7027-7034
- ²⁵ M. Signoretto, F. Menegazzo, A. Di Michele, E. Fioriniello, Effects of Support and Synthetic Procedure for Sol-Immobilized Au Nanoparticles, *Catalysts*, **2016**, 6(6), 87
- ²⁶ C. Megías-Sayago, J. L. Santos, F. Ammari, M. Chenouf, S. Ivanova, M. A. Centeno, J. A. Odriozola, Influence of gold particle size in Au/C catalysts for base-free oxidation of glucose, *Catalysis Today*, **2018**, 306, 183-190.
- ²⁷ M. Behera, S. Ram, Spectroscopy-Based Study on the Interaction between Gold Nanoparticle and Poly(Vinylpyrrolidone) Molecules in a Non-Hydrocolloid, *Nano Letters*, **2013**, 3:17
- ²⁸ M. Signoretto, F. Menegazzo, A. Di Michele, E. Fioriniello, Effects of Support and Synthetic Procedure for Sol-Immobilized Au Nanoparticles, *Catalysts*, **2016**, 6(6), 87
- ²⁹ K. Rahme, F. Gauffre, J.-D. Marty, B. Payré, C. Mingotaud, A Systematic Study of the Stabilization in Water of Gold Nanoparticles by Poly(Ethylene Oxide)–Poly(Propylene Oxide)–Poly(Ethylene Oxide) Triblock Copolymers, *J. Phys. Chem. C*, **2007**, 111, 7273–7279
- ³⁰ A. E. Deniz, H. A. Vural, B. Ortaç, T. Uyar, Gold nanoparticle/polymer nanofibrous composites by laser ablation and electrospinning, *Mater. Lett.*, **2011**, 65, 2941–2943
- ³¹ K. M. Koczkur, S. Mourdikoudis, L. Polavarapu, S. E. Skrabalak, Polyvinylpyrrolidone (PVP) in nanoparticle synthesis, *Dalton Trans*, **2015**, 44, 17883–17905
- ³² T. Deguchi, H. Yamano, S. Takenouchi, M. Iwamoto, Enhancement of catalytic activity of Pd-PVP colloid for direct H₂O₂ synthesis from H₂ and O₂ in water with addition of 0.5 atom% Pt or Ir, *Catal. Sci. Technol.*, **2018**, 8, 1002-1015
- ³³ Glucaric Acid Market Size, Share & Trends Analysis By Product (Pure Glucaric Acid, D-Glucaric Acid-1,4-lactone), By Application (Food Ingredients, Detergents, Corrosion Inhibitors), & Segment Forecasts, 2017 – 2025, <https://www.grandviewresearch.com/industry-analysis/glucaric-acid-market>
- ³⁴ Z. Walaszek, J. Szemraj, M. Narog, Metabolism, uptake, and excretion of a D-glucaric acid salt and its potential use in cancer prevention, *Cancer Detect Prev*, **1997**;21:178–90.
- ³⁵Z. Walaszek, M. Hanausek-Walaszek, J.P. Minto, T.E. Webb, Dietary glucarate as anti-promoter of 7,12-dimethylbenz[a]anthracene-induced mammary tumorigenesis, *Carcinogenesis*, **1986**; 7, 1463–6.
- ³⁶ Glucaric Acid Market Size, Share & Trends Analysis By Product (Pure Glucaric Acid, D-Glucaric Acid-1,4-lactone), By Application (Food Ingredients, Detergents, Corrosion Inhibitors), & Segment Forecasts, 2017 - 2025
- ³⁷ O. Sohst, B. Tollens, Über krystallisirte Zuckersäure (Zuckerlactonsäure), *Ann.* **1888**, 245, 1–27.
- ³⁸ <https://www.soci.org/chemistry-and-industry/cni-data/2011/4/building-block-for-change>
- ³⁹ N. Merbouh, J. F. Thaburet, M., Ibert, , F. Marsais, J. M. Bobbitt, Facile nitroxide-mediated oxidations of D-glucose to D-glucaric acid. *Carbohydrate research*, **2001**, 336(1), 75-78
- ⁴⁰ T. S. Moon, S. H. Yoon, A. M. Lanza, J. D. Roy-Mayhew, K. L. J. Prather, Production of glucaric acid from a synthetic pathway in recombinant Escherichia coli, *Appl. Environ. Microbiol.*, **2009**, 75(3), 589-595.

-
- ⁴¹ H.H. Su, Z.W. Guo, X.L. Wu, P. Xu, N. Li, M.H. Zong, W.Y. Lou, Efficient Bioconversion of Sucrose to High-Value-Added Glucaric Acid by In Vitro Metabolic Engineering, *ChemSusChem*, **2019**, 12(10), 2278-2285
- ⁴² R. Ferrando, J. Jellinek, R. L. Johnston, Nanoalloys: from theory to applications of alloy clusters and nanoparticles, *Chem. Rev.*, **2008**, 108, 845–910.
- ⁴³ I. V. Delidovich, O. P. Taran, L. G. Matvienko, A. N. Simonov, I. L. Simakova, A. N. Bobrovskaya, V. N. Parmon, Selective oxidation of glucose over carbon supported Pd and Pt catalysts, *Catalysis Letters*, **2010**, 140(1-2), 14-21.
- ⁴⁴ X. Liang, , L. B. Lyon, , Y. B. Jiang, , A. W. Weimer, Scalable synthesis of palladium nanoparticle catalysts by atomic layer deposition, *Journal of Nanoparticle Research*, **2012**, 14(6), 943.
- ⁴⁵ T. Haynes, V. Dubois, S. Hermans, Particle size effect in glucose oxidation with Pd/CB catalysts, *Applied Catalysis A: General*, **2017**, 542, 47-54.
- ⁴⁶ J. Zhang, Z. Li, J. Huang, C. Liu, F. Hong, K. Zheng, G. Li, Size dependence of gold clusters with precise numbers of atoms in aerobic oxidation of d-glucose, *Nanoscale*, **2017**, 9(43), 16879-16886.
- ⁴⁷ C. Liu, J. Zhang, J. Huang, C. Zhang, F. Hong, Y. Zhou, M. Haruta, Efficient Aerobic Oxidation of Glucose to Gluconic Acid over Activated Carbon-Supported Gold Clusters, *ChemSusChem*, **2017**, 10(9), 1976-1980.
- ⁴⁸ R. Wojcieszak, I. M. Cuccovia, M. A. Silva, Rossi, Selective oxidation of glucose to glucuronic acid by cesium-promoted gold nanoparticle catalyst, *Journal of Molecular Catalysis A: Chemical*, **2016**, 422, 35-42.
- ⁴⁹ C. Megías-Sayago, L. F. Bobadilla, S. Ivanova, A. Penkova, M. A Centeno, J. A Odriozola, Gold catalyst recycling study in base-free glucose oxidation reaction. *Catalysis Today*, **2018**, 301, 72-77.
- ⁵⁰ X. Zhang, H. Shi, Q. Chi, X. Liu, L. Chen, Cellulose-supported Pd nanoparticles: effective for the selective oxidation of glucose into gluconic acid, *Polymer Bulletin*, **2020**, 77(2), 1003-1014.
- ⁵⁰ R. Saliger, N. Decker, U. Prüße, D-Glucose oxidation with H₂O₂ on an Au/Al₂O₃ catalyst. *Applied Catalysis B: Environmental*, **2011**, 102(3-4), 584-589.
- ⁵⁰ P. Qi, S. Chen, J. Chen, J. Zheng, X. Zheng, Y. Yuan, Catalysis and reactivation of ordered mesoporous carbon-supported gold nanoparticles for the base-free oxidation of glucose to gluconic acid, *ACS Catalysis*, **2015**, 5(4), 2659-2670.
- ⁵¹ J. Lee, B. Saha, D. G. Vlachos, Pt catalysts for efficient aerobic oxidation of glucose to glucaric acid in water, *Green Chemistry*, **2016**, 18(13), 3815-3822
- ⁵² S. Solmi, C. Morreale, F. Ospitali, S. Agnoli, F. Cavani, Oxidation of d-Glucose to Glucaric Acid Using Au/C Catalysts, *ChemCatChem*, **2017**, 9(14), 2797-2806
- ⁵³ M. Comotti, C. Della Pina, E. Falletta, M. Rossi, Aerobic oxidation of glucose with gold catalyst: hydrogen peroxide as intermediate and reagent, *Advanced Synthesis & Catalysis*, **2006**, 348(3), 313-316.
- ⁵⁴ R. Saliger, N. Decker, U. Prüße, D-Glucose oxidation with H₂O₂ on an Au/Al₂O₃ catalyst, *Applied Catalysis B: Environmental*, **2011**, 102(3-4), 584-589.
- ⁵⁵ P. Qi, S. Chen, J. Chen, J. Zheng, X. Zheng, Y. Yuan, Catalysis and reactivation of ordered mesoporous carbon-supported gold nanoparticles for the base-free oxidation of glucose to gluconic acid, *ACS Catalysis*, **2015**, 5(4), 2659-2670.
- ⁵⁶ C. Megías-Sayago, J. L. Santos, F. Ammari, M. Chenouf, S. Ivanova, M. A Centeno, J. A Odriozola, Influence of gold particle size in Au/C catalysts for base-free oxidation of glucose, *Catalysis Today*, **2018**, 306, 183-190

-
- ⁵⁷ E. Menumero, R. A. Hughes, S. Neretina, Catalytic reduction of 4-nitrophenol: a quantitative assessment of the role of dissolved oxygen in determining the induction time, *Nano Lett.*, **2016**, 16, 7791–7797.
- ⁵⁸ H. Yin, Y. Zhou, S. Ai, X. Liu, L. Zhu, L. Lu, Electrochemical oxidative determination of 4-nitrophenol based on a glassy carbon electrode modified with a hydroxyapatite nanopowder, *Microchim. Acta*, **2010**, 169, 87-92
- ⁵⁹ M. Castillo, R. Domingues, M.F. Alpendurada, D. Barcelo, Persistence of selected pesticides and their phenolic transformation products in natural waters using off-line liquid solid extraction followed by liquid chromatographic techniques, *Anal. Chim. Acta*, **1997**, 353, 133-142
- ⁶⁰ P. Zhao, X. Feng, D. Huang, G. Yang, D. Astruc, Basic concepts and recent advances in nitrophenol reduction by gold- and other transition metal nanoparticles, *Coordination Chemistry Reviews*, **2015**, 287, 114–136
- ⁶¹ C. Jouannin, I. Dez, A.C. Gaumont, J.M. Taulemesse, T. Vincentand, E. Guibal, Palladium supported on alginate/ionic liquid highly porous monoliths: Application to 4-nitroaniline hydrogenation, *Appl. Catal. B*, **2011**, 103, 444
- ⁶² A.R. Siamaki, A.E.R.S. Khder, V. Abdelsayed, M.S. El-Shall, B.-F. Gupton, Microwave-assisted synthesis of palladium nanoparticles supported on graphene: A highly active and recyclable catalyst for carbon–carbon cross-coupling reactions, *J. Catal.*, **2011**, 279, 1.
- ⁶³ M.H. Liu, J. Zhang, J.Q. Liu, W.W. Yu, Synthesis of PVP-stabilized Pt/Ru colloidal nanoparticles by ethanol reduction and their catalytic properties for selective hydrogenation of ortho-chloronitrobenzene, *J. Catal.*, **2011**, 278, 1.
- ⁶⁴ H.J. Huang, H.Q. Chen, D.P. Sun, X. Wang, Graphene nanoplate-Pt composite as a high performance electrocatalyst for direct methanol fuel cells, *J. Power Sources*, **2012**, 204, 46.
- ⁶⁵ P. Dauthal, M. Mukhopadhyay, Prunus domestica Fruit Extract-Mediated Synthesis of Gold Nanoparticles and Its Catalytic Activity for 4-Nitrophenol Reduction, *Ind. Eng. Chem. Res.*, **2012**, 51, 13014
- ⁶⁶ J. Sun, Y. Fu, G. He, X. Sun, X. Wang, Catalytic hydrogenation of nitrophenols and nitrotoluenes over a palladium/graphene nanocomposite, *Catal. Sci. Technol.*, **2014**, 4, 1742
- ⁶⁷ H. Rodríguez Molina, J.L. Santos Muñoz, M.I. Domínguez Leal, T.R. Reina, S. Ivanova, M.Á. Centeno Gallego, J.A. Odriozola, Carbon Supported Gold Nanoparticles for the Catalytic Reduction of 4-Nitrophenol, *Front. Chem*, **2019**, 7:548
- ⁶⁸ S. Wunder, F. Polzer, Y. Lu, Y. Mei, M. Ballauff, Kinetic Analysis of Catalytic Reduction of 4-Nitrophenol by Metallic Nanoparticles Immobilized in Spherical Polyelectrolyte Brushes, *J. Phys. Chem. C*, **2010**, 114, 8814.
- ⁶⁹ T. Ma, W. Yang, S. Liu, H. Zhang, F. Liang, A Comparison Reduction of 4-Nitrophenol by Gold Nanospheres and Gold Nanostars, *Catalysts*, **2017**, 7, 38
- ⁷⁰ S. M. Ansar, C. L. Kitchens, Impact of Gold Nanoparticle Stabilizing Ligands on the Colloidal Catalytic Reduction of 4-Nitrophenol, *ACS Catal*, **2016**, 6, 5553–5560
- ⁷¹ P. T. Anastas, J. C. Warner, Green Chemistry: Theory and Practice, *Oxford University Press: New York*, **1998**, p.3
- ⁷² J. Lewkowski, Synthesis, chemistry and applications of 5-hydroxymethyl-furfural and its derivatives, **2001**
- ⁷³ J. J. Bozell, G.R. Petersen, Technology development for the production of biobased products from biorefinery carbohydrates the US Department of Energys Top 10 revisited, *Green Chemistry*, **2010**, 12(4), 539-554
- ⁷⁴ J. A. Moore, J. E. Kelly, Polyesters derived from furan and tetrahydrofuran nuclei, *Macromolecules*, **1978**, 11(3), 568-573

-
- ⁷⁵ A. F. Sousa, Biobased polyesters and other polymers from 2, 5-furandicarboxylic acid: a tribute to furan excellency, *Polym. Chem*, **2015**, 6(33), 5961-5983.
- ⁷⁶ J. Deng, Synthesis and properties of a bio-based epoxy resin from 2, 5-furandicarboxylic acid (FDCA), *Royal Society of Chemistry Advances*, **2015**, 5(21), 15930-15939
- ⁷⁷ H. Wang, Crystalline Capsules: Metal Organic Frameworks Locked by Size Matching Ligand Bolts, *Angewandte Chemie*, **2015**, 54(20), 5966-5970
- ⁷⁸ W. Partenheimer, Grushin, V. Vladimir, Synthesis of 2,5-Diformylfuran and Furan-2,5-Dicarboxylic Acid by Catalytic Air-Oxidation of 5-Hydroxymethylfurfural. Unexpectedly Selective Aerobic Oxidation of Benzyl Alcohol to Benzaldehyde with Metal Bromide Catalysts, *Advanced Synthesis & Catalysis*, **2001**, 343 (1), 102-111
- ⁷⁹ H. H. Li, Three luminescent metal organic frameworks constructed from trinuclear zinc (ii) clusters and furan-2, 5-dicarboxylate, *CrystEngComm*, **2015**, 17(27), 5101-5109
- ⁸⁰ M. Lomelí-Rodríguez, J. R. Corpas-Martínez, S. Willis, R. Mulholland, J. A. Lopez-Sanchez, *Polymers*, **2018**, 10, 600
- ⁸¹ M. Besson, P. Gallezot, Fine Chemicals through Heterogeneous Catalysis, *Wiley-VCH*, **2001**, 491–518
- ⁸² H. Ban, Y. Zhang, S. Chen, Y. Cheng, T. Pan, L. Wang, X. Li, Production of 2,5-Furandicarboxylic Acid by Optimization of Oxidation of 5-Methyl Furfural over Homogeneous Co/Mn/Br Catalysts, *ACS Sustainable Chemistry & Engineering*, **2020**, 8 (21), 8011-8023
- ⁸³ Y.T. Huang, J.J. Wong, C.J. Huang, C.L. Li, G.W. B Jang, 2,5-Furandicarboxylic Acid Synthesis and Use. In Chemicals and Fuels from Bio-Based Building Blocks, *Wiley-VCH Verlag GmbH & Co. KGaA*, **2016**, 191-216
- ⁸⁴ W. Partenheimer, Grushin, V. Vladimir, Synthesis of 2,5-Diformylfuran and Furan-2,5-Dicarboxylic Acid by Catalytic Air-Oxidation of 5-Hydroxymethylfurfural. Unexpectedly Selective Aerobic Oxidation of Benzyl Alcohol to Benzaldehyde with Metal=Bromide Catalysts, *Advanced Synthesis & Catalysis*, **2001**, 343 (1), 102-111
- ⁸⁵ Z. Zhang, G. W. Huber, Catalytic oxidation of carbohydrates into organic acids and furan chemicals, *Chemical Society Reviews*, **2018**, 47 (4), 1351-1390
- ⁸⁶ S. E. Davis, B. N. Zope, R. J. Davis, On the mechanism of selective oxidation of 5-hydroxymethylfurfural to 2,5-furandicarboxylic acid over supported Pt and Au catalysts, *Green Chem*, **2012**, 14, 143-14
- ⁸⁷ O. Casanova, S. Iborra, A. Corma, Biomass into chemicals: aerobic oxidation of 5-hydroxymethyl-2-furfural into 2,5-furandicarboxylic acid with gold nanoparticle catalysts, *ChemSusChem*, **2009**, 2, 1138
- ⁸⁸ B. N. Zope, S. E. Davis, R. J. Davis, Influence of Reaction Conditions on Diacid Formation During Au-Catalyzed Oxidation of Glycerol and Hydroxymethylfurfural, *Top. Catal.*, **2012**, 55, 24–32.
- ⁸⁹ C. Ferraz, M. Zielinski, M. Pietrowski, S. Heyte, F. Dumeignil, L. M. Rossi, R. Wojcieszak, Influence of Support Basic Sites in Green Oxidation of Biobased Substrates Using Au-Promoted Catalysts, *ACS Sustainable Chem. Eng.*, **2018**, 6, 16332–16340
- ⁹⁰ A. Takagaki, S. Nishimura, K. Ebitani, Catalytic Transformations of Biomass-Derived Materials into Value-Added Chemicals. *Catalysis Surveys from Asia*, **2012**, 16(3), 164-182.
- ⁹¹ L. Brown, D. Watson, Curing Phenol-Furfural Resins, *Ind. Eng. Chem*, **1959**, 51, 5, 683–684
- ⁹² B. Seemala, S. Darbha, Catalytic conversion of furfural to industrial chemicals over supported Pt and Pd catalysts, *Journal of Catalysis*, **2015**, 327, 65-77

-
- ⁹³ K. Anil, M. Amith, A. K. Kumar, M. Rajeev, K. Sukumaran, Chapter 9 - Lignocellulosic Biorefinery Wastes, or Resources? Waste Biorefinery Potential and Perspectives, **2018**, 267-297
- ⁹⁴ G. Burdock, P-Z indexes, *Encyclopedia of Food and Color Additives*. 3. Bob Stern. ,**1996**, 2359.
- ⁹⁵ B. Uma, S. Jerome Das, S. Krishnan, B. Milton Boaz, Growth, optical and thermal studies on organic nonlinear optical crystal: 2-Furoic acid, *Physica B: Condensed Matter*, **2011**, 406 (14): 2834–2839
- ⁹⁶ B. Uma, K. Sakthi Murugesan, S. Krishnan, S. Jerome Das, B. Milton Boaz, Optical and dielectric studies on organic nonlinear optical 2-furoic acid single crystals, *Optik: International Journal for Light and Electron Optics*, **2013**, 124 (17): 2754–2757.
- ⁹⁷ Q. Y. Tian, D. X. Shi, Y. W. Sha, CuO and Ag₂O/CuO Catalyzed Oxidation of Aldehydes to the Corresponding Carboxylic Acids by Molecular Oxygen, *Molecules*, **2008**, 13,948–957.
- ⁹⁸ M. Douthwaite, X. Huang, S. Iqbal, P. J. Miedziak, G. L. Brett, S. A. Kondrat, J. K. Edwards, M. Sankar, D. W. Knight, D. Bethell, G. J. Hutchings, The controlled catalytic oxidation of furfural to furoic acid using AuPd/Mg(OH)₂, *Catal. Sci. Technol.*, **2017**, 7, 5284–5293
- ⁹⁹ L. Yu, S. Liao, L. Ning, S. Xue, Z. Liu and X. Tong, Sustainable and cost-effective protocol for cascade oxidative condensation of furfural with aliphatic alcohols, *ACS Sustainable Chem. Eng.*, **2016**, 4, 1894–1898
- ¹⁰⁰ X. Tong, Z. Liu, J. Hu, S. Liao, Au-catalyzed oxidative condensation of renewable furfural and ethanol to produce furan-2-acrolein in the presence of molecular oxygen, *Appl. Catal., A*, **2016**, 510,196–203.
- ¹⁰¹ M. Douthwaite, X. Huang, S. Iqbal, P. J. Miedziak, G. L. Brett, S. A. Kondrat, J. K. Edwards, M. Sankar, D. W. Knight, D. Bethell, G. J. Hutchings, The controlled catalytic oxidation of furfural to furoic acid using AuPd/Mg(OH)₂, *Catal. Sci. Technol.*,**2017**, 7, 5284–5293
- ¹⁰² M. Manzoli, F. Menegazzo, M. Signoretto, D. Marchese, Biomass Derived Chemicals: Furfural Oxidative Esterification to Methyl-2-furoate over Gold Catalysts, *Catalysts*, **2016**, 6, 107
- ¹⁰³ C. Ampelli, G. Centi, C. Genovese, G. Papanikolaou, R. Pizzi, S. Perathoner, R.-J. van Putten, K. J. P. Schouten, A. C. Gluhoi, J. C. van der Waal, A Comparative Catalyst Evaluation for the Selective Oxidative Esterification of Furfural, *Top Catal* ,**2016**, 59:1659–1667
- ¹⁰⁴ C. P. Ferraz, A. H. Braga, M. N. Ghazzal, M. Zielinski, M. Pietrowski, I. Itabaiana Jr. , F. Dumeignil, L. M. Rossi, R. Wojcieszak, Efficient Oxidative Esterification of Furfural Using Au Nanoparticles Supported on Group 2 Alkaline Earth Metal Oxides, *Catalysts*, **2020**, 10, 430
- ¹⁰⁵ X. Tong, Z. Liu, L. Yu, Y. Li, A tunable process: catalytic transformation of renewable furfural with aliphatic alcohols in the presence of molecular oxygen, *Chem. Commun.*, **2015**, 51, 3674–3677
- ¹⁰⁶ X. Tong, Z. Liu, J. Hu, S. Liao, Au-catalyzed oxidative condensation of renewable furfural and ethanol to produce furan-2-acrolein in the presence of molecular oxygen, *Appl. Catal., A*, **2016**, 510, 196–203
- ¹⁰⁷ <https://www.researchandmarkets.com/reports/4791416/16-hexanediol-market-by-application>
- ¹⁰⁸ T.N. Smith, K.R. Hash, Modifications in the nitric acid oxidation of D-glucose, *Carbohydr. Res.*, **2012**, 350, 6–13.
- ¹⁰⁹ J.G. DeVries, T. Buntara, P. Huat Phua I.V. Melian-Cabrera, H.J. Heeres, Preparation of caprolactone, caprolactam, 2,5-tetrahydrofuran-dimethanol, 1,6-hexanediol or 1,2,6-hexanetriol from 5-hydroxymethyl-2-furfuraldehyde, *WO Pat.2011/149339 to NOW*, **2011**.

-
- ¹¹⁰ K. Chen, S. Koso, T. Kubota, Y. Nakagawa, K. Tomishige, Chemoselective Hydrogenolysis of Tetrahydropyran-2-methanol to 1,6-Hexanediol over Rhenium-Modified Carbon-Supported Rhodium Catalysts, *ChemCatChem* **2**, **2010**, 547–555.
- ¹¹¹ S.P. Burt, K.J. Barnett, D.J. McClelland, P. Wolf, J.A. Dumesic, G.W. Huber, I. Hermans, Production of 1,6-hexanediol from tetrahydropyran-2-methanol by dehydration–hydration and hydrogenation, *Green Chem.*, **2017**, *19*, 1390–1398.
- ¹¹² A. Said, D. Da Silva Perez, N. Perret, C. Pinel, M. Besson, Selective C–O Hydrogenolysis of Erythritol over Supported Rh-ReOx Catalysts in the Aqueous Phase, *ChemCatChem*, **2017**, *9*, 2768–2783.
- ¹¹³ A. Allgeier, N. Desilva, E. Korovessi, C. Menning, J.C. Ritter, S.K. Sengupta, Process for preparing 1,6-hexanediol, *WO Pat. 2013/101980*, to *E.I. Du Pont de Nemours and Company*, **2013**.
- ¹¹⁴ S.H. Krishna, D.J. McClelland, Q.A. Rashke, J.A. Dumesic, G.W. Huber, Hydrogenation of levoglucosenone to renewable chemicals, *Green Chem.*, **2017**, *19*, 1278–1285.
- ¹¹⁵ S. M. D. Santos, Hydrogenation of dimethyl adipate over bimetallic catalysts, *Catalysis Communications*, **2004**, *5* 377-381.
- ¹¹⁶ M.S. Ide, R.J. Davis, Perspectives on the kinetics of diol oxidation over supported platinum catalysts in aqueous solution, *J. Catal.*, **2013**, *308*, 50–59.
- ¹¹⁷ M. S. Ide, D. D. Falcone, R. J. Davis, On the deactivation of supported platinum catalysts for selective oxidation of alcohols, *J. Catal.*, **2014**, *311*, 295–305
- ¹¹⁸ T. Wang, M.S. Ide, M.R. Nolan, R.J. Davis, B.H. Shanks, Renewable Production of Nylon-6, 6 Monomers from Biomass-Derived 5-Hydroxymethylfurfural (HMF), *Energy Environ. Focus*, **2016**, *5*, 13-17

2 Chapter 2-Scope

The objectives and goals of the present work are to investigate the influence of stabilizers in colloidal methods like the sol-immobilization method for the synthesis of preformed Au colloidal nanoparticles and the immobilization of the synthesized Au colloidal nanoparticles on supports, for example on activated carbon. By varying the nature of stabilizer and the weight ratio of stabilizer to metal, a number of Au based catalysts were prepared and the catalytic performance of the synthesized catalysts was tested for a range of model reactions. Moreover, a characterization of the fresh catalysts was carried out by means of a number of methods and analytical techniques. In particular, in this work it was decided to study and compare three different stabilizing agents:

- Polyvinylpyrrolidone (PVP): This polymer contains lactam groups, characteristics that permit a good interaction between the Au and the polymer used (good interaction Au-O). It acts like a steric stabilizer, which means that it is a polymer that adsorbs on the particle surface, providing a protecting layer. Moreover, the N atom contained in the lactam group can interact with Au, donating electrons to the noble metal.
- Polyethylene glycol (PEG): as the PVP, the PEG acts as a steric stabilizer thanks to the O group contained in the polymer chain. However, the different structure allow it to assembly in a different configuration.
- Polyvinyl alcohol (PVA): the OH groups present on the chain make become this polymer a steric stabilizer with an additional weak electrostatic stabilization contribution, because of its polar head group and able to create an electric double layer and a lipophilic chain that provides the steric repulsion.

To determine the final morphology of the unsupported and supported metal nanoparticles, several characterization techniques were used UV-Vis, XRD, TEM, and XPS. We focused to determine the mean particle and crystallite size of Au, the particle size distribution, the oxidation state of the Au, and the surface coverage of Au onto the support for the fresh and some of the used catalysts.

The application of these materials could have considerable importance in the green chemistry field and for this reason, the catalytic performance of the synthesized catalysts for a range of important catalytic reactions was studied. The following reactions were chosen as model reactions:

- ▒ *Glucaric acid synthesis by glucose catalytic oxidation at mild reaction conditions*: starting from the most spread-out monosaccharide present in nature, it can be possible to produce glucaric acid, a promising starting material for the production of detergent, additive or plastic monomer.
- ▒ *5-(hydroxymethyl)furfural catalytic oxidation for the production of 2,5-Furandicarboxylic acid*: this latest molecule cover and important role in the sustainable industry, because it is considered the green substitute to the terephthalic acid in the production of PET.
- ▒ *Catalytic oxidation of 1,6 hexanediol to adipic acid*: the use of this diol allow to synthesize one of the nylon monomers from renovable resource and not from petroleum.
- ▒ *Catalytic furfural oxidative condensation and oxidative esterification*: both reactions lead to the formation of interesting products used as fragrances and food additives.
- ▒ *4-Nitrophenol catalytic reduction to 4-aminophenol*: this process plays a key role in the water treatment, due to the toxicity of the reagent used as a pesticide.

The glucose oxidation was the main reaction investigated in the following work and it was carried out in the research group of the University of Bologna; 4-Nitrophenol catalytic reduction and 5-(hydroxymethyl)furfural catalytic oxidation were carried out in the same research group to see the effectiveness of the catalyst prepared and to compare the catalytic performance obtained with the glucose oxidation. Instead, the catalytic furfural oxidative condensation and oxidative esterification were investigated during a period abroad spent at the University of Malaga, Spain, and the catalytic oxidation of 1,6 hexanediol to adipic acid was studied from a different research group of the University of Lille, France.

The comparison of these reactions helps to better understand which characteristics of the nanoparticles are more or less important and if there are common or different factors that play a fundamental role in the catalytic performance.

3 Chapter 3-Experimental section

3.1 Materials

3.1.1 Catalyst preparation

Tetra chloroauric(III) acid (Sigma Aldrich, 99.99 %), poly(vinyl alcohol) (PVA, Sigma Aldrich, MW 13 000–23 000 g mol⁻¹, hydrolysed 87–89 %), Polyvinylpyrrolidone (PVP, Sigma Aldrich, MW 29000 g mol⁻¹), Polyethylenglycole (PEG, Sigma Aldrich, MW 8000g mol⁻¹), sodium borohydride (Sigma Aldrich, powder, ≥98.0%) and activated carbon SX1G (AC, Norit) were used for catalyst preparation.

3.1.2 Glucose oxidation

D-Glucose (Alfa Aesar, > 99 %) and sodium hydroxide pellets (Sigma Aldrich) were used as reagents for catalytic tests. Gluconic acid sodium salt (Sigma Aldrich, 97 %), glucaric acid potassium salt monohydrate (Sigma Aldrich, ≥ 98 %), glyceric acid hemicalcium salt monohydrate (Sigma Aldrich, ≥ 97 %), sodium mesoxalate monohydrate (Sigma Aldrich, ≥ 98 %), oxalic acid dihydrate (Sigma Aldrich, ≥ 98 %), tartronic acid (Sigma Aldrich, ≥ 97 %), glycolic acid (Sigma Aldrich, 98 %), arabinose (Sigma Aldrich, ≥ 98 %), formic acid (Alfa Aesar, > 95 %), lactic acid (Alfa Aesar, 85 %), and D-glucose were used as reference commercial compounds for HPLC analysis.

3.1.3 4-Nitrophenol reduction

4-Nitrophenol (Sigma Aldrich, ≥99%) and sodium borohydride, (Sigma Aldrich, ≥98.0%) are the only reagents used for the reaction.

3.1.4 HMF oxidation

Hydroxymethylfurfural (HMF, AVA Biochem, 99%), NaOH pellet (Sigma Aldrich) are the reagents used for the catalytic test. For the calibration curves were used 2,5-furandicarboxylic acid (FDCA, Toronto Research Chemicals, 99.99%), 5-(hydroxymethyl)furan-2-carboxylic acid (HMFCFA, Toronto Research Chemicals, 99.99%), furan-2,5-dicarbaldehyde (DFF, Toronto Research Chemicals, 99.99%), 5-formylfuran-2-carboxylic acid (FFCA, Toronto Research Chemicals, 99.99%).

3.1.5 Furfural oxidation

Ethanol (VWR, 96%), Na₂CO₃ anhydrous (VWR, 100 %), Furfural (Sigma Aldrich,99%), o-xylene as internal standard (Aldrich, 99.9%). For the calibration curves, it was used 3-(2-furyl)acrolein (Sigma Aldrich, 99%) and ethyl-2 furoate (Sigma Aldrich, 99%).

3.1.6 1,6 Hexanediol oxidation

1,6-hexanediol (Sigma Aldrich, > 99%) and NaOH pellet (Sigma Aldrich) are the reagents used for the catalytic test. For the calibration curves, it was used adipic acid (Sigma Aldrich-bioextra, > 99.5%) and 6-hydroxyhexanoic acid (Sigma Aldrich, > 98 %).

3.2 Synthesis of the catalysts

Supported gold catalysts were prepared following four different procedures by sol immobilization technique to produce a catalyst with nominal metal loading of 1% wt. The choice of this technique was done because it allows to change of different parameters in a systematic way and tune the main characteristic of the final material.

3.2.1 Preparation Method A

For the preparation of 1 g of catalyst, 0.02 g of H₂AuCl₄·3H₂O (1.3×10^{-4} mol L⁻¹; 5.31×10^{-5} mol) were dissolved in 100 ml of distilled water (200.85 mg L⁻¹ of gold precursor – 0.51 M Au). Then, 0.643 mL of PVA solution (0.1010 g/mL) were added as a stabilizing agent (PVA: Au = 0.5:1 weight ratio). After 3 min, 0.0077 g of sodium borohydride was added to the solution under stirring (NaBH₄: Au = 4:1 molar ratio) to obtain a dark red colloidal solution. The pH of the solution was adjusted to 2 by the addition of concentrated sulfuric acid (8 drops). Three minutes later, 0.9947 g of support (activated carbon) was added to the solution to immobilize the gold nanoparticles. The immobilization was set under stirring at room temperature for 4 h. The catalyst was filtered using a büchner funnel with two filter papers. The slurry was washed with distilled water until the washing water reached pH 6-7. The solid was dried overnight in a watch glass at room temperature conditions. Then, a suspension was done with the catalyst in 20 mL of distilled water and kept at 60°C for 4 h under stirring. The catalyst was again filtered as previously and let dry overnight. Finally, the solid was dried in an oven at 80°C for 4 h. Figure 3.1 resume all the step followed.

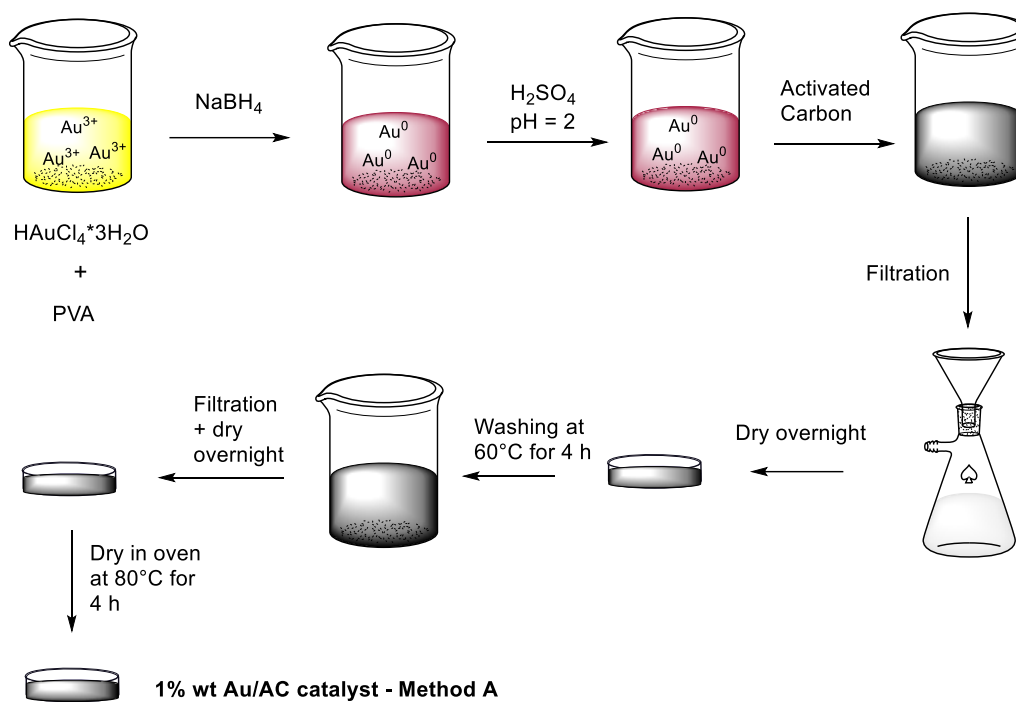


Figure 3.1: Scheme of Method A for preparation of gold-based catalyst (reference catalyst)

3.2.2 Preparation Methods B-C-D

For the preparation of 1 g of catalyst, 0.0209 g of $\text{HAuCl}_4 \cdot 3\text{H}_2\text{O}$ were dissolved in 390 mL of distilled water (53.58 mg/L of gold precursor – 1.30×10^{-4} M Au). Then, the desired volume of polyvinyl alcohol (PVA) solution (0.1010 g/mL) were added as a stabilizing agent (For the investigation of different PVA: Au weight ratio, the amount was changed as reported in Table 3.1; for the other preparation, the volume is 0.497 mL, equal to PVA: Au = 0.65:1 weight ratio). After 3 minutes, 0.0096 g of sodium borohydride dissolved in 2.5 mL of water was added to the solution under stirring (NaBH_4 : Au = 5:1 molar ratio) to obtain a red colloidal dispersion. 30 minutes later, 0.99 g of support (activated carbon) was added to the solution to immobilize the gold nanoparticles. The pH of the solution was adjusted until 2 by the addition of sulfuric acid concentrated (8 drops). The suspension was left to stirring at room temperature for 1 h. The catalyst was filtered using a büchner funnel with two filter papers. The slurry was washed with distilled water until the washing water reached pH 6-7. The solid was dried overnight in a watch glass at room temperature. From this point, Methods B, C and D changes:

For the catalyst with heat treatment (Method B, Figure 3.2): After the catalyst was heat-treated in a continuous flow reactor; the first step is a heating ramp with a rate of 5°C per minute from room temperature to Tx (120 or 200 or 250°C) in air (flow rate =20mL/min), then an isotherm step of 2 h in air. After that, the atmosphere was switched with N₂ (flow rate =20mL/min), maintaining the same temperature value for 30 minutes and finally, another isothermal step at the same temperature was kept for 1 h in H₂ atmosphere with a flow of 20 mL/min. The schematic representation of the heat treatment is reported in Figure3.3.

For the catalyst with washing treatment (Method C, Figure 3.4): A suspension was done with the catalyst in 20 ml of distilled water and kept at 60°C for 4 h under stirring. The catalyst was again filtered as previously and let dry overnight. Finally, the solid was dried in the oven at 80°C for 4 h.

For all the samples (Method D, Figure 3.5): Finally, the solid was dried in the oven at 80°C for 4 h.

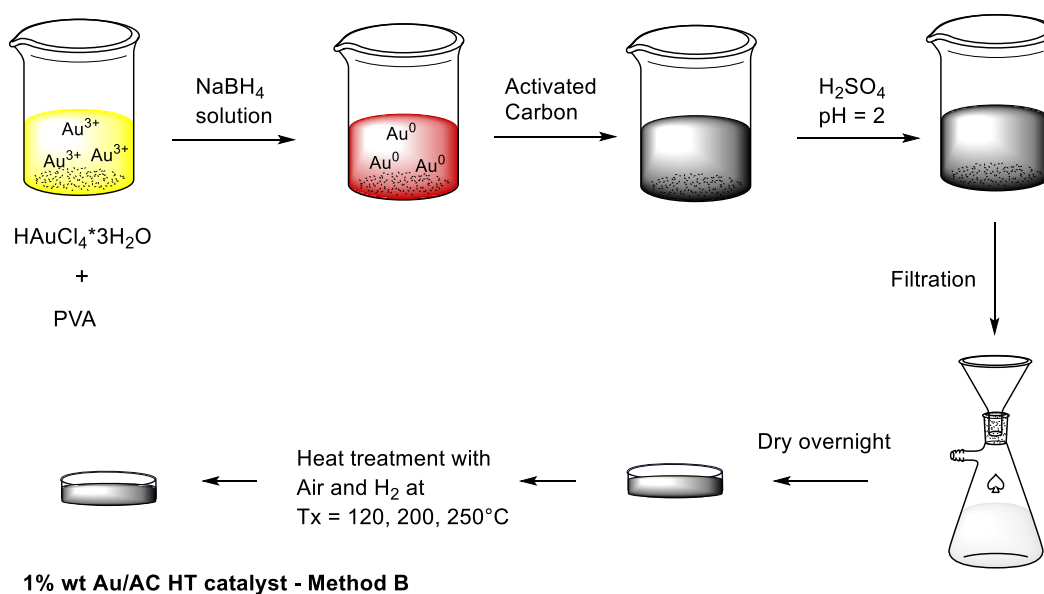


Figure3.2: Scheme of Method B for preparation of gold-based catalyst with heat treatment (120-250°C) with air/H₂

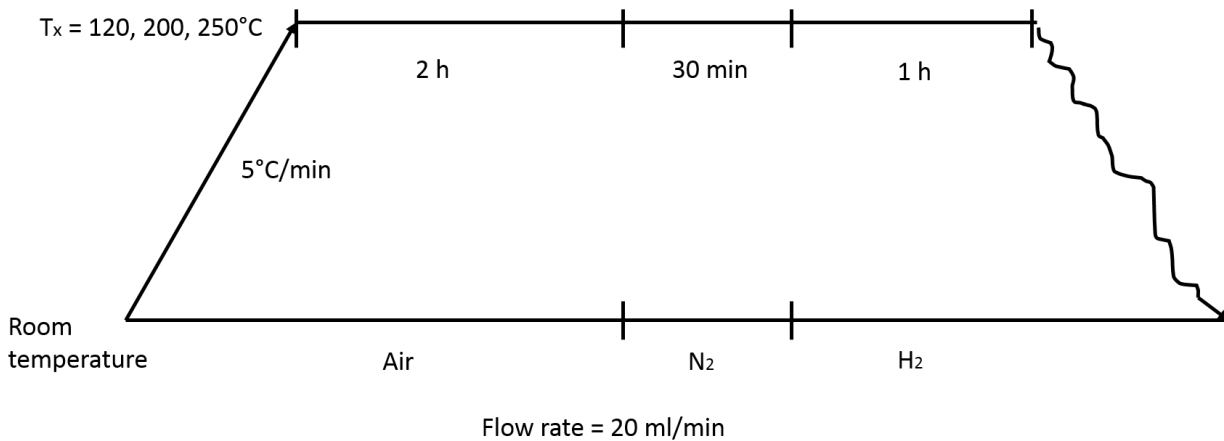


Figure 3.3: Schematic process of heat treatment of catalysts

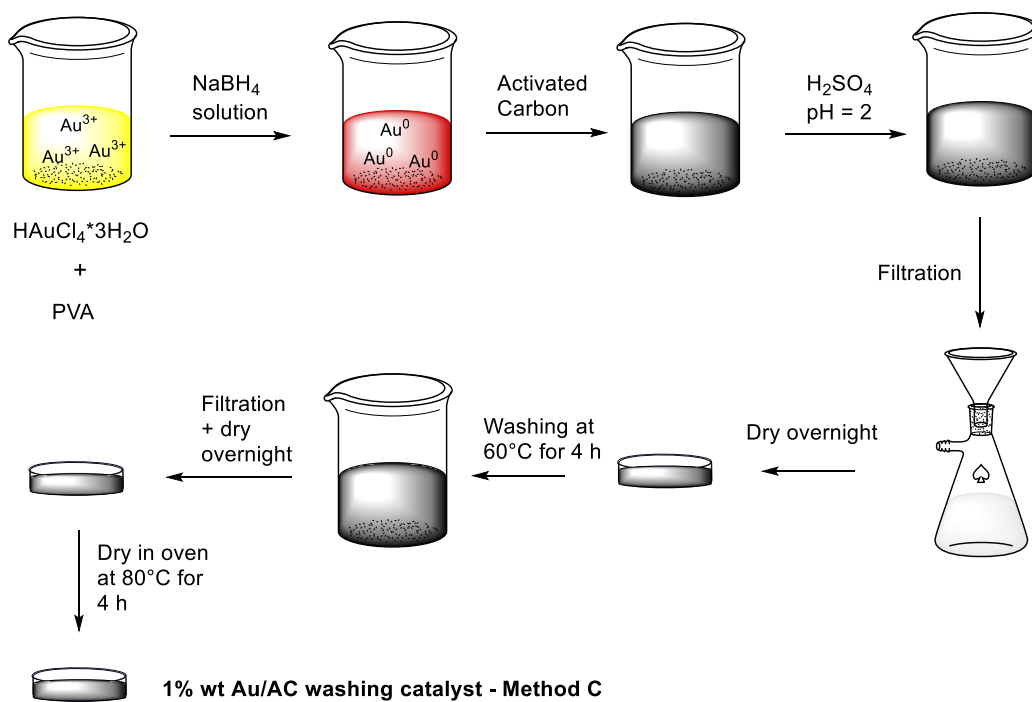


Figure 3.4: Scheme of Method B for preparation of gold-based catalyst with water washing at 60°C

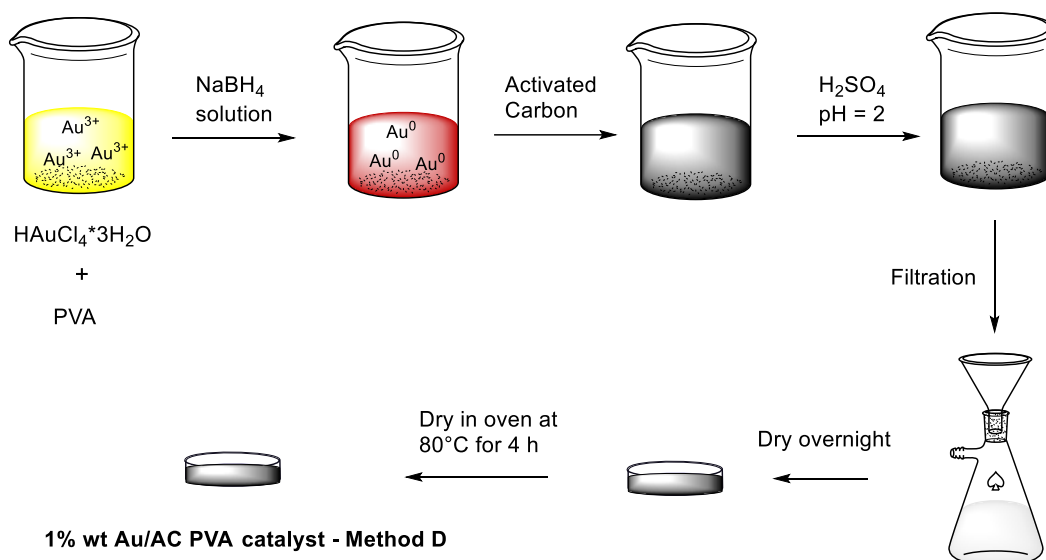


Figure 3.5: Scheme of Method B for preparation of gold-based catalyst Au/AC PVA

PVA: Au weight ratio	Volume of PVA solution 1%wt in water [mL]
0	0
0.3:1	0.29
0.6:1	0.59
1.2:1	1.19
2.4:1	2.38

Table 3.1: PVA: Au weight ratio and volume of PVA solution used

3.3 UV-VIS spectroscopy

To check the plasmon resonance peak and therefore indirectly the dimensions of the nanoparticles formed, the UV-Vis spectroscopy analysis was carried out on the colloidal solution before the immobilization step. Indeed, one of the characteristics of gold NPs is the multitude of optical and electronic properties related to surface plasmon resonance. Gold NPs display a surface plasmon resonance when the frequency of oscillating electrons present in the conduction band of the gold resonates with the frequency of incoming light radiation resulting in a plasmon band that can be observed in the UV-VIS-NIR. This special feature helps in the indirect characterization of the size and shape of nanoparticles. However, this technique permits us to estimate a range in

nanoparticles size: because the immobilization step could influence the final dimension, TEM analysis is the technique used to determine the final particle size/shape and particle size distribution. To carry on the UV analysis, 3 mL ca. of the solution was collected at different times during the preparation method: the first sample collected was the precursor solution, the second samples were the colloidal solution straight after the NaBH_4 and the third sample was after the addition and duration of 25 minutes of stirring. The spectrometer was used to observe the plasmon resonance peak related to the metallic gold nanoparticles and this was done using a Perkin Elmer UV-VIS-NIR Lambda 19 (Figure 3.6) from 750 nm to 190 nm wavelength.



Figure 3.6: UV-VIS Spectrometer Perkin Elmer UV-VIS-NIR Lambda 19

3.4 XRD

X-ray diffraction is a technique that allows to obtain information regarding the crystalline phase, crystallite size, etc. More in specific, electrons in the sample vibrate under the electric field generated by the X-ray beam and, consequently they backscatter a beam with the same wavelength as the incident beam. If these waves are in phase with each other to have constructive interference and in this way, it could be applied Bragg's law. In particular, knowing the conditions needed for diffraction, it could be possible to calculate the planes in crystal lattice and therefore, obtain the crystallographic structure, lattice distance.

$$n\lambda = 2d \sin\theta$$

n = integer (diffraction order)

λ = wavelength of the x-rays

d = distance between adjacent planes in the lattice

θ = incident angle of the x-ray beam

XRD analysis was performed with a Bragg-Brentano X'pertPro Panalytical diffractometer (Figure 3.7) using a copper anode ($K\alpha$ radiation at $\lambda = 1.5418 \text{ \AA}$) as the source of X radiation with 0.08° step size and acquisition time of 1300 s per step in $36 - 41^\circ 2\theta$ range. All the XRD analysis were performed on powder samples.



Figure 3.7: Images of Bragg-Brentano X'pert Pro Panalytical diffractometer

This instrument was employed for the calculation of the mean gold crystallite size of Au/AC catalysts; more precisely, it was applied the Scherrer's equation for the Au peak at $38.28^\circ 2\theta$, corresponding to the (111) Au plane. The Scherrer's equation correlates the signal width with the dimension of the crystal through the following mathematical formula:

$$FWHM(2\theta) = \frac{K \lambda}{L \cos\theta}$$

FWHM = Full Width Half Maximum

λ = wavelength

L = crystallite size

K = the Scherrer constant

3.5 TEM

Transmission electron microscopy is an analytical technique used for the characterization of surfaces obtained by the transmission of electrons through a sample. The electrons can be created from a tungsten filament and then, accelerated by an electric potential (100-300 keV), collimated and finally focused on the sample thanks to the use of special lenses. The technique requires the use of vacuum conditions. It was observed that the generated electrons interact with the surface of the sample and a part of them is transmitted without undergoing interaction with the sample. This fraction of electrons is captured by a fluorescent screen on which is obtained an enlarged image of the sample. TEM analyses were performed to evaluate the size and the distribution of the Au nanoparticles presence on the catalyst. It was carried out using a TEM/STEM FEI TECNAI F20 microscope operating at 200 keV. Samples were prepared by suspending in ethanol and treated by ultrasound for 15 min. A drop of the suspension was deposited on "quantifoil-carbon film" supported by a grid of Cu. The preparation was dried at 120°C and analyzed. In order to determinate the nanoparticles average size and the distribution, for each sample it was measured the diameter of a minimum of 400 nanoparticles.

3.6 X-ray photoelectron spectroscopy (XPS)

From the XPS technique, information on the surface chemical composition and oxidation states of the elements can be obtained, both in conductive and insulating materials. This analytical technique is based on the irradiation with high energy photons on the surface of the sample. The radiation energy is higher than the bonding of the electrons in the atoms and this is why sample electrons leave it with a kinetic energy that is equal to the excess energy of the photon concerning the binding energy. In this way, it is possible to identify the atoms present on the surface and to quantify them thanks to the proportionality between the atomic intensity and the intensity measured by XPS.

The XPS spectra were recorded with a Physical Electronic PHI 5700 spectrometer (Figure 3.8), fitted with an Electronics 80-365B multi-channel hemispherical electron analyzer and an X-ray excitation source of Al K α 1486.6 eV. High-resolution spectra were recorded using a concentric hemispherical analyzer with a constant energy step of 29.35 eV, irradiating an analysis area of 100 μm in diameter. On the other hand, the binding energy was determined with a precision of ± 0.4 eV, using as reference the C 1s signal of the adventitious carbon at 284.8 eV. The pressure in the analysis chamber was kept below 5-10 Pa. The PHI ACCESS ESCA-F V6 software was used for the acquisition of analysis data. A Shirley-type background was subtracted from the signals. The spectra that were recorded were analyzed with Gauss-Lorentz type curves, to determine with greater precision, the binding energy of the atomic levels of the different elements.

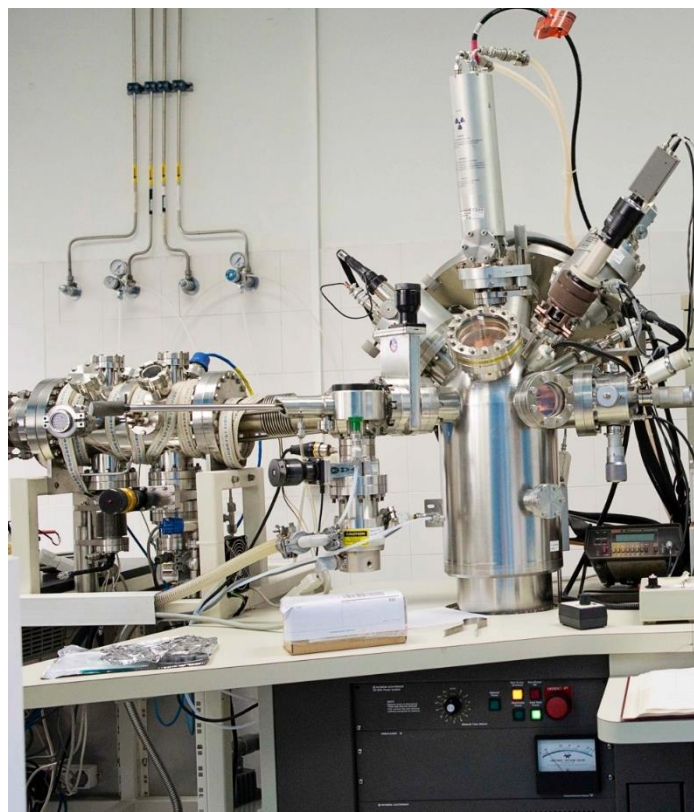


Figure 3.8: XPS instrument- System PHI Model 5700

3.7 Analytical procedures and protocols

3.7.1 Glucose oxidation

The oxidation reaction experiments were performed in an autoclave batch reactor of 50 mL capacity (Figure 3.9). The reactor consists of a stainless-steel vessel connected to the top cover via a flanged joint. The reactor has coupled a pressure gauge, a steel capillary for the introduction of a thermocouple (the thermocouple is not in direct contact with the solution inside the reactor), an inlet pipeline, and an outline pipeline, both controlled by an interception valve. The autoclave has also a reversible security valve (relief valve) which was set to 40 bar to ensure the safety of the reaction. To control the temperature and the stirring rate, the reactor is set on a heating and magnetic stirring plate and a second thermocouple to indicate the real temperature inside the reactor.



Figure 3.9: Batch reactor system used for the glucose oxidation reaction

The experimental procedure of the catalytic test consists of the following steps: a reaction solution is prepared by measuring 0.7895 g of glucose dissolved in 15 mL of distilled water to obtain an aqueous solution of 5% wt of glucose (0.29 M glucose). Then, 0.5263 g (0.01315 mol) of sodium hydroxide was added to obtain a molar ratio Glu:NaOH of 1:3; and the desired amount catalyst was added. After adding the reagents and catalyst to the vessel, a magnetic stirrer bar was introduced to maintain the solution under stirring. The vessel was tightly closed and the autoclave was purged with O₂ (three times); then gaseous oxygen (as oxidant agent) was introduced (10bar). The reactor was placed in contact with a heating mantle that allows it to reach the set-point temperature (60°C) through feedback heating control with the thermocouple. The magnetic stirrer was switched on to guarantee the diffusion and homogeneity of the reagents. Once the solution had reached 60°C, the solution reaction was kept under these experimental conditions. At the end of the reaction time, the reactor mixture was cooled down by placing it on an ice bath for 10 minutes to quench the reaction. The reaction mixture was collected and centrifuged at 4500 rpm for 15 min to separate the liquid from the catalyst. The final volume was measured with a cylinder and a sample was taken for subsequent analysis and storage. The catalyst was left to dry at ambient conditions overnight. To identify and quantify all the chemical compounds present in the solution, the analytical technique that was chosen and used is the High-performance liquid chromatography (HPLC) was used. The reaction mixture quantitative analyses were carried out using an Agilent 1260 Infinity Quaternary HPLC system (Figure 3.10). Analyses were performed using 0.0025 M sulfuric acid in ultra-pure water

as eluent with a flow of 0.5 ml/min. The injection system consisted of a six-way valve with an injection volume of 20 μ l. Two Rezex ROA-H+ (8%) 300x7.8 mm ion exclusion columns connected in series were used for the separation of products. A diode array detector (DAD) set to 202 nm was used to detect organic acids and a refractive index detector (RID) was used to detect monosaccharides. The column compartment was thermostated at 80°C while the RID was kept at a constant temperature of 40°C.



Figure 3.10: High pressure liquid chromatography instrument

Keeping the same conditions of analysis, quantification and identification of the compounds in the reaction mixture was carried out by means of comparison the retention time of each standard commercial substance prepared with the one obtained in the reaction. Moreover, the determination of the response factor (RF) with the preparation and the analysis of the external calibration curve, leading us to quantify the concentration of each product detected in the liquid phase and to know the conversion and the yield of each molecule and the carbon balance. Table 3.2 shows all analytes calibrated reported with the detector was used, the retention time (RT), and response factor (RF). Two examples of calibration curves were reported in Figure 3.11.

Name	Detector	RT (min)	RF
Oxalic Acid	UV	16	3915953
Mesoxalic Acid	UV	16.7	758839
Tartronic Acid	UV	19.2 (19.25-18.66)	750193
2-Keto-D-glucose	UV	20.34 (20.29-20.03)	310104
Tartaric acid	UV	21.4 (21.24-20.99)	538930
Glucaric acid	UV	21.43 (21.39-21.35)	518704
5-Keto-D-glucose	UV	21.74	539617
Gluconic acid from UV	UV	23.7 (23.7)	380806
Glucose	RID	23.9 (23.91-23.89)	65775693
Gluconic acid from RID	RID	23.97 (23.99-23.95)	53942132
Mannose	RID	25.25 (25.29-25.28)	84153868
Fructose	RID	25.66 (25.59-25.58)	63730195
Arabinose	RID	27.54 (27.46-27.45)	55289287
Glyceric acid	RID	27.7	61926976
Glycolic acid	UV	30.57 (30.57-30.56)	107842
Lactic acid	RID	31.97 (31.65-31.64)	21059006
Formic acid	UV	34 (34-33.95)	92081

Table 3.2: List of molecules (reagent and products) detected by HPLC method, retention time and response factor

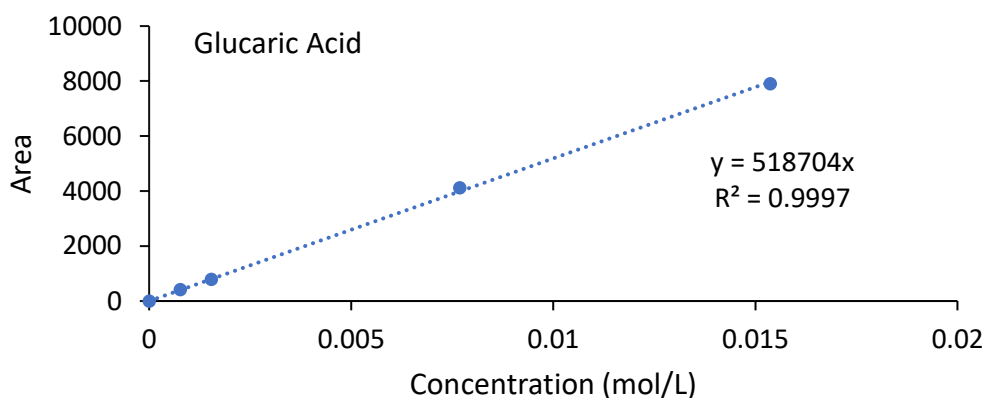
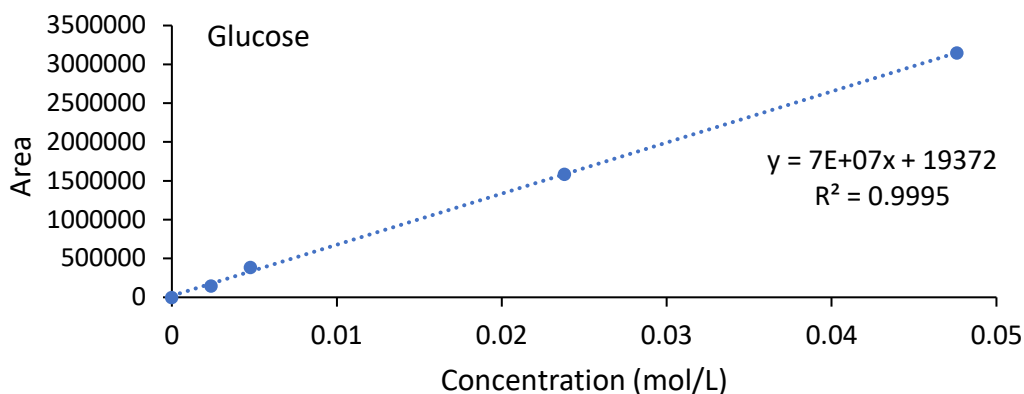


Figure 3.11: Calibration curves of standard solutions: correlation between concentration and HPLC area reported for glucose and glucaric acid

Once RF was determined for each substance, the quantification of each species could be done; at the beginning, the number of moles was calculated in the following way:

$$n_i = \frac{A_i}{RF_i} * \frac{V_{sol}}{1000}$$

n_i = Number of moles

A_i = Chromatogram peak area

RF_i = Response factor

V_{sol} = Volume of the solution [mL]

After calculating the moles of each species, it is possible to find glucose conversion and product yield, as it is shown with the following equation:

$$X = \frac{n_{glucose(t=0)} - n_{glucose(t=f)}}{n_{glucose(t=0)}} * 100$$

X = Glucose conversion

$n_{glucose(t=0)}$ = Initial number of moles of glucose

$n_{glucose(t=f)}$ = Final number of moles of glucose

$$Y_i = \frac{n_i * C_f}{n_{glucose(t=0)}} * \frac{V_{sol}}{1000} * 100$$

$$C_f = \frac{\text{atoms of Carbon in the molecule of the product}}{\text{atoms of Carbon in glucose}}$$

However, the peak of glucose and glucaric acid are overlapped in the refractive Index Detector (RID) chromatogram and this could represent a problem for the quantification of all the species. Although, the glucose signal at the UV detector is not relevant and for this reason, we can quantify and subtract the gluconic acid “contribution” and apply the following formula:

$$n_{GLU} = \frac{A_{RID\ GO+GLU} - \frac{A_{DAD\ GO}}{m_{DAD\ GO}} * F_{RID\ GO}}{RF_{RID\ GLU}} * \frac{V_{sol}}{1000}$$

N_{GLU} = moles of glucose

$A_{RID\ GO+GLU}$ = area of the peak in RID chromatogram related to gluconic acid and glucose

$A_{DAD\ GO}$ = Area of the peak in DAD chromatogram related to gluconic acid

$RF_{DAD\ GO}$ = Response factor of gluconic acid in DAD

$RF_{RID\ GO}$ = Response factor of gluconic acid in RID

$F_{RID\ GLU}$ = Response factor of glucose in RID

V_{sol} = Final Volume of the solution [mL]

There are also the glyceric acid and arabinose that show the same behavior. However, it cannot be possible to apply the same strategy because there is no proportion between the theoretical sum of single areas and the area of GC peaks. Since these two compounds had a response

factor similar to that of the RID detector, both were quantified by using an mean response factor applying the formula:

$$n_{\text{glyceric acid+arabinose}} = \frac{A_{\text{RID glyceric acid+arabinose}}}{\frac{RF_{\text{arabinose}} + RF_{\text{glyceric acid}}}{2}} * \frac{V_{\text{sol}}}{1000}$$

$n_{\text{glyceric acid+arabinose}}$ = Number of moles of glyceric acid and arabinose

RF= Response factor

V_{sol} = Volume of the reaction mixture [mL]

$A_{\text{RID glyceric acid+arabinose}}$ = Peak's area corresponding to glyceric acid and arabinose

3.7.2 4-Nitrophenol reduction

In literature are reported several set-ups to carry out this reaction. However, the use of Au/AC as catalyst, and in particular of active carbon as support, requires a deep investigation. Indeed, the AC possesses a high surface area that can allow the adsorption of reagents and products. Therefore, to quantify and minimize the carbon absorption contribution of 4-nitrophenol (4-NP), three different reaction experimental procedures were used and compared:

1) Round bottom flask

The reaction was carried out in a 250 mL round-bottom flask (Figure 3.12) equipped with a magnetic stirrer set at 900 rpm, at room temperature (20°C). At first, a 4-NP 2.0×10^{-4} M solution was added to the round bottom flask, then the desired amount of fresh aqueous solution of NaBH_4 9.0×10^{-3} M was added and mixed in the round bottom flask. Once mixed with the fresh solution of sodium borohydride, the colour of 4-NP solution has changed to bright yellow. After that, the catalyst was added (for test 1 320mg/L; for test 2 80mg/L). To check the reaction behaviour as a function of time, 3.5 mL of the reaction solution was withdrawn periodically, filtered with a PTFE 0.22 μm syringe filter to remove the catalyst, and added into a quartz cuvette with an optical path of 1 cm to record a UV-Vis spectrum. The absorbance (A) of the reaction solution was recorded by the UV-Vis spectrometer as a function of reaction time to monitor the conversion of 4-NP.

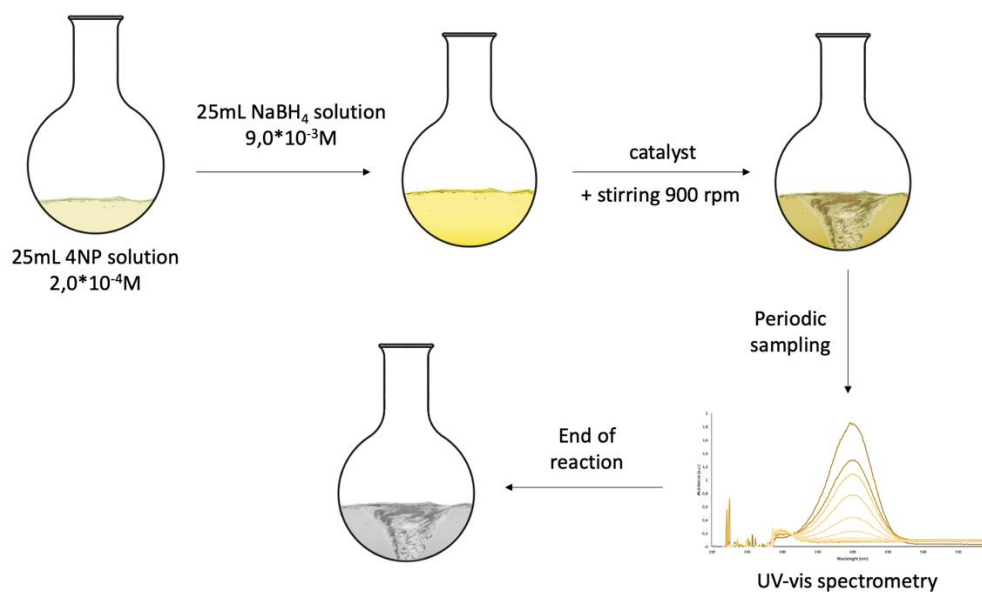


Figure 3.12: Scheme of round-bottom flask reaction setup

2) Cuvette set up

The catalyst was added firstly inside a 50mL beaker (80 mg/L), then 25 ml of $2.0 \cdot 10^{-4}$ 4-NP solution was added, trying to avoid the eventual catalyst particles floating on the surface of the liquid (Figure 3.13). 25 mL of a fresh aqueous NaBH_4 solution ($9.0 \cdot 10^{-3}$ M) were added, straight away and this was the starting reaction time ($t = 0$). After mixing, 3.5 mL of the suspension was drawn from the beaker and poured in a glass cuvette to measure the absorbance periodically, every 2.50 minutes.

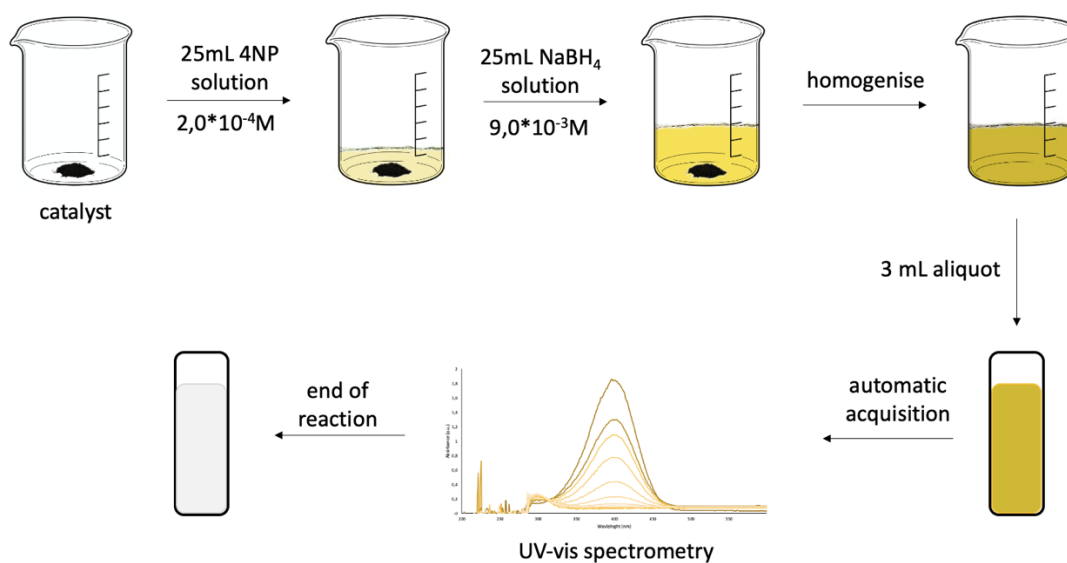


Figure 3.13: Scheme of cuvette reaction setup

UV-Vis spectroscopy is a useful technique to perform quantitative determination of the concentration of aromatic compounds and conjugated organic molecules, like the 4-nitrophenol and the 4-aminophenol. It is possible to apply the Lambert-Beer law, which allows correlating the absorbance of a solution to the concentration of the chemical species in solution with the following formula:

$$A = \epsilon * l * C$$

Where A is the absorbance, ϵ is the molar extinction coefficient (expressed in $M^{-1}cm^{-1}$), l is the optical path length and depends on the cuvette (normally 1 cm), and C is the concentration of the species in the solution. The molar extinction coefficient was obtained by calibration, in particular from the dependency concentration/absorbance (Figure 3.14).

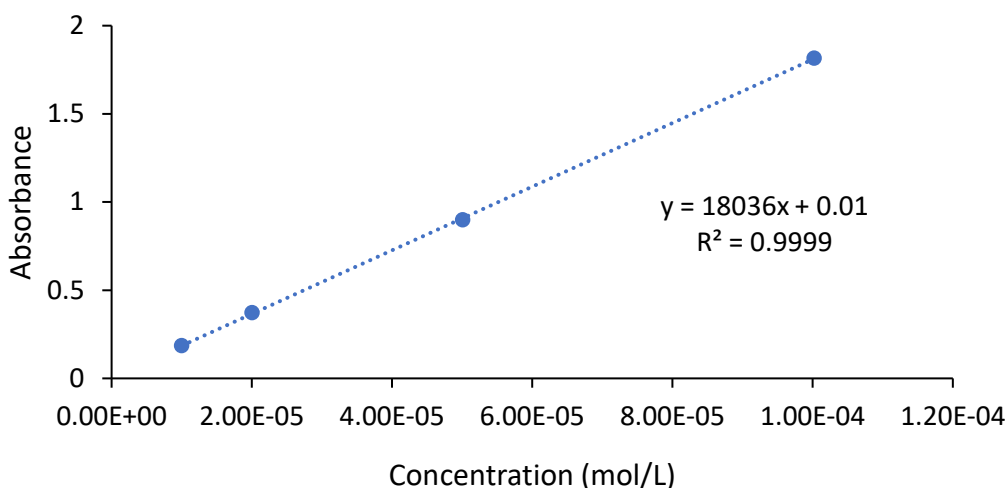


Figure 3.14: Calibration curves of standard solutions: correlation between concentration and solution absorbance at 400nm

4-nitrophenol in the basic environment and in solution with $NaBH_4$ has a UV-vis peak at $\lambda_{max} = 400$ nm as the molecule deprotonates in the form of nitrophenolate. The instrument used was a Perkin Elmer UV-VIS-NIR Lambda 19 used for nitrophenol concentration measurements using a wavelength range going from 600 to 200 nm. AC adsorption and/or reaction progression was monitored by UV-vis spectroscopy using the absorbance at 400 nm (corresponding to 4-NP characteristic UV-vis peak) to determine 4-NP concentration at the time of the analysis. To determine the concentration, the Lambert-Beer law was applied, using the molar extinction coefficient obtained thanks to the calibration ($\epsilon=18100 Lmol^{-1}cm^{-1}$). 4-nitrophenol conversion was obtained with the formula:

$$4 - NP \text{ adsorption or } X\% = \frac{C_0 - C_t}{C_0} * 100$$

Where C_0 is the initial 4-NP concentration and C_t is 4-NP concentration at the time, which the UV-Vis spectrum was recorded.

After that, the kinetic constant of the reaction was determined: the natural logarithmic function of the concentration ratio comes from the assumption that in presence of large excess of NaBH_4 , its concentration can be approximated as constant with time hence leaving only the nitrophenol concentration in a pseudo-first order reaction rate³⁵:

$$k_{app} = -\frac{dC}{dt}$$

Where C is nitrophenol concentration; t represents time; k_{app} represents the apparent kinetic constant; k_{app} contains the sodium borohydride approximated-constant concentration and other parameters that are constant if the reaction conditions are fixed.

After integration of this differential equation using as extremes C_0 and C_t for the C variable and imposing the initial time as $t = 0$, it can be obtained:

$$\ln \frac{C_t}{C_0} = -k_{app} * t$$

This equation can be interpreted with t as the independent variable and $\ln(C_t / C_0)$ as the dependent variable, $-k_{app}$ represents the slope of the straight line so identified. By plotting the points obtained experimentally in a graph that presents reaction time on the x axis and $\ln(C_t / C_0)$ on the y axis. Interpolating the experimental points with a fitting straight line, the slope of the latter represents the term $-k_{app}$ of the reaction.

However, to evaluate the real contribution of the catalytic reaction, an $E_{extrapolated}$ was calculated subtract, for each time, the $X_{absorbed}$ from the X_{total} . From the extrapolated conversion values, it is possible to obtain the natural logarithmic function that allows calculating the real apparent kinetic

constant for a given catalyst. The ratio C_t/C_0 can be expressed as a function of the extrapolated conversion ($X_{extr}\%$):

$$\frac{C_t}{C_0} = 1 - \frac{\%X_{extr}}{100}$$

4-aminophenol is the only product of the reaction, so theoretically the conversion corresponds with the product yield. To verify the presence of 4-aminophenol as only product, a mass spectrometer analysis or an NMR could be carried on.

3.7.3 HMF oxidation

The catalytic tests were carried out in an autoclave reactor (100 mL capacity, Figure 3.15), equipped with a mechanical stirrer and measurement tools for temperature and pressure.



Figure 3.15: Batch reactor system used for the HMF oxidation reaction

The desired amounts of an aqueous solution of HMF and the catalyst were loaded in the reactor. Then the autoclave was purged with O_2 (three times) and then pressurized at 10 bar and the temperature was increased to $70^\circ C$ and the reaction mixture was stirred for the whole experiment. Initial time (time zero) for the reaction was considered when the set point temperature was reached (after 10 min). At the end of the reaction, the reactor was cooled to room temperature and the

solution was filtered. 1mL of the reaction mixture was diluted 5 times and the final solution was analyzed with HPLC technique. For this purpose, the column operated is an Aminex HPX- 87H 300 mm × 7.8 mm column, using a 0.005 M H₂SO₄ solution as mobile phase. The compound identification and quantification were achieved by using external calibration method and using reference commercial samples and Figure 3.16 are reported the calibration curves for HMF and FFCA as an example.

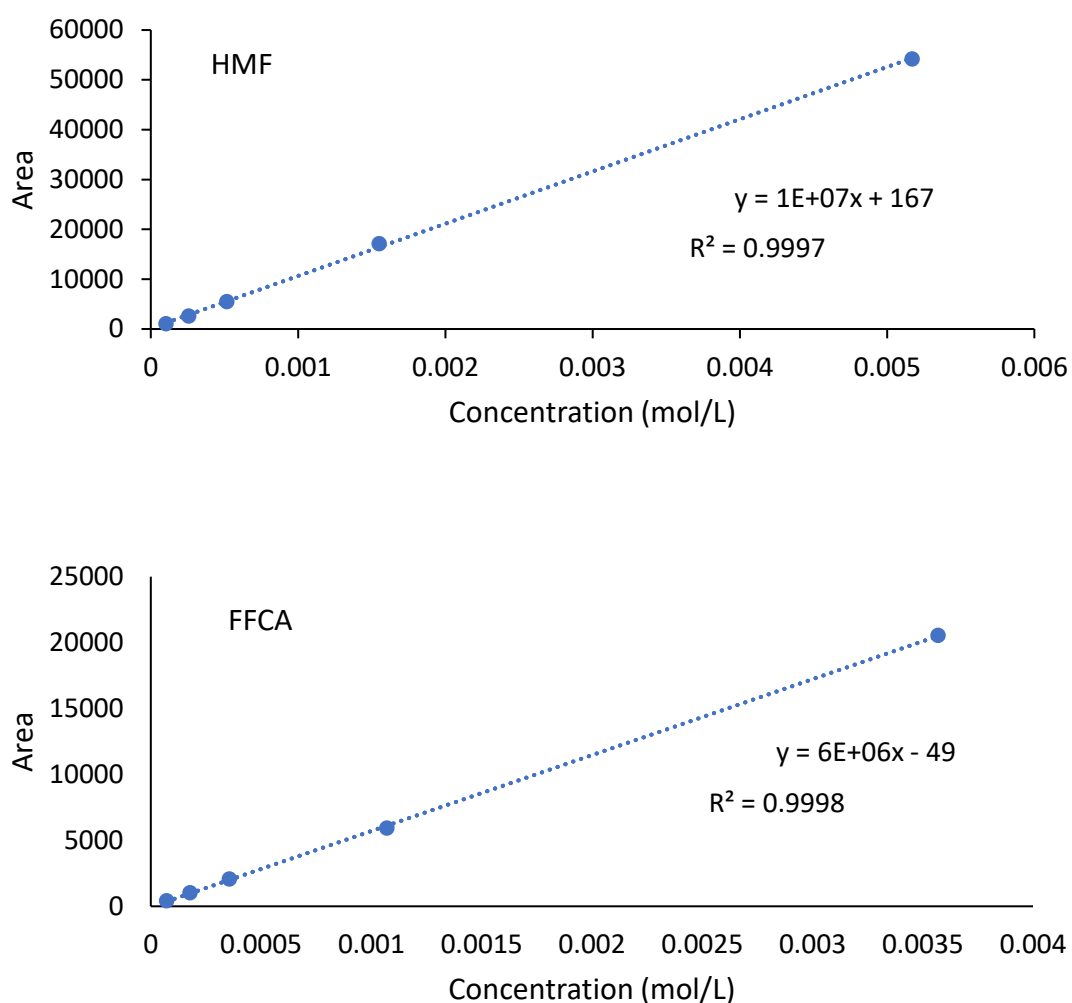


Figure 3.16: Calibration curves of standard solutions: correlation between concentration and HPLC area reported for HMF and FFCA

To evaluate conversion and yields, at first is useful the initial concentration of HMF. All the parameters were calculated with the following formulas:

$$C_{0,HMF} = \frac{m_{HMF}}{MW_{HMF} * V_R}$$

$C_{0,HMF}$ =Initial concentration of HMF

m_{HMF} = Weight HMF

MW_{HMF} = Molecular weight HMF

V_R = Volume reaction

$$X_{HMF} = 100 * \left(1 - \frac{A_{HMF}}{RF_{HMF}} * \frac{DF}{C_{0,HMF}} \right)$$

$$Y_i = 100 * \frac{A_i}{RF_i} * \frac{DF}{C_{0,HMF}}$$

X_{HMF} = HMF conversion

Y_i = Yield of component i

A_i = HPLC Area of component i

RF_i =Response factor of component i

DF = Dilution Factor

3.7.4 Furfural oxidative condensation

This reaction was studied during the abroad period carried on in the university of Malaga-Spain.

The catalytic tests were carried out in a batch reactor (Figure 3.17), a stainless-steel autoclave with a Teflon glass inside and the reaction conditions used were previously established in the researched group.



Figure 3.17: Batch reactor system used for the furfural oxidation reaction

In particular, 6mL of a mixture of ethanol and o-xylene (internal standard, volume ratio EtOH:O-xylene 1:0.0067) was added in the reactor with 25mg of catalyst, 0.1g of base (Na_2CO_3), and 86 μL of furfural. Then, the reactor was closed and, after a purge step, 6 bar of molecular oxygen was loaded. After that, the reactor was set in a hot plate to heat and keep the reactor at 120°C and a stirring rate of 350 rpm. After 6h, the vessel was removed from the plate and the liquid was separated from the solid; the liquid phase was analyzed through gas chromatography, using a TBR-14 column, a FID detector and the following method (Figure 3.18):

- Isotherm step at 40°C for 1 minute
- Heating step 2°C/min until 70°C
- Isotherm step at 70°C for 1 minute
- Heating step 5°C/min until 220°C
- Isotherm step at 220°C for 20 minutes

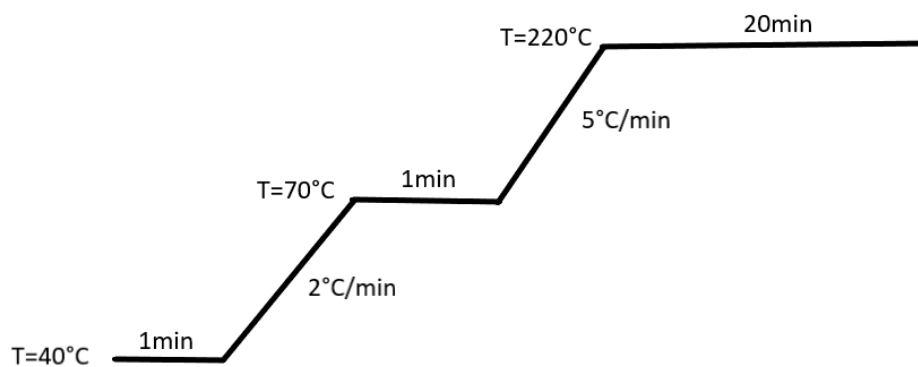


Figure 3.18: Heating ramp used for GC analyses

The solid instead was filtrated and washed with water to remove the sodium carbonate in excess. Also here the quantification of the compounds and the calculation of conversion and yield was obtained by the determination of the response factor for each chemical compound. Here in Figure 3.19 are reported the calibration curves for furfural and furan-2-acrolein as an example.

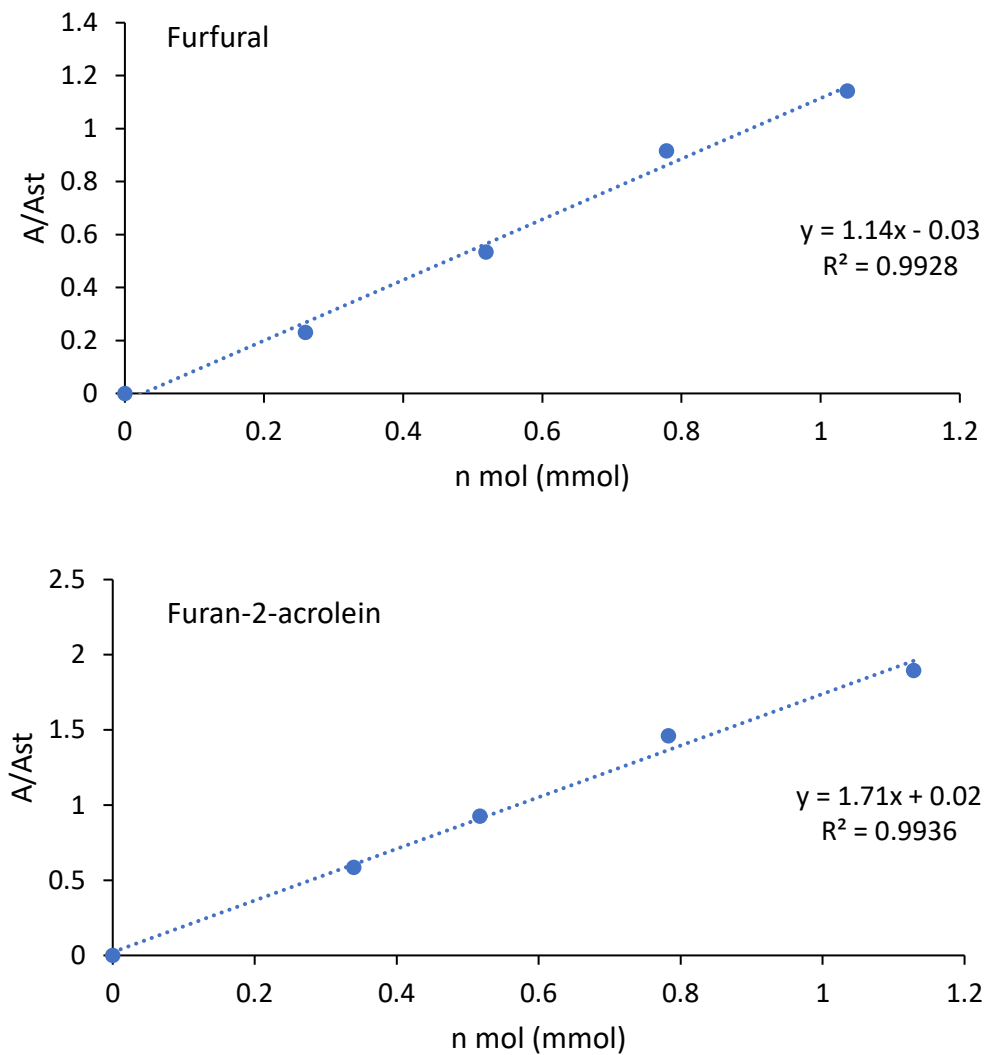


Figure3.19: Calibration curves of standard solutions: correlation between number of mole and the ratio between A and A standard. Here are reported the curve for furfural and furan-2-acrolein

The response factor determined from the curve slope permits to calculate conversion and yields as reported in the formulas below:

$$\frac{A_i}{A_{st}} = RF * n_i$$

$$n_i = \frac{A_i}{A_{st}} * \frac{1}{RF}$$

$$X_{fur} = \frac{n_{0fur} - n_{fur}}{n_{0fur}}$$

$$S_i = \frac{n_i}{n_{0fur} - n_{fur}}$$

$$Y_i = X_{hmf} * S_i$$

A_i = Area substance

A_{st} = Area internal standard

n_i = Number of mol component i

RF= Response factor

X_{fur} = Furfural conversion

Y_i = Yield of component i

S_i = Selectivity of component i

3.7.5 1,6 hexanediol (HDO) oxidation

The catalytic oxidations were carried out from the research group in France, Lille and they have used two catalytic reactors. The screening of the Au/AC catalysts was carried out with a multi-reactor system (see Figure 3.20 below). It consists of 24 parallel batch reactors with a final volume of 6 mL; each reactor was loaded with an aqueous HDO solution (2 mL, 14 mmol L⁻¹) with and without base (NaOH, 2 equivalent) and the considered Au-based catalyst (ca. 5-10 mg). The reaction was carried out at 15 bar of air, 110 °C, 600 rpm for the reaction time of 4 h. At the end of the reactions, the reactor was cooled to room temperature, the pressure was released, and the suspension was collected and filtered with a nylon membrane filter 0.2 µm.

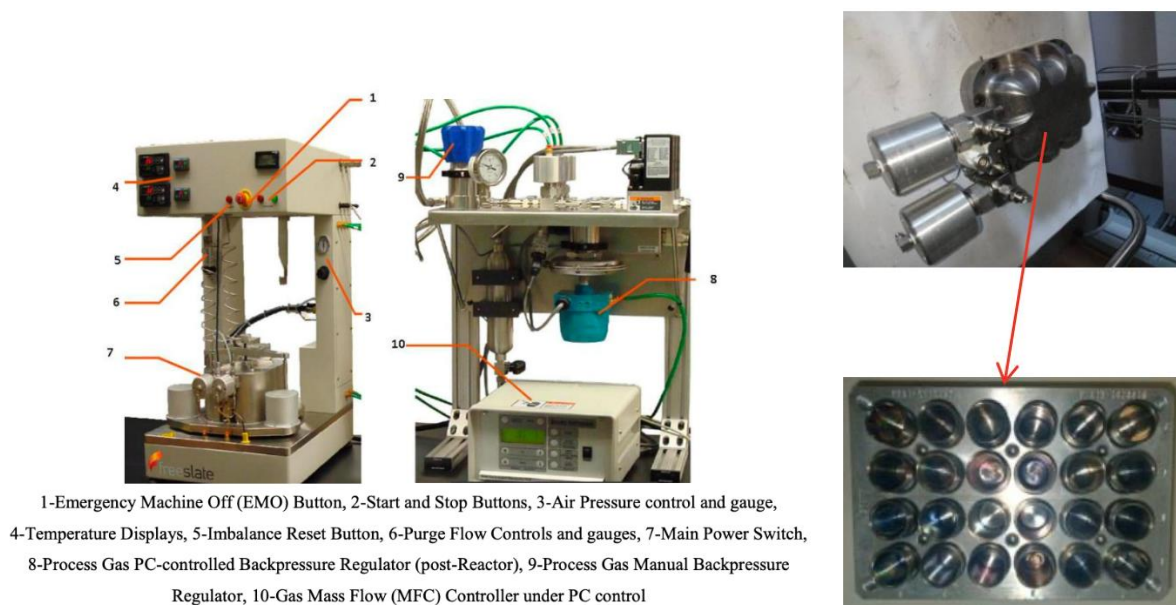


Figure 3.20: SPR pressure reactor from Unchained Labs and SPR block reactor and 24 reactor plate

Instead, the time on line for specific catalysts was carried out with the second type of reactor, which is an autoclave reactor with a capacity of 30 mL equipped with a high precision heating system and

a mechanical stirrer (Figure 3.21). This reactor permits also to removal liquid samples during the catalytic test. In the beginning, an aqueous solution (20 mL) of HDO (with 2 equivalents of NaOH) and the amount of catalyst that corresponds to the HDO/metal molar ratio of 100 were introduced into the reactor. After this, the reactor was closed and purged with a flow of air. The reaction was carried out under 15 bar of air, 110 °C, 600 rpm during 4 h. The 4 hours of reaction started just when the system reached the right temperature (110°C).

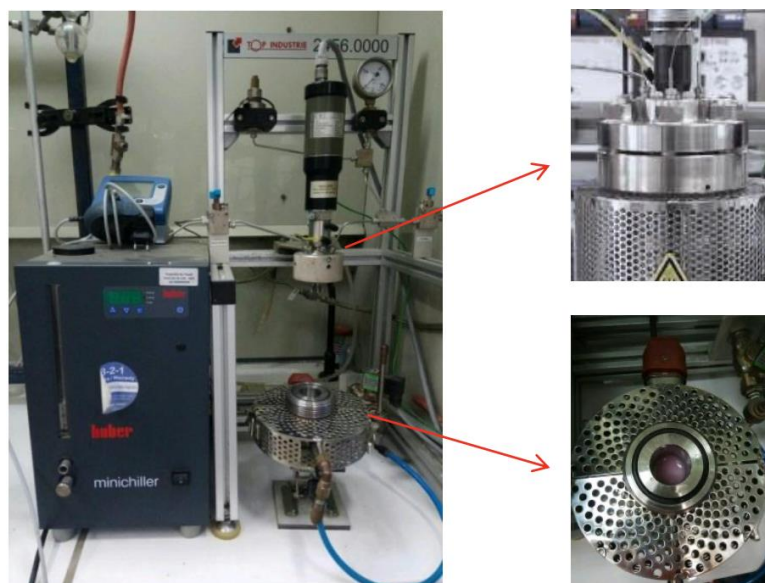
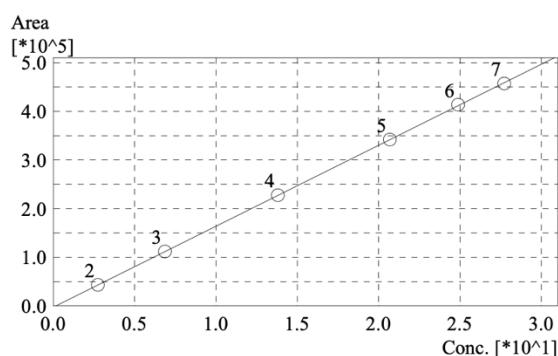


Figure 3.2:TOP Industry autoclave reactor

AA, HDO, and HHA were analyzed by High Performance Liquid Chromatography (HPLC, Waters 2410 RJ) equipped with refractive Index (RI) and UV detectors and a Rezex ROA–organic Acid H⁺ column (Ø 7.8 mm x 300 mm). Diluted H₂SO₄ (5 mM, 0.5 mL min⁻¹) was used as a mobile phase. The response factor was determined experimentally for the commercial compounds and Figure 3.22 report an example of that.

ID# : 1
 Name : AA
 Quantitative Method : External Standard
 Function : $f(x)=16650.5*x-2854.12$
 Rr1=0.9999806 Rr2=0.9999612 RSS=5.396437e+006
 MeanRF: 1.628016e+004 RFS: 3.959749e+002 RFRSD: 2.432254
 FitType : Linear
 ZeroThrough : Not Through
 Weighted Regression : None
 Detector Name : Detector B



#	Conc.(Ratio)	MeanArea	Area
2	2.760984	42864	42823
			43099
			42669
3	6.880283	111725	111949
			111631
			111594
4	13.81324	227165	227346
			226920
			227228
5	20.70738	342068	341943
			342375
			341886
6	24.89321	413302	412350
			412229
			415326
7	27.72904	457261	457261

Figure 3.22: Correlation between concentration of standard solutions and HPLC areas

It was, therefore, possible to calculate conversion (X), selectivity (S), and carbon balance (CB), according to the following formulas:

$$X \text{ HDO } (\%) = \frac{n \text{ HDO}_0 - n \text{ HDO}_f}{n \text{ HDO}_0} \times 100$$

$$S \text{ product } (\%) = \frac{n \text{ product}_f}{n \text{ HDO}_0 - n \text{ HDO}_f} \times 100$$

$$\text{Carbon balance (CB)} = \frac{n \text{ HDO}_f + n \text{ AA}_f + n \text{ HA}_f}{n \text{ HDO}_0} \times 100$$

Where n HDO_i is the initial moles of HDO, n HDO_f is the final moles of HDO, n product_f is the final moles of products, n AA_f is the final moles of adipic acid, and n HA_f is the final moles of HA.

4 Chapter 4- Supported gold catalysts: effect of preparation methods

4.1 Preparation Method: Old (Method A) VS New method (Method D)

At first, the intention was to investigate how the characteristics of the supported metal nanoparticles could affect the reaction behavior and for this reason, it was decided to use the sol-immobilization for the preparation of the catalysts presented in the following Chapters. The methodology used previously in our laboratory research corresponds to Method A, but for the preparation of the catalysts presented in the following chapters, it was chosen to change slightly the steps for the synthesis. In particular, Method D provides:

- Lower concentration of Au precursor: low concentration of gold could avoid the growth of colloidal Au nanoparticles when they are already formed;
- Longer reaction time before adding the support: even if higher time facilitates the growth of the colloidal Au nanoparticles (it was proved from the UV-Vis spectra in the following part), this modification ensures us that all the gold precursor was reduced to form Au colloidal nanoparticles.

Method B and Method C are further modifications of Method D; in particular Method B provides a heat treatment and Method C a washing step, both carried on at the end of the immobilization step. However, these two methods will be treated in the following section.

To understand how much the modification from Method A to Method D could affect the catalyst morphology, TEM analysis was done on the two samples prepared.

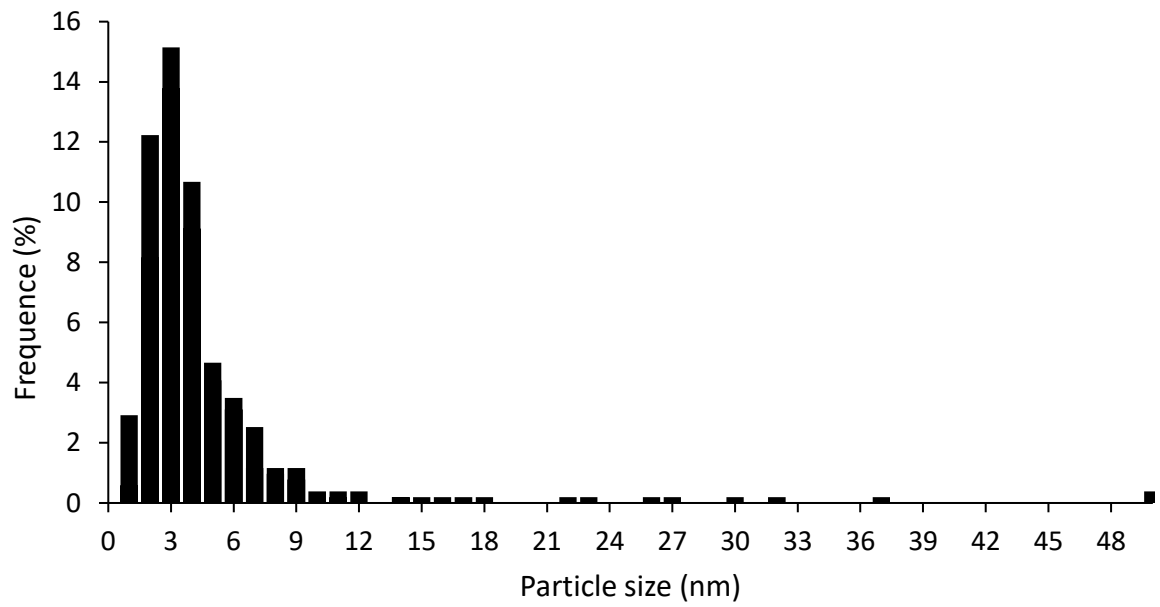
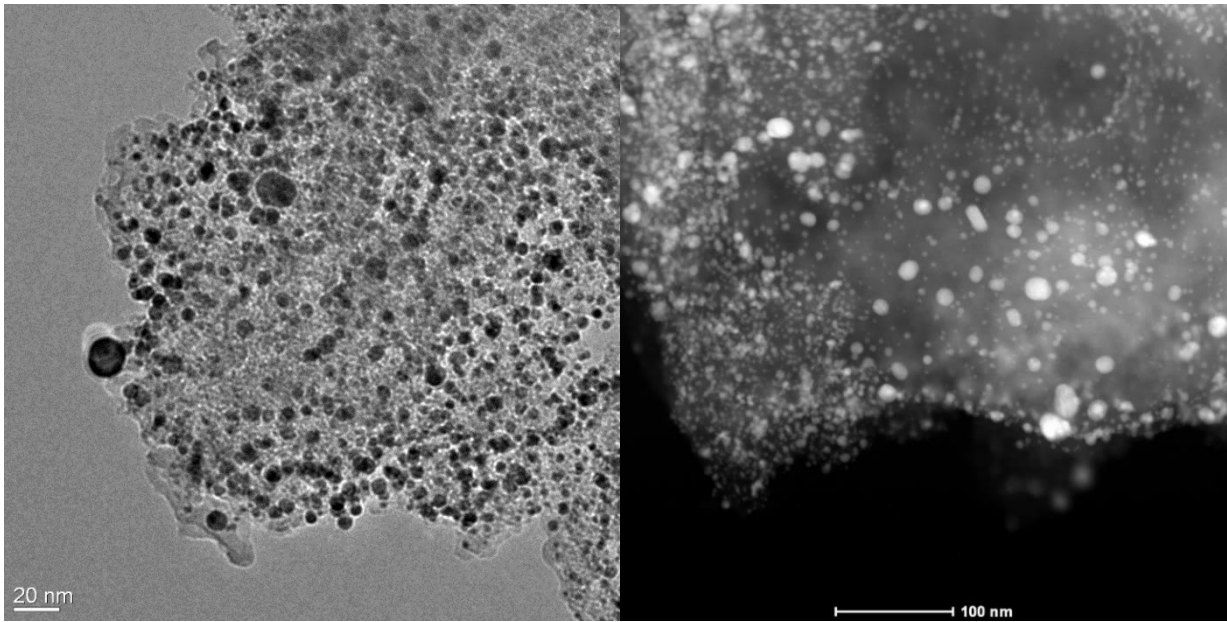


Figure 4.1: TEM, STEM analysis, and particle size distribution of Au/AC prepared with Method A

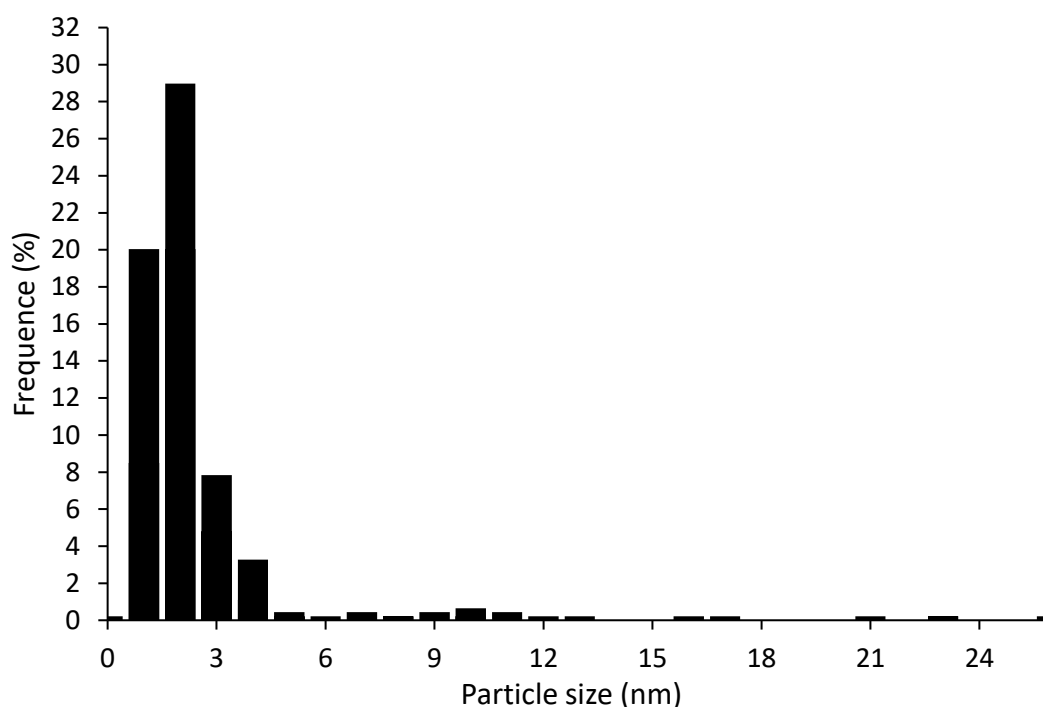
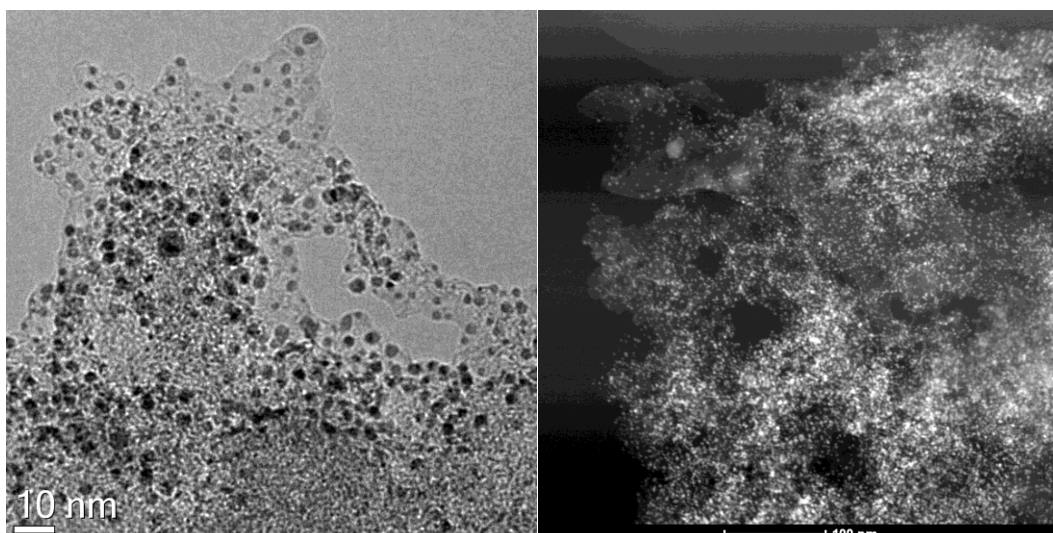


Figure 4.2: TEM, STEM analysis and size distribution of Au/AC prepared with Method D

From the comparison between Figure 4.1 and Figure 4.2, it can be noticed that both methods provide the formation of spherical nanoparticles. The modification done in Method D provided the smallest nanoparticles and well distribution of them, as could be seen from the TEM and STEM analysis: with Method A, the mean particle size obtained is 4.1 nm (standard deviation = 1.9 nm), but with Method D the mean particle size is equal to 2.4 nm (standard deviation = 1.6 nm). The comparison between these two methods showed also how the sol-immobilization method permits the synthesis of different nanoparticles with different mean particle size and particle size

distribution by easily changing some steps of the synthesis. However, for the next study of the synthesis, it was decided to use Method D as the starting experimental procedure.

4.2 Preparation Method: Au/AC-PVA series

It was decided to focus on the systematic study of the supported gold preformed colloidal nanoparticles changing some parameters like the nature of the polymer or the amount of the polymer added during the experimental procedure.

To tune the dimension of the nanoparticles (NPs), several synthetic approaches exist; one of them is the systematic modification of the stabilizing agent amount that could influence the particle size. This is why many Au samples with a different stabilizing agent (example polyvinyl alcohol or polyvinyl pyrrolidone) and different stabilizer to Au weight ratio were prepared, to study the influence and nature of stabilizer and the amount of stabilizer in the final morphology of the nanoparticle and later in terms of catalytic performance. The catalysts were prepared with the sol immobilization Method D, as it is described in the previous section. To analyze the Au species formed during the synthesis step, UV-Vis spectra were recorded in all the main steps of the preparation method (reduction of gold precursor and formation of Au colloidal nanoparticles).

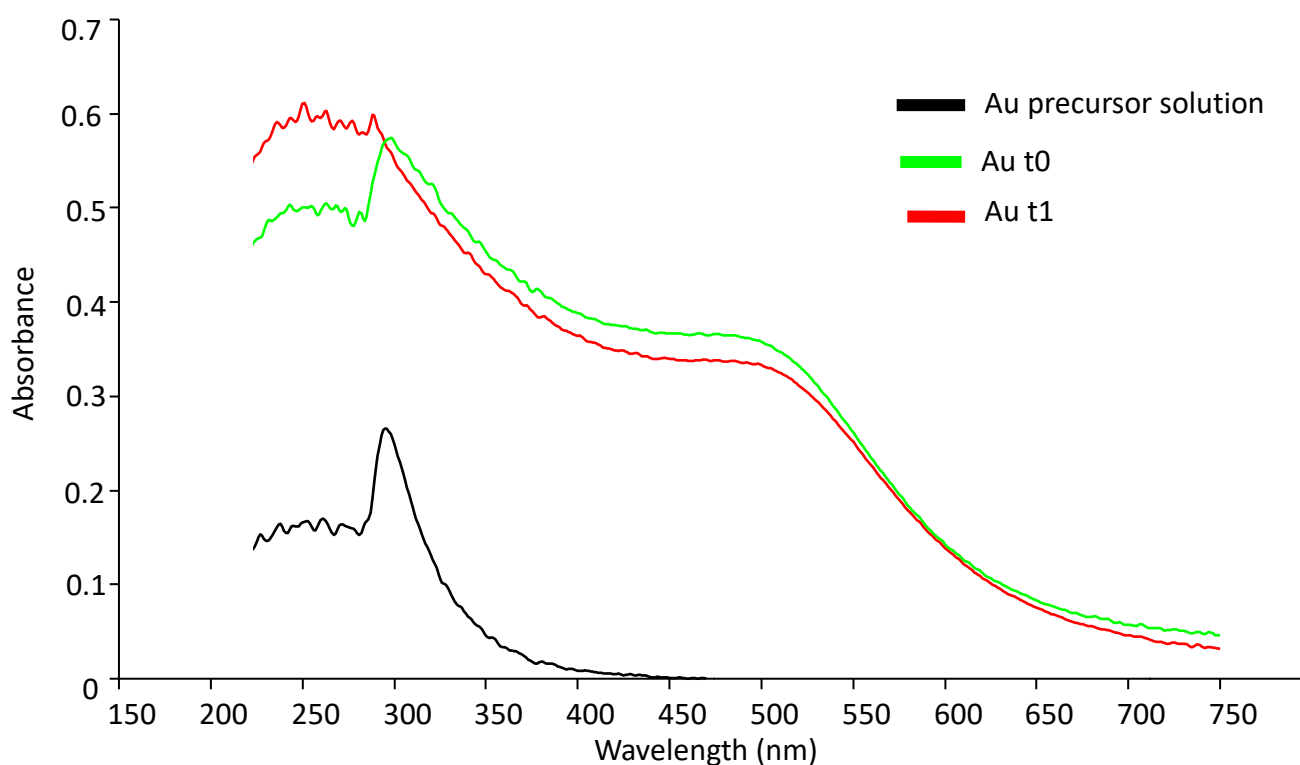




Figure 4.3: UV-Vis spectra of gold precursor and gold colloidal nanoparticles; (: Au precursor solution; : Au colloidal at t=0min after NaBH₄ addition; : Au colloidal at t = 25min after NaBH₄ addition, called t1). Bottom picture: photo of the gold precursor solution (left) and the gold colloidal nanoparticles prepared

In particular, the black line in Figure 4.3 represents the UV-Vis spectrum of the Au precursor solution. It shows a narrow peak around 300 nm, corresponding to the pale-yellow color of Figure 4.3a. “Aut0” and “Aut1” (the green and the red line in Figure 4.3) correspond to the UV-Vis spectra after 3 and 25 minutes of NaBH₄ addition, respectively. The spectra show a new peak around 500 nm, corresponding to the characteristic plasmon peak.¹¹⁹ Indeed, Au metal fine particles interact with a photon, giving the surface plasmon resonance and induces a strong absorption in the UV-Vis field. The surface plasmon resonance (SPR) band intensity and wavelength depend on factors affecting the electron charge density on the particle surface, such as the metal type, particle size, shape, structure (Figure 4.4 reported the relationship between the size of the nanoparticles with the λ of the plasmonic peak). Knowing that and comparing these three spectra, it could be deduced that the precursor reduces in the colloidal solution, while the size of the gold nanoparticles increases a little with time (there is a little blue shift compared to the Aut0 with Aut1).

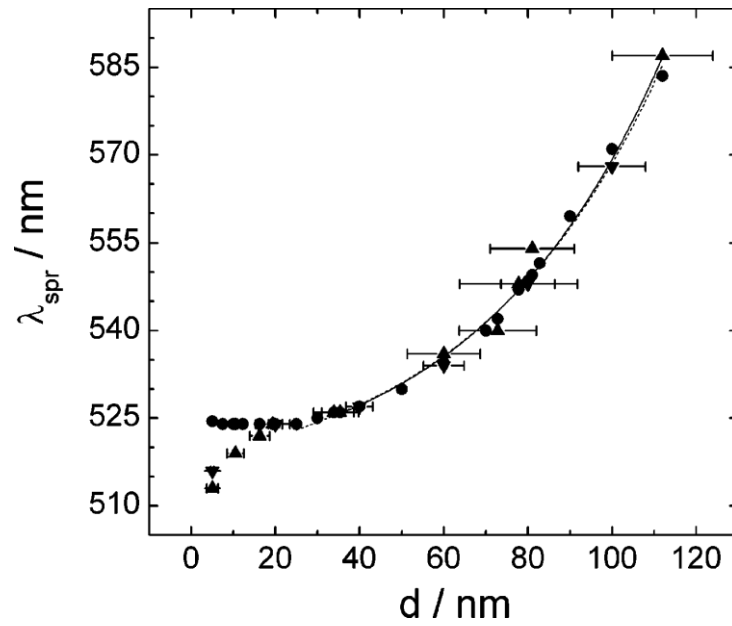


Figure 4.4: Position of the surface plasmon resonance peak (λ_{spr}) as a function of the particle diameter for GNPs in water: calculated (circles); experimentally measured (downward-pointing triangles, commercial GNPs; upward-pointing triangles, in-house synthesized GNPs). An exponential fit to the theoretical (experimental) data for $d > 25$ nm is shown as a dotted (dashed) line

As it is reported in the paper of Wolfgang Haiss et al.¹²⁰ and showed in Figure 4.4, the dimension of the metal nanoparticles changes the position of the surface plasmon peak. Using this correlation, Au colloidal nanoparticles were prepared with different amount of stabilizing agent (weight ratio stabilizing agent: Au from 0 to 2.4) and UV-Vis spectra were collected after 25 min.

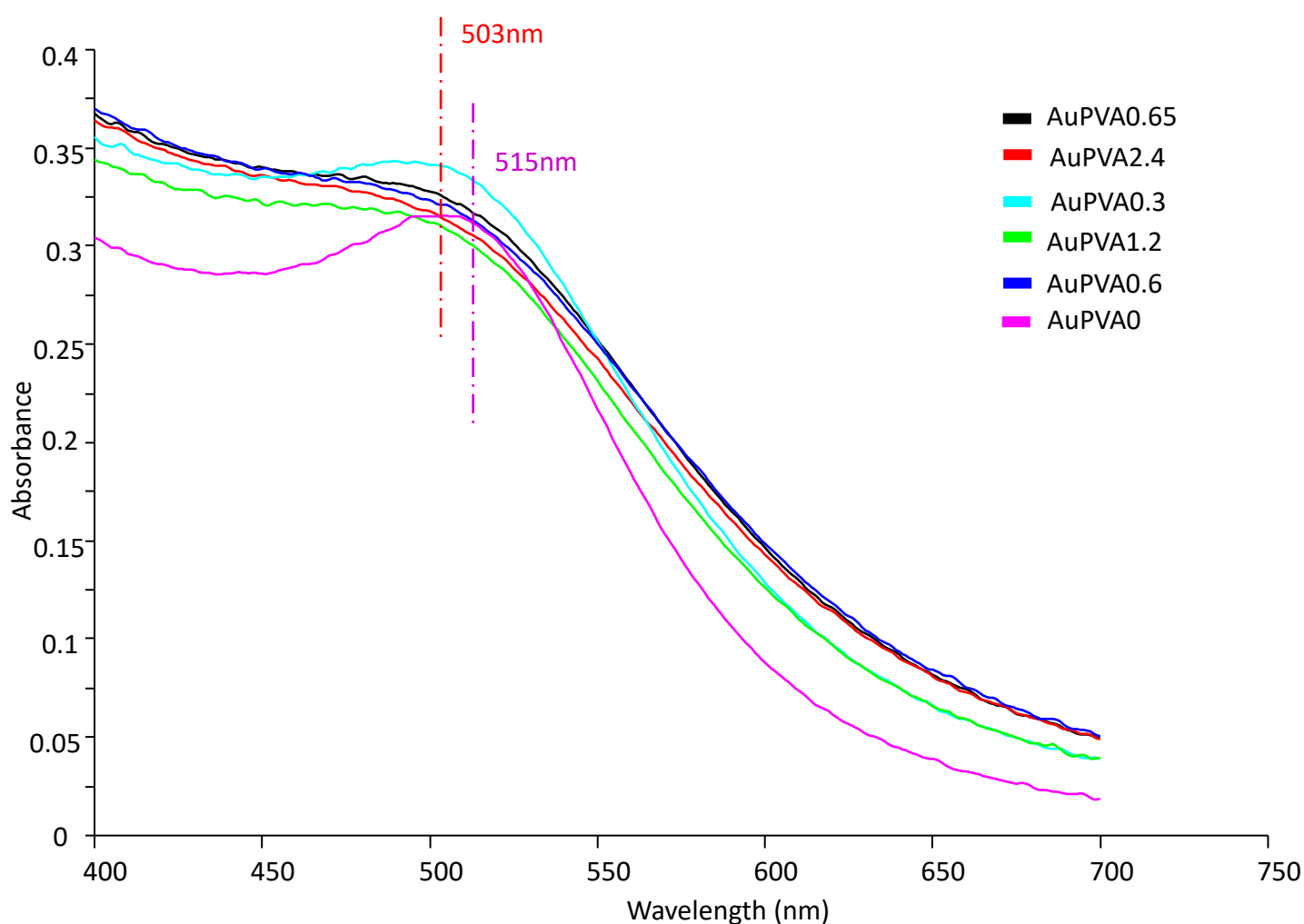


Figure 4.5: UV-VIS spectra of Au colloidal solutions with different Au:PVA weight ratio

The comparison of the different UV-Vis spectra recorded (Figure 4.5) shows that with increasing the amount of PVA from a polymer: Au weight ratio of 0 to 2.4, the plasmonic peak became broad and shifted to a lower wavelength; in particular, AuPVA0 shows the plasmonic peak at 515nm and AuPVA2.4 at 503nm. These results confirm that a higher amount of PVA facilitates the formation of smaller nanoparticles in the colloidal solution. After that, the Au colloidal nanoparticles were immobilized (as reported in Method D) on the activated carbon and after the immobilization step (addition of support) and post-treatment, the catalysts were submitted to a series of analyses. X ray diffraction (XRD) is one of the techniques used and allows us to establish the Au crystalline size presented in the samples. Each crystal plane gives a diffraction peak in a specific position and the main ones for gold nanoparticles are:

- Au (111): $\sim 38^\circ 2\theta$
- Au (200): $\sim 44^\circ 2\theta$

- Au (220): $\sim 64^\circ 2\theta$
- Au (311): $\sim 77^\circ 2\theta$

Usually, for Au nanoparticles, the most intense peak is the one related at the 111 facets/planes; for this reason and because of the low metal loading used (1% wt), the method used is focused in the region nearby $38^\circ 2\theta$; XRD patterns are shown in Figures 4.6.

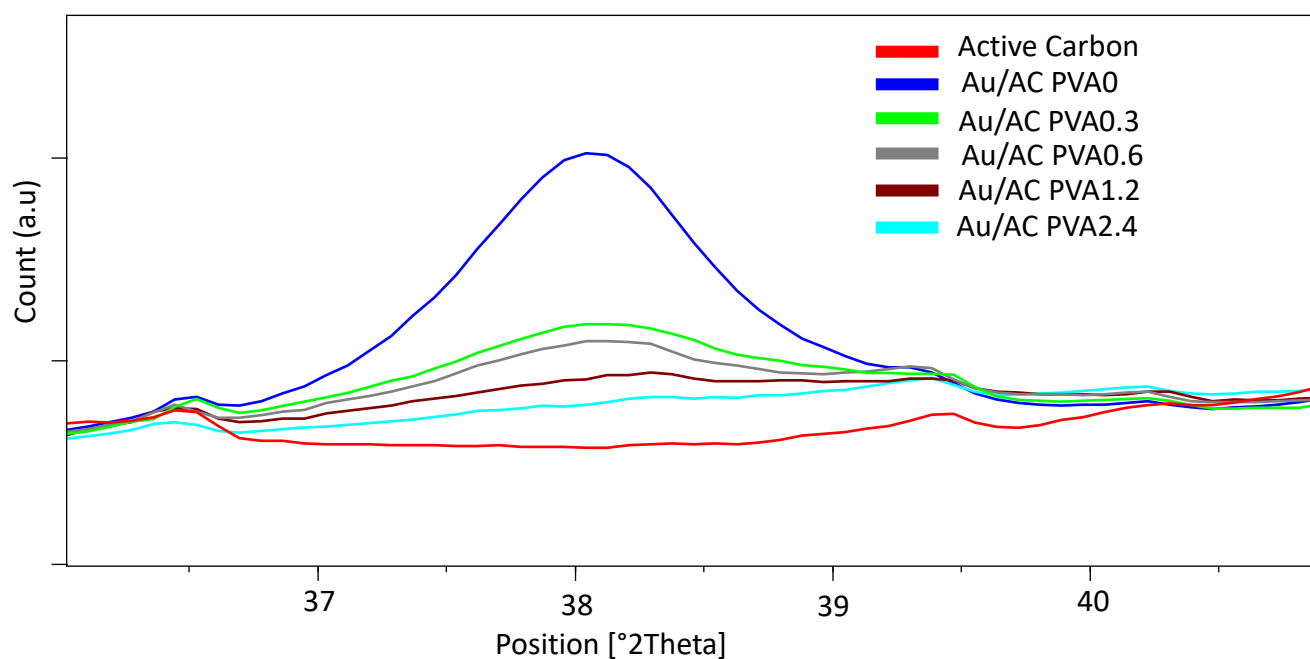


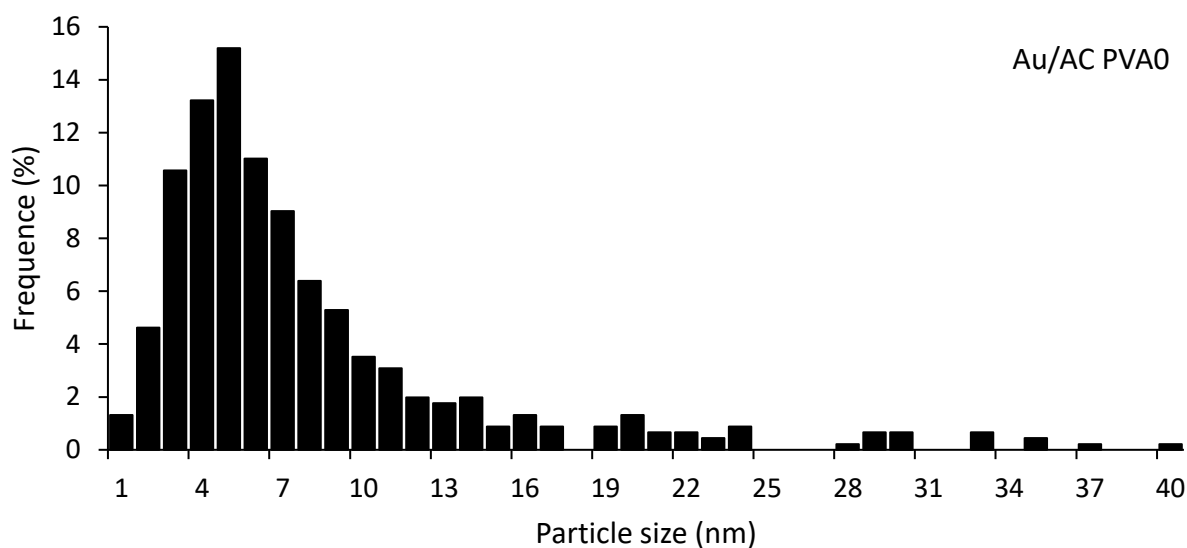
Figure 4.6: XRD patterns of activated carbon and Au/AC samples

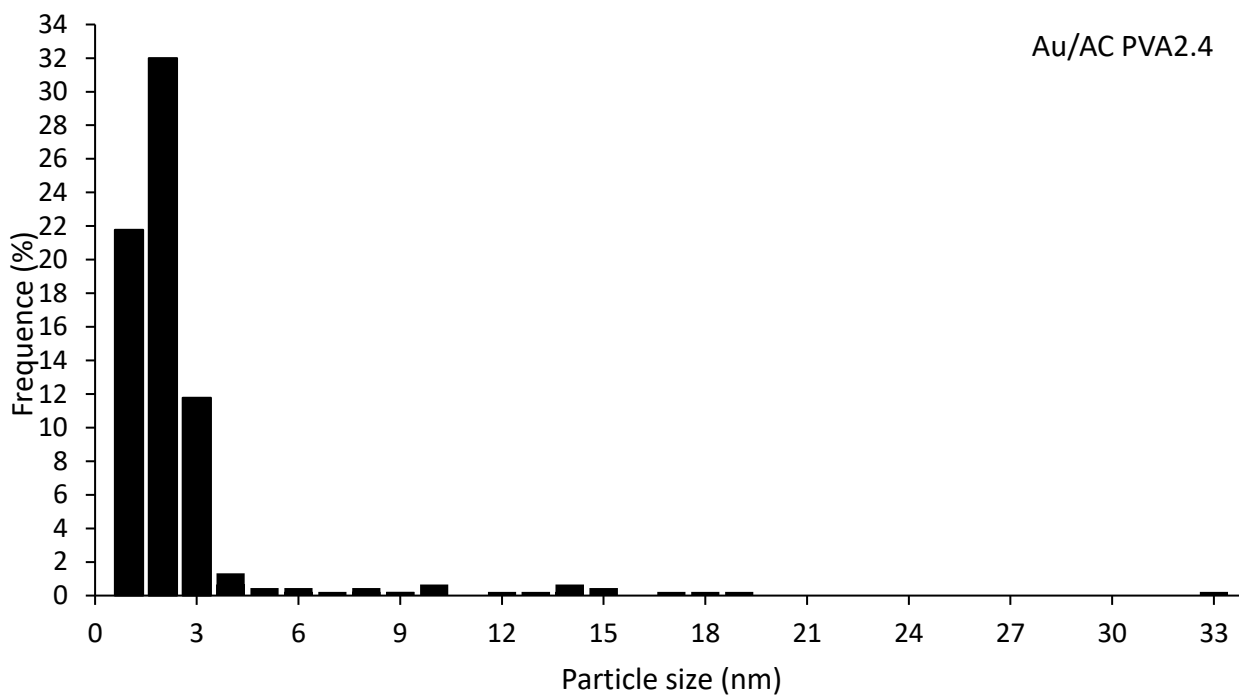
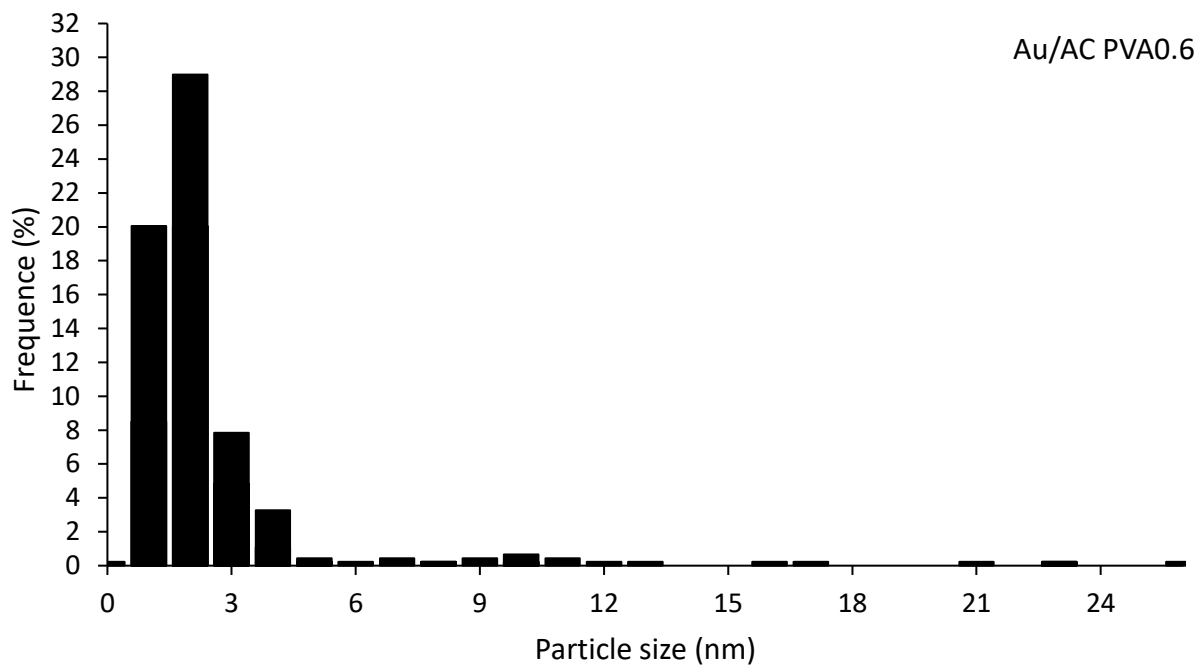
The diffraction peak present in the XRD pattern at $38.2^\circ 2\theta$ corresponds to the highest signal of gold, which is the plane Au (111). It was reported also the diffractogram of the carbon, to prove that there is no diffraction peak overlapping given by the support used. XRD pattern clearly showed a broadening of the diffraction peak of Au as PVA concentration increased. This was ascribed to the decrease of the dimension of the crystal size and with the Scherrer equation, it is possible to calculate the mean crystallite size of Au. Indeed, this formula correlates the diameter with the broadening at half the maximum intensity and the result are reported in Table 4.1. However, as the crystallite size of Au is lower than 5 nm, the precision and accuracy of this method are lower, therefore we focused on the trend of crystallite size to compare the results presented.

Catalyst	Au mean crystallite size (nm)
Au/AC PVA0	6.4
Au/AC PVA0.3	3.6
Au/AC PVA0.6	3.1
Au/AC PVA1.2	2.6
Au/AC PVA2.4	2.2

Table 4.1: Mean crystallite size values of the Au/PVA series obtained by XRD analysis

Comparing the results obtained with the UV-Vis spectroscopy and the powder XRD analysis, we can suggest that the immobilization step keeps constant the trend of the values obtained for the mean particle size. However, to have a proper comparison of the effect of the PVA on the final mean particle size of Au on the supported Au nanoparticles and the dispersion, transmission electron microscopy (TEM) analysis of the samples is required.





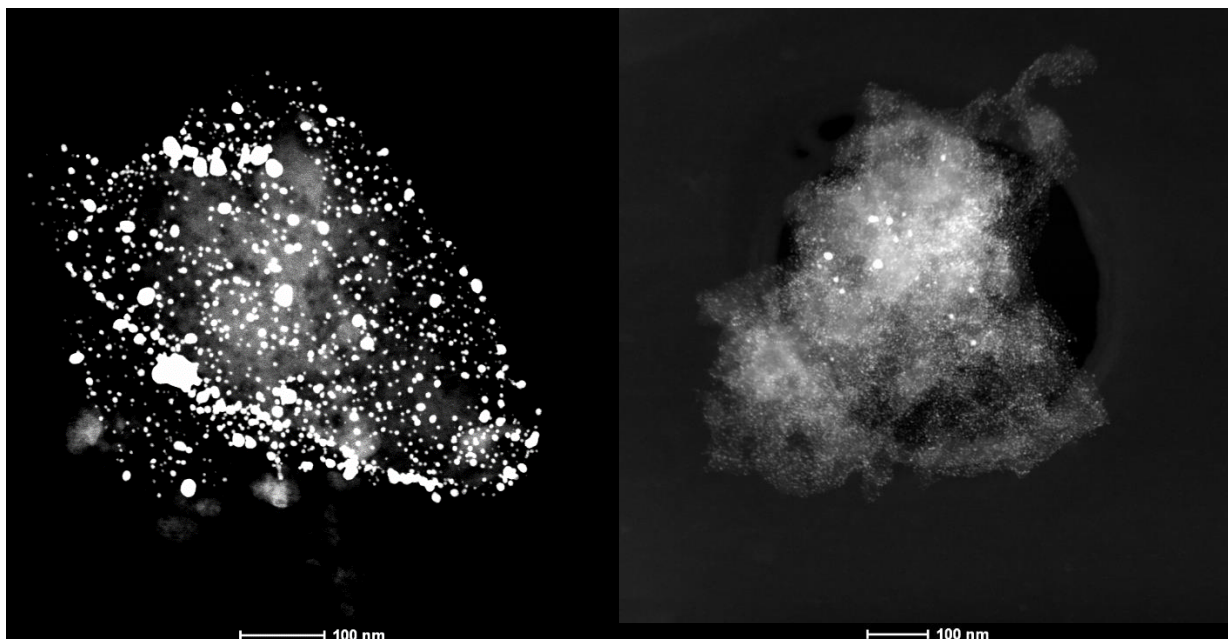


Figure 4.7: Histograms of particle size of Au/AC PVA0- Au/AC PVA0.6 and Au/AC PVA2.4. STEM-HAADF analysis of Au/AC PVA0 and Au/ACPVA2.4

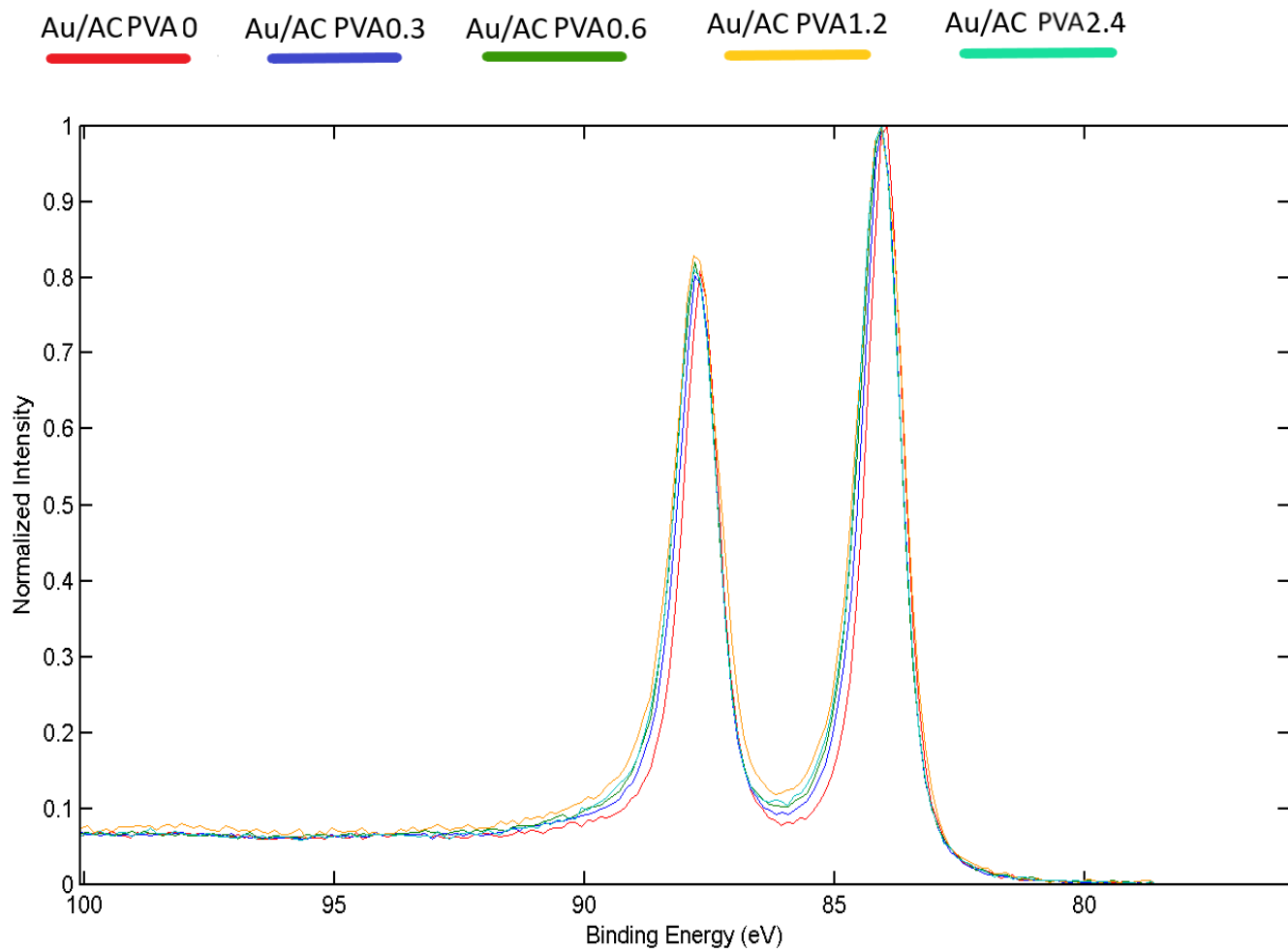
Figure 4.7 shows the STEM-HAADF analysis of AuPVA0, Au PVA0.6, and AuPVA2.4. In particular, TEM analysis is based on a statistical analysis of the number of Au nanoparticles that were counted to calculate the mean particle size and particle size distribution on specific areas of the sample analyzed; instead, XRD analysis measures a mean crystallite size given by all nanoparticles in conjunction, with limitations of the sensitivity of this technique below 3 nm. Both values are valid, and they can provide a very good idea of the mean particle size of NPs on the support. If we compare the results, the dimensions obtained with the XRD analysis are in good agreement with the one calculated with the TEM, confirmed the method validity and the Scherrer equation applicability (Table 4.2). Moreover, the STEM is useful to find other information, like the NPs dispersion on the support. If we compare the STEM analysis of Au/AC PVA0 with Au/AC PVA2.4, it could be noticed that sample Au/AC PVA0 shows the presence of large nanoparticles and agglomeration of Au nanoparticles possibly due to poor dispersion onto the support. On the other hand, Au/AC PVA2.4 shows fewer agglomerate particles and a good distribution on the surface, showing that the stabilizing agent is necessary to obtain small and well-distributed nanoparticles on the surface of the support. In the end, these analysis confirm the trend already observed by XRD analysis: the stabilizing agent helps the formation of small nanoparticles, avoiding the agglomeration and the aggregation during the preparation method; the higher is the amount of PVA, the smaller is the

mean particle size of the Au nanoparticles. Bigger Au nanoparticles for the sample without stabilizing agent and areas where agglomeration of Au nanoparticles was observed.

Catalyst	Mean crystallite size (nm) by XRD	Mean particle size (nm) by TEM± Standard Deviation
Au/AC PVA0	6.4	7.9 ± 6.3
Au/AC PVA0.3	3.6	4.3 ± 3.6
Au/AC PVA0.6	3.1	2.7± 1.6
Au/AC PVA1.2	2.6	2.6 ± 2.1
Au/AC PVA2.4	2.2	2.4 ± 1.2

Table 4.2: Comparison between Au/AC nanoparticles size by XRD and TEM analysis

The XPS technique, as a surface sensitive technique, could help to understand better other characteristics of the catalyst preparation, since the oxidation state of the metal and the surface coverage could be determined.



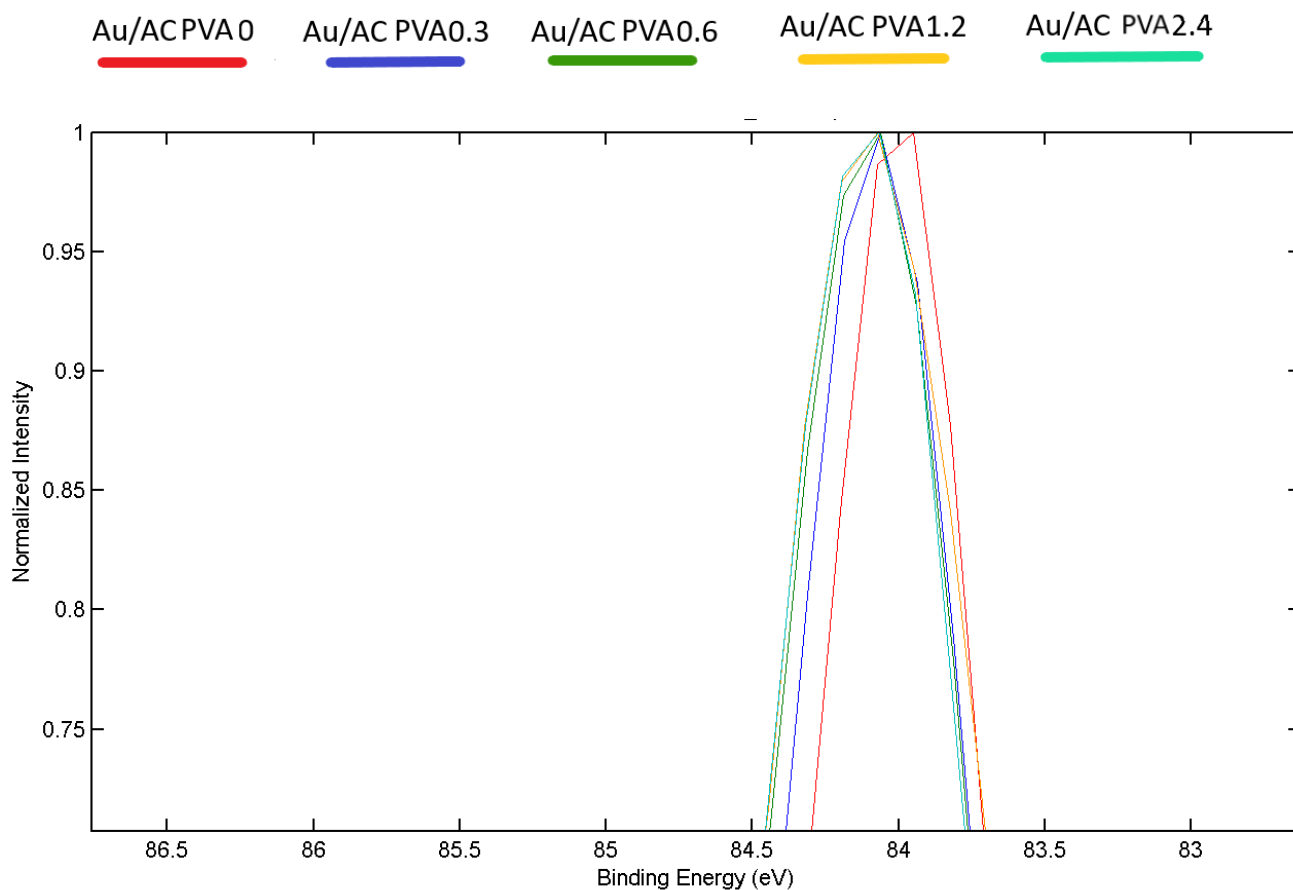


Figure 4.8: XPS spectra of Au4f $_{7/2}$ and Au4f $_{5/2}$ for Au/AC PVA series; zoom on the Au4f $_{7/2}$ peaks

Samples	BE Gold [eV]
Au/AC PVA0	84.0
Au/AC PVA0.3	84.1
Au/AC PVA0.6	84.1
Au/AC PVA1.2	84.1
Au/AC PVA2.4	84.1

Table 4.3: Binding energy value of Au4f $_{7/2}$ for Au/AC PVA series

In Figure 4.8 are reported the two signals for the Au (4f) peaks, (Au4f $_{7/2}$ (low energy line), Au4f $_{5/2}$ (high energy line) with an area ratio of 3/4. The determination of the oxidation state of the gold presence on the surface of the catalyst could be carried out by analyzing the peak of the gold: in particular, the binding energy position (84 eV, Table 4.3) and the slight asymmetry of the peaks suggest the presence of Au(0)¹²¹ (there is no contribution of Au⁺ and Au³⁺ that would give a peak at

84.7 eV and 86 eV respectively) and indicate the presence of Au nanoparticles in metallic state. Moreover, the values of Au on the surface and the surface atomic ratio Au/C for this series of samples are reported in Table 4.4. The XPS technique is a surface sensitive analysis and this is why the percent of gold is higher than the metal loading (depends on metal particle size and also depends on the porosity of the support and the location of metal nanoparticles on the surface and within the pores of the supports). Analyzing the trend for the Au% and the surface atomic ratio Au/C, it can be seen two different trends (Figure 4.9): the particle size decrease from 7.8nm (Au/AC PVA0) to 4.3nm (Au/ACPVA0.3) was accompanied with an increase of the surface atomic ratio Au/C (from 0.028 to 0.039) and the amount of gold on the surface (from 2.6% to 3.5%). However, even if the dimension continues to decrease with a higher amount of stabilizing agent (2.4nm for Au/AC PVA2.4), the surface atomic ratio Au/C and the Au % decrease (for Au/AC PVA2.4 the values are 1.8% 0.022 respectively). In the beginning the decrease of particle size increase the Au surface available; however, for Au/AC PVA 0.6, Au/ACPVA1.2 and Au/ACPVA2.4 the trend changed completely. A possible reason could be that higher amount of PVA could cover the surface of the metal that goes from 3.5% for the Au/AC PVA0.3 to 1.8% for Au/ACPVA2.4. Moreover, smaller nanoparticles can be within the pores of the support; the analysis carried on the AC shows a total pore volume equal to 0.6686 cm³/g, the presence of micro pore (V=0.3563 cm³/g) and also meso-macro pore (V= 0.2846 cm³/g). The pore diameter range for this last type is between 2-300 nm, therefore it is possible that small nanoparticles could be inside the pore, giving lower the surface Au coverage in agreement with previous reports and with literature.^{122, 123}

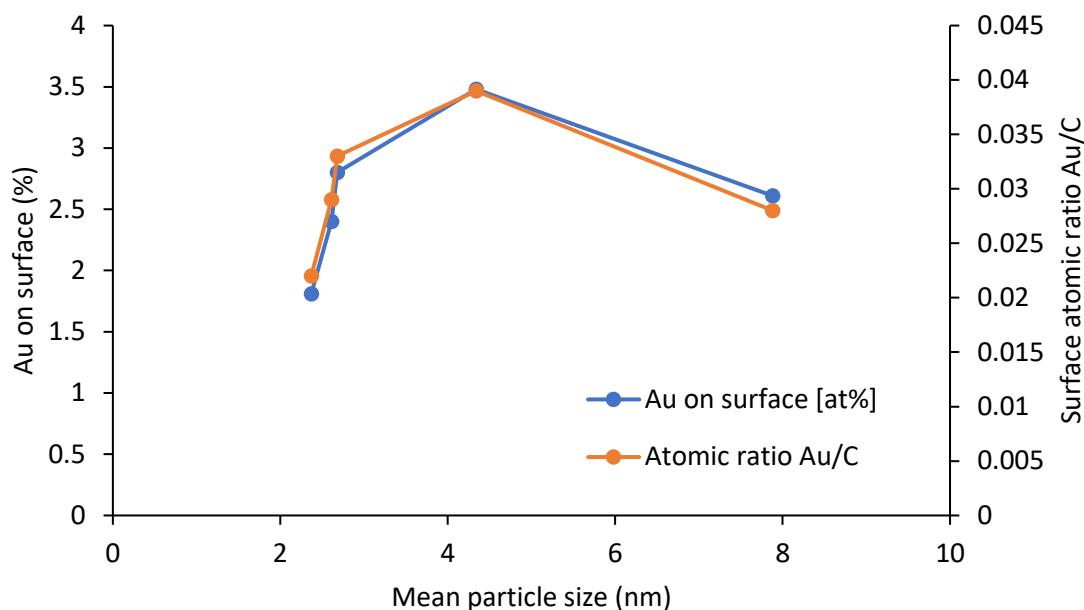


Figure 4.9: Atomic percentage of Au on surface and surface atomic ratio Au/C in function of the mean particle size for Au/AC PVA series

Samples	BE Gold (eV)	Au on surface (at%)	Surface atomic ratio Au/C	Mean particle size (nm) (TEM)
Au/ACPVA0	84.0	2.6	0.028	7.9
Au/ACPVA0.3	84.1	3.5	0.039	4.3
Au/ACPVA0.6	84.1	2.8	0.033	2.7
Au/ACPVA1.2	84.1	2.4	0.029	2.6
Au/ACPVA2.4	84.1	1.8	0.022	2.4

Table 4.4: Binding energy value of Au4f_{7/2}, gold atomic percentage on surface, surface atomic ratio Au/C and mean particle size for Au/AC PVA series.

To obtain an analysis on the relative content and amount of PVA covered the Au surface and support (we can't differentiate the quantity of PVA that covers Au and support) and to investigate the blocking action of the polymer, the surface atomic ratio Au/C measured by XPS was reported as the function of the PVA amount (Figure 4.10). It is possible to observe an initial increase in the Au/C atomic ratio from Au/AC PVA0 to Au/AC PVA0.3 (from 0.028 to 0.039), then the value drops until 0.022 for Au/AC PVA 2.4. The main reason could be that the decrease of mean particle size causes an initial increase of the atomic ratio Au/C but at a higher amount of PVA may cover the surface of gold nanoparticles, causing a decrease in the value (to notice that Au/AC PVA2.4 shows a lower

value of Au/C surface atomic ratio than Au/AC PVA0). The observed trend confirms the previous hypothesis.

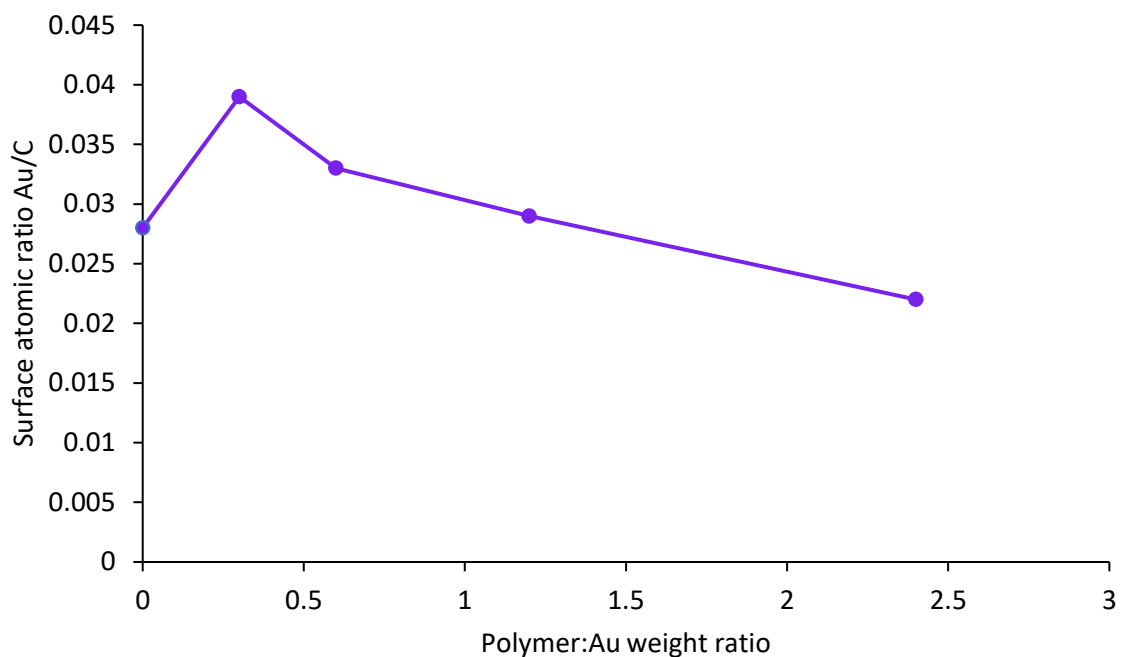


Figure 4.10: Correlation between surface atomic ratio Au/C and the polymer: Au weight ratio for Au/AC PVA series

Moreover, the observation of the peak in Figure 4.12 corresponding to C_{1s} reveals the presence of a shoulder around 286 eV that become more intense when the PVA amount increase. The presence of more OH group due to the higher amount of polymer make increase the contribution of C-O, which correspond to the peak at ~ 285.6 eV. The not total hydrolyzation of the PVA used and, consequently, the presence of an acetate group, make increase slightly the peak at ~ 286.6 eV, obtained from the C=O group (Figure 4.11 shows the different C contribution described).

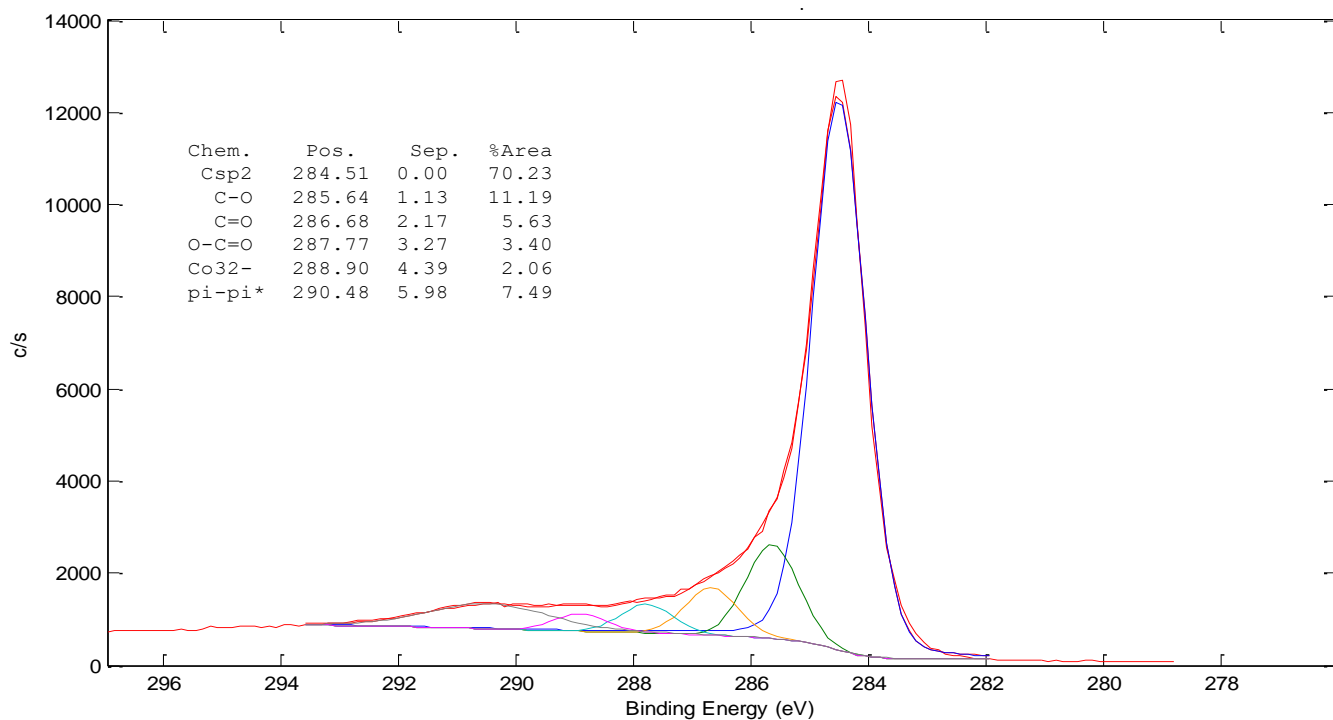


Figure 4.11: Example of deconvolution for XPS spectra of C_{1s} for active carbon

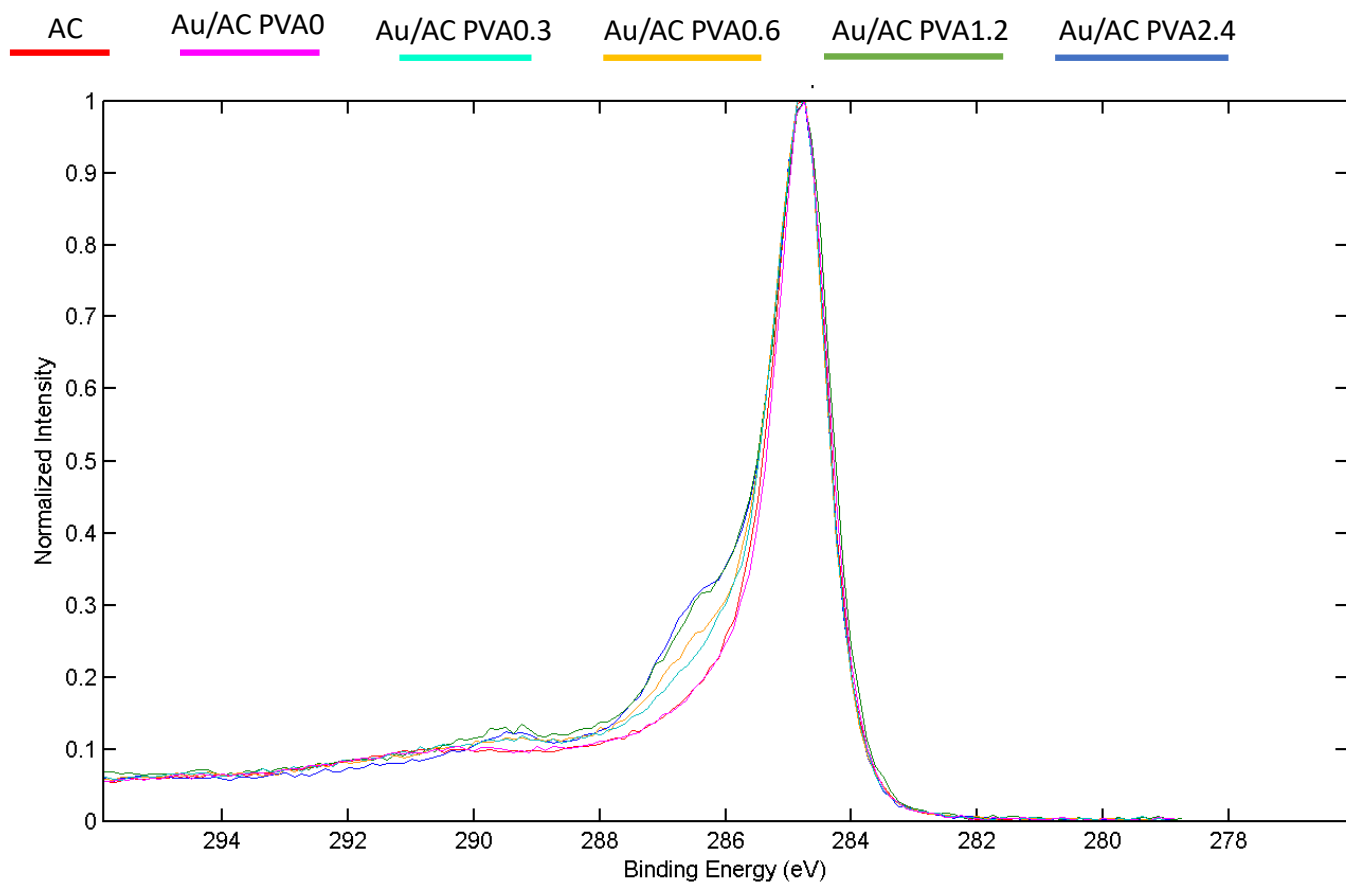


Figure 4.12: XPS spectra of C_{1s} for Au/AC PVA series

4.3 Preparation Method: Effect of heat treatment and washing step on the Au NPs

The research of a reliable methodology to remove the excess of stabilizing agent from the surface of metal nanoparticles and the support is appealing, therefore two different experimental approaches to remove the PVA stabilizer from the active sites of gold nanoparticles and the catalyst surface were tested. The first one provides the addition of a washing step at 60°C after the overnight drying step (Method C). Theoretically, the hot water helps to solubilize the excess of PVA in the catalyst and avoid or minimizes the aggregation of the nanoparticles thanks to the mild conditions used. The other method used is a heat treatment on the final catalyst (Method B). The idea is to modify the conformation of the polymer and maybe to remove partially the PVA from the surface through decomposition. Mainly, the treatment was carried out with a flow of oxygen and in a range of different temperatures were chosen based on the fact that the decomposition temperature of PVA is around 250°C, (120-200-250°C). Therefore, the main idea is to use a mild heat treatment where the PVA can be removed effectively without a significant agglomeration or aggregation of Au nanoparticles.

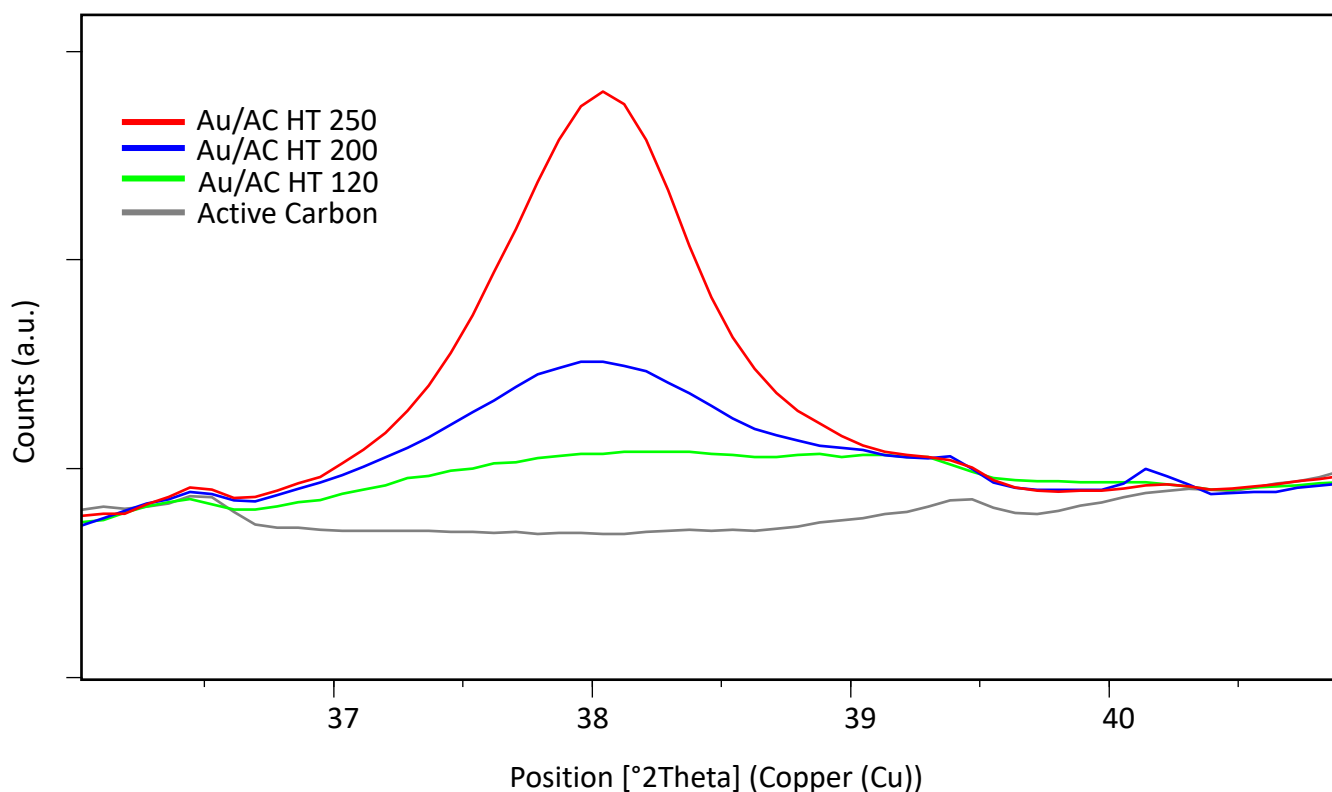


Figure 4.13: XRD patterns of active carbon, Au/AC heat treated samples

The heat treatment of the catalyst with high temperature, especially over 300 °C can lead to the agglomeration of the nanoparticles present on the surface, especially when weak metal-support interactions exist, as in the case of activated carbon materials. It is well known that the metal-support interaction is stronger in the case of metal oxides as the chosen supports, like TiO₂, ZrO₂, CeO₂, etc.¹²⁴ To check the thermal stability of gold nanoparticles, XRD analyses were carried out for each sample and the XRD patterns were used for calculating the mean crystallite size based on the Scherrer equation. The width of the XRD pattern (Figure 4.13) decreases when the heat treatment temperature increase, so the crystallite size increase; the application of the Scherrer equation confirms that the interaction with carbon as the chosen support isn't enough strong to avoid the aggregation and an increase of the dimension of nanoparticles. Indeed, the value increases from 3.1 nm for the sample not treated to 7.5 nm for Au/AC HT250, doubling the crystallite size of Au (Table 4.5). To see if the results obtained have the same trend, TEM analyses were carried out on the samples. The mean particle size calculated from TEM analysis are reported in Table 4.5 and confirms the NPs dimension trend. Moreover, the increase of the temperature leads a larger particle size distribution: the standard deviation pass from 1.6 for Au/AC no treated to 4.1 for Au/AC HT250.

Catalyst	Mean crystallite size (nm) by	Mean particle size (nm) by
	XRD	TEM ± Standard Deviation
Au/AC no treat	3.1	2.7 ± 1.6
Au/AC HT120	2.9	4.2 ± 2.3
Au/AC HT200	4.1	4.9 ± 2.9
Au/AC HT250	7.5	5.8 ± 4.1

Table 4.5: Crystallite size and mean particle size diameter of Au/AC heat-treated obtained by XRD analysis and TEM analysis

A further important observation to emphasize is the dispersion of Au nanoparticles as a function not only of Au nanoparticle size but also as a function of PVA: Au weight ratio. If we compare the STEM analysis of Au/AC PVA0 with Au/AC HT 250 (Figure 4.14), it can be noticed that even if the dimensions of the nanoparticles are similar, the presence of PVA in Au/AC HT250 guaranteed a well distribution of gold even after an high-temperature treatment.

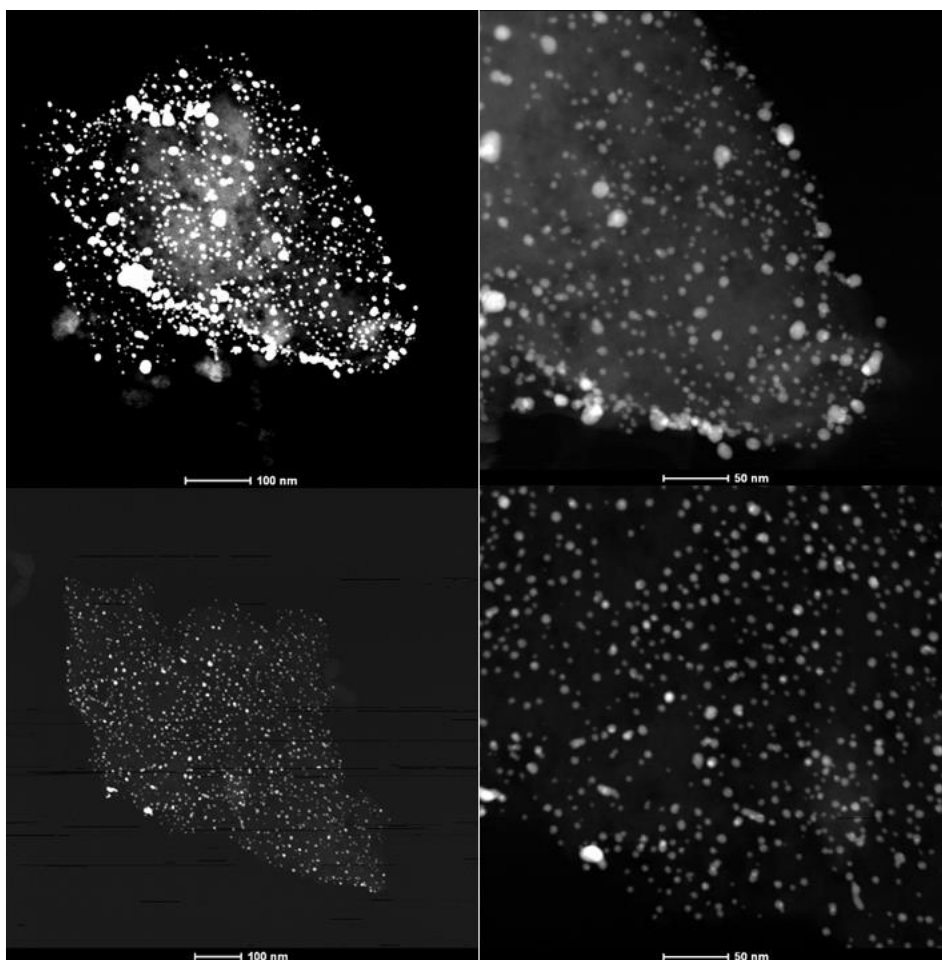


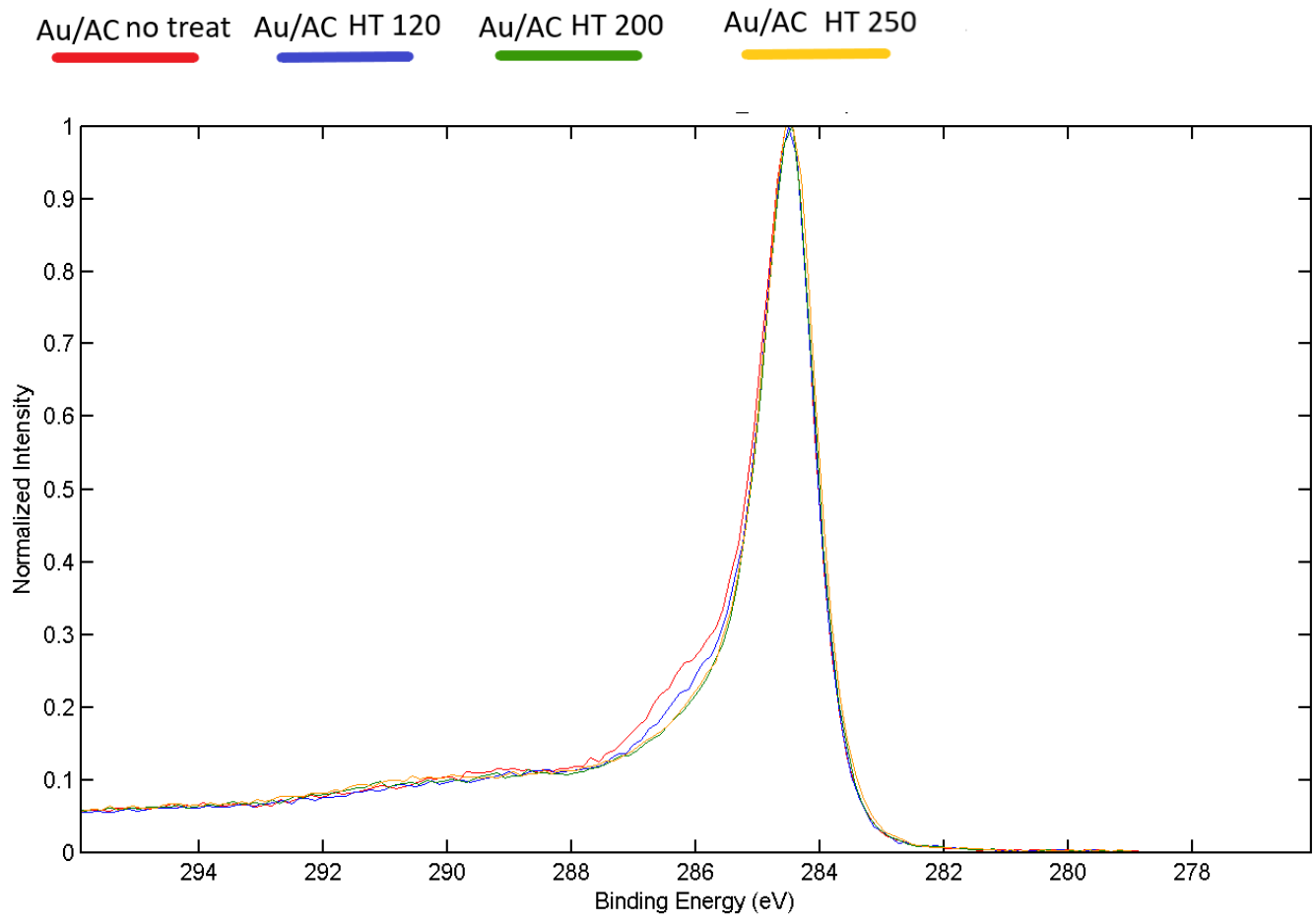
Figure 4.14: STEM analysis and comparison between Au/AC PVA0 (figures above) and Au/AC HT250 (figures below)

Moreover, the XPS data give us more information about the effectiveness of the chosen heat treatment. In particular, from Table 4.6 below, it can be noticed that the surface atomic ratio Au/C of the no treated sample and Au/AC HT120 can be considered equal even if the dimensions of the nanoparticles are different (2.7nm vs 4.2nm). This result could be ascribed to a partial removal and/rearrangement of the polymer on the surface of the metal and support. However, the increase of the temperature leads to an increase of the nanoparticles dimension, with a significant decrease of the Au content on the surface (from 2.8% for Au/AC HT120 to 1.1% for the Au/AC HT250).

Samples	Au on surface (at%)	Surface atomic ratio Au/C	Mean particle size (nm) (TEM) ± Standard Deviation
Au/AC no treat	2.8	0.033	2.7 ± 1.6
Au/AC HT120	2.8	0.032	4.2 ± 2.3
Au/AC HT200	2.7	0.029	4.9 ± 2.9
Au/AC HT250	1.1	0.012	5.8 ± 4.1

Table 4.6: Au atomic percentage on surface, surface atomic ratio Au/C and mean particle size for Au/AC HT series

As it has already been done for the Au/AC PVA series, the comparison between the XPS C1s signal of this type of catalyst could give some suggestions about the effective removal of the stabilizing agent. As it could be seen from Figure 4.15, the red curve represents the sample without any treatment and the C=O and C-O contributions around 287eV due to the presence of PVA are well visible. When the heat treatment was carried out at 120 °C, this shoulder starts to decrease (blue curve) and this contribution is quite low for the Au/AC HT 200 and Au/AC HT 250 (green and yellow curve respectively). From this comparison seems that the amount of stabilizing agent has decreased on the surface as a function of heat treatment.



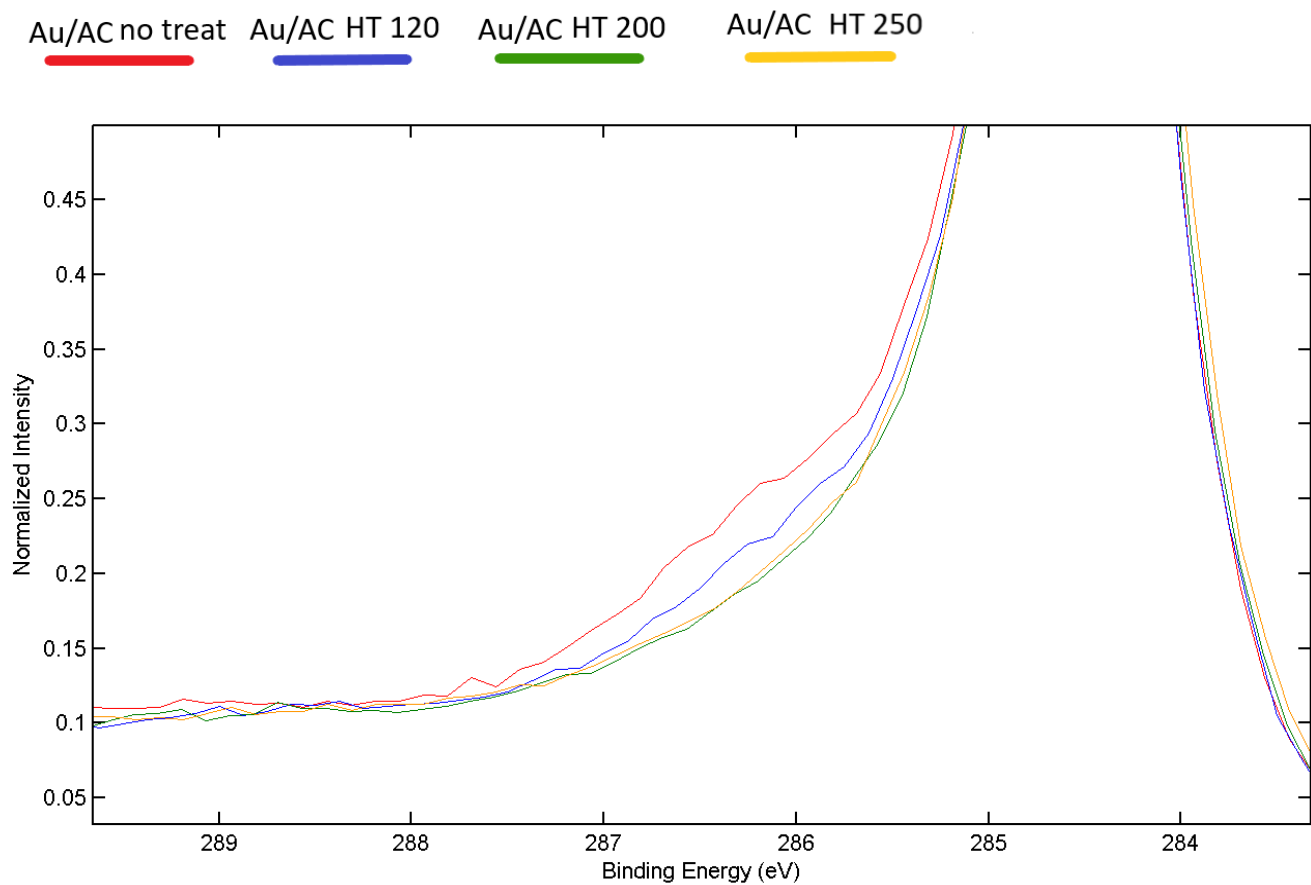


Figure 4.15: XPS spectra of C_{1s} for Au/AC HT series

4.4 Preparation Method: Choice of stabilizer, PVA vs PVP and PEG

The change of the polymer used as a stabilizing agent could affect the characteristics of the Au NPs present on the catalyst. In this work, it was decided to compare three different polymers with different characteristics (as it was explained in Chapter 1): Polyvinylpyrrolidone (PVP), Polyethylene glycol (PEG), and Polyvinyl alcohol (PVA). The weight ratio of stabilizing agent: Au was kept 0.65 for all the materials to compare the final morphology of the catalyst and their catalytic behavior.

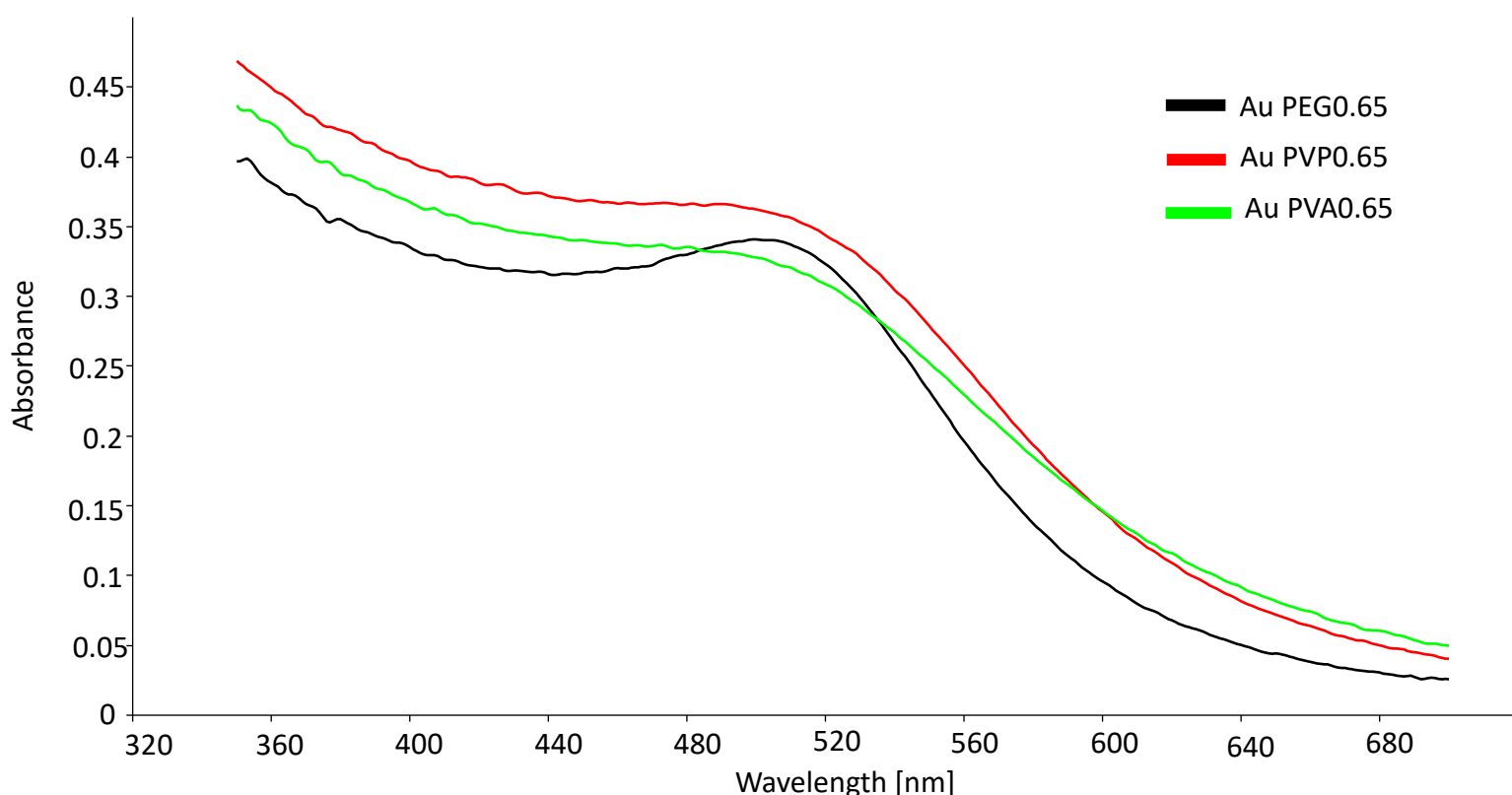


Figure 4.16: UV-Vis spectra for AuPVA0.65, AuPVP0.65 and AuPEG0.65 after 25min from the NaBH_4 addition

As it has already been done for the PVA series, the UV-Vis spectroscopy could be useful to have structural information about the dimension NPs range and the effectiveness of the polymers; this could be done by comparing the position and the shape of the surface plasmon resonance peak. From the UV-Vis spectra for the synthesized Au colloidal nanoparticles by varying the nature of the stabilizer (Figure 4.16), the most remarkable difference is in the PVP colloidal Au solution. Indeed, the Au colloidal nanoparticles capped with PVP as the chosen stabilizer, surface plasmon resonance peak appeared sharper than the PEG and PVA solution, suggesting the formation of bigger nanoparticles. However, as it has already been seen in the PVA series, from UV-Vis spectroscopy it

is not possible to define a precise size from the value of λ . After this evaluation, the gold NPs were immobilized following Method D (see Chapter 2). To confirm the trend observed and to verify if the immobilizing step affects the mean crystallite/particle size, XRD analysis on the final catalyst was carried out. The XRD pattern and the Scherrer equation confirm the presence of larger nanoparticles using the PVP as polymer, indicating a crystallite size of Au around 6 nm (see Table 4.7). Despite the colloidal result, also the PEG leads to the formation of larger nanoparticles, with a crystallite size around 6nm similar to the result obtained with PVP. The comparison of the values suggests that the PVA is the best stabilizing agent at the chosen experimental conditions, giving the smaller mean crystallite size obtained (3.1 nm).

Sample	Mean crystallite size (nm)
Au/AC-PVA 0.65	3.1
Au/AC-PVP0.65	6.4
Au/AC-PEG 0.65	6.4

Table 4.7: Mean Au crystallite nanoparticle size calculated using Scherrer equation

To confirm the characterization data obtained from XRD, the TEM analysis was carried out to determine the mean Au nanoparticle size, and particle size distribution via the TEM micrographs. The results are reported below in Figures 4.17, 4.18, 4.19. The comparison between the three Au/AC functionalized with the different polymers shows that when we use PVA as the chosen stabilizer, the best result is obtained in terms of mean Au particle size and narrow particle size distribution and dispersion of the Au nanoparticles on the support. Indeed, it helps the formation of small nanoparticles (mean Au nanoparticle size of 2.7 nm for Au/AC PVA0.65 against 5.2 nm for Au/AC PVP0.65 and 5.5 nm for Au/AC PEG0.65). Moreover, if we compare the STEM analysis and the statistical particle size distribution it is noticeable how PVA and PVP (Figure 4.17 and Figure 4.18) allow a good dispersion and PEG (Figure 4.19) allow the formation of nanoparticles with different range of Au nanoparticles, therefore a broader particle size distribution.

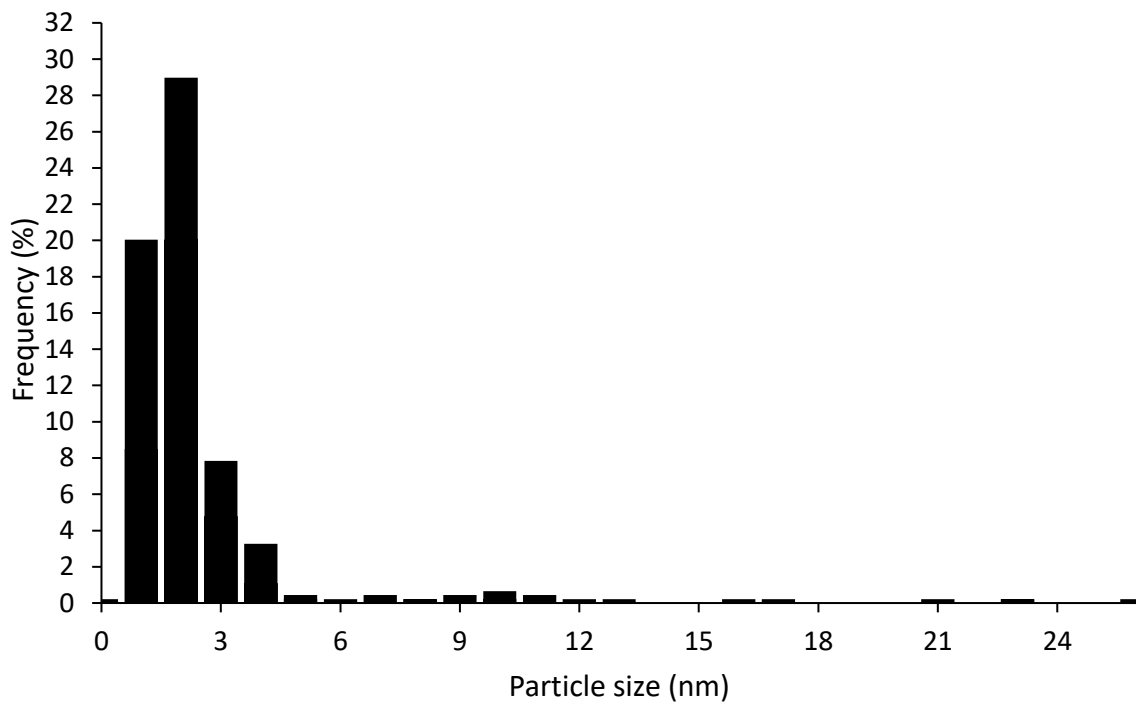
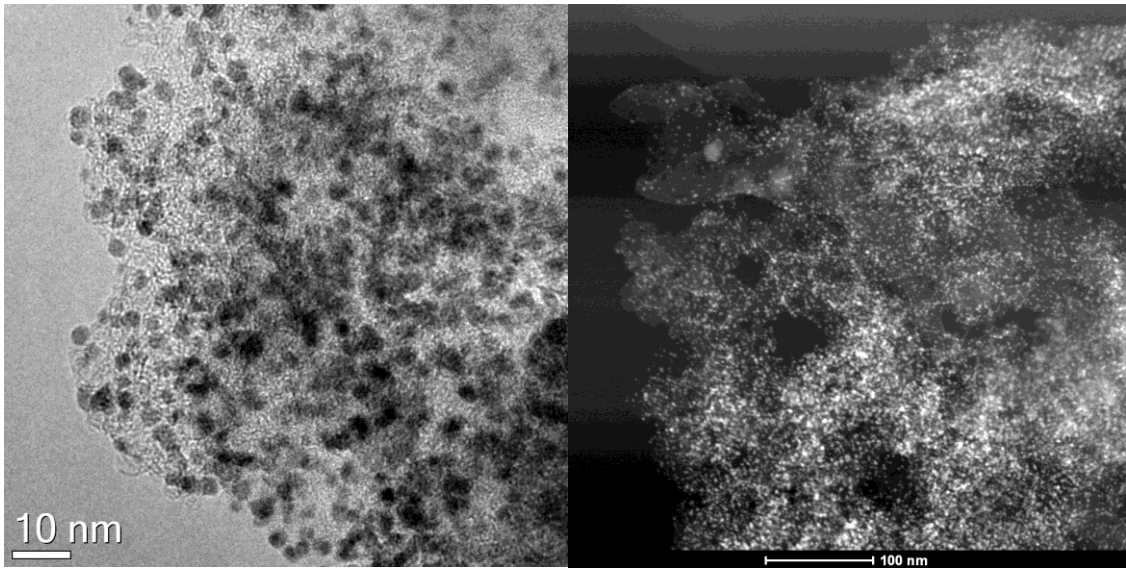


Figure 4.17: STEM/TEM analysis and histograms of particle size of Au/ACPVA0.65

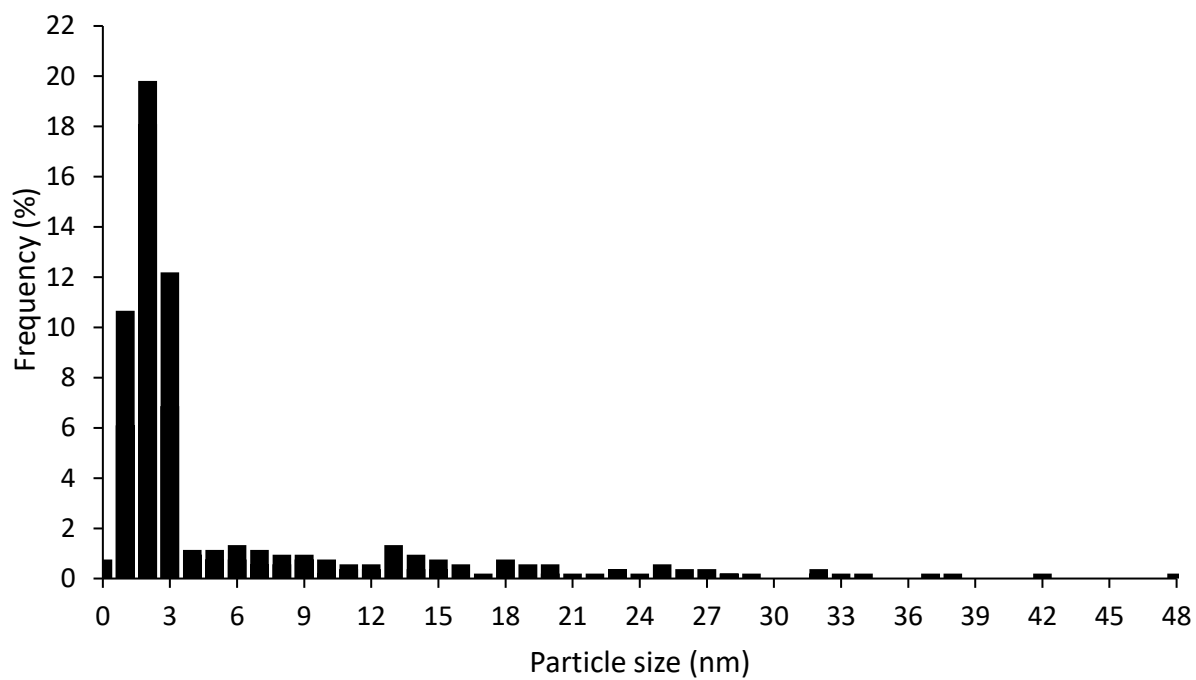
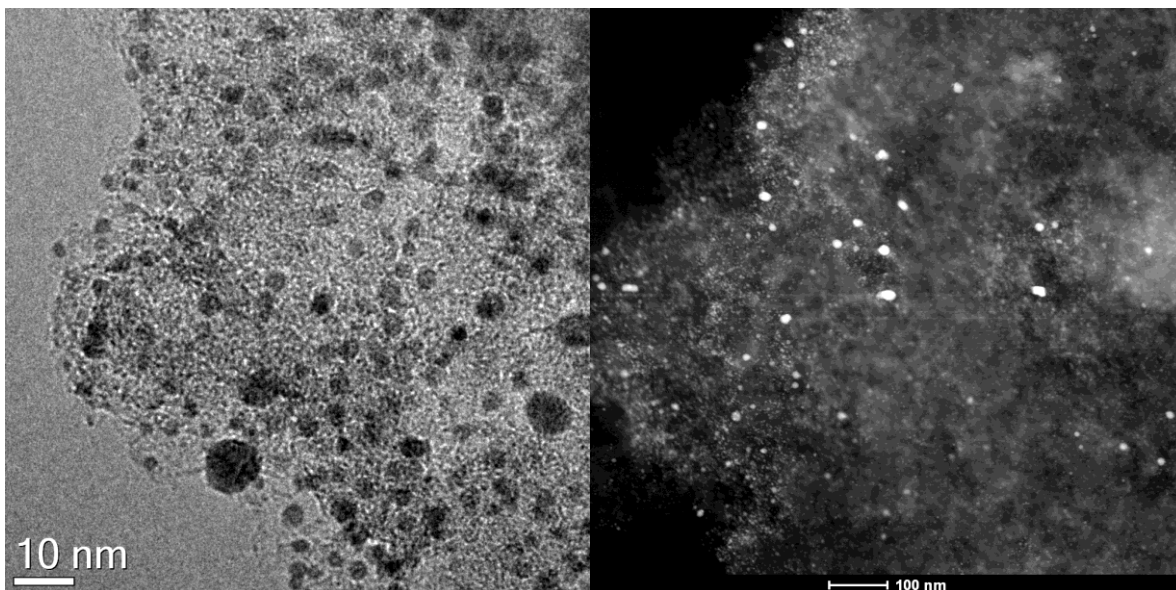


Figure 4.18: STEM/TEM analysis and histograms of particle size of Au/ACPVP0.65

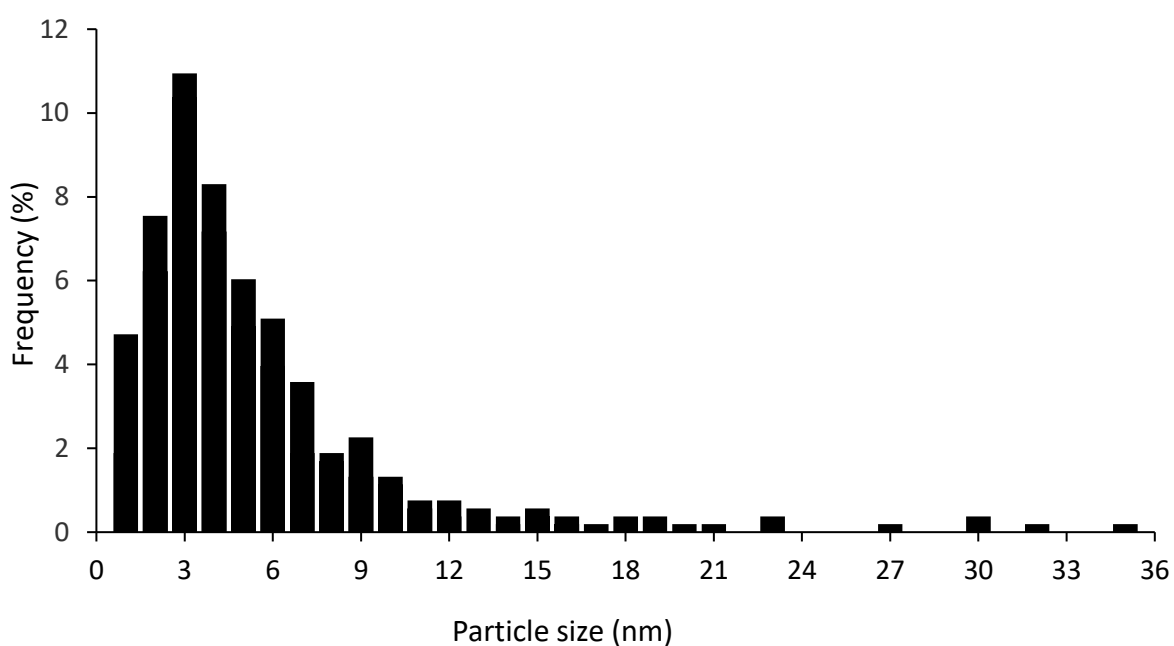
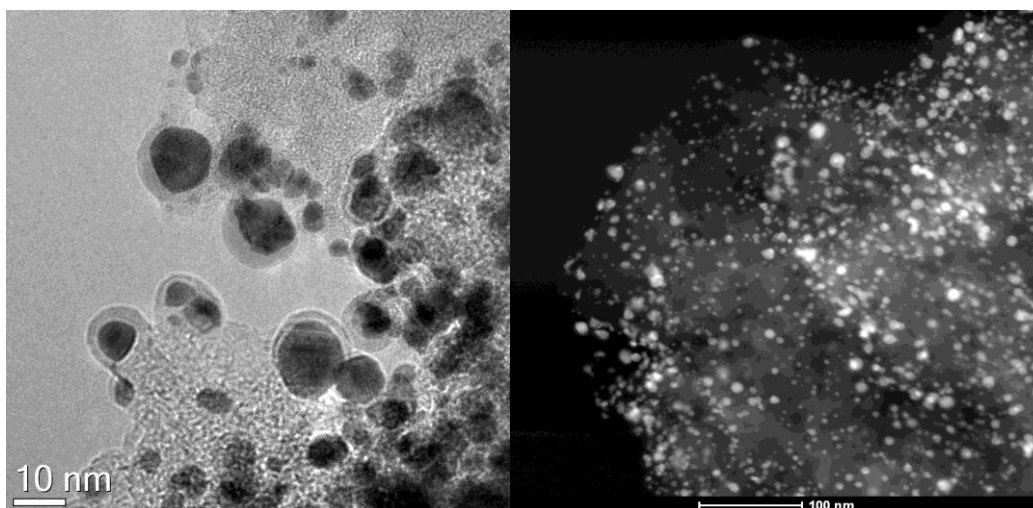


Figure 4.19: STEM/ TEM analysis and histograms of particle size of Au/ACPEG0.65

Sample	Mean crystallite size (nm) by XRD	Mean particle size (nm) by TEM ± Standard Deviation
Au/AC-PVA 0.65	3.1	2.7 ± 2.6
Au/AC-PVP0.65	6.4	5.2 ± 6.8
Au/AC-PEG 0.65	6.4	5.5 ± 4.3

Table 4.8: Mean crystallite size and mean particle size for Au/AC PVA0.65, Au/AC PVP0.65 and Au/AC PEG0.65

The mean particle size of Au obtained by TEM analysis (Table 4.8) shows that the same weight ratio polymer: Au did not permit to obtain similar nanoparticles dimensions. A deeper investigation is necessary to see if a higher amount of stabilizing agent is required and this is why it was decided to prepare Au/AC PVP and Au/AC PEG series with different weight ratio of polymer: Au.

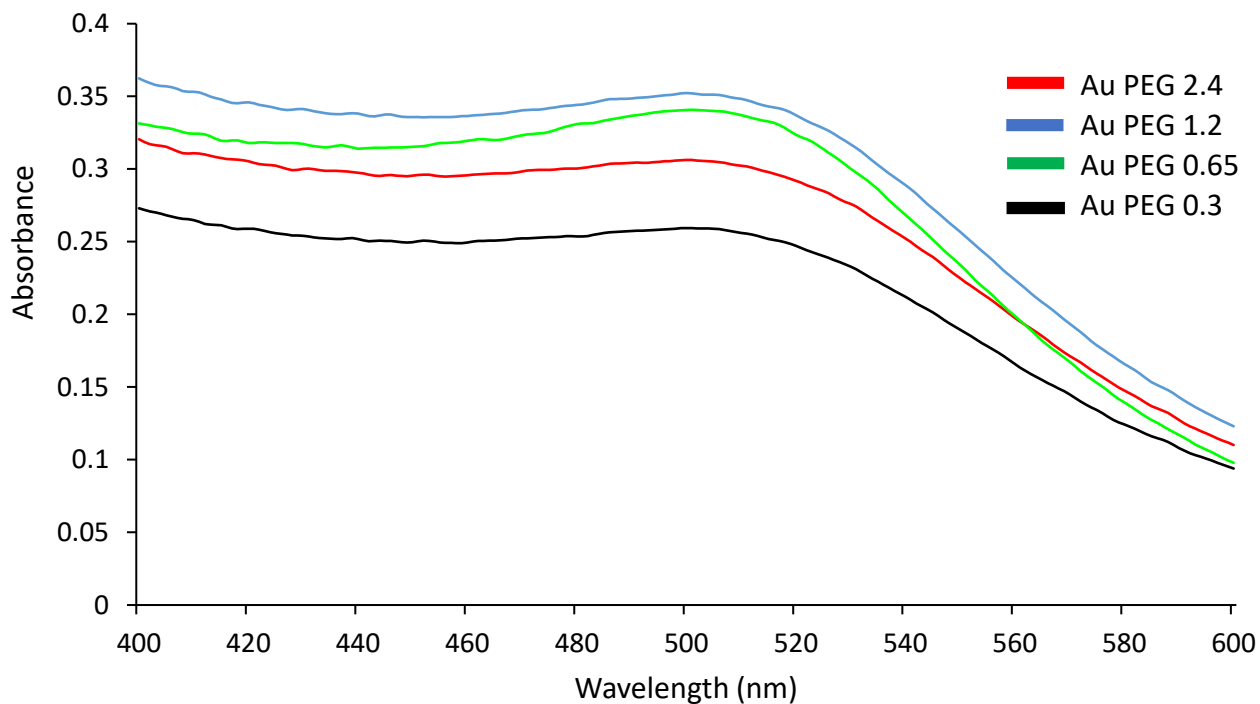


Figure 4.20: UV-Vis spectra for Au/AC PEG series after 25min from the NaBH_4 addition

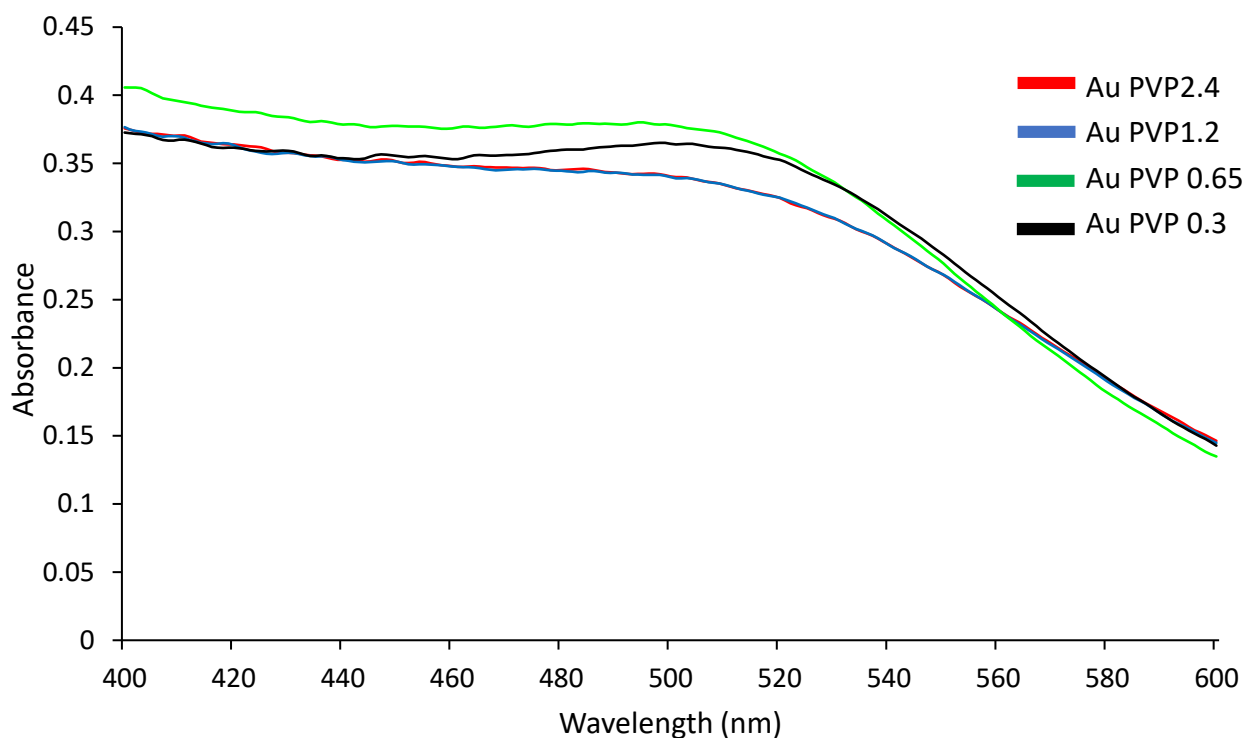


Figure 4.21: UV-Vis spectra for Au/AC PVP series after 25min from the NaBH₄ addition

Initially, the preparation step of the Au colloidal nanoparticles synthesized by PEG (Figure 4.20) and PVP (Figure 4.21) was followed by UV-Vis spectroscopy and all the colloidal solutions showed a surface plasmon resonance peak around 500 nm and, therefore, an indication of the formation of small nanoparticles. In Table 4.9 it is reported the λ_{\max} extract 25minute after the adding of the NaBH₄. For both series, big differences are not evident and the shift could be attribute to the instrumental error (± 2 nm): the Au nanoparticles stabilized by PVP gave a surface plasmon resonance which varies from 498 nm to 500 nm; the increase of PEG amount causes a slight decrease in the λ_{\max} from 503 nm to 501 nm.

PVP: Au weight ratio	λ_{\max} at 25 minutes (nm)	PEG: Au weight ratio	λ_{\max} at 25 minutes (nm)
0.3:1	498	0.3:1	503
0.65:1	500	0.65:1	503
1.2:1	497	1.2:1	502
2.4:1	497	2.4:1	501

Table 4.9: SPR peak values from UV-vis spectra for AuPVP and AuPEG series after 25 minutes from the addition of NaBH₄

However, the results show a quite different trend in comparison to the Au colloidal nanoparticles synthesized by PVA (see Section 4.2). In particular, PVP-stabilized Au colloids have generally broader UV-Vis peaks, except for the UV-Vis spectrum corresponding to the sample Au-PVP0.3 which seems sharper. The UV-Vis spectra of samples Au-PVP1.2 and Au-PVP2.4 are overlapping, suggesting that the preformed Au colloidal nanoparticles have similar dimensions. It can be further deduced that at an Au:PVP weight ratio of 1.2 the nanoparticle environment reached a maximum in PVP concentration and doubling the Au- PVP to 2.4 does not produce any significant size effect on the preformed Au nanoparticle.

Instead, for the Au-PEG series seems that Au-PEG 0.3 and 2.4 show the broadest peak of the series. However, to confirm the trend obtained from the UV-Vis spectra, it is necessary to collect the XRD patterns and calculate the mean crystallite size of Au of the supported colloidal nanoparticles.

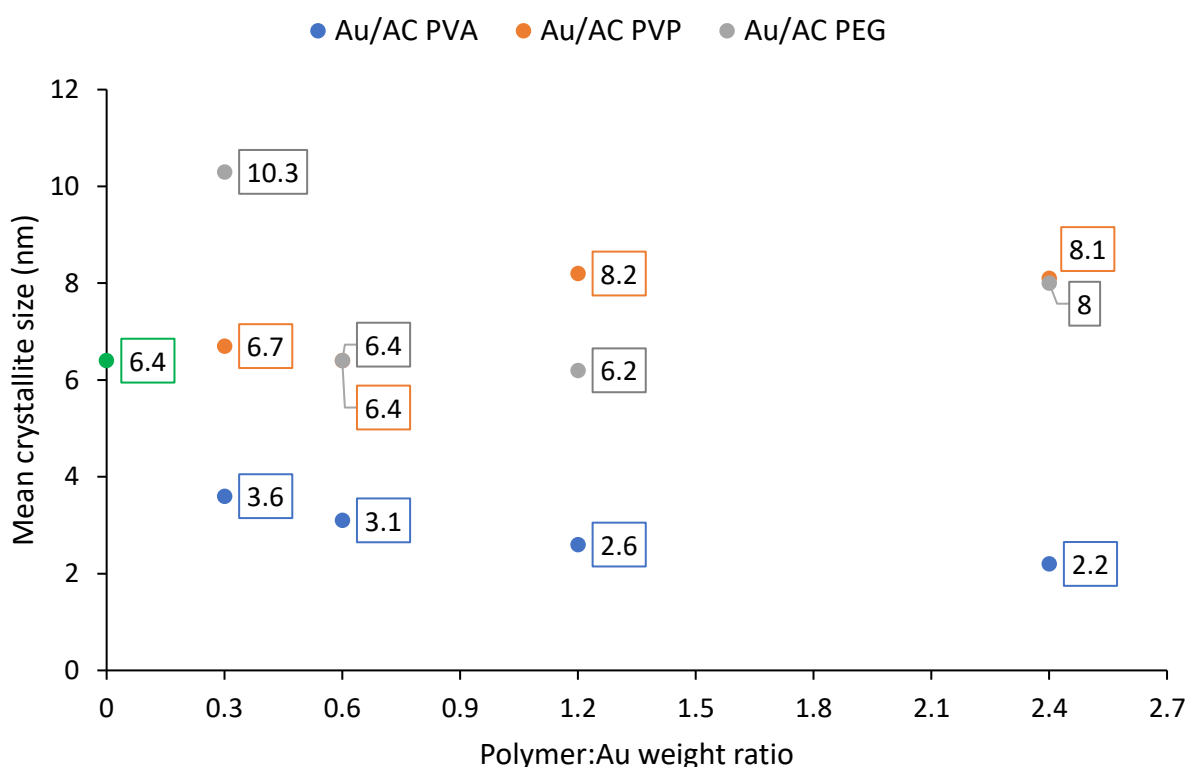


Figure 4.22: Mean crystallite size in function with the polymer: Au weight ratio for Au/AC PVA, Au/AC PVP and Au/AC PEG series

In Figure 4.22 are reported the mean crystallite size obtained with the different stabilizing agents as a function of stabilizer amount used during the synthesis. For the Au/AC PVP series, a weight ratio of Au to the chosen stabilizer of 0.3 and 0.65 does not affect the crystallite size for Au/AC (6.7nm for Au/AC PVP0.3 and 6.4nm for Au/AC PVP0.65); indeed, it appears similar to the value obtained

without a stabilizer agent (Au/AC PVA0 6.4nm). Moreover, the increase of PVP does not reduce the crystallite size, which reaches the value of 8.1 nm for Au/AC PVP 2.4.

The PEG behaves differently: it is observable that the increase of PEG from the ratio 0.3 to 0.65 leads to an Au crystallite size decrease from 10.2 nm to 6.4 nm, then remains stable doubling the PEG amount. In the end, the maximum amount of PEG leads to the formation of large Au particles with a value of 8.1 nm. As has already been seen in Section 4.2, by increasing the amount of PVA, the nanoparticles are better stabilized and lead to the formation of spherical Au particles. The PVP instead is required in small quantities to form the smallest nanoparticles because higher amounts lead to the formation of NPs with a higher dimension; instead, PEG acts as a good stabilizer only at an intermediated Au to PEG weight ratio. These data required further analysis by using TEM, however, it can be concluded that PVA seems the best polymer to form the smallest gold nanoparticles in this presented study.

To confirm the data obtained, in particular for the Au/AC PVP series, the TEM analysis was carried out and Table 4.10 reports the comparison between these two trends.

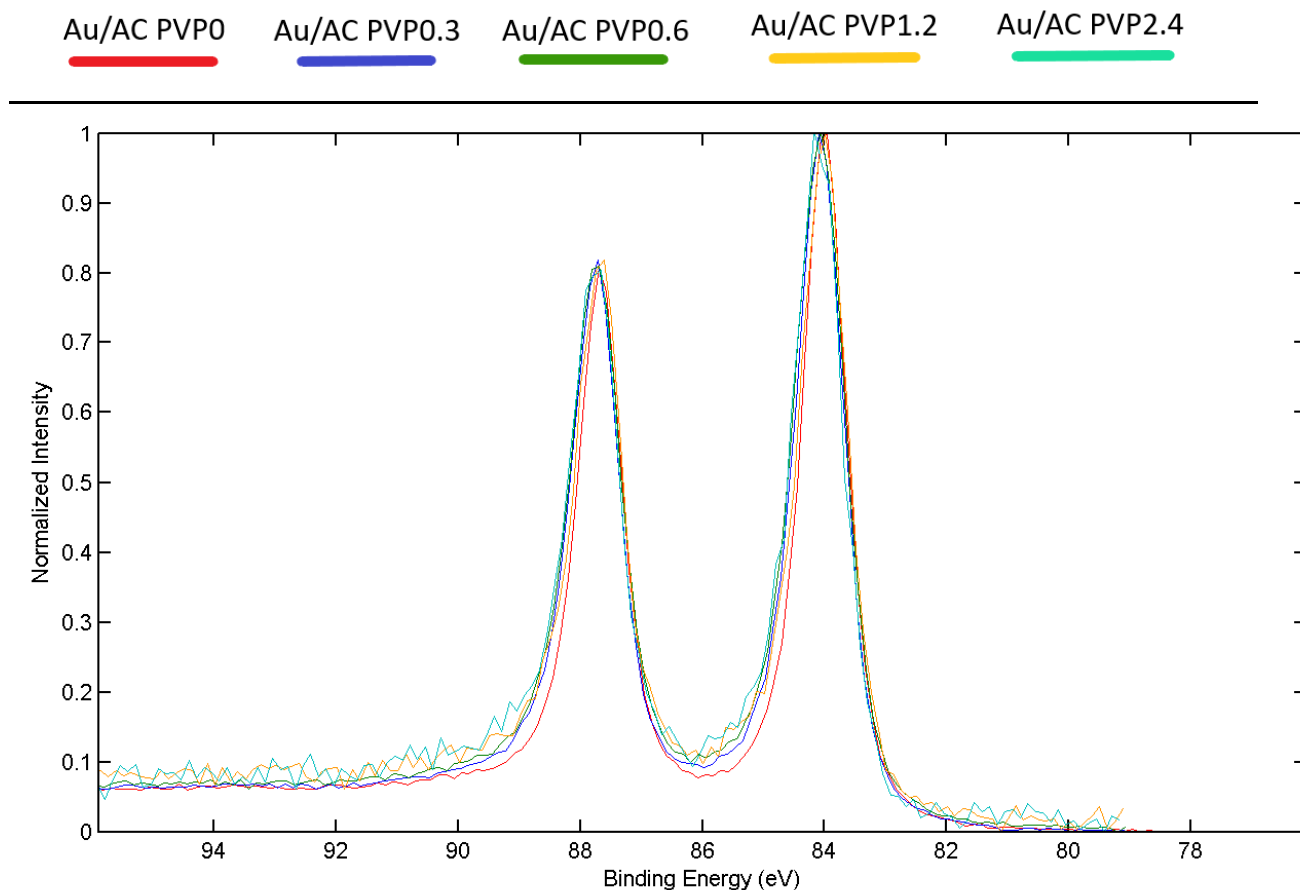
Catalyst	Mean crystallite size (nm) by XRD	Mean particle size (nm) by TEM± Standard Deviation
Au/AC PVP0.3	6.7	5.5 ± 3.6
Au/AC PVP0.6	6.4	5.6 ± 3.9
Au/AC PVP 1.2	8.2	7.4 ± 4.7
Au/AC PVP2.4	8.1	8.4 ± 4.9

Table 4.10: Mean crystallite size and mean particle size for Au/AC PVP series

The TEM data confirm the trend obtained with the Scherrer equation, suggesting that probably a small amount of PVP is required to form small and stable NPs with good dispersion on the surface of the support.

The use of PVP as a stabilizer agent could affect also the gold binding energy value; for example Behera and co-workers compared the Binding energy (BE) of a AuNPs solution and the BE of a AuNPs solution with PVP. They report a shift from 86.75eV to 86.23 eV (Au4f_{5/2} signal for AuNPs and AuNPs with PVP) and they attribute this behaviour to the interfacial interaction between the Au NP and

PVP molecule.¹²⁵ However, for the Au/AC PVP series this shift is not so much marked and the polymer presence does not change the oxidation state of Au present: as it has already seen for the Au/AC PVA series, the binding energy of 84 eV (values reported in Table 4.11 below) and the asymmetrical shape of the peak (Figure 4.23) prove that for the Au/AC PVP series, gold is present only in the metallic state.



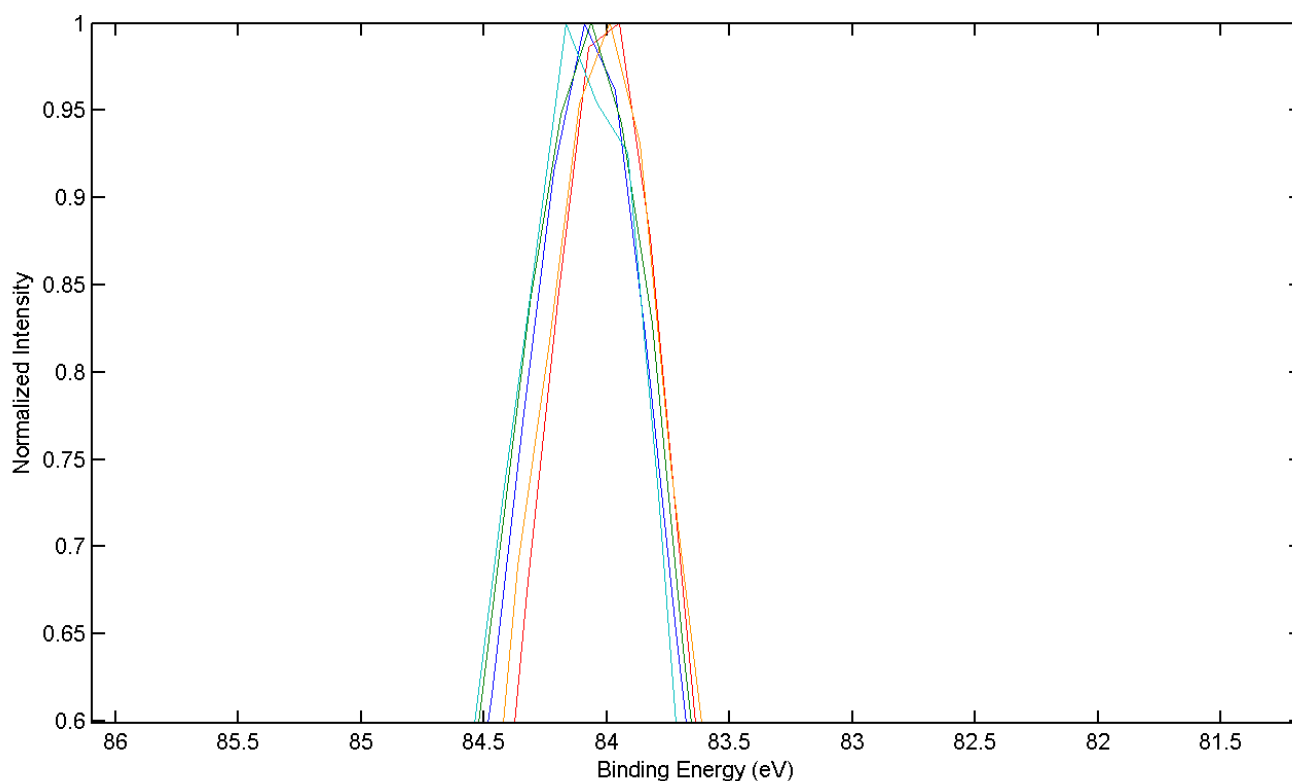


Figure 4.23: XPS spectra of Au4f $_{7/2}$ and Au4f $_{5/2}$ for Au/AC PVP series. Zoom on the Au4f $_{7/2}$ peak

The surface atomic ratio Au/C and the Au present in the surface follow the same trend for the Au/AC PVP series (Table 4.11 below): the samples without the stabilizer agent showed a 2.6% for the Au on the surface and a 0.028 in atomic ratio Au/C; just adding the lower amount of PVP, the gold available on the surface reduces until 1.4% and the surface atomic ratio Au/C reduces to 0.016. The lower value was reached for a higher amount of polymer used during the preparation method for Au/AC PVP2.4 the percentage of Au on the surface is equal to 0.1% and the surface atomic ratio Au/C is 0.0013). Two hypotheses could explain these trends: the increase of Au mean particle size proven with the TEM analysis could expose lower Au surface, therefore, decreasing the atomic ratio Au/C and the gold on the surface, as it was represented in Figure 4.24. However, the surface atomic ratio Au/C of Au/AC PVPO (0.028) and the samples Au/AC PVPO.3 (0.016) Au/AC PVPO.6 (0.013) suggest that the NP size is not the only factor and the increase of stabilizing agent can cover the Au surface.

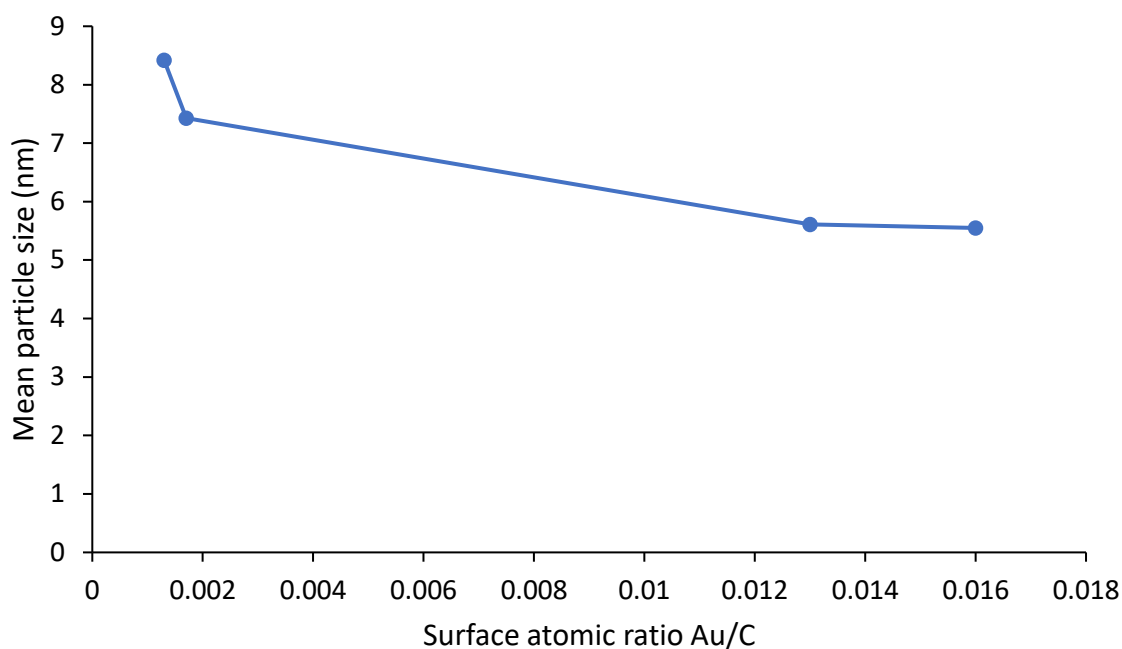


Figure 4.24: Correlation between mean particle size and surface atomic ratio Au/C for Au/AC PVP series

Samples	BE Gold [eV]	Au on surface [at%]	N on surface [at%]	Surface Atomic ratio Au/C
Au/AC PVPO	84.0	2.6	-	0.028
Au/AC PVPO.3	84.0	1.4	2.1	0.016
Au/AC PVPO.6	84.0	1.2	3.3	0.013
Au/AC PVP1.2	84.0	0.2	3.1	0.0017
Au/AC PVP2.4	84.1	0.1	3.6	0.0013

Table 4.11: Binding energy value of Au4f_{7/2}, gold atomic percentage on surface, nitrogen atomic percentage on surface, surface atomic ratio Au/C and mean particle size for Au/AC PVP series

Moreover, the nitrogen atom could be detected as N% on the surface and it can be an indicator of the amount of stabilizing agent present; the polymer chain is formed from monomers contained a 5-membered lactam group. Excluding Au/AC PVP1.2, the amount of nitrogen (see Table 4.11 above) due to the presence of lactam group in the PVP has a higher value from 2.1% to 3.6%, when the PVP amount has increased (Au/ACPVP0.3 and Au/ACPVP2.4 respectively). Further confirmation of the polymer presence arises from the C1s signal. From Figure 4.25 it could be seen that the shoulder at ~286 eV due to the C=O contribution, increase from Au/AC PVPO.3 to Au/ACPVP2.4, with an expectation on Au/ACPVP 1.2 that do not follow the trend.

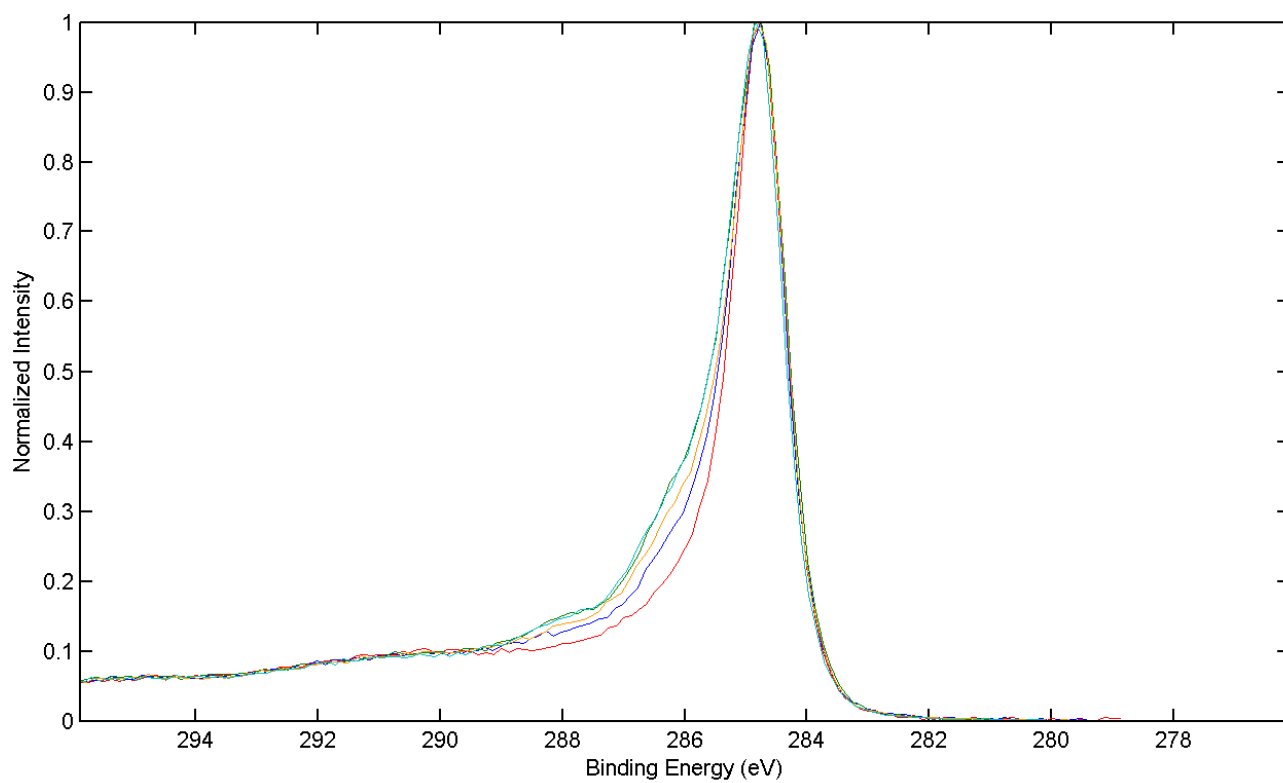
Au/AC PVP0

Au/AC PVP0.3

Au/AC PVP0.6

Au/AC PVP1.2

Au/AC PVP2.4



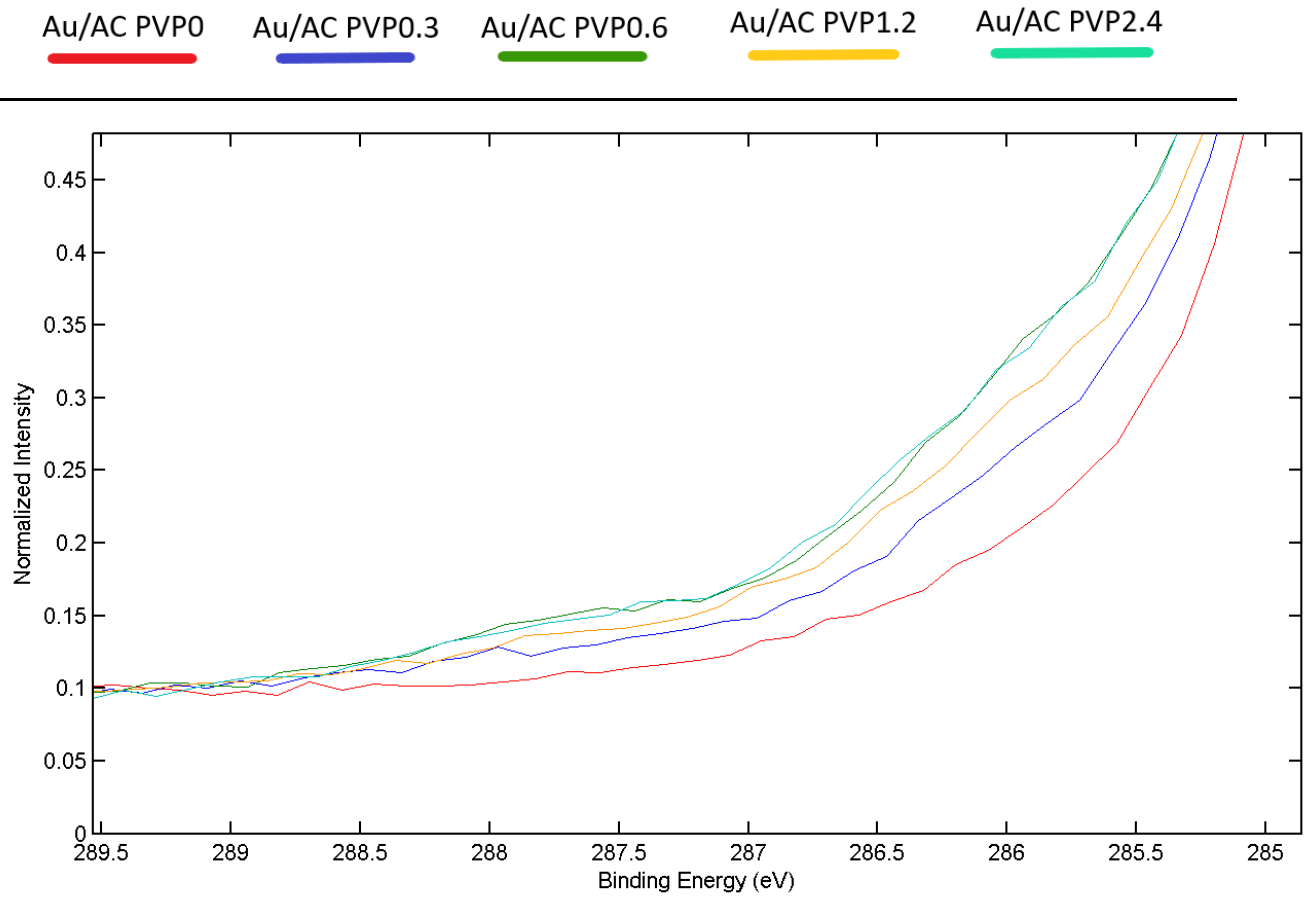


Figure 4.25: XPS spectra of C_{1s} for Au/AC PVP series

-
- ¹¹⁹ X. H. Mostafa, E. S. Mostafa, Gold nanoparticles: Optical properties and implementations in cancer diagnosis and photothermal therapy, *Journal of Advanced Research*, **2010**, 1(1):13-28
- ¹²⁰ W. Haiss, N. T. K. Thanh, J. Aveyard, D. G. Fernig, Determination of size and concentration of gold nanoparticles from UV-vis spectra, *Anal. Chem.*, **2007**, 79, 4215-4221
- ¹²¹<https://xpssimplified.com/elements/gold.php>
- ¹²² C. Bianchi, S. Biella, A. Gervasini, L. Prati, M. Rossi, Gold on Carbon: Influence of Support Properties on Catalyst Activity in Liquid-Phase Oxidation, *Catalysis Letters*, **2003**, 85, 1–2,
- ¹²³ C. Bianchi, F. Porta, L. Prati, M. Rossi, Selective liquid phase oxidation using gold catalysts, *Topics in Catalysis*, **2000**, 13, 231–236
- ¹²⁴ J. Engel, S. Francisa, A. Roldan, The influence of support materials on the structural and electronic properties of gold nanoparticles – a DFT study, *Phys. Chem. Chem., Phys.*, **2019**, 21, 19011-19025
- ¹²⁵ M. Behera, S. Ram, Spectroscopy-based study on the interaction between gold nanoparticle and poly(vinylpyrrolidone) molecules in a non-hydrocolloid, *Int Nano Lett*, **2013**, 3, 17

The reactor system doesn't allow for a continuous adjustment of the pH and the production of the acid molecule during reaction decrease this value. For this reason, it was decided to work with a high base excess, a condition that, however, promotes other side reactions, like the reaction of isomerization to fructose and mannose. This is why, even if the tests were carried on for a short time and with a small amount of catalyst, the reaction and the experiment set up do not permit to reach conversion lower than 80%, avoiding a good establishment of it.

Stirring rate (rpm)	Glucose conversion %	Gluconic acid yield %	Glucaric acid yield %	Isomers ^a yield %	Others ^b yield %
400	89	53	1	8	20
600	83	64	2	6	13
800	83	70	2	2	7
1000	87	53	15	1	18
1200	90	54	16	0	20

Table 5.1: Effect of stirring rate on glucose oxidation. Reaction conditions: 15 min, 60 °C, 10 bar O₂, Glu: Au: NaOH molar ratio of 1000:1:3000. ^a Isomers corresponding to fructose and mannose combined. ^b Other byproduct correspond to all the byproduct comes from C-C cleavage reaction and retroaldolic: Formic acid, Oxalic acid, Mesoxalic acid, Tartaric acid, Tartronic acid, Lactic acid, 2KDG, 5KDG, Glycolic acid, glycolic acid

However, from the data reported in Table 5.1 it can be noticed that by increasing the stirring rate (stirring rate can influence the presence of mass transfer limitations and to ensure perfect mixing and to avoid segregation of both fluid and solid catalyst) an increase of glucaric acid formation was observed and reached a plateau above 800 rpm (Glucaric acid yield 15%) indicating the stirrer speed at this range has a minor effect in the conversion of gluconic acid to glucaric acid and hence, the reaction is in kinetic regime. By accelerating the oxidation reaction, the competition with isomerization of glucose decreases dramatically to less than 1% of fructose and mannose, and no formation was detected at all at 1200 rpm. In fact, it is well-known that alkaline environment promotes higher yields to glucaric acid with noble metal nanoparticles but also accelerates the isomerization of glucose. This last reaction can be "switched off" by increasing the stirring rate. To corroborate this assumption and to calculate the number of isomers formed during the preparation of the solution in the reactor until it reaches the desired temperature, two experiments were set at time zero. Since glucose is a very reactive molecule, lower conversions are needed to study the

initial rate. The reaction mixture was set up at 1200 rpm or 0 rpm and stopped when it reached 60°C.

Stirring rate (rpm)	Glucose conversion %	Gluconic acid yield %	Glucaric acid yield %	Isomers ^a yield %	Others ^b yield %
0	43	1	0	26	10
1200	86	68	9	0	10

Table 5.2: Effect of stirring rate on glucose oxidation at time zero. Reaction conditions: 0 min (until the reaction reaches 60 °C), 10 bar O₂, Glu: Au: NaOH molar ratio of 1000:1:3000. ^aIsomers corresponding to fructose and mannose combined. ^bOther byproduct correspond to all the byproduct comes from C-C cleavage reaction and retroaldolic: Formic acid, Oxalic acid, Mesoxalic acid, Tartaric acid, Tartronic acid, Lactic acid, 2KDG, 5KDG, Glycolic acid, glycolic acid

As it can be seen from Table 5.2, when no stirring was present at all in the reaction mixture, a very low amount of gluconic acid was obtained (0.9% yield of GO) and no glucaric acid was formed even in the presence of the catalyst. Meanwhile, a high quantity of isomeric products is formed (25% yield of isomers) indicating the isomerization of glucose predominance. Therefore, vigorous agitation is required to ensure the homogeneity of the mixture and the mass transferring of the substrate to the available active sites inside the pores of the activated carbon where the gold nanoparticles could be deposited. For the result obtained, the following tests were carried out at 1000 rpm.

To understand better how each byproduct is formed, it is useful to study how the concentration of these species varies as a function of reaction time. Following the experimental conditions established in the previous section, the reaction (kinetic studies) was followed at reaction times of 15, 30, 60, and 120 minutes.

Time (min)	Glucose conversion %	Gluconic acid yield %	Glucaric acid yield %	Glucaric acid selectivity %	Others ^a yield %
15	87	53	15	17	20
30	90	44	20	22	25
60	93	38	24	26	28
120	92	32	25	27	30

Table 5.3: Glucose conversion and Gluconic acid and Glucaric acid formation through time. Reaction conditions: 60 °C, 1000 rpm, 10 bar O₂, Glu: Au: NaOH molar ratio of 1000:1:3000.^a Other byproduct correspond to all the byproduct comes from C-C cleavage reaction and retroaldolic: Formic acid, Oxalic acid, Mesoxalic acid, Tartaric acid, Tartronic acid, Lactic acid, 2KDG, 5KDG, Glycolic acid, glycolic acid

From the data obtained (Table 5.3) it can be noticed that the conversion of glucose is fast at the initial time of the reaction; for example after only 15 minutes of reaction, the conversion of glucose has reached 87% and the main product that was formed is the gluconic acid (53%), one of the primary products. Since aldehyde groups are easily oxidizable, a high concentration of gluconic acid is expected at short reaction times in agreement with previous studies. While in the case of the formation of glucaric acid, the oxidation of alcohol group -CH₂OH requires the first dehydrogenation to -CHO followed by oxidation to -COOH, which is a more demanding step, therefore it is a slower step. After the initial reaction time, the gluconic acid yield started to decrease (from 53% at t = 0 to 32% at 120 minutes), demonstrating the intermediate nature of GO; meanwhile the glucose conversion was almost constant, and the glucaric acid yield was increased, including the yield of other byproducts (Figure 5.2). These data also suggest that the major part of the additional byproducts were formed from the reaction starting from GO (see Figure 5.3), whereas the glucaric acid was quite stable (this was investigated by use GO and GA as starting material and controlling the intermediates and final products). Another interesting fact is that the value of GA yield appeared constant after 60 minutes of reaction. This result indicates that the further oxidation of gluconic acid slows down during the progress of the reaction, leading to the formation of by-products. This could be explained if we consider the blocking of the active surface sites of the catalyst by glucaric acid and similar byproducts. The reactants and products have a multifunctional nature where they can interact with the catalyst via multiple groups. Glucose and gluconic acid absorb possibly with similar strength to the active site (-CHO and -COOH group respectively) whereas, glucaric acid can interact by both C=O groups (belonging to the carboxylic groups) with the Au surface of the catalyst.

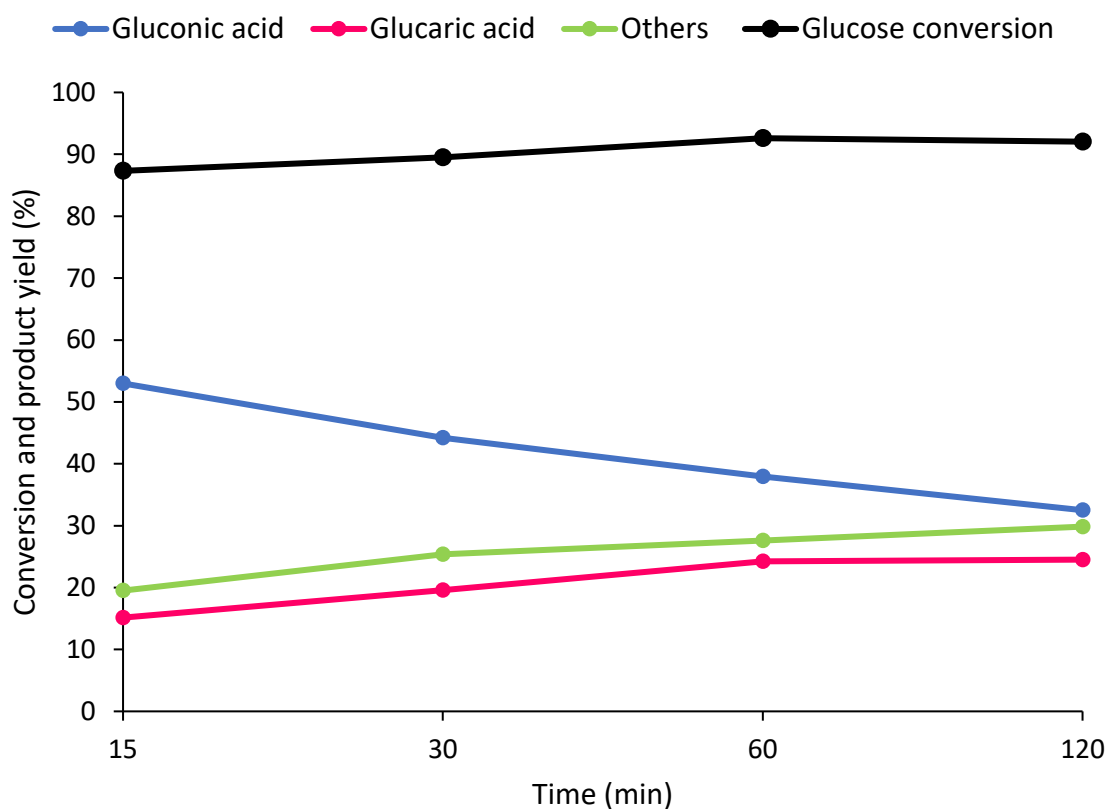


Figure 5.2. Glucose conversion and formation of GO, GA and other byproducts as a function of reaction time. Reaction conditions: 60 °C, 1000 rpm, 10 bar O₂, Glu:Au:NaOH molar ratio of 1000:1:3000

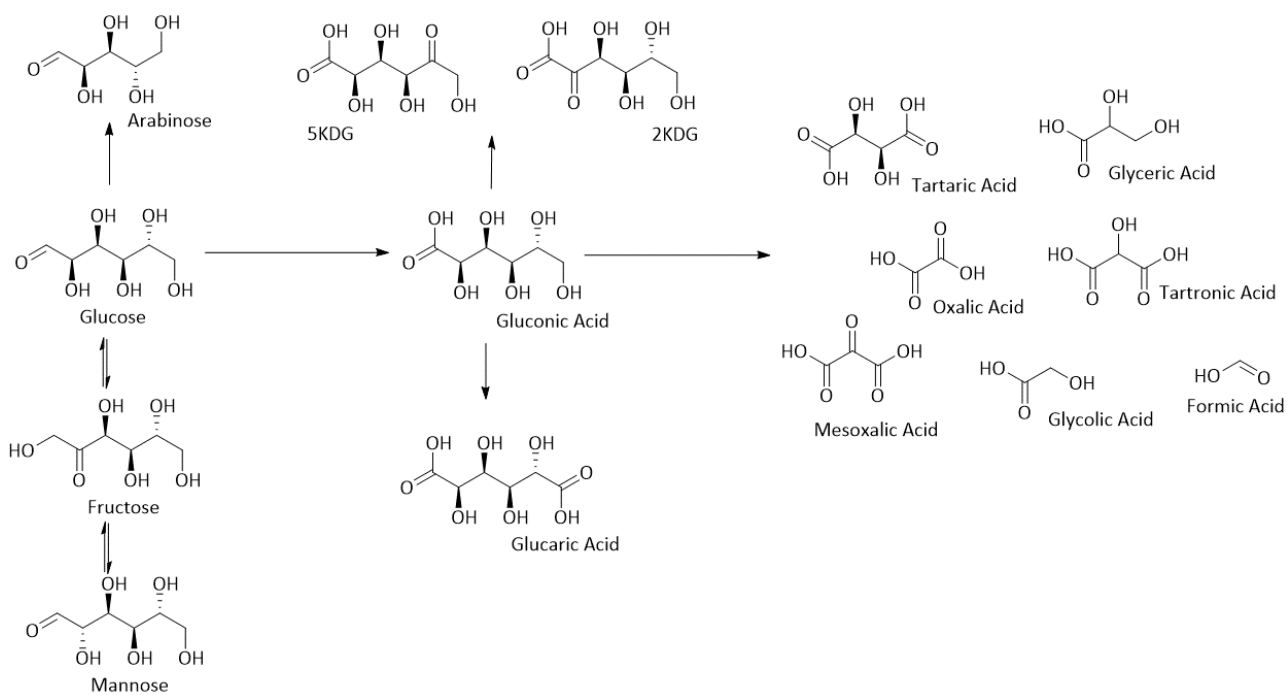


Figure 5.3: Reaction network and reaction pathways for the glucose oxidation

A further interesting screening that could help to optimize the reaction parameters and to understand the reaction mechanism is the metal:glucose molar ratio. The effect of Au:Glu molar ratio (1/500 to 1/1500) was studied to understand the influence of the mass of catalyst in terms of activity and yield to specific products. The results are presented in Table 5.4.

Au:Glu molar ratio	Glucose conversion %	Gluconic acid yield %	Glucaric acid yield %	Isomers^a yield %	Others yield %
1:500	92	31	28	0	32
1:1000	93	38	24	1	27
1:1500	90	40	19	2	26

Table 5.4: Study of Au:Glu ratio (changing the amount of catalyst). Reaction conditions: 1 h, 60 °C, 1000 rpm, 10 bar O₂, Glu:NaOH molar ratio of 1:3. ^a Isomers corresponding to fructose and mannose. Other byproduct correspond to all the byproduct comes from C-C cleavage reaction and retroaldolic: Formic acid, Oxalic acid, Mesoxalic acid, Tartaric acid, Tartronic acid, Lactic acid, 2KDG, 5KDG, Glycolic acid, glycolic acid

It can be noted that glucose conversion is very high in all the cases. Isomers yield slightly increases as the catalyst quantity decrease. Conversely, glucaric acid concentration decreases as Au:Glu molar ratio decreases. The yield to other compounds remains similar (~26%) in 1:1000 and 1:1500 molar ratios meanwhile glucose conversion remains the same (~92%) for molar ratios 1:500 and 1:1000. Higher metal:substrate molar ratios generate a higher amount of glucaric acid (28% yield GA at Au:Glu molar ratio or 1:500) due to the increasing number of active sites available for the chemical transformation.

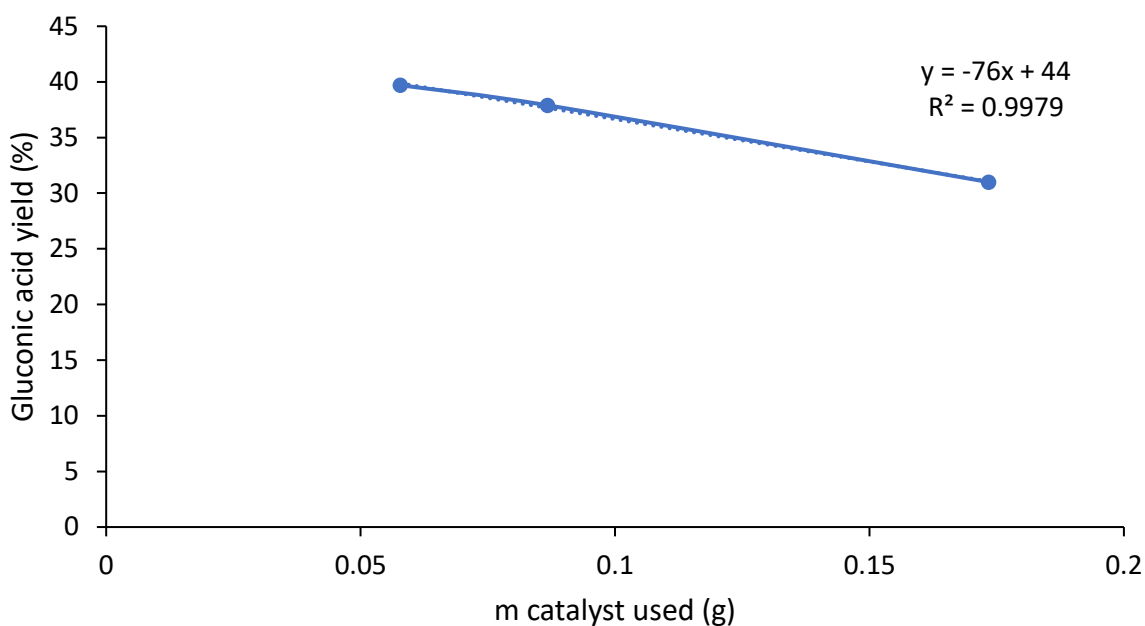


Figure 5.4: Correlation between gluconic acid yield and amount of catalyst used in Table 5.4

To evaluate if the reaction conditions are consistent with a kinetic or diffusion regime, the GO yield was reported in function of the amount of catalyst used (Figure 5.4). Usually this correlation is done by plotting the reagent conversion with the amount of catalyst, however, the high glucose conversion does not permit this comparison. The relationship observable could be attributed to a linear one, with an R^2 equal to 0.9979, so the reaction parameter lead us to work in a kinetic regime.

5.2 Glucose oxidation: Screening of Au/AC PVA series

After the optimization of the reaction parameters, the catalytic performance of Au/AC-PVA series was evaluated. Small metal nanoparticles have a high metal surface area and, usually, higher catalytic activity. To see if this trend is observed in the chosen reaction models, the series of synthesized materials were tested for the oxidation of glucose as the first model reaction. The reaction conditions and the analysis method are the same reported in the experimental part and here in Table 5.5 and Figure 5.5 are reported the results obtained.

Catalysts	Glucose conversion %	Gluconic acid yield %	Glucaric acid yield %	Gluconic acid selectivity %	Glucaric acid selectivity %	Others ^a yield %
Au/AC PVA0	92	38	22	41	24	28
Au/AC PVA 0.3	90	36	22	40	24	29
Au/AC PVA 0.6	91	37	22	40	25	29
Au/AC PVA 1.2	91	39	20	42	22	27
Au/AC PVA 2.4	90	44	17	49	19	25

Table 5.5: Screening of catalysts for the Au/AC PVA series. Reaction conditions: 1 h, 60 °C, 1000 rpm, 10 bar O₂, Glu:Au:NaOH molar ratio of 1000:1:3000.^a Other byproduct correspond to all the byproduct comes from C-C cleavage reaction and retroaldolic: Formic acid, Oxalic acid, Mesoxalic acid, Tartaric acid, Tartronic acid, Lactic acid, 2KDG, 5KDG, Glycolic acid, glycolic acid

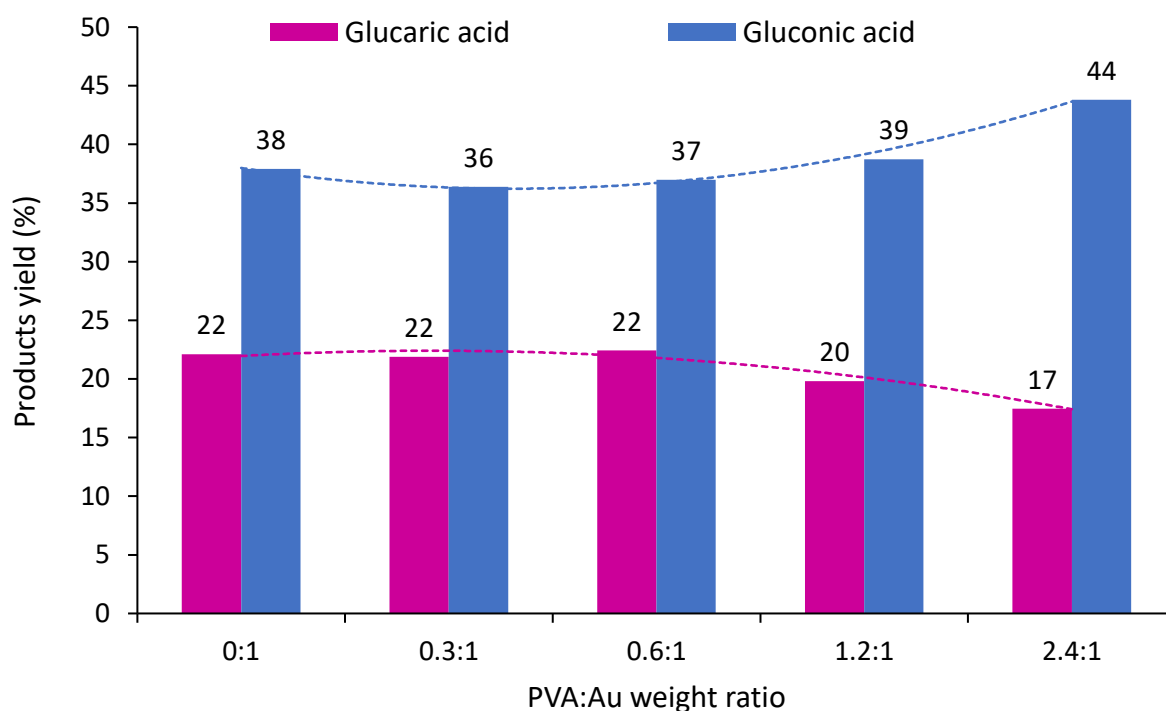


Figure 5.5: Catalytic screening of catalysts Au/AC PVA series. Reaction conditions: 60 min, 60 °C, 1000 rpm, 10 bar O₂, Glu:Au:NaOH molar ratio of 1000:1:3000

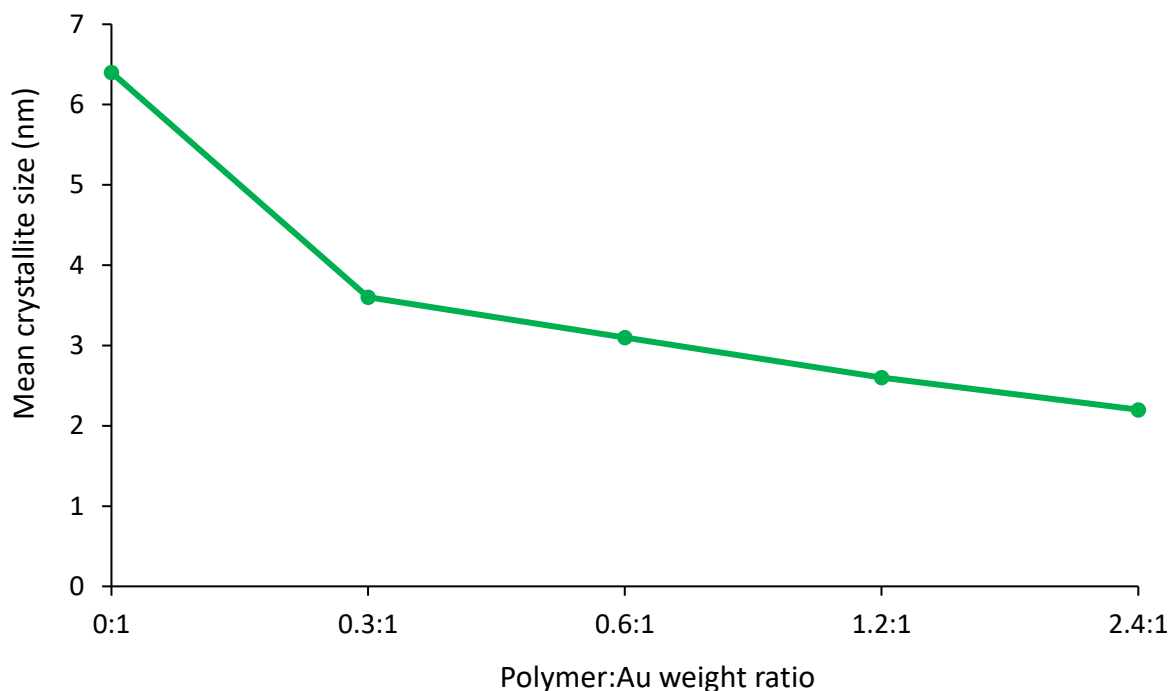


Figure 5.6: Comparison between and mean crystallite size of Au based on XRD analysis and the polymer: Au weight ratio for Au/AC PVA series

The catalytic trends obtained from the reactions are quite peculiar. At 1 hour of reaction, similar glucose conversions are obtained (~90%) for all the Au/AC PVA series; however, lower conversions are necessary to study the initial rates and to obtain a useful comparison in terms of initial activity. However, the glucaric acid yield slightly decreases when PVA: Au weight ratio increases (22% for Au/AC PVA0 vs 17% for Au/AC PVA2.4), meanwhile the gluconic acid shows the opposite trend. From Figure 5.6 it can be noticed that an increase in PVA: Au weight ratio leads a decrease in terms of particle size: Au nanoparticle size seems to show an influence in terms of controlling the activity and productivity of intermediate and final products. Thereby, reactions of a duration of 15 minutes were performed with catalysts Au/AC PVA0, Au/AC PVA1.2, and Au/AC PVA2.4 to evaluate the initial activity and understand better the consecutive reactions as a function of reaction time.

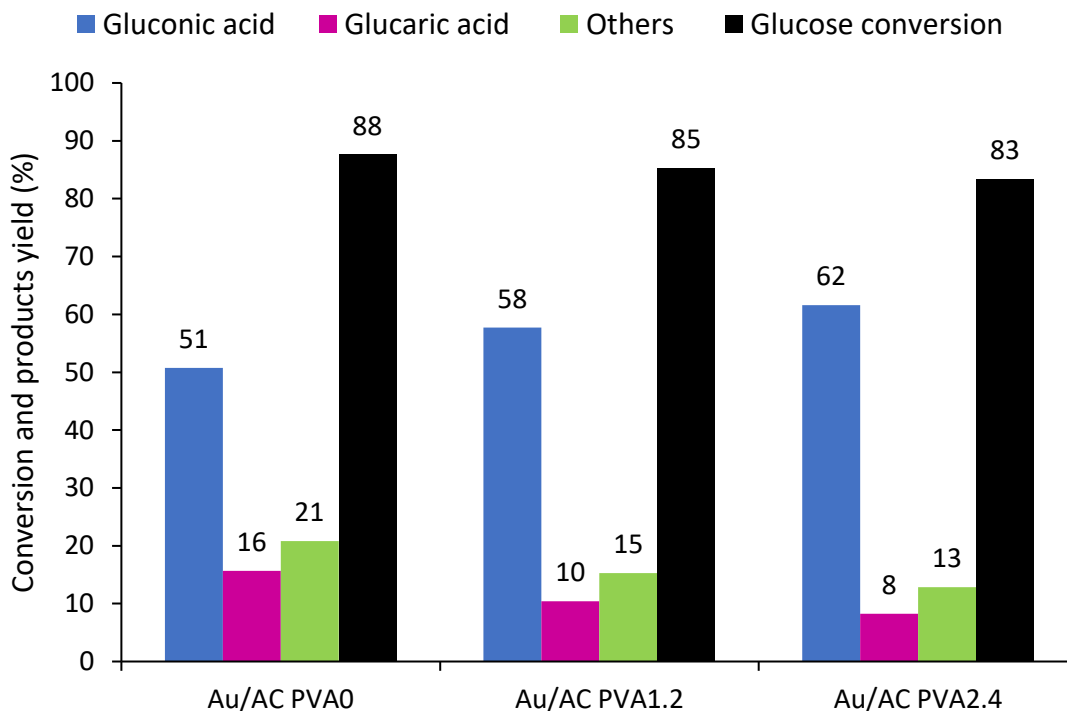


Figure 5.7: Catalytic screening of catalysts Au/AC PVA series. Reaction conditions: 15min, 60 °C, 1000 rpm, 10 bar O₂, Glu: Au:NaOH molar ratio of 1000:1:3000

Figure 5.7 shows that glucose conversion decreased as the PVA amount increased in the synthesized catalysts: Au/AC PVA0 reached 88% in glucose conversion, but Au/ACPVA2.4 stopped at 83%. The quantity of glucaric acid decreased as the PVA concentration increased in the catalysts (16% for Au/AC PVA0 vs 8% for Au/AC PVA 2.4), while the opposite trend was observed for gluconic acid yield. It seems that the initial rate of the reaction is slower in the catalyst with a higher amount of PVA despite the fact Au/AC PVA2.4 has the smallest mean diameter size of Au nanoparticles of the series of catalysts prepared (mean particle size of 2.4 nm). One of the possible reasons for the observed catalytic trend could be attributed to the fact that PVA could be partially blocking the active sites in the nanoparticles. This behavior was more evident at reaction time of 15minutes and in this case, the PVA presented at the highest PVA to Au weight ratio in the catalyst seems to influence to a higher degree the reaction rate and product distribution than the Au nanoparticle, when the dimensions of Au nanoparticles are in a similar range. For reaction time equal to 1hour, partial solubilization of PVA could occur (PVA is soluble in water and dissolves at 60°C) and active sites start to be available. The characterization of Au/AC PVA series in Chapter 4 showed that the catalyst with a lower amount of PVA shows higher surface atomic ratio Au/C because of the blocking

action of the polymer. To verify if this is the parameter that more affects the catalytic activity, the correlation between yield and Au on the surface could be useful.

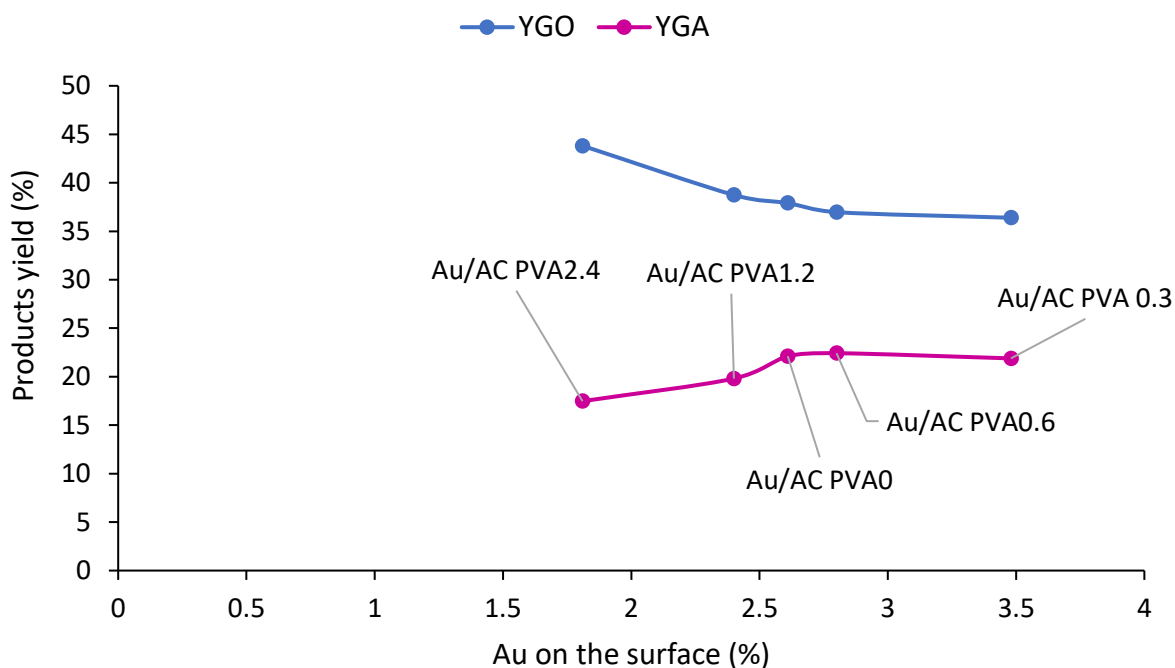


Figure 5.8: Correlation between the glucaric acid (GA) and gluconic acid (GO) yield and atomic percentage of Au on the surface

Figure 5.8 shows the yield of GO and GA after 1 hour in the function of gold presence on the surface (to highlight this comparison, the weight ratio of PVA to Au was reported as a label on the data in Figure 5.8). From the results, it seems that dimensions and relative amount of PVA do not directly correlate with the catalytic activity of the catalyst, but it is the presence of Au on the surface that plays a key role in it. Indeed, it seems that increasing the availability of the gold surface content on the surface of the catalyst enhances the conversion of GO to the formation of GA. This parameter does not depend only on the dimension of the nanoparticles (smaller is the diameter, higher is the surface of gold available), but also on the coverage of the nanoparticles with PVA.

5.3 Glucose oxidation: Effect of heat treatment vs washing to conversion and yield

Due to the blocking action of PVA seen in the previous section, it could be crucial to the study of catalyst method preparations act to remove the excess of the stabilizing agent from the surface of

metal nanoparticles. The treatments here compared are quite different: the washing step provides mild temperature (60°C) in aqueous solution for a long time (4h) (Method C) instead, the heat treatment includes a dry step in the presence of oxygen and after in hydrogen flow, at a higher temperature (from 120°C to 250°C) (Method B). In this way, it was possible the preparation of a Au/AC HT series and of a Au/AC washed sample.

Samples	Au on surface (at%)	Surface atomic ratio Au/C	Mean particle size (nm) (TEM)
Au/AC no treat	2.8	0.033	2.7
Au/AC HT120	2.8	0.032	4.2
Au/AC HT200	2.7	0.029	4.9
Au/AC HT250	1.1	0.012	5.8

Table 4.6: Au atomic percentage on surface, surface atomic ratio Au/C and mean particle size for Au/AC HT series

The surface atomic ratio Au/C trend already seen in Table 4.6 could give us some clue about the catalytic trend that we could observe in terms of the activity of the series of catalysts: the sample Au/AC HT120 shows a similar surface atomic ratio in comparison with Au/AC no treated, even in the Au NPs size is higher. A possible explanation is that the heat treatment allow the rearrangement/partial remotion of the polymer and the higher availability of gold active sites. However, it is necessary to test this set of catalysts to see if these approaches help to increase the activity/selectivity of the reaction.

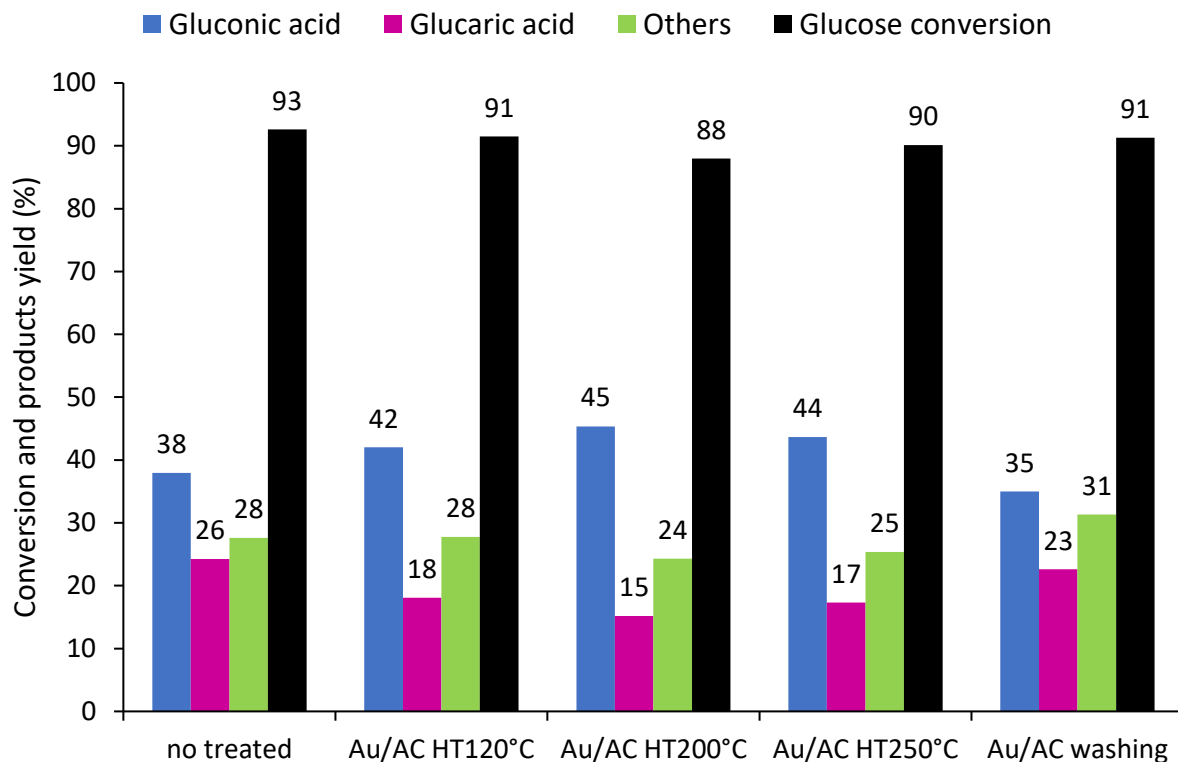


Figure 5.9: Screening of catalysts Au/AC PVA series. Reaction conditions: 1 h, 60 °C, 1000 rpm, 10 bar O₂, Glu: Au: NaOH molar ratio of 1000:1:3000

Different treatments can influence differently the morphology of the catalyst and therefore the catalytic behavior, but from the catalytic data obtained after 1 hour of the reaction (see Figure 5.9), it can be seen that all the treatments don't change dramatically the results in terms of yield of products. Specifically, the treatments did not affect the conversion that remained stable at around 90%. However, the yields of GO, GA and other byproducts obtained using the different experimental protocols could give some interesting information. It can be seen that the washing step seem to give a lower yield of gluconic acid (35% and 38% for the Au/AC washing and the Au/AC no treated respectively); however, the yield in GA worsen due to the increase of other byproduct amounts (23% for Au/AC washing against 26% for Au/AC no treated). These data indicate that the washing step facilitates the removal of PVA and therefore the availability of the active sites; however, at the same time, we observed an increase of the byproducts, due to the C-C scission and the retroaldolic reactions.

Instead, the effect of heat treatment, especially at a temperature above 120 °C, showed that when the temperature use in the heat treatment increased, the gluconic acid yield was increased (38% for Au/AC no treat, 44% for Au/AC HT250), whereas, a decrease of GA and other by-products was

observed. However, this yield of products did not change drastically when the variation of the heat treatment temperature was in the range of 120-250 °C. To evaluate and understand better the catalytic behavior of this system, the reactions were carried out at shorter reaction times, for example at 15 minutes.

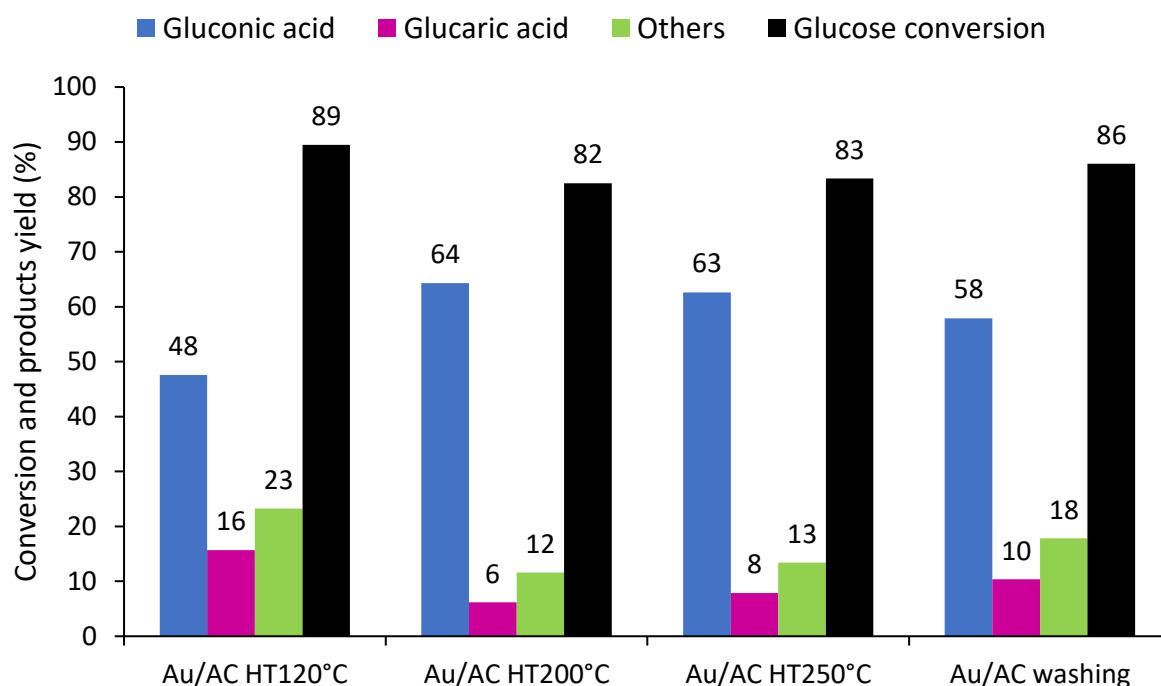


Figure 5.10: Screening of catalysts for the Au/AC PVA series. Reaction conditions: 15min, 60°C, 1000 rpm, 10 bar O₂, Glu: Au:NaOH molar ratio of 1000:1:3000

In Figure 5.10 it can be observed that the Au/AC HT120°C catalyst had the best initial catalytic performance (16% yield of GA) followed by the Au/AC washing catalyst (10% yield GA). Meanwhile, Au/AC HT200°C and Au/AC HT250°C catalysts showed the poorest catalytic performance of the four catalysts at 1 hour and 15 minutes of reaction. This could be due to the increase of the mean nanoparticle size of Au during the heat treatment and the incomplete removal of PVA ligand over the surface of the catalyst. In particular, Au/AC HT250°C has a larger mean nanoparticle size of Au (5.8 nm against 4.9 nm and 4.2 nm for Au/AC HT200°C and Au/AC HT200°C respectively) but maybe at higher calcination temperature a higher amount of PVA was removed, since the thermal decomposition of pure PVA occurs at 250°C, therefore, a higher number of active sites are free for accessibility of substrate/intermediates. Hence, a mild calcination treatment at 120°C Air/H₂ or washing with water at 60°C seem to offer an effective treatment (as previously reported in

literature⁶⁴) to clean off the catalyst surface without altering the original mean nanoparticle size (crystallite size of 3.1 nm).

5.4 Glucose oxidation: Catalytic performance of Au/ACPVA- Au/ACPVP- Au/ACPEG

The other series of catalysts that were prepared are the one where the stabilizing agent was changed, using polyethylene glycol (PEG), and polyvinyl pyrrolidone (PVP). It was already seen that keeping constant the weight ratio of polymer to Au, (the amount of polymer), the mean particle size for Au/AC PEG 0.65 and Au/AC PVP0.65 was higher than Au/AC PVA0.65 (see Table 5.6).

Sample	Mean particle size (nm) by TEM ± Standard Deviation
Au/AC-PVA 0.65	2.7 ± 2.6
Au/AC-PVP0.65	5.2 ± 6.8
Au/AC-PEG 0.65	5.5 ± 4.3

Table 5.6: Mean crystallite size values of the Au/PVA0.65, Au/AC PVP0.65, Au/AC PEG 0.65 obtained by XRD analysis

However, the evaluation of the catalytic performance on Au/AC PVA series showed that NP size could not be the main factor that influences the catalytic activity and for this reason, the synthesized catalysts with PVP and PEG chose as stabilizer were evaluated for the selective oxidation of glucose, therefore to make a comparison of the effect of different stabilizers nature. The results are shown in Figure 5.11.

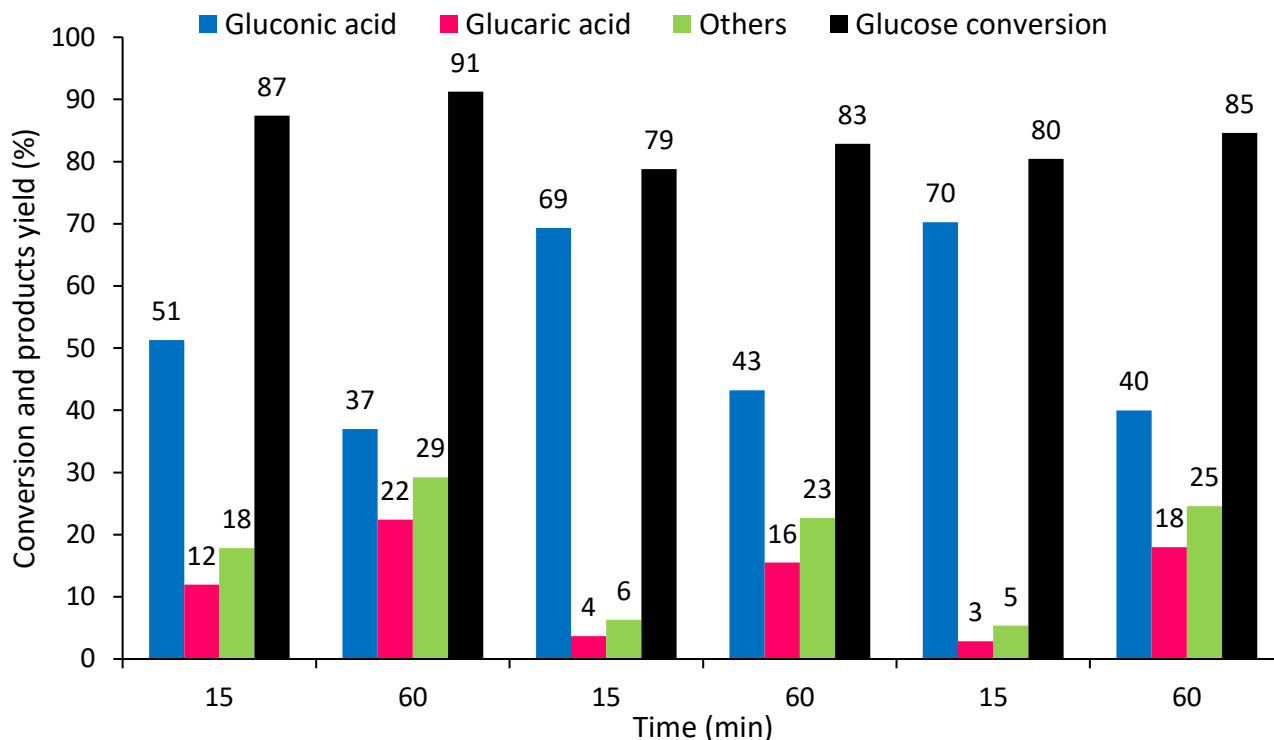


Figure 5.11: Catalytic test for Au/ACPVA, Au/ACPVP, Au/ACPEG. Reaction conditions: 15 min or 60min, 60 °C, 1000 rpm, 10 bar O₂, Glu: Au: NaOH molar ratio of 1000:1:3000

At first, the comparison was carried out at an initial reaction time of 15 minutes; at this reaction time it is possible to notice that Au/AC PVA0.65 is the sample that gives different data in comparison with the other two samples prepared with PVP and PEG as the chosen stabilizer: the yield of Gluconic acid (GO) for Au/AC PVA0.65 is 51% against 69% and 70% obtained for Au/ACPVP0.65 and Au/AC PEG0.65 respectively. Moreover, the yields of Glucaric acid (GA) and Other by-products are higher for the sample with PVA (YGA 12% against 4% for Au/ACPVP0.65 and 3% for Au/AC PEG0.65 - Y Other 18% against 6% for Au/ACPVP0.65 and 5% for Au/AC PEG0.65). This difference between the catalysts Au/ACPVA0.65 to Au/AC PVP0.65 and Au/ACPEG0.65 probably is due to the size of Au nanoparticles; in particular, the smallest size obtained with PVA increases the availability of the active sites and the initial reaction rate. This is why with the Au/AC PVA0.65 it was obtained a lower amount of GO that convert to give a higher amount in GA and other byproducts. After 1 hour the performance of the three catalysts are quite similar: in particular, for all the catalyst it was obtained YGO around 40%, GA yield of ~20% and 25% for the other byproduct yield (the samples containing PVA seems the one who gives a high amount of GA (22%)). The size of the Au NPS is no more a discriminating factor and it appears that a longer reaction time decreases the differences between

stabilizing agents. This can be due to the solubilization of the stabilizer and structural rearrangement on the surface of the catalyst of the polymer.

The lower activity at short reaction time for the supported colloidal nanoparticles prepared by using PVP and PEG could be also ascribed to the stronger binding of the stabilizing agent on the Au surface that can block the available active sites or the inadequate amount of stabilizing agent which lead to the formation of big nanoparticles. To evaluate if there is an optimized amount for these two polymers like in the case of PVA, a systematic study was made by varying weight ratio of polymer to Au, therefore the nominal amount of the polymer, with values of weight ratio of polymer to Au from 0 to 2.4. Figure 4.22 reported the NPs dimension for all the catalysts prepared.

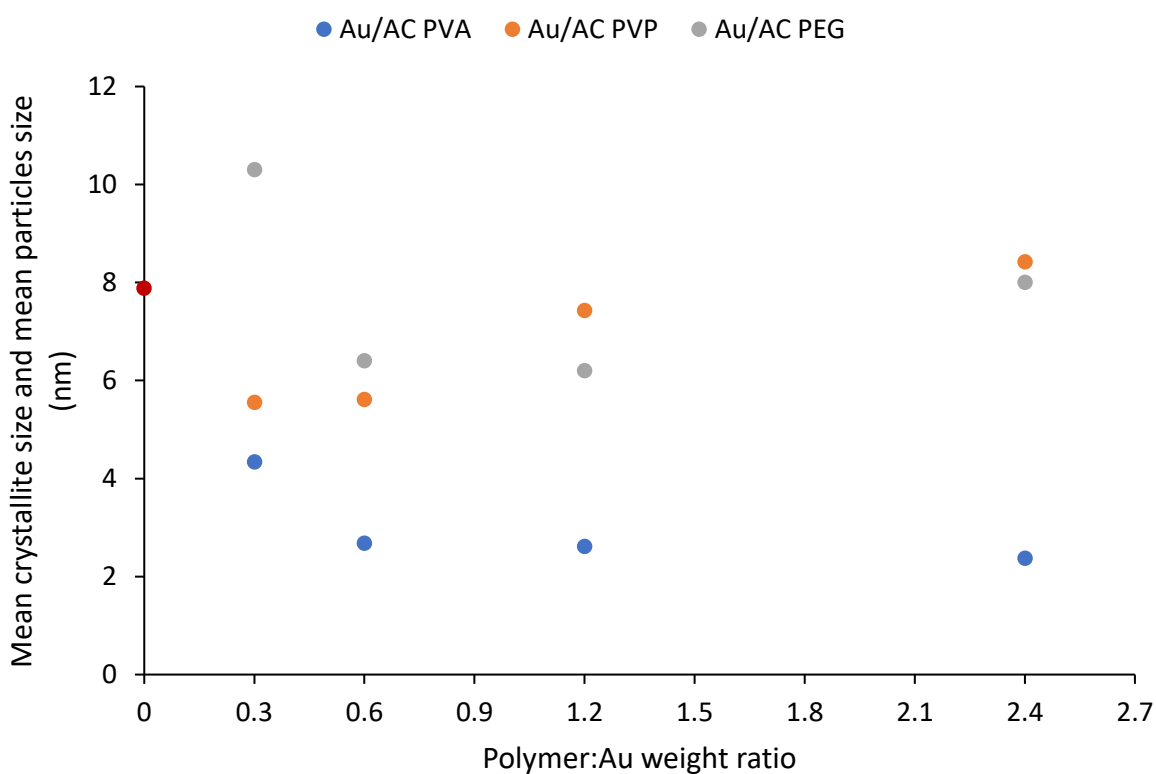


Figure 4.22: Mean crystallite size and mean particle size in function with the polymer: Au weight ratio for Au/AC PVA, Au/AC PVP and Au/AC PEG series

Furthermore, these series of catalysts were tested to study the activity and the behavior in our reaction. The results obtained after 15 minutes of reaction time are reported here in Figures 5.12 and 5.13.

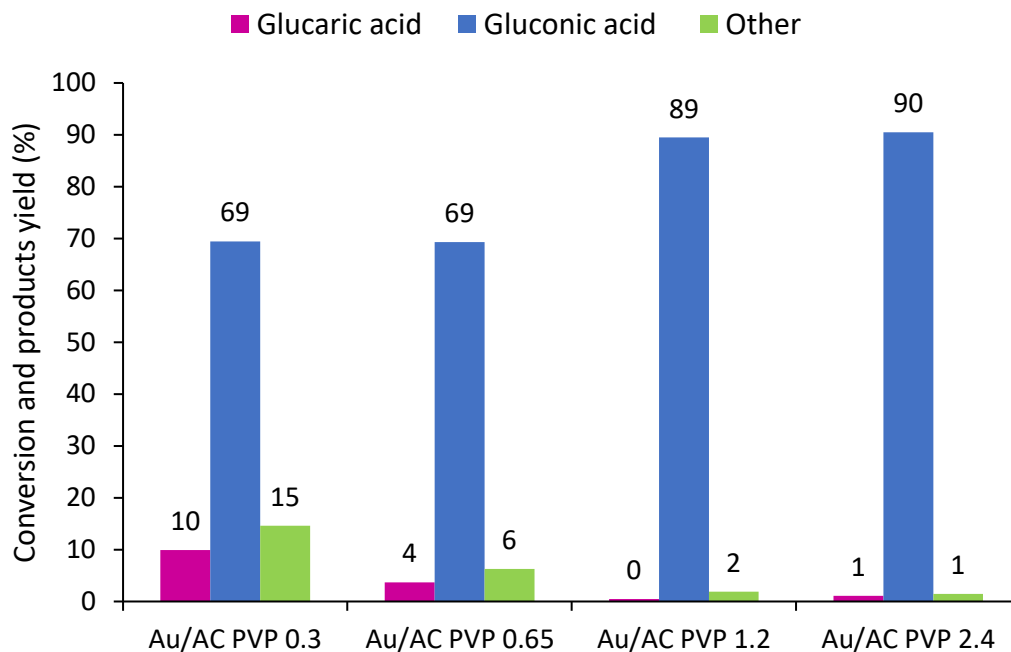


Figure 5.12: Screening of catalysts Au/AC PVP series. Reaction conditions: 15min, 60°C, 1000 rpm, 10 bar O₂, Glu:Au:NaOH molar ratio of 1000:1:3000

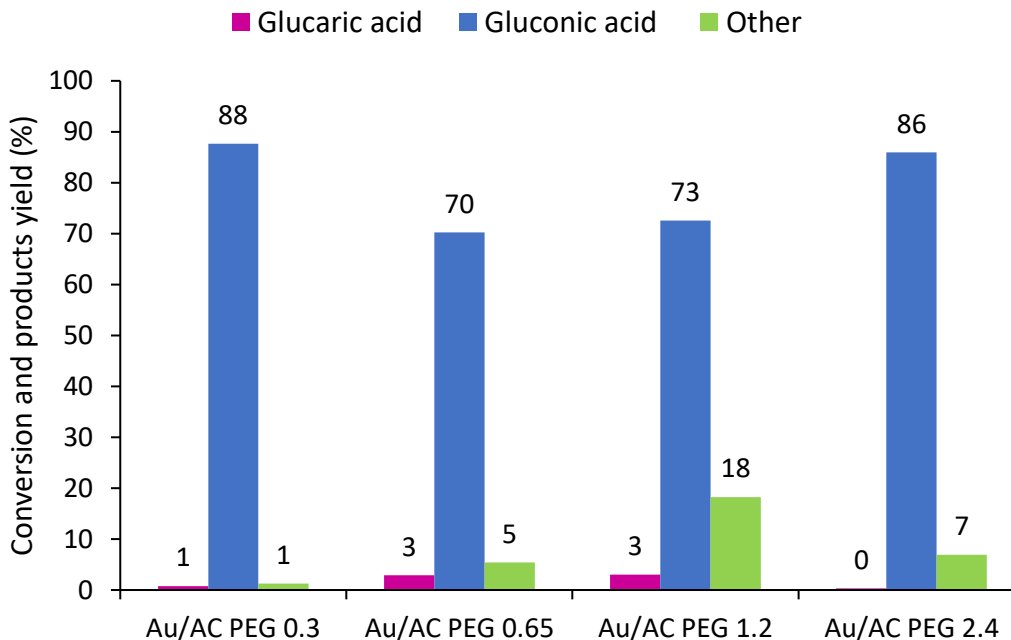


Figure 5.13: Screening of catalysts Au/AC PEG series. Reaction conditions: 15min, 60°C, 1000 rpm, 10 bar O₂, Glu:Au:NaOH molar ratio of 1000:1:3000

On the contrary to the series of catalysts prepared by PVA, the parameter that seems to influence more at short time of reaction is the size of the nanoparticles. Indeed, the Au/AC PVP series and the

Au/AC PEG show that the samples with the smallest nanoparticles lead to a higher tendency to oxidize the gluconic acid to glucaric acid or to form other byproducts. Moreover, the Au/AC PVP trend suggests that a higher amount of stabilizing agent blocks the gold active site, stopping the reaction (Figure 5.12). Indeed Au/AC PVP 2.4 leads to a GA yield of 1% against the 10% obtained with Au/AC PVP 0.3. Moreover, the XPS analysis carried out on the Au/AC PVP series showed that the increase of the amount of polymer leads to a decrease of the Au/C atomic ratio, data that are in agreement with the decreasing yield of GA (Figure 5.14).

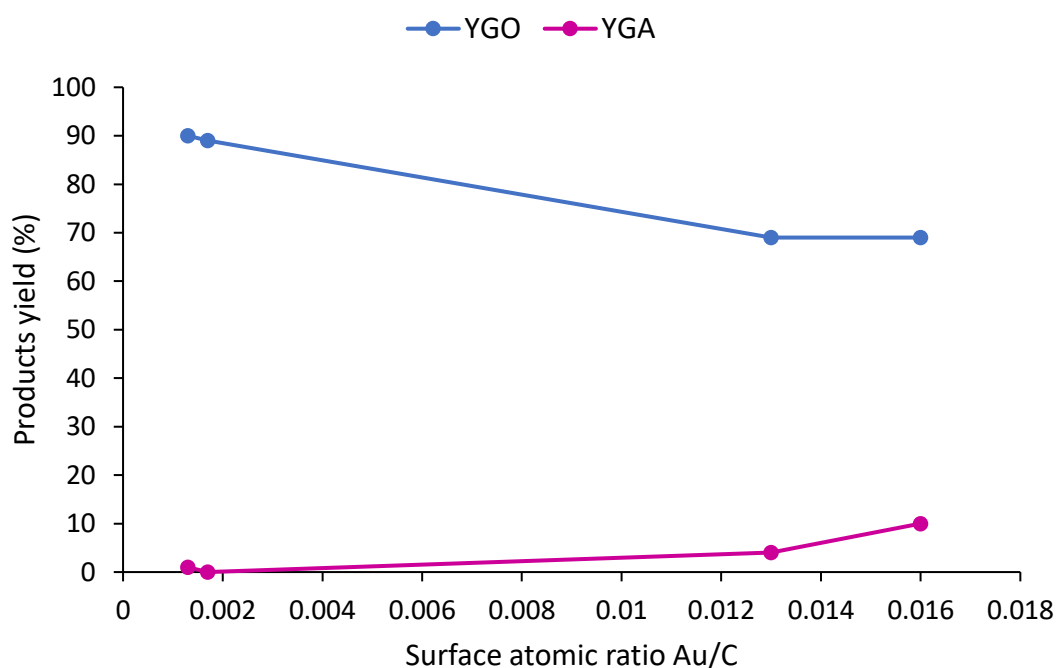


Figure 5.14: Correlation between glucaric acid (GA) and gluconic acid (GO) yield with surface atomic ratio Au/C obtained by XPS analysis

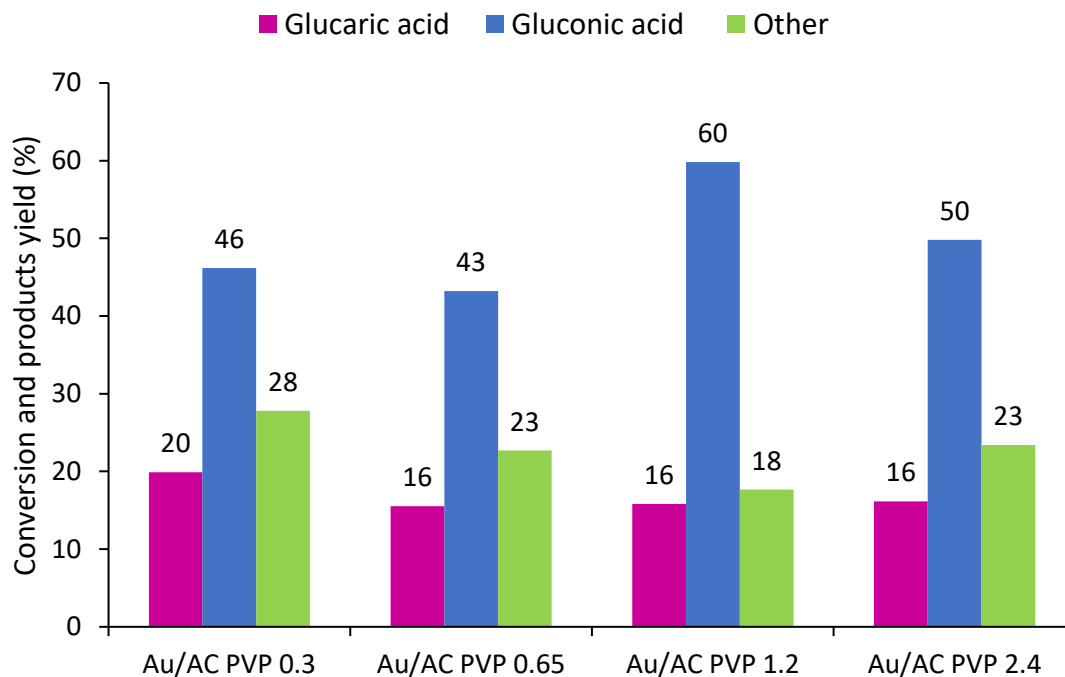


Figure 5.15: Screening of catalysts Au/AC PVP series. Reaction conditions: 1 h, 60 °C, 1000 rpm, 10 bar O₂, Glu: Au: NaOH molar ratio of 1000:1:3000

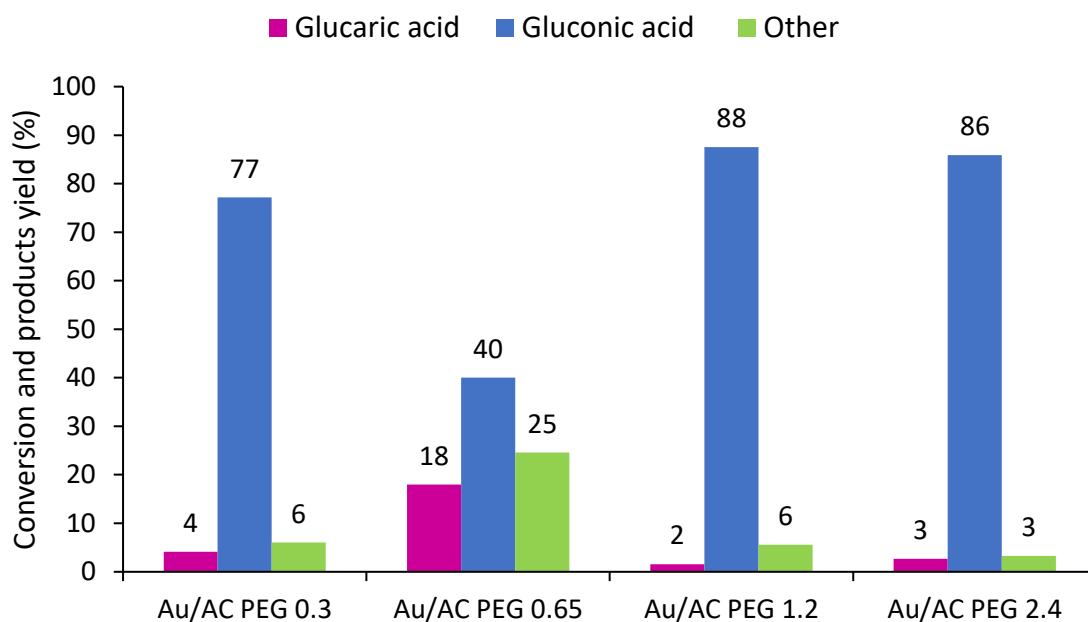


Figure 5.16: Screening of catalysts Au/AC PEG series. Reaction conditions: 1 h, 60 °C, 1000 rpm, 10 bar O₂, Glu: Au: NaOH molar ratio of 1000:1:3000

After 1 hour of reaction, the reaction trend appears quite different. In particular, the Au/AC PVP catalysts (Figure 5.17) seem to have a similar behavior even if the amount of polymer changes drastically. A reasonable explanation for this phenomenon could be the partial solubilization of the

polymer; the PVP could have higher solubility in water, so probably the presence of water as a solvent and the 60°C of reaction help the polymer removal and the access to the new active site of gold, also for Au/AC PVP2.4. It is also evident that the nanoparticles size is not the only factor that influences the reaction in the experimental condition tested. In fact, the results reported in Figure 5.16 suggest that PEG seems to block completely the second step of the reaction, leading a higher yield of gluconic acid (excluding Au/AC PEG 0.65, the Au/AC PEG series gives an average YGO ~83% against YGO ~50% for Au/AC PVP series).

6 Chapter 6-4-Nitrophenol reduction

6.1 4-Nitrophenol reduction: Effect of substrate adsorption on the support

The possible use of Au/AC PVA, Au/AC PVP, and Au/AC PEG series for the 4-nitrophenol reduction could have a double relevance: as it was seen from Chapter 1, the 4-nitrophenol reduction (Figure 6.1) has relevance in the water-waste treatment and the possible production of 4-aminophenol (paracetamol precursor). Moreover, this reaction was considered a model reaction due to the simplicity of the experimental conditions (room temperature and pressure) and the analysis system; therefore, it could be useful to evaluate the behavior of different catalysts.

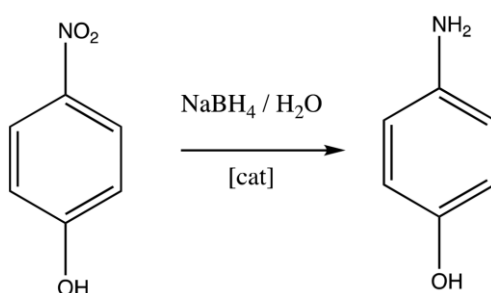


Figure 6.1: Reaction scheme of 4-nitrophenol reduction to 4-aminophenol

However, before testing the catalyst prepared, an initial evaluation of the precursor has to be made. Since activated carbon has a very high surface area ($A_{\text{BET}} = 1049 \text{ m}^2/\text{g}$), a possible effect that could be observed is the partial adsorption of the nitrophenol in solution.^{100,101} To evaluate these phenomena as well as to understand the appropriate catalyst concentration and reaction conditions to be used for catalysts activity determination, it was collected the optical spectrum of 4-nitrophenol $1.0 \times 10^{-4} \text{ M}$ with different amounts of activated carbon with different experimental conditions and experimental protocols. The methods used were summarized in Table 6.1.

Test	AC (mg/L)	Reactor	Stirring	Adsorption
1	320	Round-bottom flask	Yes, ~1000 rpm	>90%
2	80	Round-bottom flask	Yes, ~1000 rpm	40%
3	80	Cuvette	No	25%

Table 6.1: Conditions for the adsorption tests. $[4\text{-NP}] = 1.0 \times 10^{-4} \text{ M}$, $[\text{NaBH}_4] = 4.5 \times 10^{-3} \text{ M}$, $V = 50 \text{ mL}$. Tests 1 and 2 were carried out using round-bottom flask setup; for test 3, cuvette setup

Generally, for this reaction, the optimal substrate to metal molar ratio to explore the catalytic activity is in a range of 2 to 6.¹⁰² To make sure that it was possible to notice a difference in catalytic activity caused by stabilizer agents, it was decided to start from ratio 6 since a higher substrate:metal molar ratio results in a lower reaction rate.

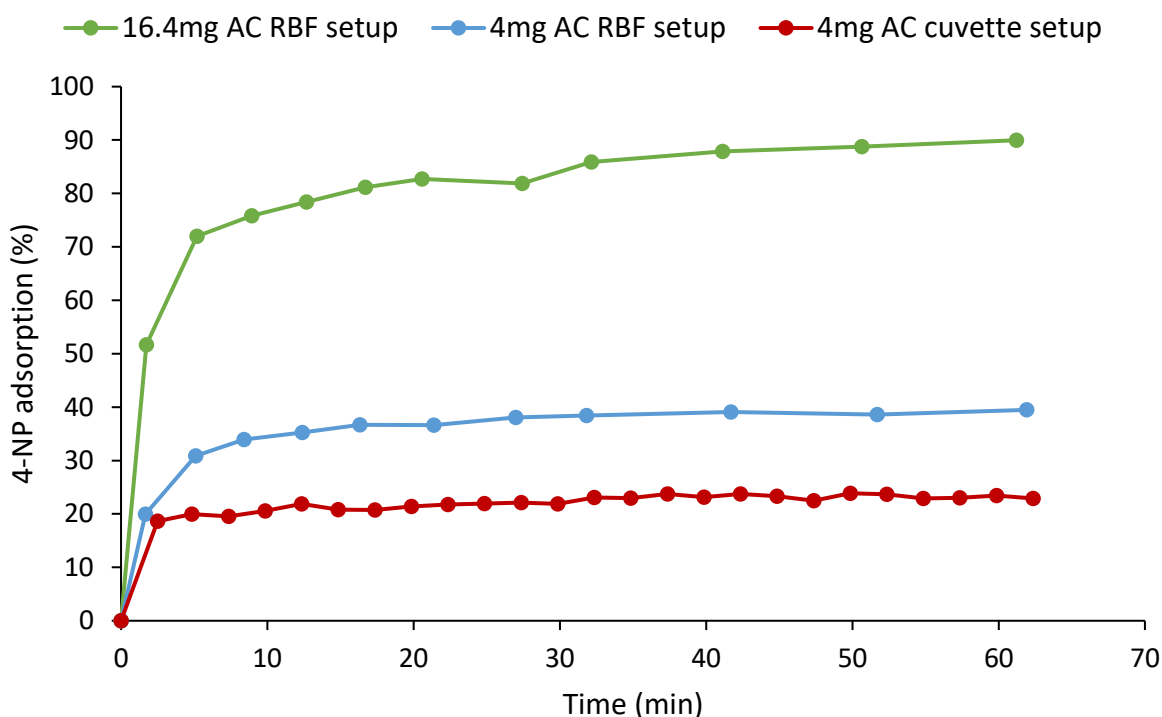


Figure 6.2: Adsorption of nitrophenol by active carbon under conditions of test 1, test 2 and test 3. Adsorption is calculated from experimental measurements as $(C_0 - C_t)/C_0$ and expressed as a percentage

Using the round-bottom flask setup as we have described in Chapter 3, the resulting amount of carbon (320 mg/L) proved to be enough to remove alone up to 90% of the nitrophenol in solution

(green line, Figure 6.2). Even reducing the amount of carbon to a quarter of the initial quantity (80 mg/L), physical adsorption of nitrophenol is still consistent (blue line, Figure 6.2). In test 3, the concentration of 80 mg/L without stirring proved to limit the physical adsorption to 25% (red line, Figure 6.2).

6.2 4-Nitrophenol reduction: Optimization of reaction setup

The adsorption tests the previous section highlight the influence of the different experimental protocols used. The three experimental protocols identified were tested for the possibility to distinguish the catalytic activity of the supported Au nanoparticles from the simple adsorption and to analyze the effect of the preparation procedure on their activity. These preliminary tests were executed using the series of catalysts prepared with PEG as the chosen stabilizer (Au/AC PEG set) and Figure 6.3 shows the resulting curves from the reaction with each sample from the set Au/AC PEG obtained using Test 1 as reaction set up.

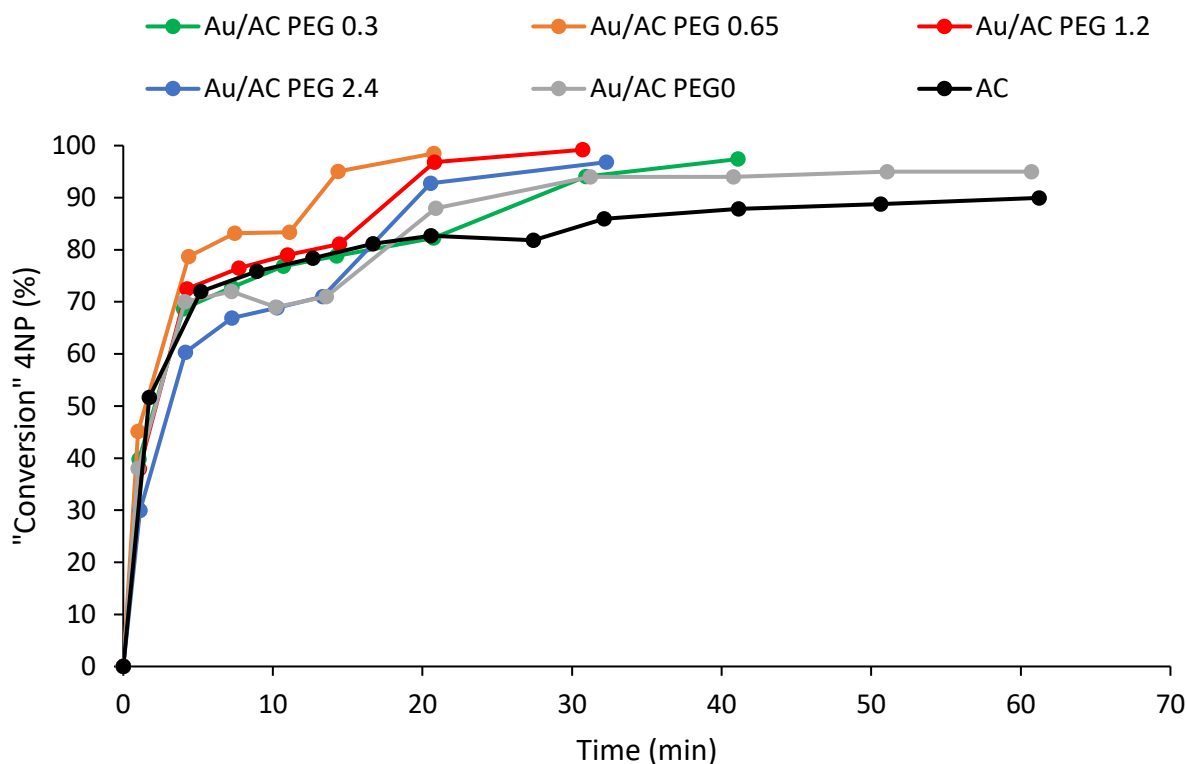


Figure 6.3: 4-nitrophenol conversion from catalytic reduction with Au/AC PEG set carried out using the round-bottom flask setup. Reaction conditions: $[4\text{-NP}] = 1.0 \times 10^{-4} \text{ M}$, $[\text{NaBH}_4] = 4.5 \times 10^{-3} \text{ M}$, $V = 50 \text{ mL}$, $[\text{catalyst}] = 320 \text{ mg/L}$, stirrer speed = $\sim 1000 \text{ rpm}$

From Figure 6.3 it can be seen that 4-nitrophenol conversion is high due to the adsorption on the support and catalytic activity. The curves obtained from the catalytic tests show a trend similar to

AC for the initial part, although they don't strictly overlap: this can be interpreted in terms of an altered adsorption capacity of the catalysts compared to AC due to the presence of the pre-formed colloidal nanoparticles and the stabilizing agent which could cover the surface. The latter in particular could displace from the nanoparticle into the AC's pores decreasing the final surface area, suggested also by the fact that the sample with the highest PEG: Au weight ratio is the one that shows the most evident reduction in adsorption capacity. The second part of the curves can be identified when the slope sharply increases, although for just one (Au/AC PEG0.3, Au/AC PEG0.65, Au/AC PEG1.2) or two (Au/AC PEG2.4) intervals of time. This change can be attributed to catalytic activity, but it has not been reported before so not much information is available on this. It is interesting to note that the slope increase shows up at different times for the various samples: after 10 minutes for Au/AC PEG0.65, after 13 minutes for Au/AC PEG2.4, after 16 minutes for Au/AC PEG1.2, and finally after 20 minutes for Au/AC PEG 0.3. The whole series of the supported nanoparticles convert 4-nitrophenol to > 97%, while AC reaches a plateau after 80% 4-NP removal. This allows us to confirm that the Au/AC PEG series shows catalytic activity towards 4-nitrophenol reduction, although this setup is not suitable for quantitative analysis for AC-based catalysts and this is why the second setup was tested (Figure 6.4).

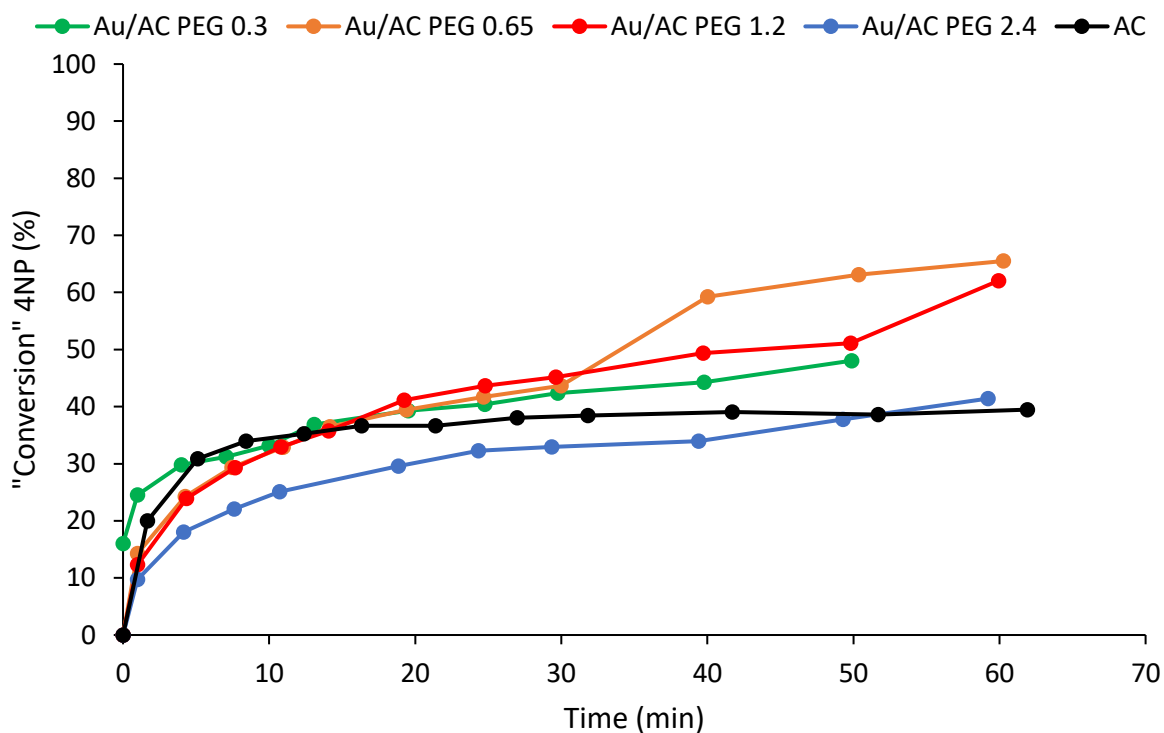


Figure 6.4: 4-nitrophenol conversion from catalytic reduction with Au/AC-PEG set carried out using the round-bottom flask setup. Reaction conditions: $[4\text{-NP}] = 1.0 \times 10^{-4} \text{ M}$, $[\text{NaBH}_4] = 4.5 \times 10^{-3} \text{ M}$, $V = 50 \text{ mL}$, $[\text{catalyst}] = 80 \text{ mg/L}$, stirrer speed = $\sim 1000 \text{ rpm}$

In this case, all the catalysts showed a decreased 4-nitrophenol adsorption and therefore conversion compared to naked AC at initial times; moreover, the hypothesis that the stabilizing agent could block the surface of carbon can be confirmed because the sample with a higher amount of PEG (Au/AC PEG2.4) shows a lower “conversion” in comparison with the carbon. Hence, the effect of active metallic surface area decrease is even more evident than in figure 6.3. Also, the maximum conversion measured is 66% by Au/AC PEG0.65 after 60 minutes, but it is not unexpected as the catalyst concentration is $\frac{1}{4}$ respective to the previous setup. Catalytic activity, in this case, is distinguishable for samples Au/AC PEG0.65 and Au/AC PEG1.2 only, and they both show the slope increase after 30 and 50 minutes respectively. The scope of this reaction setup is clearly to discard to test preformed Au nanoparticles supported on AC.

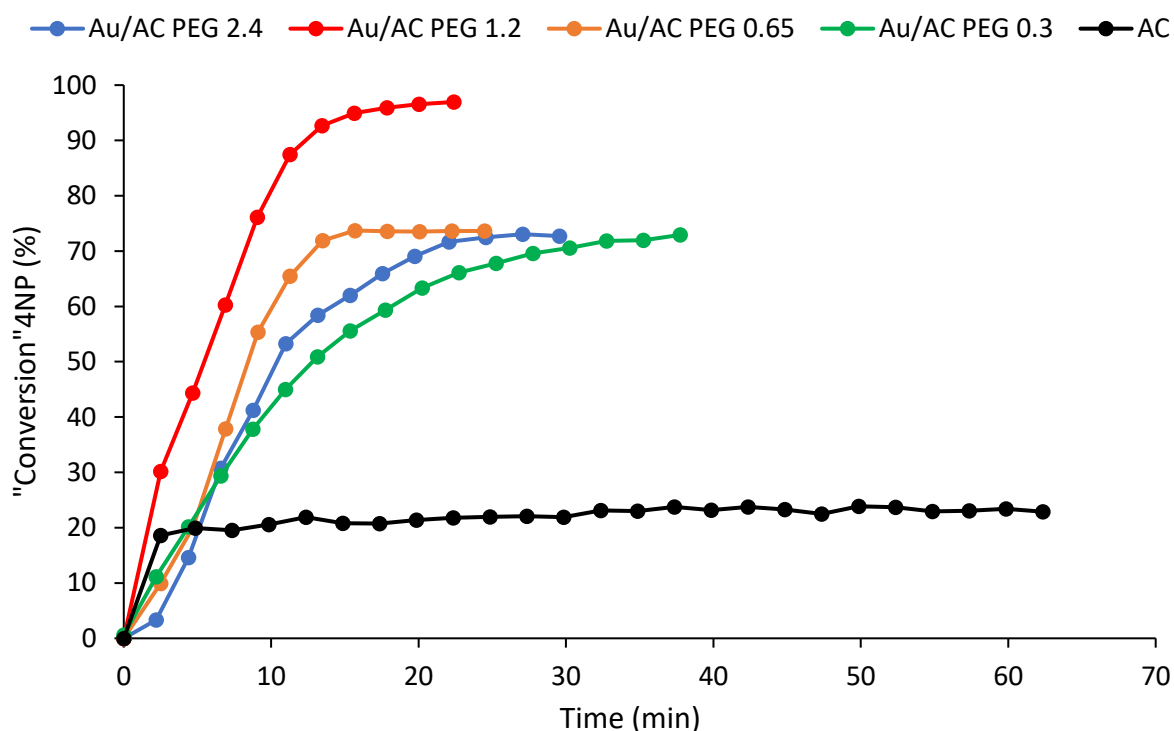


Figure 6.5: 4-nitrophenol conversion from catalytic reduction with Au/AC-PEG series carried out using the cuvette setup. Reaction conditions: $[4\text{-NP}] = 1.0 \times 10^{-4} \text{ M}$, $[\text{NaBH}_4] = 4.5 \times 10^{-3} \text{ M}$, $V = 50 \text{ mL}$, $[\text{catalyst}] = 80 \text{ mg/L}$, stirrer speed = 0 rpm

Lastly, the reaction experimental setup that corresponds to “test 3” in Table 6.1 was tested with the series of Au/AC-PEG catalysts (Figure 6.5). 4-NP removal by AC adsorption is rather low, to begin with: it reaches a plateau at about 20% 4-NP removal after just 2.5 minutes. The catalytic activity of all Au/AC PEG samples is identifiable and doesn’t seem to be negatively affected by AC adsorption of the substrate as was the case for previous tests (the discussion dealing with the Au/AC series will

be evaluated in the next paragraph). Eventually, this reaction experimental setup seems to be the most appropriate for quantitative analysis of reaction kinetics for the particular reaction using highly adsorbing carbon materials.

6.3 4-Nitrophenol reduction: Screening of the catalysts

From the tests carried out on activated carbon, an appropriate set up to screen catalytic activity of the materials was found in the cuvette setup. This is because it allows to minimize physical adsorption by the support and this is why all the reaction was carried out following the cuvette procedure for every sample, to allow comparison of the results.^{126,127} After the determination of the real conversion (X_{extrap}), it was possible to evaluate the k_{app} for all the catalysts prepared.

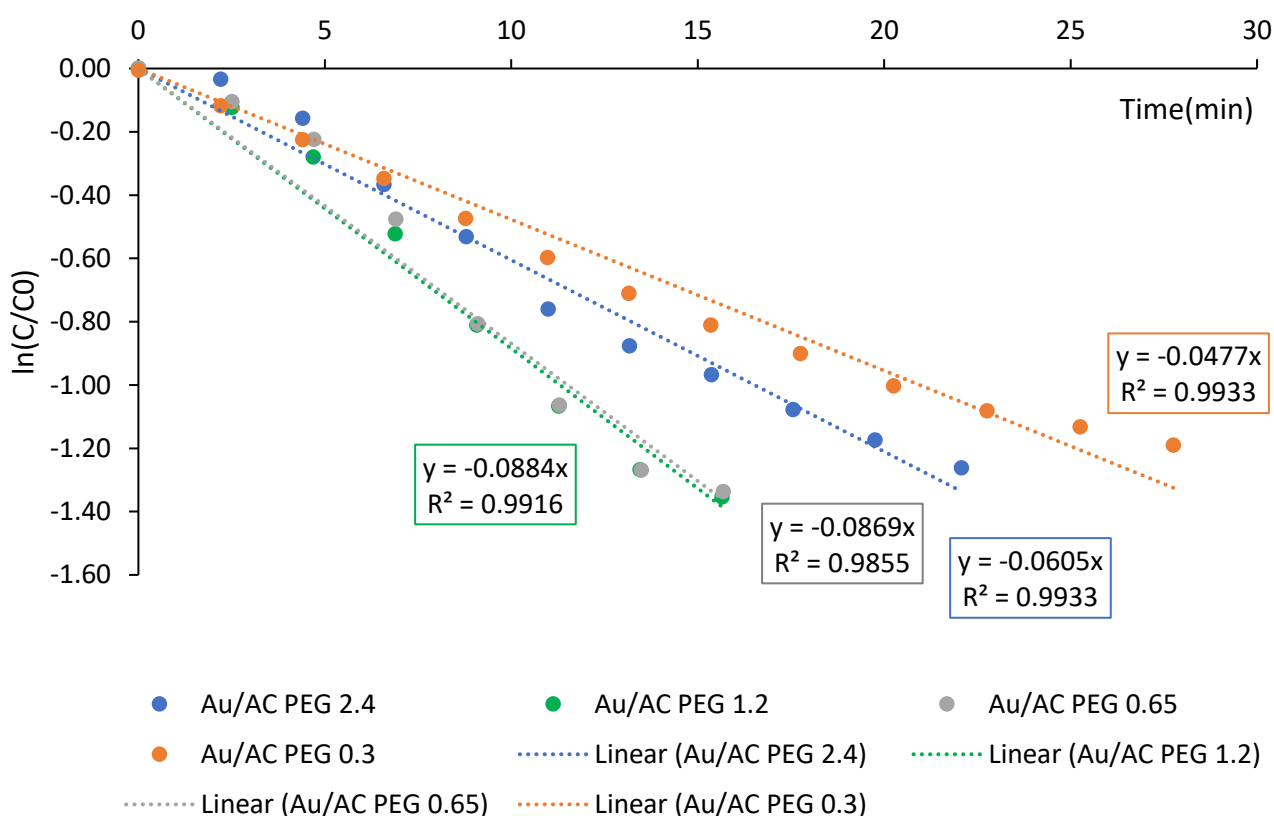


Figure 6.6: The pseudo first-order reaction curves for the 4-nitrophenol catalytic reduction by Au/AC PEG series of catalysts; k_{app} values are represented by the slope of the trendlines, for which R^2 values are shown

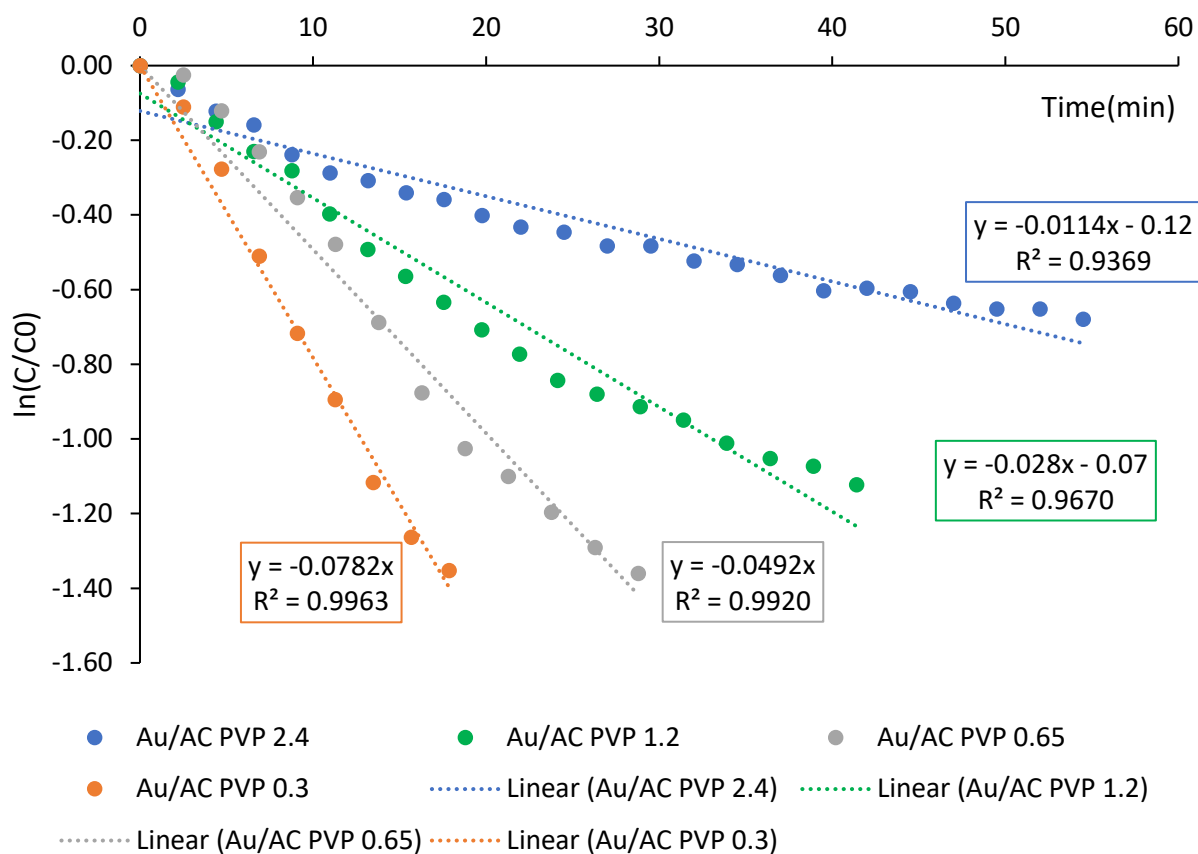


Figure 6.7: The pseudo first-order reaction curves for the 4-nitrophenol catalytic reduction by Au/AC PVP series of catalysts

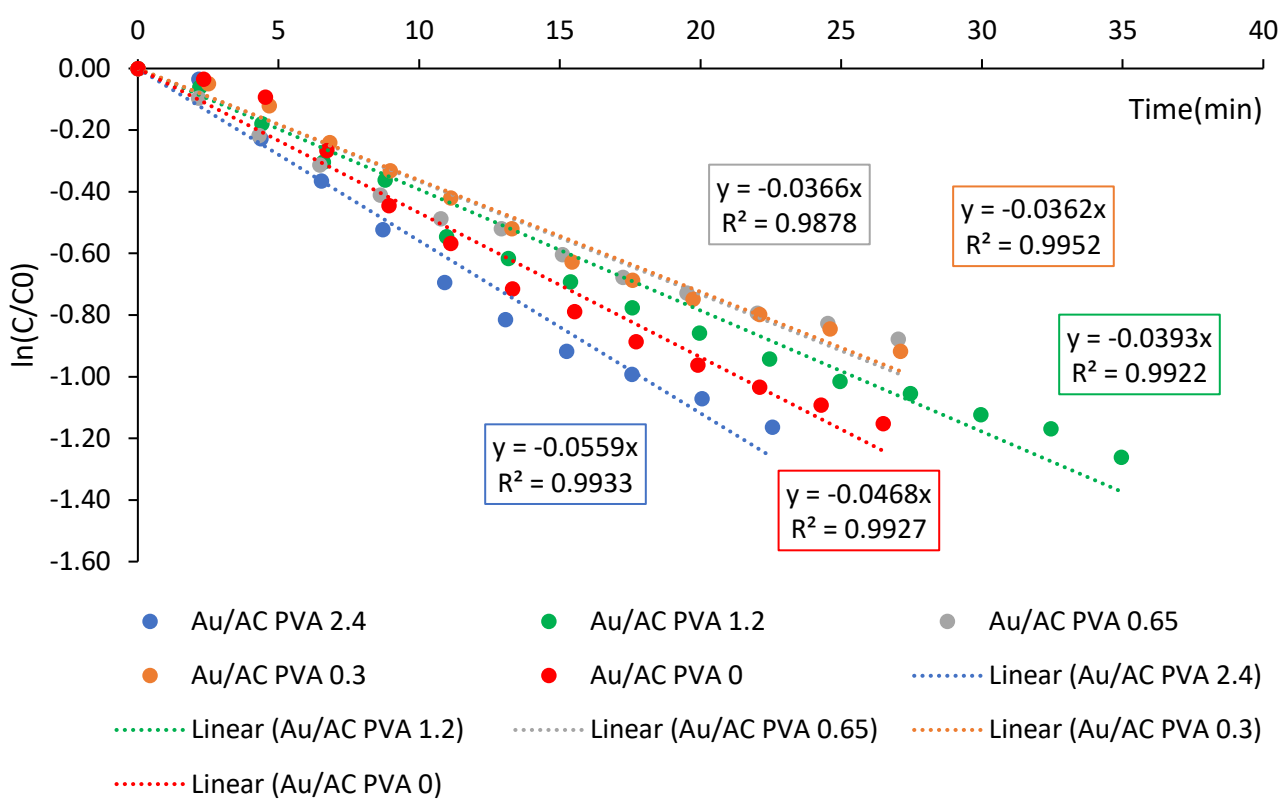


Figure 6.8: The pseudo first-order reaction curves for the 4-nitrophenol catalytic reduction by Au/AC PVA series of catalysts.

All the k_{app} values obtained for all the catalysts tested showed in Figure 6.6, 6.7 and 6.8 are grouped in Table 6.2.

Sample	k_{app} (min ⁻¹)	Mean Nanoparticle size	
		(nm)	
Au/AC PEG 0.3	0.048	10.3 ^a	
Au/AC PEG 0.65	0.087	6.4 ^a	
Au/AC PEG 1.2	0.088	6.2 ^a	
Au/AC PEG 2.4	0.061	8.0 ^a	
Au/AC PVP 0.3	0.078	5.5 ^b	
Au/AC PVP 0.65	0.049	5.6 ^b	
Au/AC PVP 1.2	0.028	7.4 ^b	
Au/AC PVP 2.4	0.011	8.4 ^b	
Au/AC PVA 0.3	0.036	4.3 ^b	
Au/AC PVA 0.65	0.037	3.1 ^b	
Au/AC PVA 1.2	0.039	2.6 ^b	
Au/AC PVA 2.4	0.059	2.3 ^b	
Au/AC PVA 0	0.047	7.8 ^b	

Table 6.2: List of the samples with their respective obtained k_{app} and supported Au nanoparticle size. ^a Crystallite mean size obtained from XRD patterns by application of Scherrer equation. ^b Mean nanoparticle diameter obtained by TEM analysis

The comparison between catalysts with the same or different stabilizing agent could give different information in terms of structure-activity relationships.

It is well-known that nanoparticle size has an important influence on catalytic activity. For this reason, the kinetic constant obtained for nitrophenol reduction with each of the AC-supported Au nanoparticle catalysts was plotted against the respective Au nanoparticle size, derived from the XRD patterns by applying the Scherrer equation or from TEM analysis.

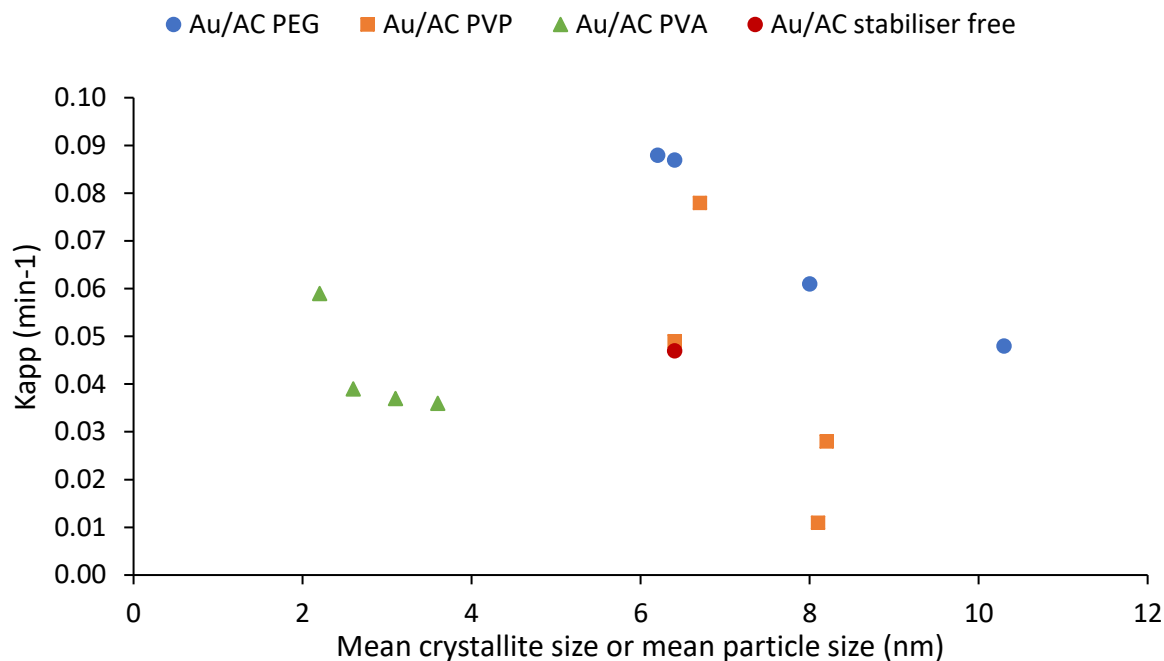


Figure 6.9: The values of k_{app} of the three catalyst sets obtained for the 4-nitrophenol reduction with the cuvette setup are plotted against mean nanoparticle diameter. Labels indicate the polymer: Au weight ratio

From figure 6.9 it is possible to notice that for each set, smaller nanoparticles show higher activity, in agreement with the works of Ghosh group¹²⁸ and Dasong et al.¹²⁹

The Au/AC PVA series is the one that showed the smaller mean Au particle sizes, however, it shows lower catalytically active compared to the other two sets. The series of Au/AC PEG catalysts show an overall better catalytic performance, and the best catalytic performance among the three sets is obtained with the samples Au/AC PEG 0.65 and Au/AC PEG 1.2 (k_{app} = 0.087 min^{-1} and 0.088 min^{-1} respectively). On the other hand, the series of Au/AC PVP catalysts do not show a clear catalytic trend based on the reported catalytic activities, since the sample Au/ACPVP0.3 has k_{app} = 0.078 min^{-1} comparable to Au/AC PEG0.65 and Au/AC PEG1.2, while sample Au/AC PVP2.4 and Au/AC PVP1.2 (k_{app} = 0.028 min^{-1} and 0.011 min^{-1} respectively) have lower catalytic activity than Au/AC PVA0.3 (has k_{app} = 0.036 min^{-1}). For this reason, the dimension of the Au nanoparticles isn't the only factor that contributes to the reaction activity but also the nature of the polymer that was used as the chosen stabilizer. To understand better how this impact in the k_{app} , it was plotted the obtained catalytic constant against the stabilizer: Au weight ratio to elucidate the effect of this parameter on catalytic activity.

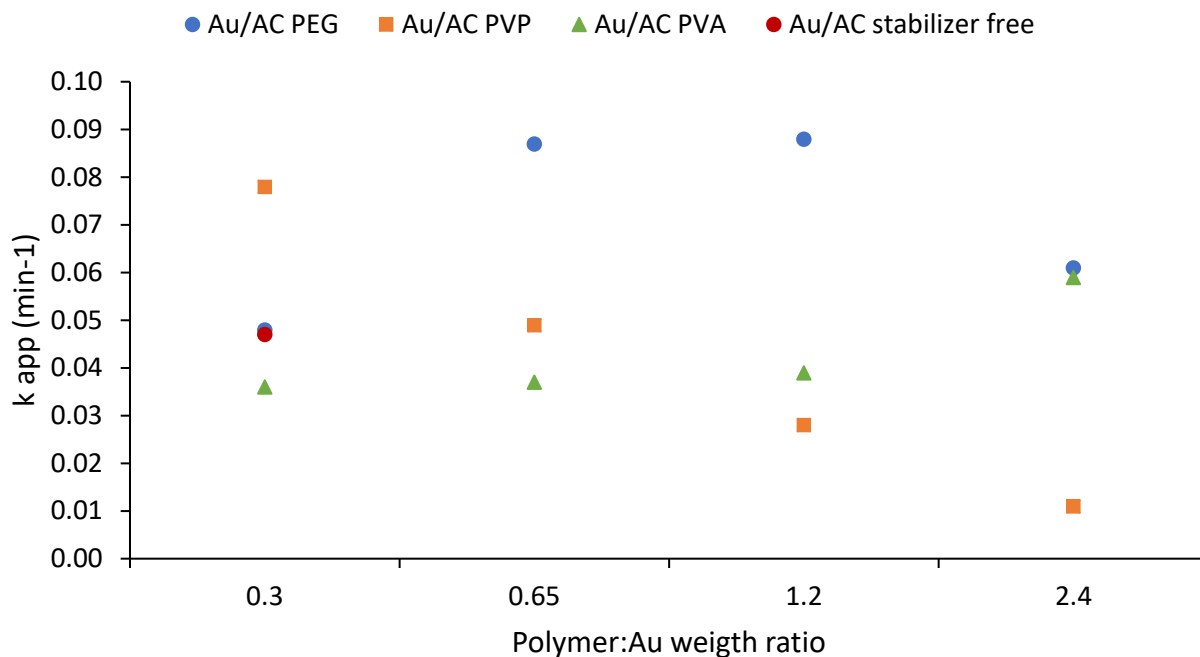


Figure 6.10: The values of k_{app} of the three catalyst sets obtained for the 4-nitrophenol reduction with the cuvette setup are plotted against the stabilizer:Au weight ratio

From the catalytic data presented in Figure 6.10, it can be noticed that PEG is the polymer that shows better catalytic results when the Au to polymer weight ratio as varied. The Au/AC PEG set shows comparable activity for the PEG:Au ratios 0.65 ($k_{app} = 0.087 \text{ min}^{-1}$) and 1.2 ($k_{app} = 0.088 \text{ min}^{-1}$), for the PEG:Au 2.4 ratio the activity decreases ($k_{app} = 0.061 \text{ min}^{-1}$) but the least active sample of the set is Au/AC-PEG0.3 with $k_{app} = 0.048 \text{ min}^{-1}$. This could be ascribed to two different factors: the first could be the way how PEG is adsorbed and interacted on the surface of the gold and also on the Au-support interface and which configuration assumes in water, leaving more free active sites on the surface in comparison with the other polymers. Moreover, the presence of a lactame group for the PVP could coordinate the Au surface through N and donates electrons from N to the metal. In particular, the series of Au/AC PVP set shows higher activity at the lower PVP:Au weight ratio. The activity decreases as the PVP:Au ratio increases: the catalytic activity of the lower PVP:Au (Au/AC PVP0.3) is sevenfold the activity of the sample with the highest PVP:Au (Au/AC-PVP2.4), from $k_{app} = 0.078 \text{ min}^{-1}$ to $k_{app} = 0.011 \text{ min}^{-1}$ respectively. Au/AC PVP 0.65 and Au/AC PVP 1.2 show intermediate activity.

The sample without stabilizer (Au/AC PVA0) is not affected by the blocking effect of the polymer and with a k_{app} of 0.048 min^{-1} has activity comparable to the samples Au/AC PEG0.3 and Au/AC PVP0.65.

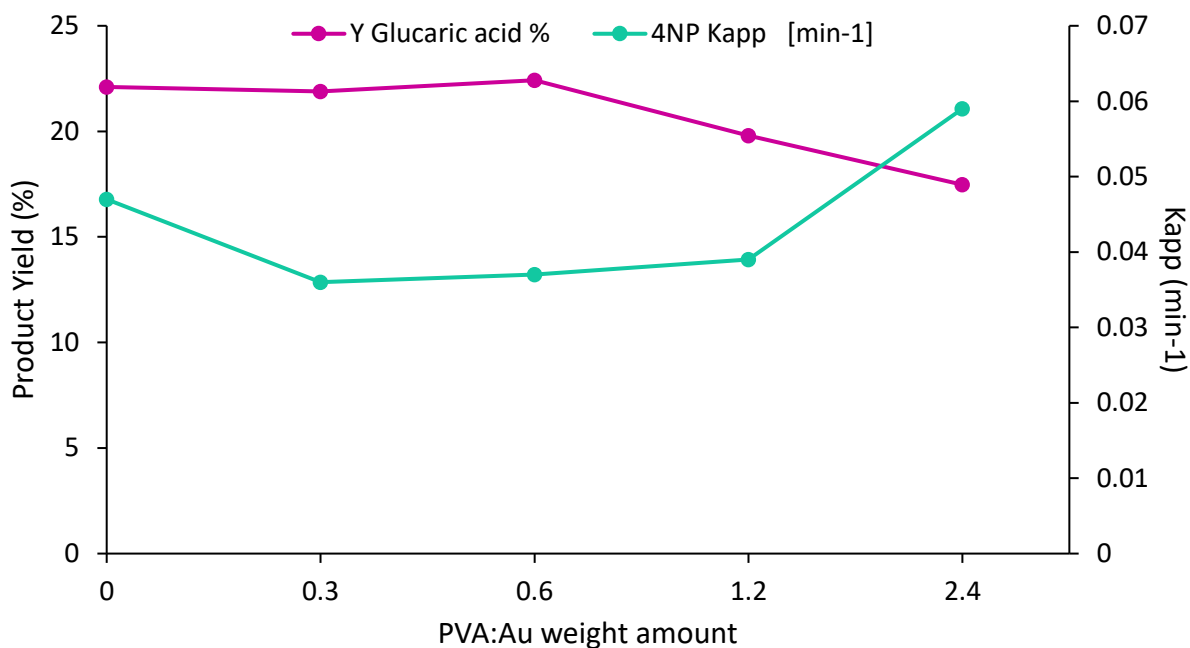


Figure 6.11: Correlation between the GA yield and Kapp of 4-nitrophenol reduction with the PVA: Au weight amount

Moreover, it is very interesting to compare the behavior of the same catalyst series for different reactions. To analyze the data, it was considered as an activity indicator the GA yield and the Kapp and this is why in Figure 6.11 it was reported the GA yield and the 4NP k_{app} versus the PVA: Au weight ratio. As it can be noticed, the trends for these two reactions are the opposite. These results indicate that different structural characteristic of the catalyst affects the activity of the reaction.

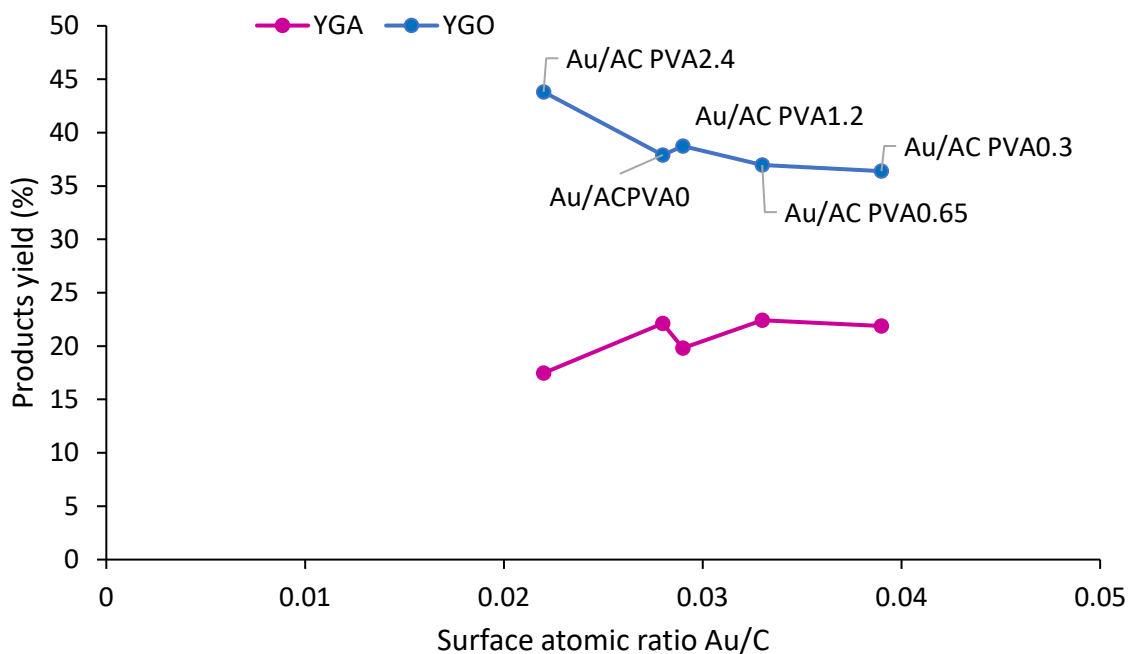


Figure 6.12: GA and GO yield in function of surface atomic ratio Au/C of Au/AC PVA series

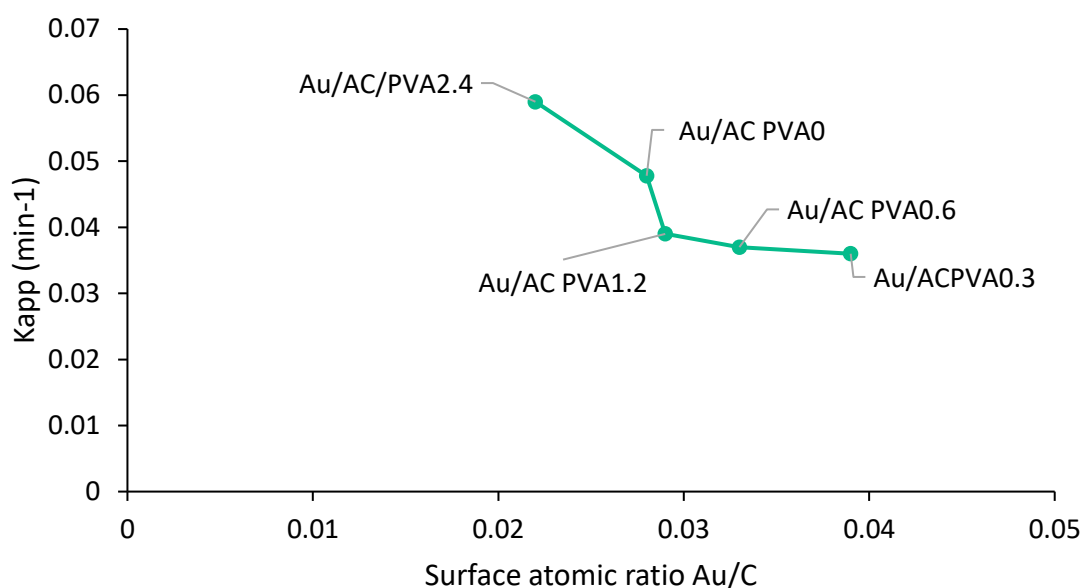


Figure 6.13: *K_{app}* of 4-nitrophenol reduction in function of surface atomic ratio Au/C of Au/AC PVA series

For example, the comparison between Figure 6.12 and Figure 6.13 shows how the surface atomic ratio of Au/C of the Au from XPS analysis for the Au/AC PVA series affects in a completely different way the two reactions; for the glucose oxidation, higher availability on the surface of support of gold active sites seems to facilitate the conversion to GA, on the contrary, the 4-NP shows the opposite trend. Therefore we have to take into account how the active surface sites affect the adsorption and binding configuration of the reactants and intermediates and consequently influence the final catalytic activity and yield to specific products.

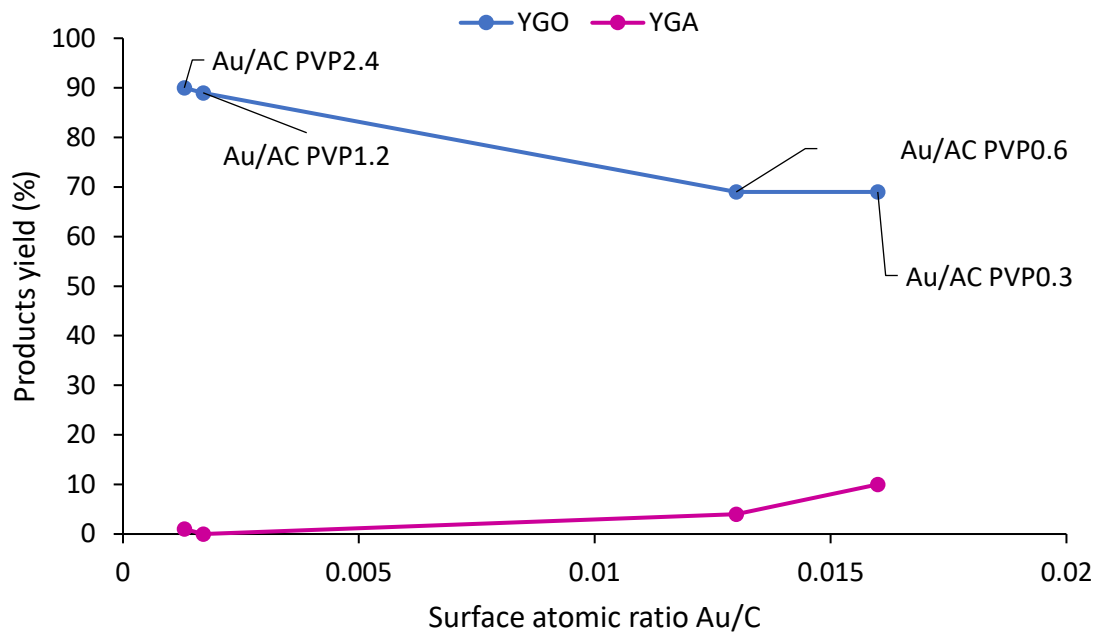


Figure 6.14: gluconic acid (GA) and gluconic acid (GO) yield in function of surface atomic ratio Au/C of Au/AC PVP series

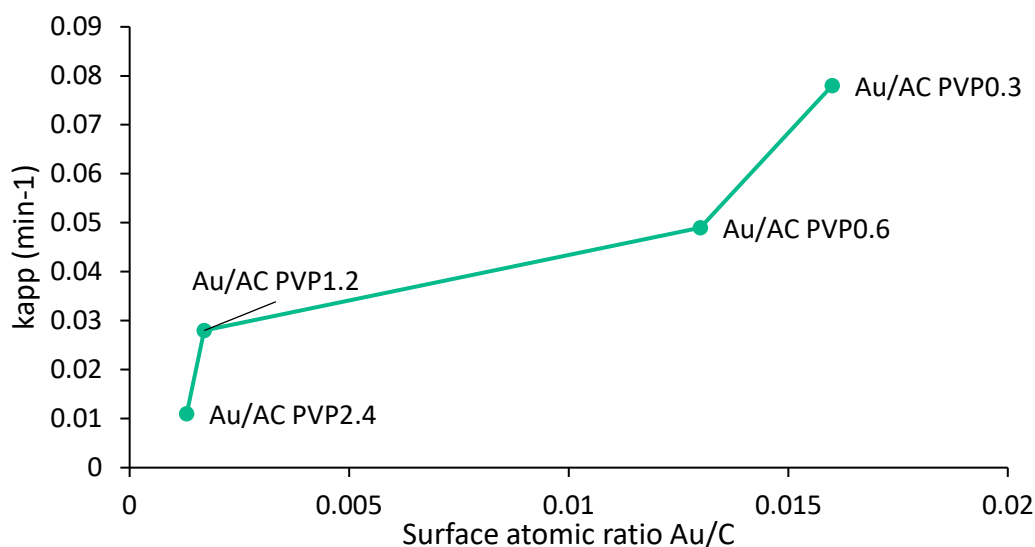


Figure 6.15: Kapp of 4-nitrophenol reduction in function of surface atomic ratio Au/C of Au/AC PVA series

Completely different is the scenario for the Au/AC PVP series (Figure 6.14 and Figure 6.15), where for both reactions, the catalytic activity seems to be enhanced when there is an increase of surface atomic ratio Au/C. However, it has to be considered that the structure of the reagent, the reaction condition, and the kind of reaction is completely different and maybe could affect our final evaluation. For this reason, the comparison with other oxidation reactions could help us to understand if the parameters are the same or we have a different trend.

¹²⁶ Seo, Catalytic reduction of 4-nitrophenol with gold nanoparticles synthesized by caffeic acid, *Nanoscale Research Letters*, **2017**,12:7

¹²⁷ K. Naseem, R. Begum, W. Wu, Core/shell composite microparticles for catalytic reduction of p-nitrophenol: kinetic and thermodynamic study, *Appl. Organometal. Chem.*, **2016**, 1–8

¹²⁸ S. Panigrahi, S. Basu, S. Praharaj, S. Pande, S. Jana, A. Pal, S.K. Ghosh, T. Pal, Synthesis and Size-Selective Catalysis by Supported Gold Nanoparticles: Study on Heterogeneous and Homogeneous Catalytic Process, *J.Phys. Chem. C*, **2007**, 111, 4596

¹²⁹ Y. Mei, G. Sharma, Y. Lu, M. Drechsler, T. Irgang, R. Kempe, M. Ballauff, High Catalytic Activity of Platinum Nanoparticles Immobilized on Spherical Polyelectrolyte Brushes, *Langmuir*, **2005**, 21, 12229

7 Chapter 7-Furan compounds oxidation

7.1 Hydroxymethylfurfural oxidation

As it was seen from the previous section, the study of an oxidation reaction could be easier compared with the glucose oxidation reaction. In particular, the investigation of HMF oxidation to 2,5-furandicarboxylic acid (FDCA) could be matched easily with glucose oxidation: HMF and glucose have the same starting functional group (the terminal OH group and an aldehyde group), and the oxidation reactions lead to the formation of diacid molecules. Furthermore, Chapter 1 has already shown the research interest for the HMF oxidation to FDCA in the industry field: HMF can be obtained from the dehydration of sugars and FDCA has several applications in the polymer industry.

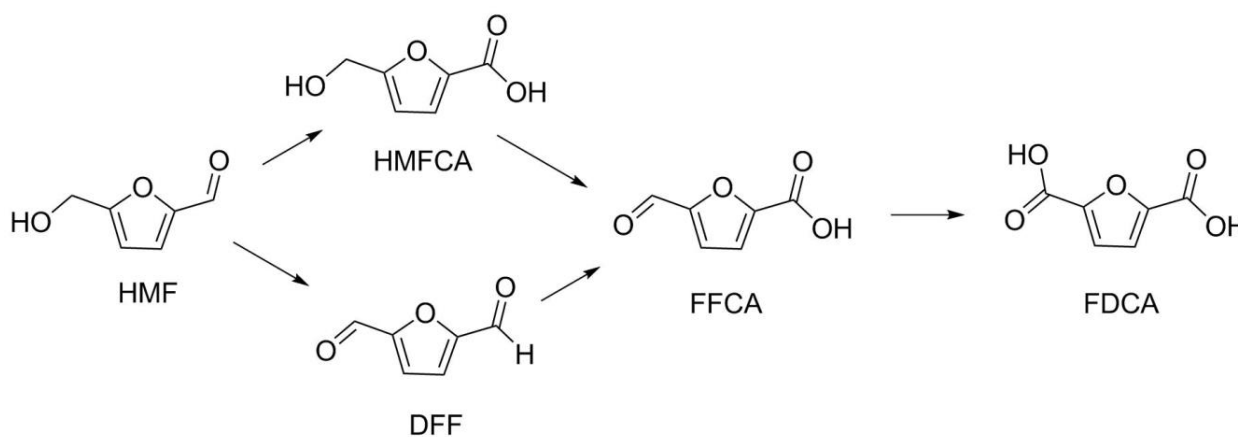


Figure 7.1: Reaction pathway of HMF oxidation to FDCA

In Figure 7.1 is represent the reaction pathway of the HMF oxidation. The oxidation can proceed through two different partially oxidized intermediates: the 5-hydroxymethyl-2-furancarboxylic acid (HMFCFA) and 2,5-diformylfuran (DFF). The formation of these intermediate could be influenced by the reaction condition: for example, it was observed that high pH value promotes the formation of HMFCFA, the intermediate thermodynamically more stable. Both intermediates subsequently oxidized to 5-formyl-2-furancarboxylic acid (FFCA) before further oxidation to FDCA.¹³⁰

7.1.1 HMF oxidation: Effect of the reaction time to conversion and yield

At first, it was studied how the intermediates and products evolve with reaction time, in order to analyze the reaction kinetics for the reaction.

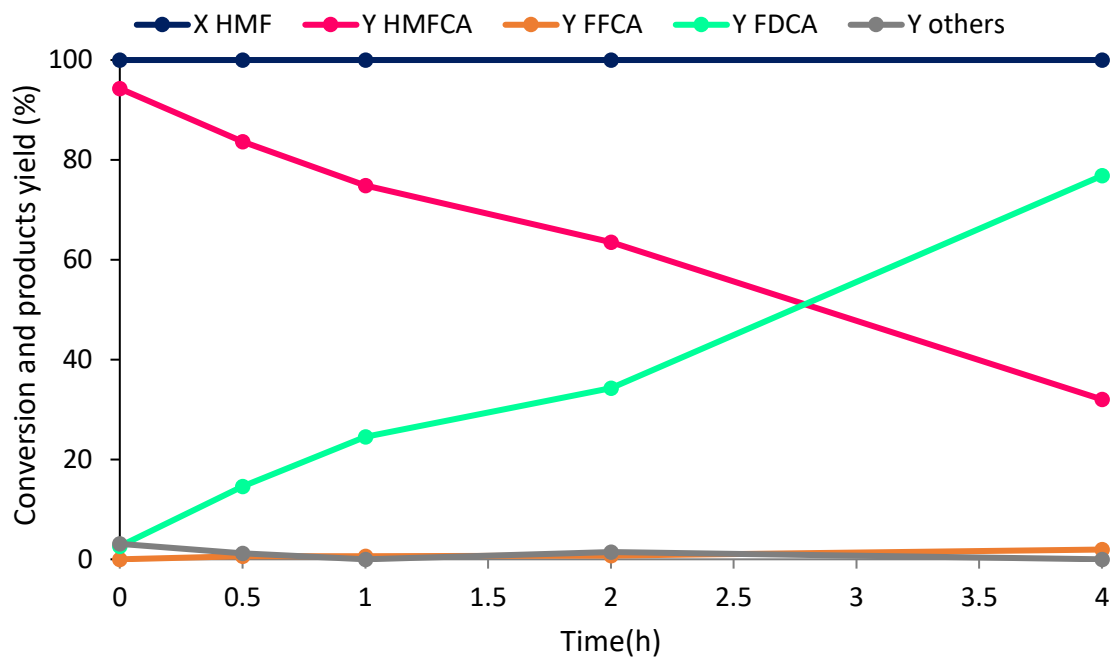


Figure 7.2: Conversion and products yield in function of the reaction time. Reaction Parameter: $T=70^{\circ}\text{C}$, $P=10$ bar, NaOH:HMF 4:1, HMF:Au 100:1. Catalyst used: Au/AC PEG 0.65

In Figure 7.2 are reported the HMF conversion and the yields of 2,5-furandicarboxylic acid (FDCA), 5-hydroxymethyl-2-furancarboxylic acid (HMFCFA), and 5-formyl-2-furancarboxylic acid (FFCA) at 0 min, 30 min, 1 hour, 2 hours, and 4 hours as a function of reaction time. The values recorded at short times show that the oxidation of the HMF aldehyde group to the HMFCFA carboxylic acid is very fast; even at $t = 0$ (it is considered when the set point temperature was reached) the conversion of HMF is complete and HMFCFA yield is 94%. FDCA and FFCA are not detected at the initial time. The reaction time affects the formation and yield of HMFCFA; after 30 minutes the yield has decreased to 86% and continued to decrease until reaching the value of 32% after 4 hours of reaction. At the same time, the yield of FDCA increased. These two trends suggest that HMFCFA plays the role of intermediate of the reaction for the formation of FDCA, as shown in the mechanism in Figure 7.1. Moreover, the yield of FDCA increased with longer reaction time, starting from 14% at 30 minutes and reaching 77% after 4 hours. The other intermediate proposed FFCA is not detected for any time; this is because the aldehyde group is high reactivity and it converts directly in the carboxylic acid (FDCA). Moreover, the chosen reaction conditions and the choice of the catalyst doesn't lead to the formation of any by-products from the HMF polymerization, namely with "Other".

7.1.2 HMF oxidation: Screening of the catalysts

The screening of catalyst as a function of reaction time confirms the role of HMFCAs as intermediates in the reaction¹³¹; as it was done for the glucose oxidation, the trend of the yield of HMFCAs could help to understand better the effectiveness of the catalyst. After that, it was compared to the three series of catalysts and Figure 7.3 shows the results obtained testing the Au/AC PVA series.

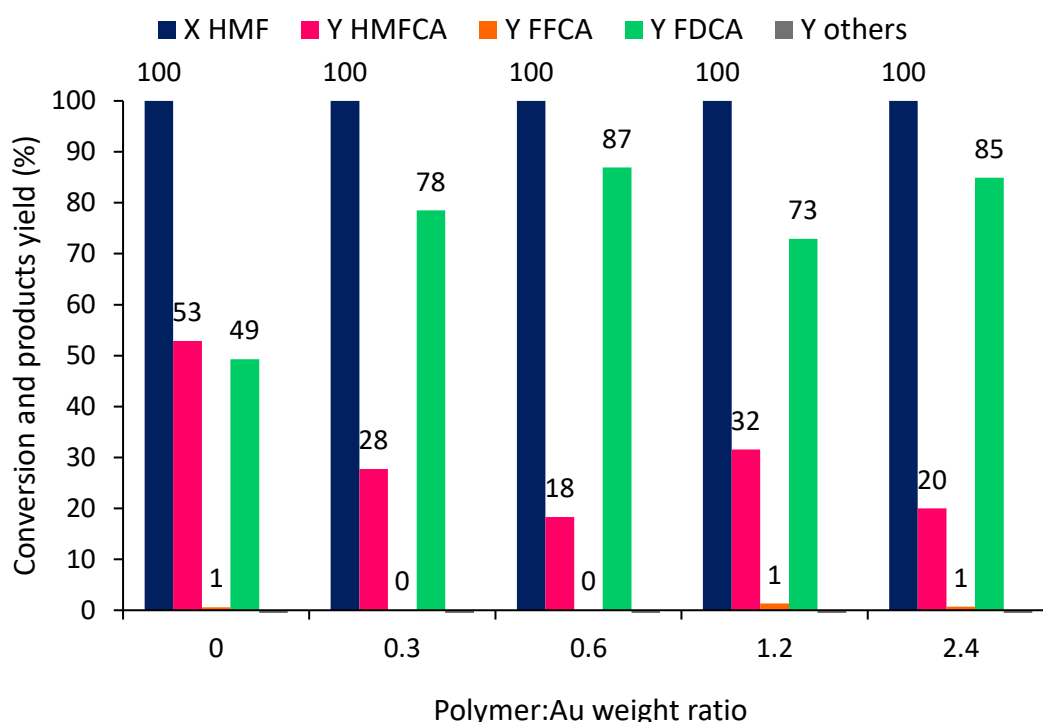


Figure 7.3: Conversion and products yield in function of polymer: Au weight ratio for Au/AC PVA series. Reaction Parameter: $T = 70^{\circ}\text{C}$, $P = 10 \text{ bar}$, $t = 4 \text{ h}$, $\text{NaOH:HMF } 4:1$, $\text{HMF:Au } 100:1$

All the catalysts at the chosen reaction conditions permit to reach 100% of HMF conversion. The other common observation for all the catalysts studied is that the FDCA formation passes through the HMFCAs intermediate and not from the DFF, but this is mainly due to the strong basic conditions used that make the carboxylic acid more thermodynamically stable. The increase of PVA amount from Au/AC PVA0 to Au/AC PVA0.6 leads to an enhanced catalytic activity: the HMFCAs yield decreased from 53% to 18%, the intermediate was converted to FDCA from 49% to 87% at the end of the reaction. Probably this initial trend is related to the decrease of the size of the Au nanoparticles as the amount of the polymer increases, with the optimum sample to be the one with the PVA to Au weight ratio of 0.6. The Au/AC PVA 2.4 shows a similar catalytic behavior, instead,

Au/AC PVA1.2 seems to be less reactive; a higher amount of stabilizing agent doesn't affect in a better way the performance of the catalyst. Without considering the sample Au/AC PVA 1.2, from Figure 7.4 seems that the nanoparticles dimension is the main parameter that affects the catalyst behavior: smaller dimensions lead to higher FDCA yield.

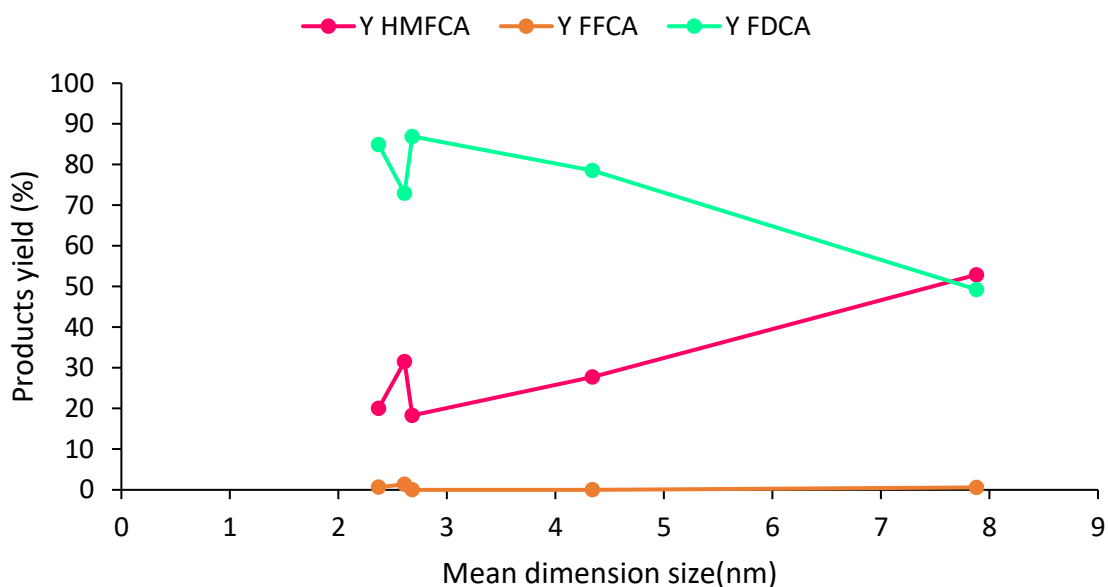


Figure 7.4: Products yield in function of mean dimension size by TEM analysis for Au/ACPVA series

For the Au/AC PVA series, it was already seen that nanoparticle size of Au and surface atomic ratio Au/C do not have a linear correlation because the stabilizing agent could block or partially cover the active sites of Au (see Table 4.4). To understand better if gold surface availability could influence the reaction behavior and if there is a correlation, the surface atomic ratio Au/C was plotted against the Yield of HMFCA and FDCA obtained (Figure 7.5).

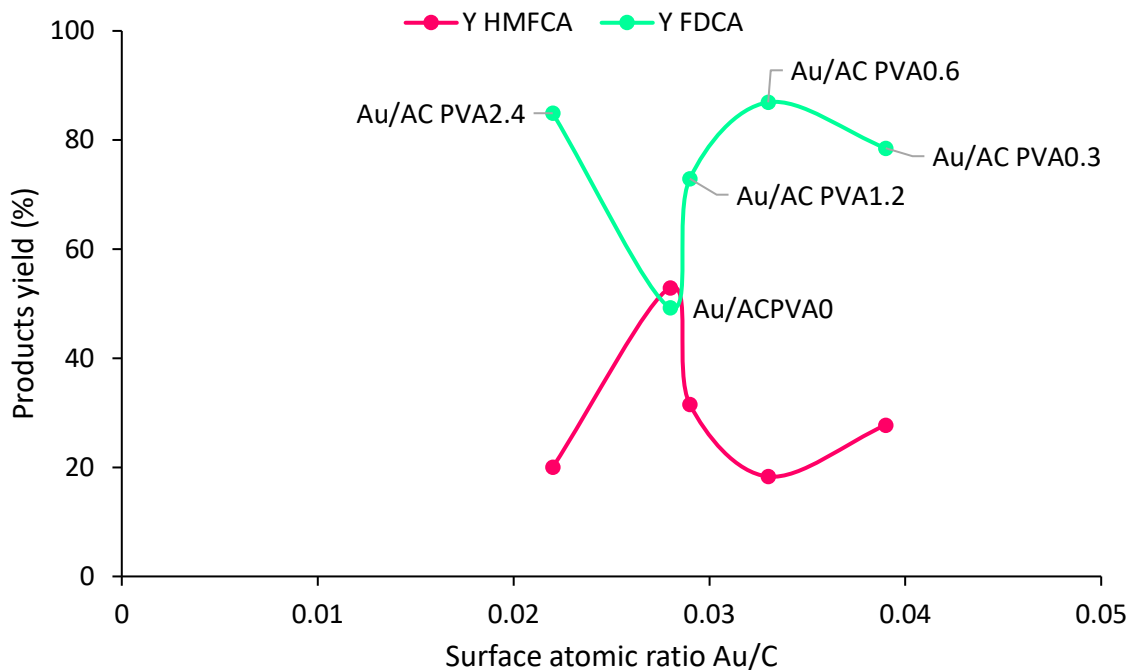


Figure 7.5: Products yield in function of surface atomic ratio Au/C by XPS analysis for Au/ACPVA series

The trend of surface atomic ratio Au/C vs yield FFCA is not reported because the amount of FFCA is low, even non-present in some reactions. Moreover, because the HMFCFA is the intermediate of the FDCA and there is no other by-side reaction starting from it, its trend is specular to the one observed for FDCA; for this reason, in the following part, it was analyzed just the trend of FDCA. It is evident how the trend here reported is completely different from the one seen for Glu oxidation and 4NP reduction. Initially, low surface atomic ratio of Au/C (Au/AC PVA2.4 have 0.022) seems to give high FDCA yield (85%); then the increase of surface atomic ratio of Au/C makes drop the product yield until 45 %, the lower value recorder for Au/AC PVA0. However, Au/AC PVA0.6 and Au/AC PVA0.3, which shows the higher surface atomic ratio of Au/C, gives FDCA yield comparable with the one of Au/ACPVA2.4. This parameter is not the one that affects directly the reaction behaviour.

As it was seen for the glucose oxidation, the higher amount of PVA is expected to block active sites, therefore higher amount of polymer was expected to lead a lower formation of the FDCA; however, HMF oxidation reaction is performed at higher temperature and longer reaction time, parameters that can promote the PVA solubilization.

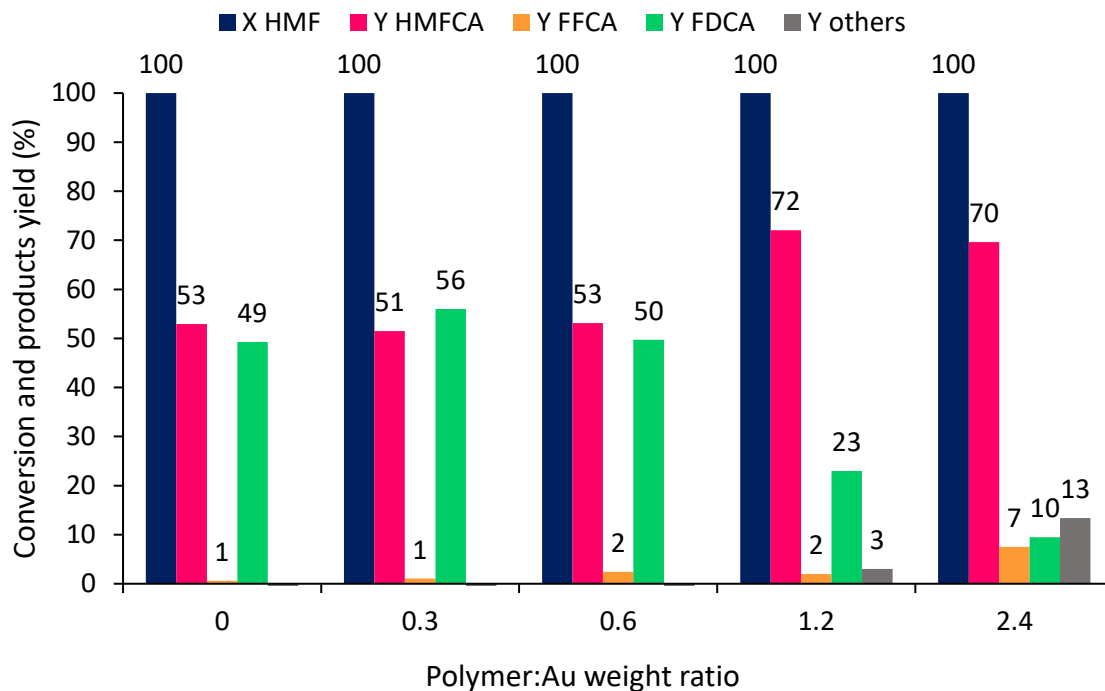


Figure 7.6: Conversion and products yield in function of polymer: Au weight ratio for Au/AC PVP series . Reaction Parameter: $T=70^{\circ}\text{C}$, $P=10\text{ bar}$, $t=4\text{h}$, $\text{NaOH:HMF } 4:1$, $\text{HMF:Au } 100:1$

The Au/AC PVP series instead have a completely different trend (Figure 7.6); Au/AC PVP0.3 showed a slight improvement compared to the one without stabilizing agent (Y FDCA Au/AC PVP0= 49% vs Au/AC PVP0.3 =56%). However, a further increase of PVP amount leads to a reduction in catalytic activity, causing a decrease in FDCA yield, an increase of the intermediate species (for Au/AC PVP2.4, a 7% in FFCA was seen) and the formation of other byproducts. As it was seen in Chapter 4, a higher PVP: Au weight ratio leads to the formation of bigger particle sizes. The FDCA yield decreasing could be ascribed to the NP dimension and the PVP increasing; the smallest nanoparticles of Au/AC PVP0.3 (5.5nm) lead to a higher amount of the final product, which decreases until 10% when the dimension is 8.4nm (Au/AC PVP2.4).

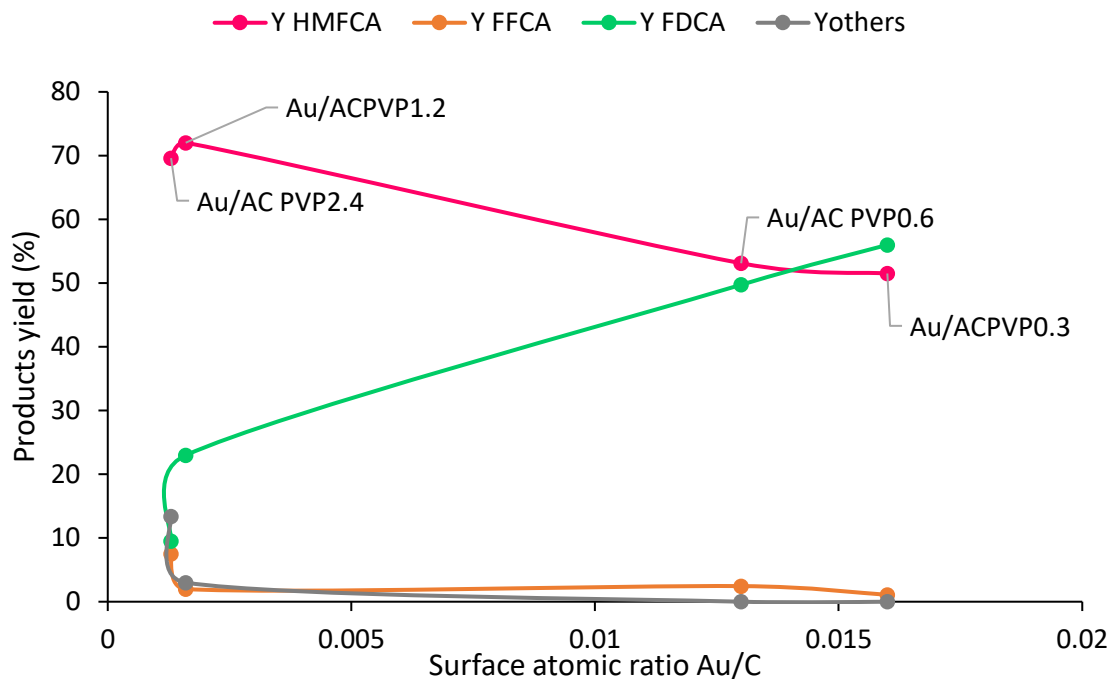


Figure 7.7: Products yield in function of surface atomic ratio Au/C by XPS analysis for Au/AC-PVA series

Moreover, for the Au/AC PVP series, it was seen that the surface atomic ratio Au/C and the particle size have the same trend when the polymer amount increase; the comparison between the yield obtained with the surface atomic ratio Au/C gives a trend similar with the other reactions seen: an increase of Au available on the surface helps the formation of FDCA and the conversion of HMFCA (Figure 7.7). Au/AC PVP 0.3 is the one with higher surface atomic ratio Au/C and generates the higher Y in FDCA.

The last series that was screened is the Au/AC PEG series (Figure 7.8). After a worsening in performance for Au/AC PEG0.3 (FDCA Yield Au/ACPEG0 =49% vs Au/ACPEG0.3 =38%), Au/ACPEG 0.6 gives the best result of the series, with 77% of FDCA yields. After that, the increase of PEG amount doesn't lead to catalytic improvement in terms of yield, and the FDCA yield drops to 34%. Also for this series of catalysts seems that the nanoparticles dimension is the most important factor that affects the reaction; Au/AC PEG 0.6 and Au/ACPEG 1.2.

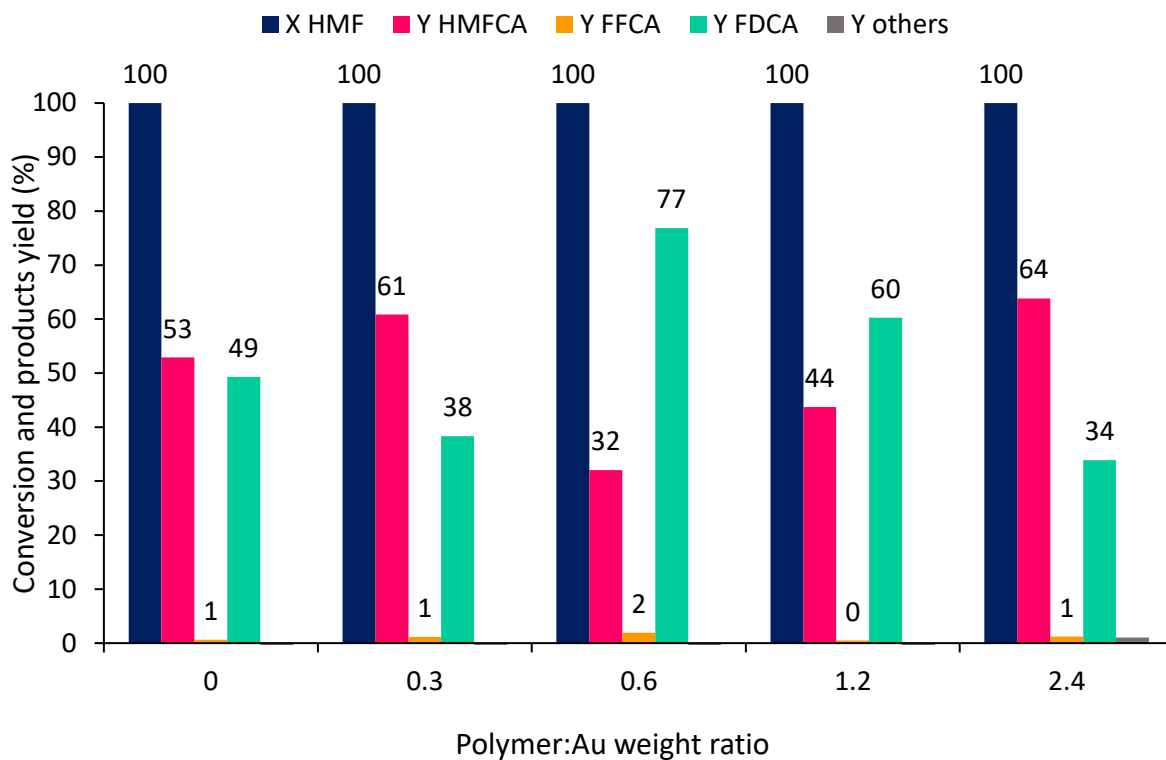


Figure 7.8: Conversion and product yield in function of polymer: Au weight ratio for Au/AC PEG series . Reaction Parameter: $T=70^{\circ}\text{C}$, $P=10\text{ bar}$, $t=4\text{h}$, $\text{NaOH:HMF } 4:1$, $\text{HMF:Au } 100:1$ (molar ratio).

For all the catalysts the dimension of the nanoparticles seems the main factor that influences the reaction behavior (see Figure 7.9). The Au/AC PVA set is the one that shows the smallest dimension and the highest FDCA yield. However, also the nature of the polymer plays a key role: there are four catalysts with a NPs dimension around 6nm (6.2, 6.4, 6.4 and 6.7 nm), but the samples that use PEG as a stabilizing agent (green dots) are more efficient than the one with PVP.

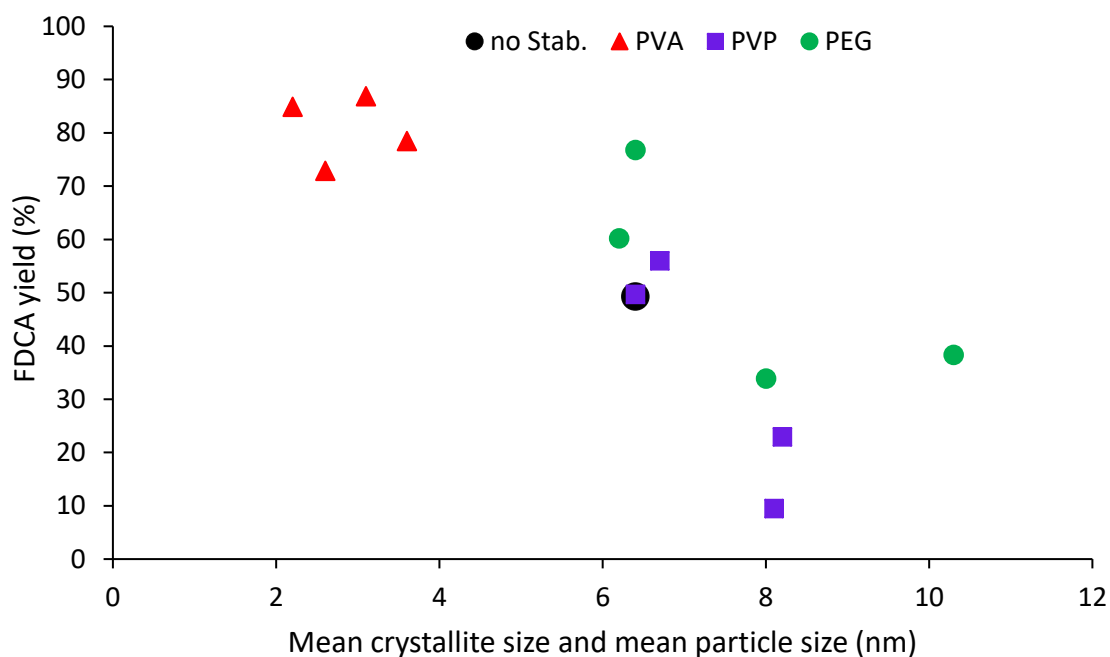


Figure 7.9: FDCA yield in function of mean crystallite size (by XRD) and mean particle size (by TEM) of Au/AC PVA, Au/AC PVP, Au/AC PEG series.

7.2 Furfural oxidative condensation-esterification

Like HMF, furfural is another furan compound that could be used as bio-derivates building blocks, with a very high potential for biorefineries development.¹³² Different reactions can be studied using the furfural as starting reagent, but in this work, we focus our attention to the oxidation reaction. Moreover, if alcohol with a H group in position α is used as solvent instead of water, this can be involved in the reaction mechanism, giving rise to two different pathways: the oxidative condensation and the oxidative esterification.

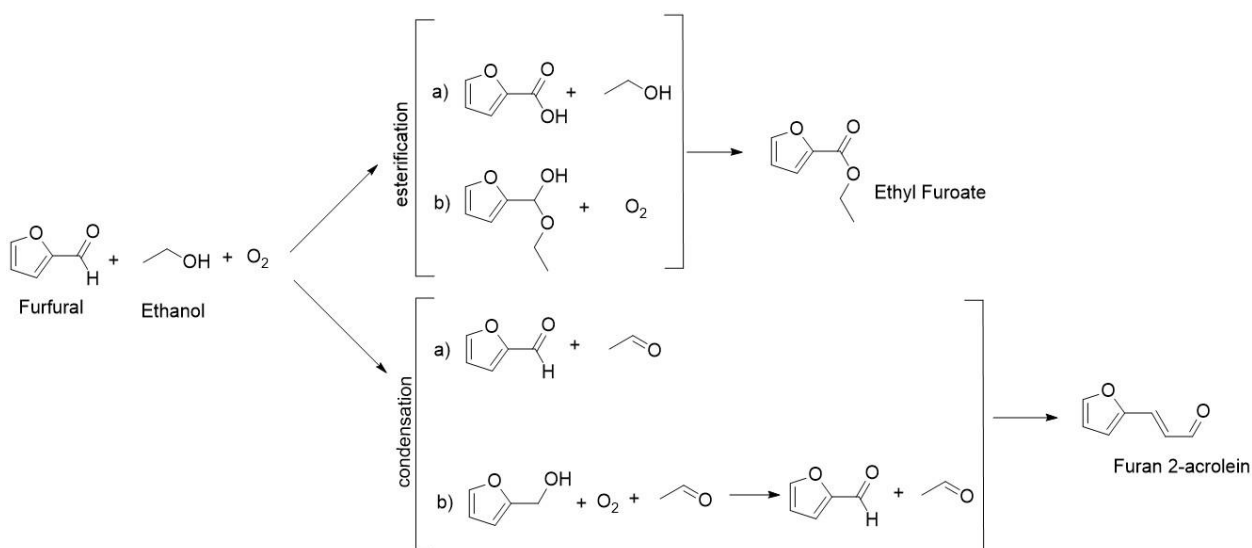


Figure 7.10: Reaction pathway for furfural oxidative condensation and oxidative esterification

Figure 7.10 shows the different pathways of the reaction. At first, several first step may be occur: for the esterification 1a) oxidation of furfural with O₂ or 1b) semi acetal reaction of furfural with ethanol; for the condensation 2a) oxidation of ethanol with O₂, (the condensation of furfural with ethanol hardly happens). In the following, the product ethyl furoate can be obtained via a) esterification of 2-furoic acid or b) the oxidation of ethoxy(furan-2-yl) methanol, while the product furan-2-acrolein can be attained from the condensation of furfural with acetaldehyde.¹³³

The industrial interest for these reactions and for the two different products in the fragrance sector was already shown in Chapter1; however, the study was focused on the furan 2-acrolein production.

7.2.1 Furfural oxidation: Effect of the reaction time to conversion and yield

To evaluate a mechanism, it is necessary to perform a number of experiments including (i) monitoring the progress of reaction varying the reaction time (time on line), (ii) the study using the intermediates as reactants and (iii) computational studies.

As reported in literature, the two reactions follow a parallel mechanism and in order to investigate it, the progress of the reaction was studied by analyzing samples periodically (0, 2, 4, 6, and 8 hours). During the progress of the reaction, the conversion of the substrate and the selectivity/yield of intermediates and products were determined.

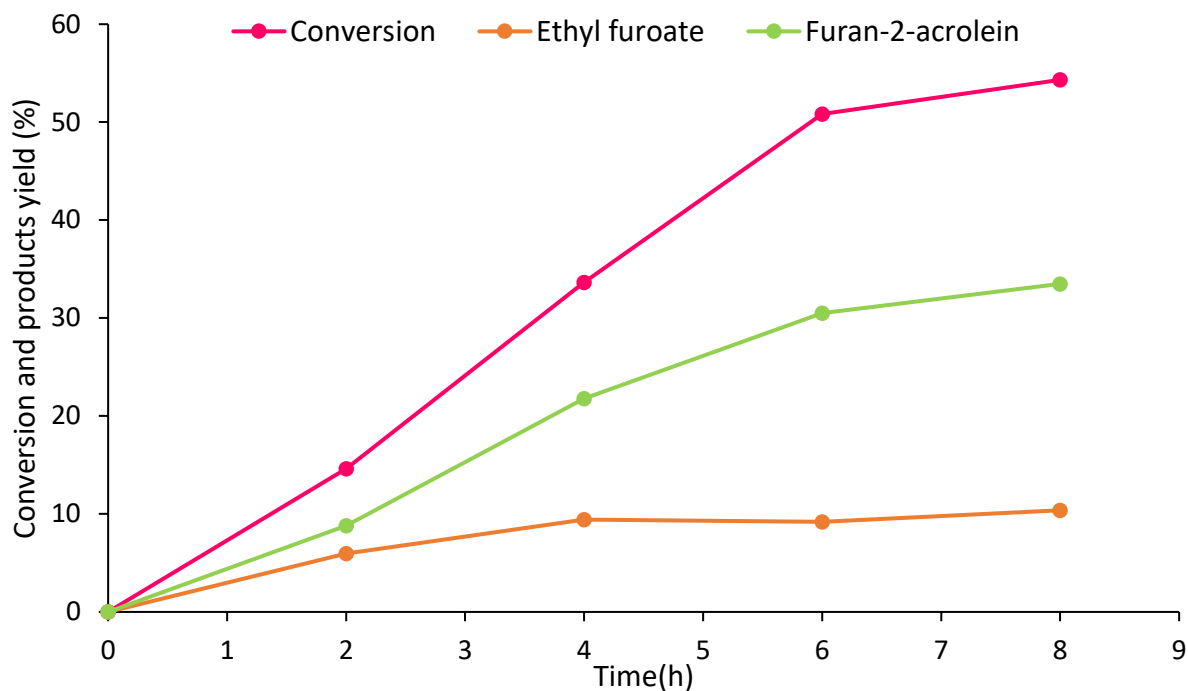


Figure 7.11: Reaction trend at different times. Reaction condition: Furfural 86 μ L, EtOH 6mL, 0.025mg catalyst, 0.1g Na₂CO₃, T = 120°C, stirrer speed = 350rpm. Catalyst used=Au/AC PVA2.4

Figure 7.11 shows the catalytic data obtained as a function of reaction time. At time 0 (*it is considered when the set point temperature was reached*), no furfural (Fur) conversion and product yield were detected, which means that there is no conversion at zero time. After 2 hours, the Fur conversion is only 14%, indicating the rate of reaction is slow, then a linearly increase to 34% and 51% after 4 and 6 hours of reaction was observed. After 8 hours, the conversion slightly increased, reaching only 54%. The ethyl furoate (EtFur) yield does not change drastically with time: from 6% after 2 hours, the yield reached at 9-10% after 4 hours. The furan-2-acrolein (Fur2Acr) instead has a trend more similar to the conversion: starting from 8% at 2 hours, it increases to 22% and 30% after 4 hours and 6 hours, respectively, then it reached a maximum value of 33% after 8 hours. For the catalytic trend obtained, it could be seen the increase of reaction time from 6 to 8 hours did not increase drastically the conversion and the product yields; moreover, the difference between Fur conversion and yield sum from 4 to 6 hours started to increase from 2% to 10%. The reasons for the decrease of carbon balance could be related to the fact that some chemical species start to adsorb in an irreversible way on the surface of the catalyst. From the GC analysis no other chemical species were detected. Tong et al¹³⁴ have showed that the increase of reaction time leads to an increase in

the amount of other products no specified; further GC MS analysis could be done to verify this possibility. For all these reasons, the catalytic tests were performed at 6 hours.

7.2.2 Furfural oxidation: Screening of the catalysts

The next step of investigation focused on the screening of the Au/AC PVA series and investigate the catalytic performance.

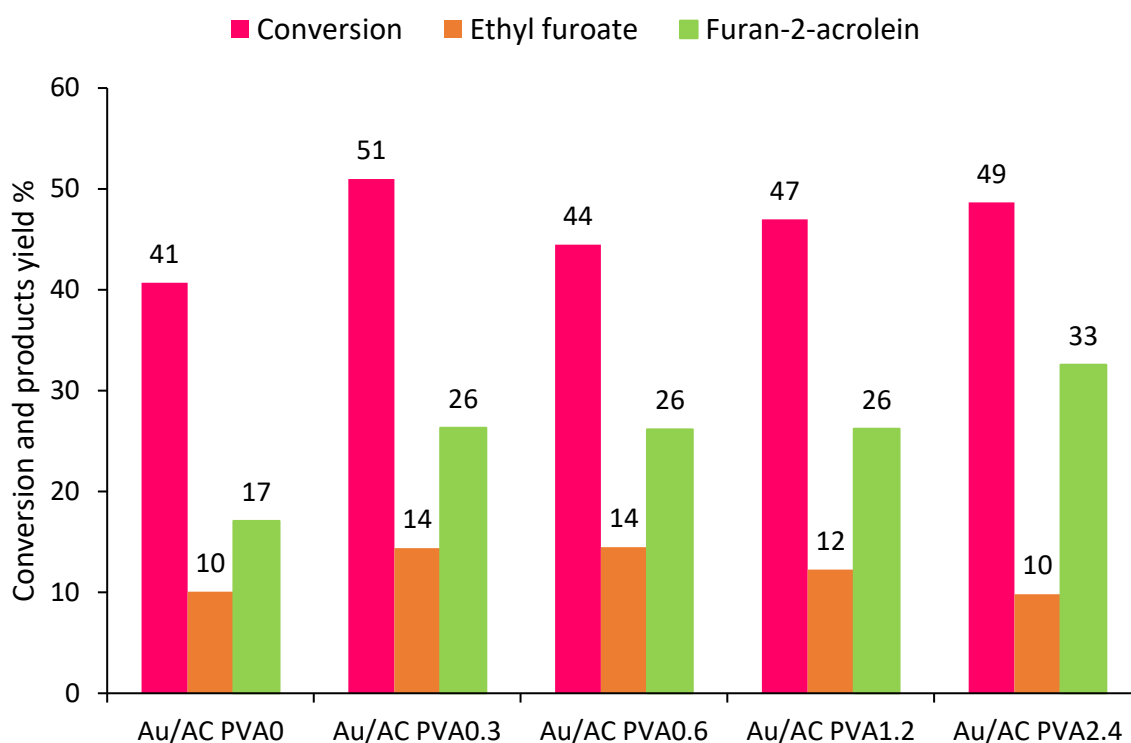


Figure 7.12: Reaction trend for Au/AC PVA series. Reaction condition: Furfural 86 μ L, EtOH 6 mL, 0.025 mg catalyst, 0.1g Na_2CO_3 , $T = 120^\circ\text{C}$, $t = 6$ hours, stirrer speed = 350rpm

In Figure 7.12 are reported the catalytic results of the series of the catalysts investigated as a function of the PVA to Au weight ratio used, (0-2.4) in terms of furfural (Fur) conversion and yields of ethyl furoate (EtFur) and furan 2-acrolein (Fur2Acr). It can be observed that the conversion of Fur does not change drastically, oscillating between 41% (Au/AC PVA0) and 51% (Au/AC PVA0.3). The difference between the Fur conversion and the yield sum was around 10%; to evaluate if this phenomena could be ascribed to the Fur adsorption on the support, a test using only the activated carbon was carried out. However, the support didn't show this effect, therefore the lower carbon balance due to adsorption on the support could be excluded. Moreover, the yield trends for the two products are quite different. In particular, the EtFur yield slightly increase by increasing the PVA

amount from Au/AC PVA0 to Au/ACPVA0.6, reaching the maximum yield of 14% for the Au/AC PVA0.6. However, higher PVA: Au weight ratio seems to cause a yield decrease and for Au/AC PVP2.4 it was obtained a value of 10%. However, the difference between the value are not dramatically big, so the variation could be attributed to the experimental error. Regarding the Fur2Acr, the formation of smaller nanoparticles is facilitated by increasing the amount of PVA, as we have shown previously, and can promote the formation of Fur2Acr, which shows an increase from 17% for Au/AC PVA0 to 33% for Au/AC PVA2.4. The selectivity reported in Figure 7.13 also confirmed the trend already seen for the EtFur and Fur2Acr yields and it is clear that Au/AC PVA2.4 gives the higher selectivity for the condensation product.

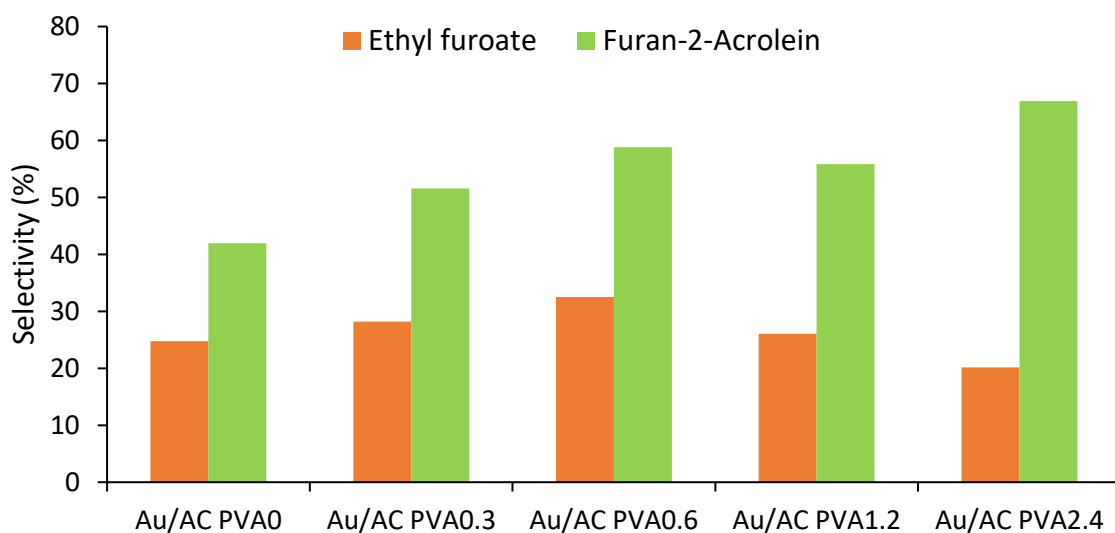


Figure 7.13: Reaction trend for Au/AC PVA series. Reaction condition: Furfural 86 μ L, EtOH 6mL, 0.025mg catalyst, 0.1g Na_2CO_3 , $T=120^\circ\text{C}$, $t=6\text{hours}$, stirrer speed =350rpm

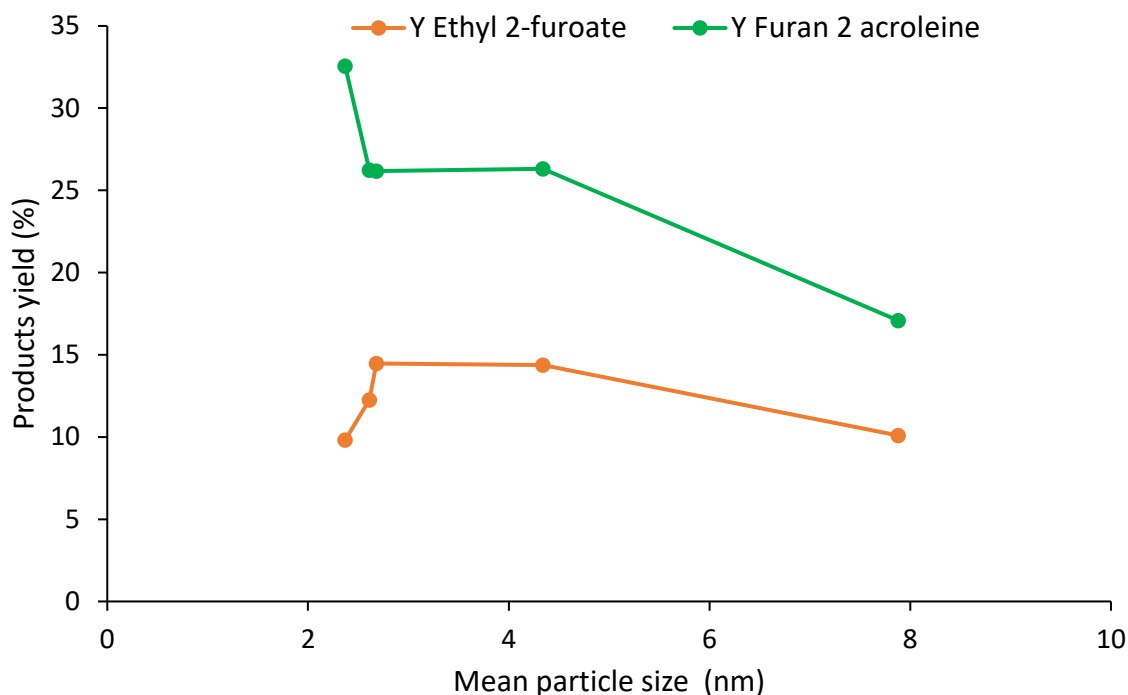


Figure 7.14: Products yield in function of mean particle size of Au/AC PVA series

In order to identify a possible structure-activity relationship, the yield of the desired products as a function of Au particle size was plotted (Figure 7.14) and it illustrates how the size of the Au nanoparticles could influence the yield reported for the catalysts tested. The two yield trends are quite different: for the smaller Au nanoparticles (2.4 nm), ethyl furoate (EtFur) yield is very low, reaching 10%. A slight increase of dimension leads to an increase in the EtFur yield until reaches 14%; the value remains constant for 2.7 nm and 4.3 nm. The additional increase in the size to 7.8 nm, however, causes a decrease to 10%. One hypothesis is that the highest amount of PVA of Au/AC PVA2.4 seems to give low yield of EtFur, whereas similar NP dimension (2.4 nm for Au/AC PVA2.4, 2.6nm for Au/ACPVA1.2, 2.7 nm for Au/AC PVA0.6) but at low PVA amount seems to increase the yield. At higher mean particle size (above ~5 nm), the yield to EtFur decreases again. Therefore, it is evident from the results that an optimum ratio between PVA to Au weight ratio is needed as an optimum value of mean Au particle size. The furan-2-acrolein (Fur2Acr) yield instead decreases with the increase of the mean particle size of the Au nanoparticles: yield of 33% was reached for the Au/AC PVA2.4 with the smaller Au nanoparticles (2.4nm), then the yield decreases to 17% for the sample with mean particle size of Au of 7.8 nm (Au/ACPVA0).

Moreover, the comparison between the product yields and surface atomic ratio of Au/C was valuated.

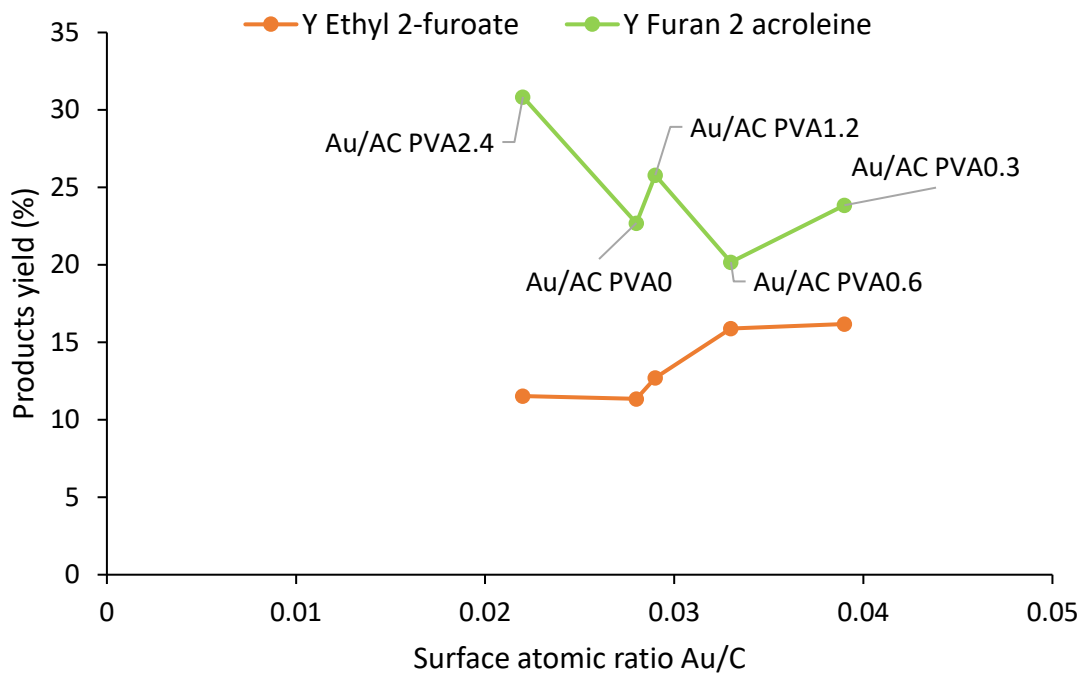


Figure 7.15: Products yield in function of surface atomic ratio Au/C for Au/AC PVA series

From Figure 7.15 it can be seen two different trends. The ethyl furoate yield shows an increase with the higher surface atomic ratio Au/C, even if it not linear as seen for glucose oxidation. Instead, the Fur2Acr has a completely different trend: Au/AC PVA2.4 is the sample with lower surface atomic ratio Au/C (0.022) but it is the one that gives the higher amount of product; the following catalyst for surface atomic ratio Au/C Au/AC PVA0 instead gives the lower yield (17%). Higher surface atomic ratio Au/C give yield between these two extremes.

In Chapter4 it was studied the effect of heat treatment and washing step to investigate the influence of the partial removal of the stabilizer in terms of catalytic performance for the glucose oxidation. In particular, it was seen that mild treatment condition like the washing (Au/AC washing) or heat treatment at 120°C (Au/AC HT 120°C) gave higher glucaric acid yield in comparison with the sample treated at higher temperature (Au/AC HT 200°C and Au/AC HT 250°C). As these samples was tested for the glucaric synthesis, they were used as a catalyst for the furfural oxidation.

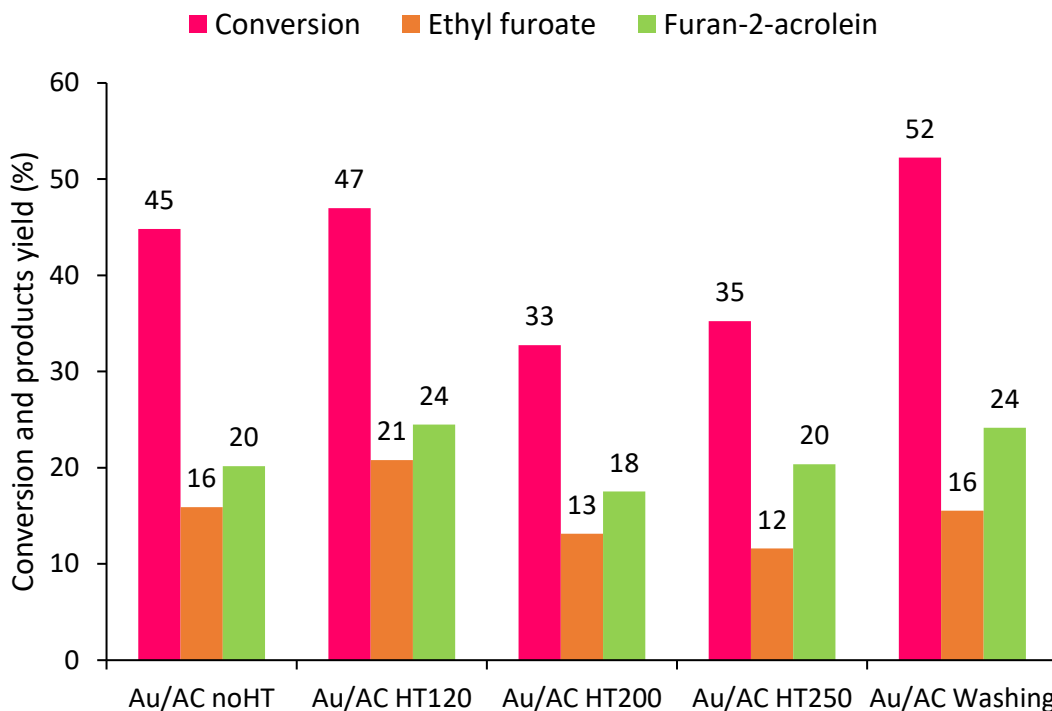


Figure 7.16: Reaction trend for Au/AC HT series. Reaction condition: Furfural 86 μ L, EtOH 6 mL, 0.025 mg catalyst, 0.1 g Na_2CO_3 , $T = 120^\circ\text{C}$, $t = 6$ hours, stirrer speed = 350 rpm

The results in Figure 7.16 are following the same trend as the one obtained with the previously oxidation reactions. From the results obtained for the furfural oxidation, the experimental procedures of heat treatment at 120°C and washing were the most effective, since the synthesized catalysts based on these experimental procedures have shown the best catalytic results. It can be seen a slight increase of furfural conversion (Au/AC no treated gives 45% against 47% and 52% for Au/AC HT 120°C and Au/AC washing respectively) and Fur2Acr yield (20% for the Au/AC no treated, 24% for Au/AC HT 120°C and Au/AC washing). The higher temperature used (over 120°C) in the heat treatment has a clear effect on the conversion and for the yield of ethyl furoate. In particular, the conversion decreased from 45% to 33% for Au/AC HT 200°C and 35% for Au/AC HT 250°C ; the EtFur yield seems to show a slight decrease from 16% to 13% and 12% for Au/AC HT 200°C and Au/AC HT 250°C ; the Fur2Acr yield have the same value, from 20% to 18% and 20% for Au/AC HT 200°C and Au/AC HT 250°C .

The reason why Au/AC HT120 seems more efficient than Au/AC HT200 and HT250 has already been observed for the glucose oxidation and could be as well as applied for the furfural reaction.

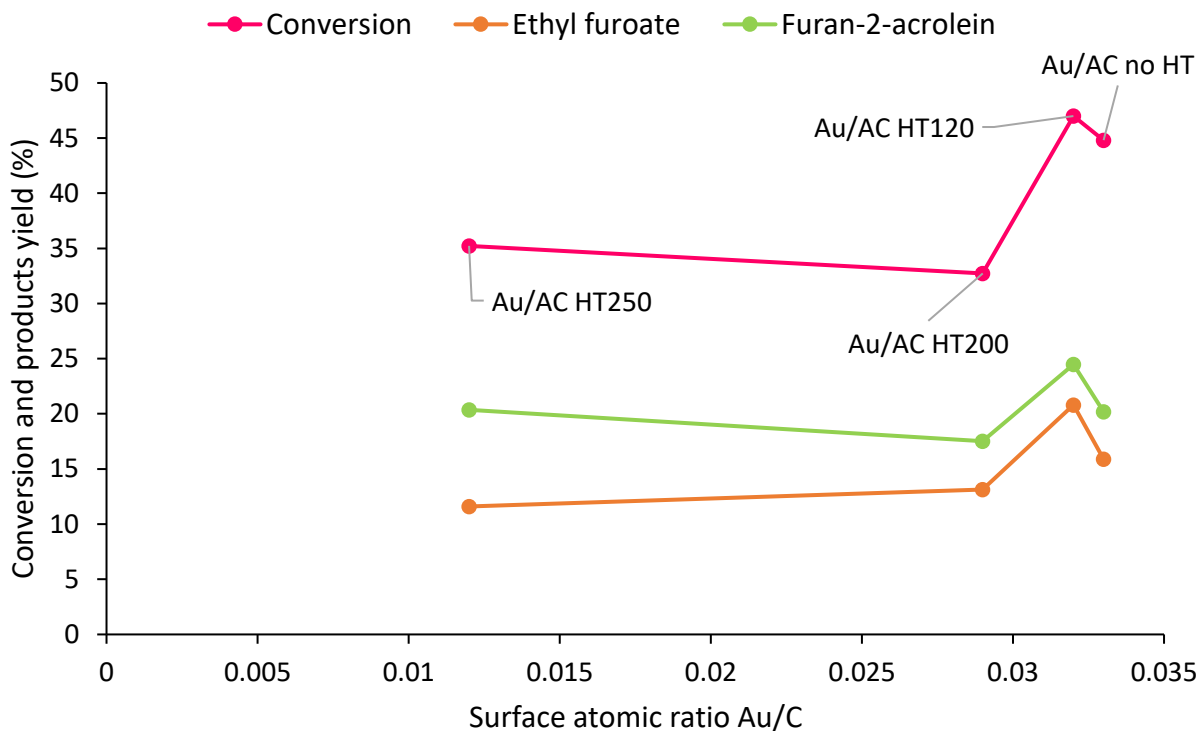


Figure 7.17: Products yields in function of surface atomic ratio Au/C for Au/AC HT series

Figure 7.17 correlates the conversion of furfural and product yields with the surface atomic ratio Au/C for Au/AC HT120, Au/AC HT200 and Au/AC HT250. The mild conditions used for Au/AC HT120 permit to increase the number of active sites without a significant increase of the mean Au particle size; in this way, the surface atomic ratio Au/C is higher (0.032) respect to the series of catalysts and also furfural conversion, ethyl furoate, and furan-2-acrolein yields values were the higher of the series. The increase of the mean particle size for Au/AC HT200 (4.9nm) and Au/AC HT250 (5.8nm) decreases the surface atomic ratio Au/C (0.029 and 0.012) and gives a lower performance in terms of conversion and product yield.

Finally, the Au/AC PVP series were tested. The conversion of furfural decreased drastically by increasing the amount of PVP presented: for Au/AC PVP0, the conversion was 50%, then conversion decreased to 10% for Au/AC PVP0.3 and to 8% for Au/AC PVP2.4. The same trend was observed for the products: the Ethyl-2-furoate has a 10% yield for the samples in the absence of polymer, but when the PVP is present, the yield decreased to 2% for Au/AC PVP0.3 and 1% for Au/AC PVP2.4. The

furan-2-acrolein yield was 21% in the absence of PVP, and then decreased to 4% and 2%, respectively.

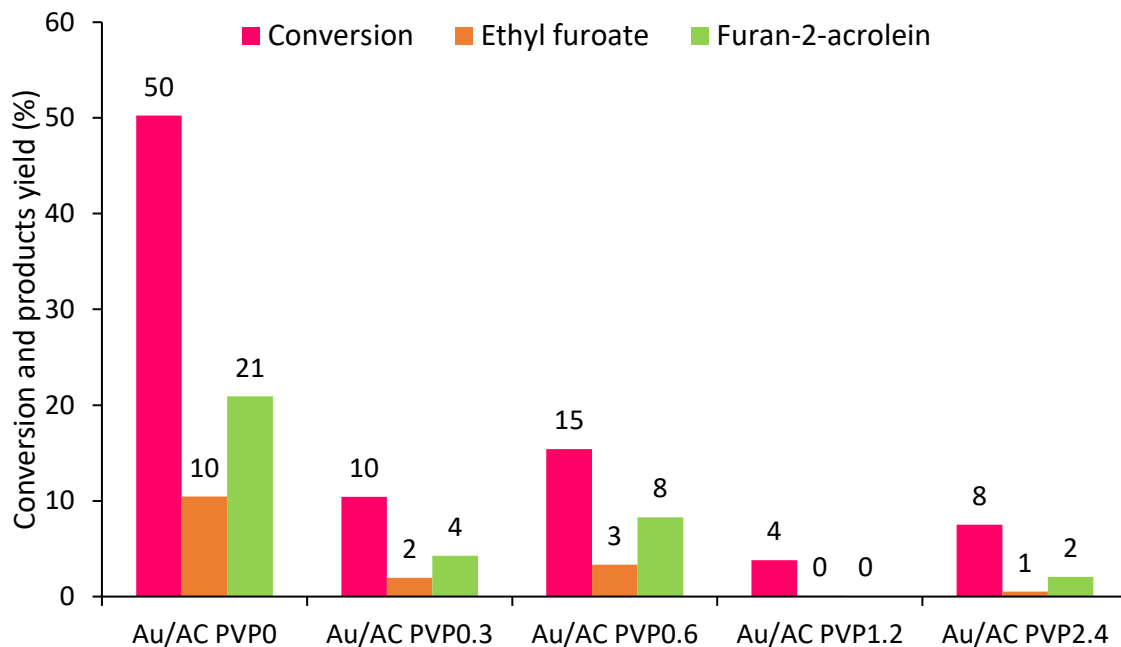


Figure 7.18: Reaction trend for Au/AC PVP series. Reaction condition: Furfural 86 μ L, EtOH 6mL, 0.025mg catalyst, 0.1g Na_2CO_3 , $T=120^\circ\text{C}$, $t=6\text{hours}$, stirrer speed =350rpm

The trend from Figure 7.18 seems slightly fluctuating; this could be due to the low yield and conversion obtained, which could be affected more from the experimental error (the determination of deviation standard is reported in Table 7.1); however, it seems that an increase in the surface atomic ratio Au/C that is accompanied with a decrease of particle size of Au and simultaneously the decrease of the stabilizing agent weight ratio, facilitates the catalytic activity for this series of catalyst in terms of conversion and yield. However, this trend change after a specific PVP: Au weight ratio, and the treadlines reported in Figure 7.19 appears like a volcano plot trend.

	X Fur	YEtFur	Y Fur-2-Acr
Test 1	44	12	31
Test 2	48	10	33
Test 3	49	10	26
Average	47	11	30
Standard Deviation	2	1	4

Table 7.1: Reproducibility of catalytic tests

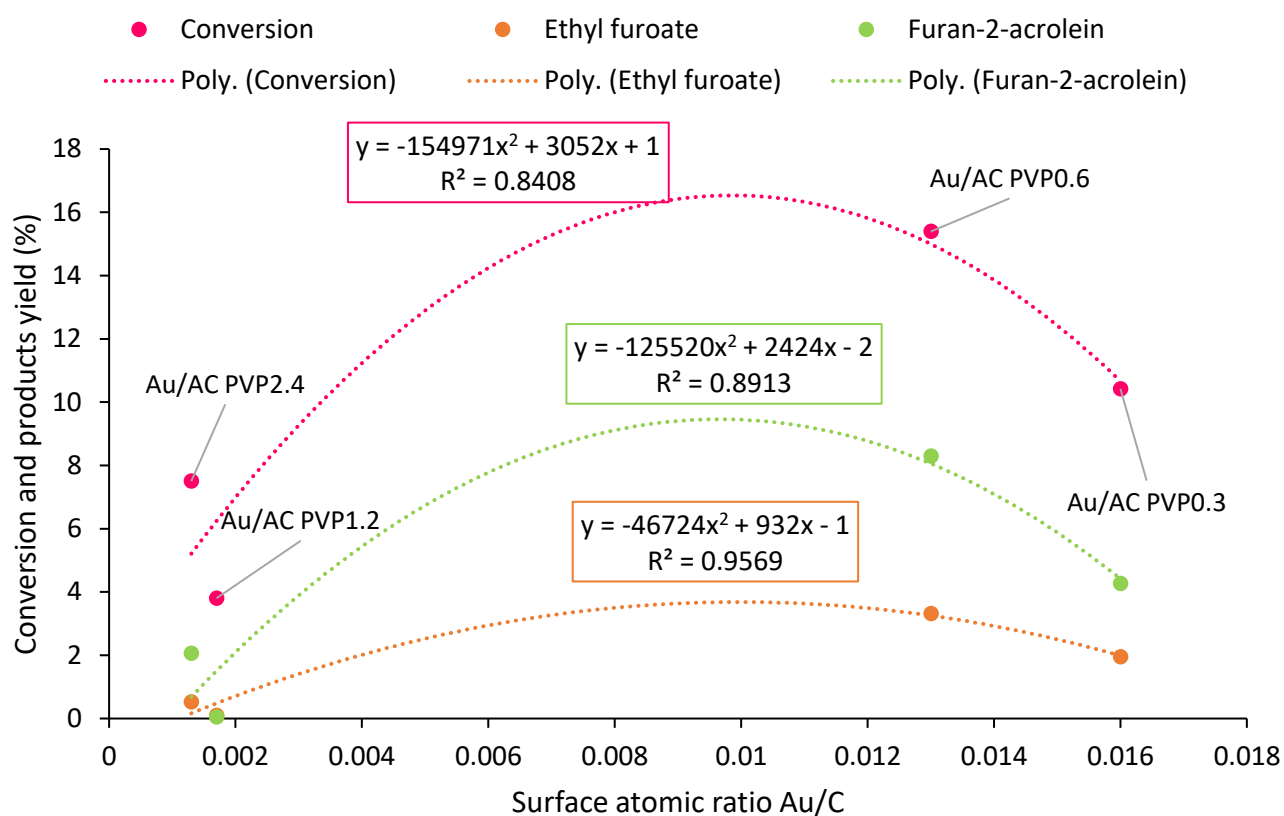
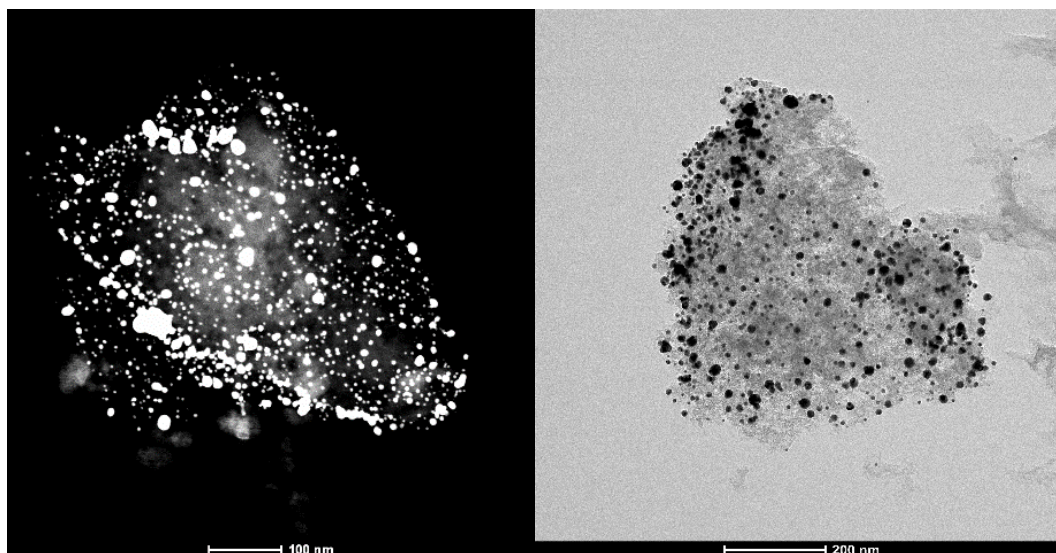


Figure 7.19: Products yield in function of surface atomic ratio Au/C for Au/AC PVP series

7.2.3 Furfural oxidation: Effect of reaction temperature

The effect of temperature on the oxidative condensation/esterification of furfural with ethanol was investigated to evaluate how this reaction parameter could influence the product selectivity and

the furfural conversion. To do that, it was decided to carry on tests at 110°C, 130°C, 140°C and 150°C. However, the high temperature and long reaction time can affect the morphology of the supported nanoparticles. To study the morphology of the fresh and used catalysts (reaction condition: T = 120°C, t = 6hours, N = 350rpm), TEM analysis was carried out for the Au/AC PVA0, Au/ACPVA0.3, and Au/AC PVA2.4.



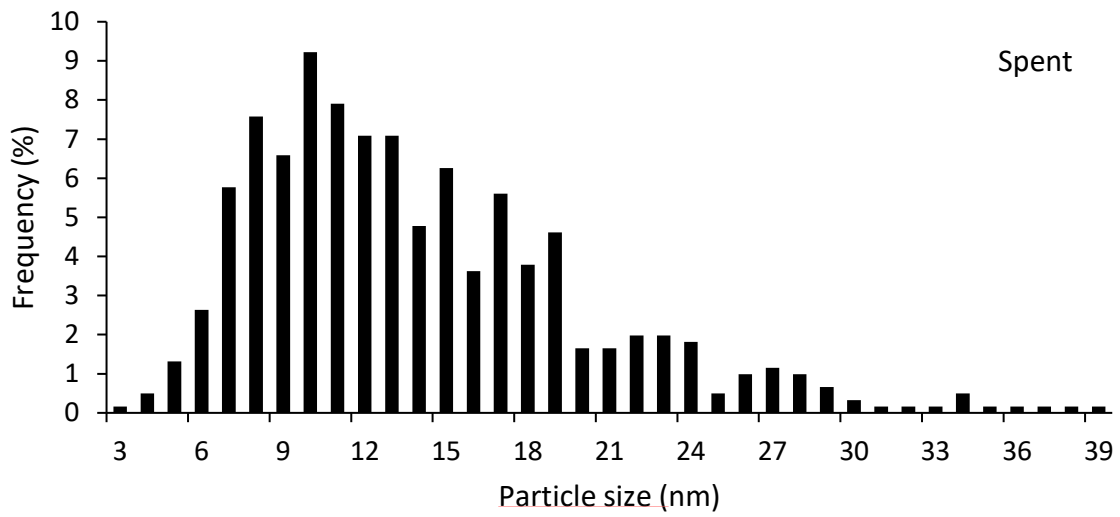
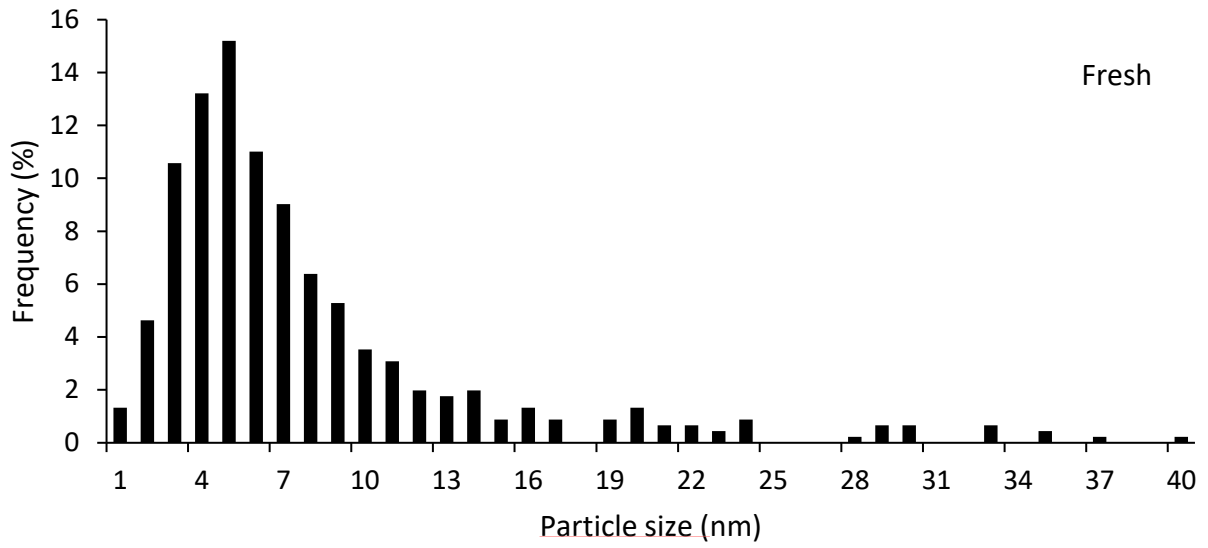
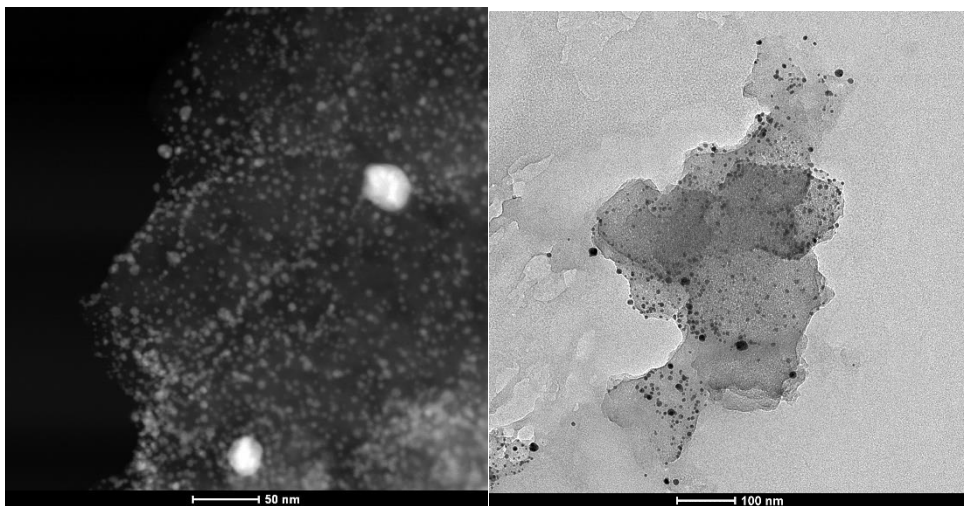


Figure 7.20: STEM analysis of Au/AC PVAO fresh, TEM analysis of Au/AC PVAO spent, size distribution for Au/AC PVAO fresh and spent



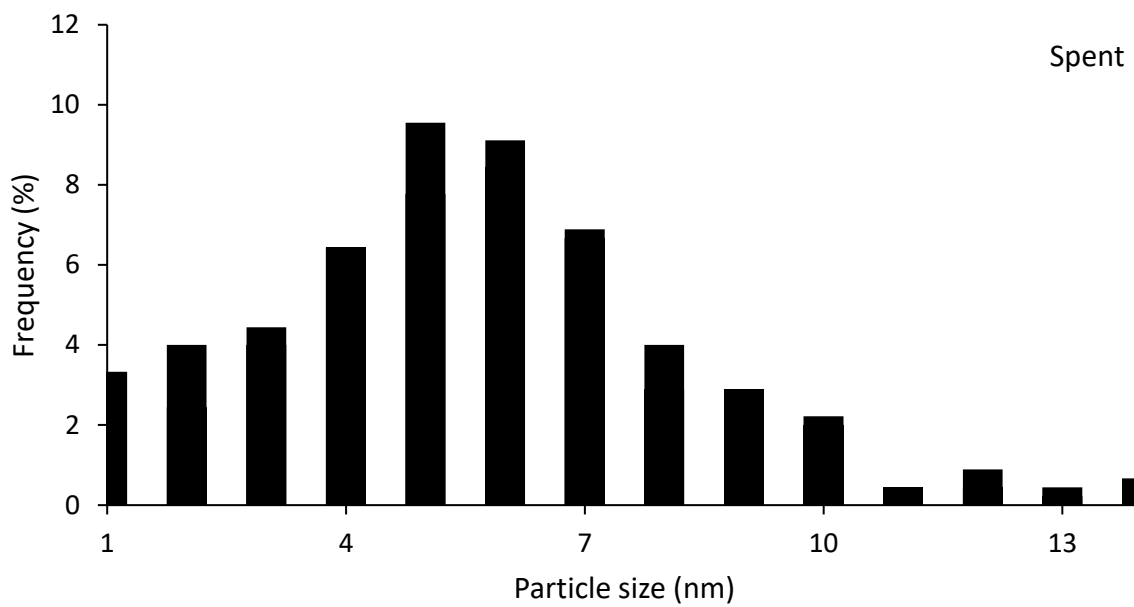
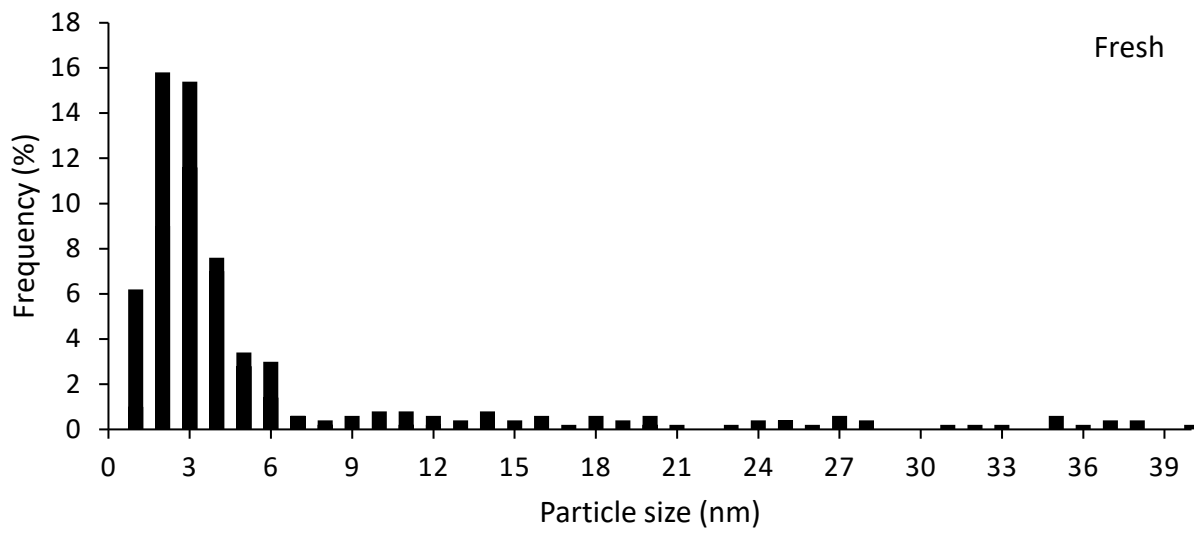


Figure 7.21: STEM analysis of Au/AC PVA0.3 fresh, TEM analysis of Au/AC PVA0.3 spent, size distribution for Au/AC PVA0.3 fresh and spent

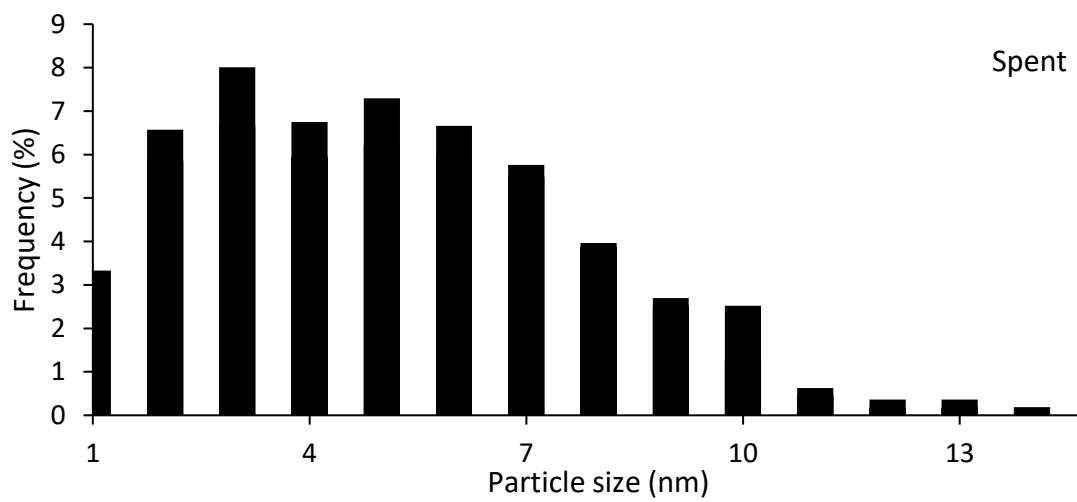
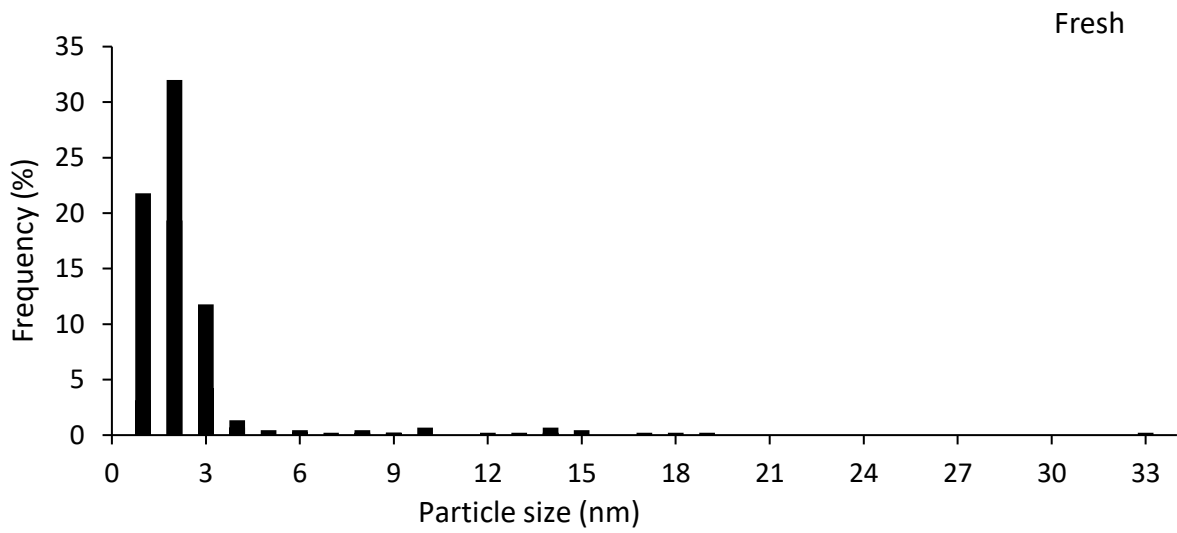
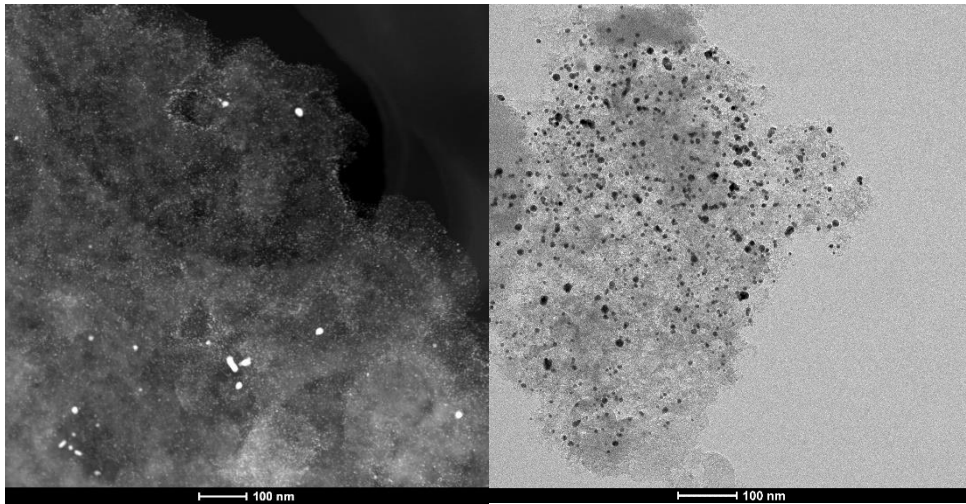


Figure 7.22: STEM analysis of Au/AC PVA2.4 fresh, TEM analysis of Au/AC PVA2.4 spent, size distribution for Au/AC PVA2.4 fresh and spent

In Figures 7.20, 7.21, 7.22 are reported the STEM analysis of the fresh catalyst and the TEM analysis for the catalyst recovered after the reaction. The comparison between the histograms and analysis shows that the reaction parameter used to carry on the catalytic test, in particular a temperature of 120°C and a reaction time of 6h, has led to an increase of the nanoparticle dimension for all the samples (Table 7.2); in particular, the mean particle size of Au nanoparticles has increased and the particle size distribution is more heterogeneous, indicating that part of the smaller Au particles has agglomerated. The sample that is more sensitive to the reaction temperature used, is the catalyst Au/ACPVA0, where the mean particle size of Au, has increased from 7.8nm to 14 nm. The main reason for the significant increase of mean particle size of Au could be attributed to the absence of a stabilizing agent which limits the agglomeration of Au nanoparticles as it is observed for the Au/AC PVA0.3 and Au/AC PVA2.4 samples.

Samples	Mean nanoparticle size of Au by TEM (nm) -Fresh samples	Mean nanoparticles size of Au by TEM (nm) -spent samples
PVA0	7.9 ± 6.3	14.0 ± 6.4
PVA0.3	4.3 ± 3.6	6.1 ± 3.0
PVA2.4	2.3 ± 1.2	5.5 ± 2.6

Table 7.2: Comparison between mean size dimension by TEM for Au/AC PVA fresh and spent

The sample Au/AC PVA2.4 was chosen to investigate further the effect of the reaction temperature due to (i) the smallest mean particle size of Au, (ii) the best stability showed during the reaction and (iii) the good selectivity to Fur2Acr.

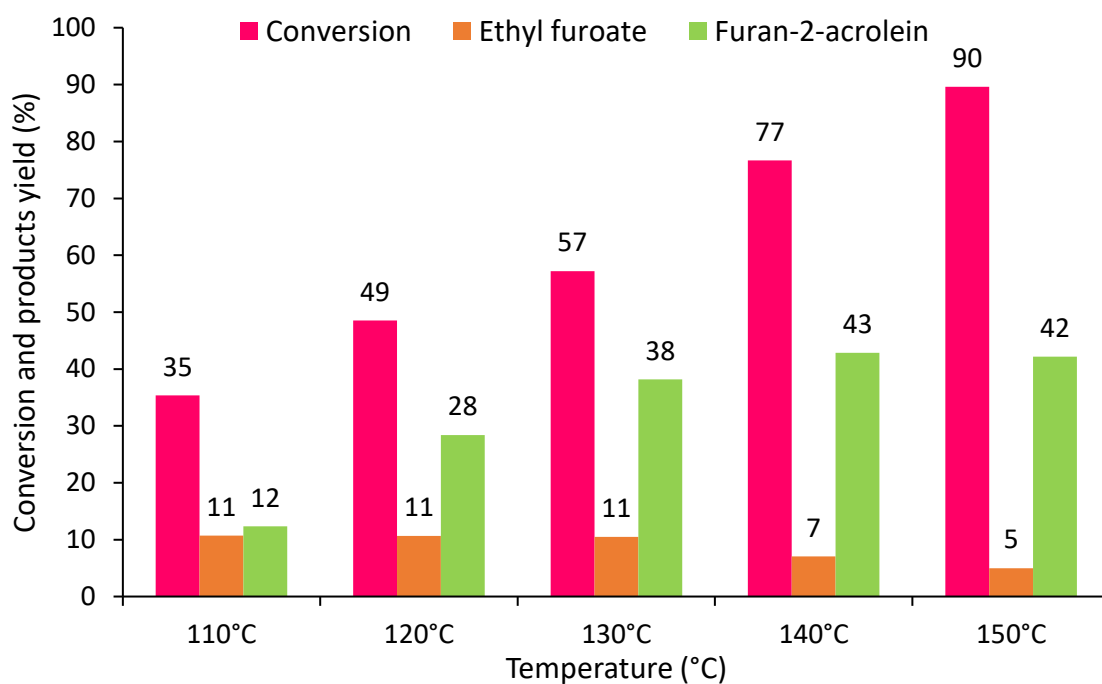


Figure 7.23: Reaction trend in function of temperature. Condition: Furfural 86 μ L, EtOH 6mL, 0.025mg catalyst, 0.1g Na_2CO_3 , $T=x^\circ\text{C}$, $t=6\text{hours}$, stirrer speed =350rpm. Catalyst used: Au/AC PVA2.4

Figure 7.23 shows the Fur conversion and yields of the products as a function of reaction temperature. It can be seen that the increase of temperature (from 110°C to 150°C) improves the conversion of the reagent, starting from 35% at 110°C until 90% at 150°C. In terms of yield of products, the increase of reaction temperature seems not to affect drastically the yield of EtFur, which slightly decrease from 11% to 5%; in the case of Fur2Acr yield, the increase of reaction temperature has increased the yield from 12% at 110°C to 43% at 140°C.

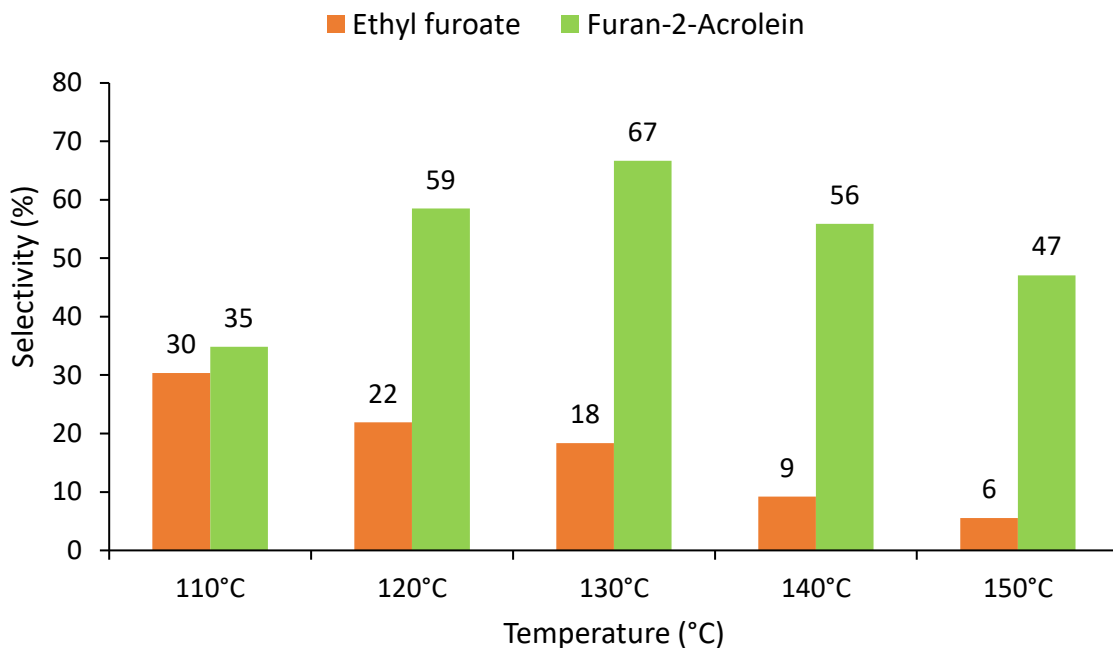


Figure 7.24: Reaction trend in function of temperature. Condition: Furfural 86 μ L, EtOH 6mL, 0.025mg catalyst, 0.1g Na₂CO₃, T=x°C, t=6hours, stirrer speed =350rpm. Catalyst used: Au/AC PVA2.4

The selectivity trend showed in Figure 7.24 instead shows that 130°C is the best temperature to operate, having the best selectivity in Fur2Acr (67%). Despite the good selectivity, the high temperature leads to a worsening in terms of carbon balance, which reaches 50% at 150°C. The loss of carbon balance could be due to the formation of furfural polymerization product (the solution color is darker as shown in Figure 7.25 and it is observable a small peak at the GC for high retention time); moreover, another small peak for low retention time seen from GC analysis is probably ascribable to light product due to ethanol reactions, as Tong and coworkers have reported.¹³⁵



Figure 7.25: Samples of reaction solution of catalytic test reported in figure 7.23

It has already been seen that Au/AC HT120°C gives a slight improvement in catalytic performance for furfural reaction. To see if the increase of the temperature can modify the yield in the two products, a temperature investigation from 120°C to 150°C was carried out also for Au/AC HT120.

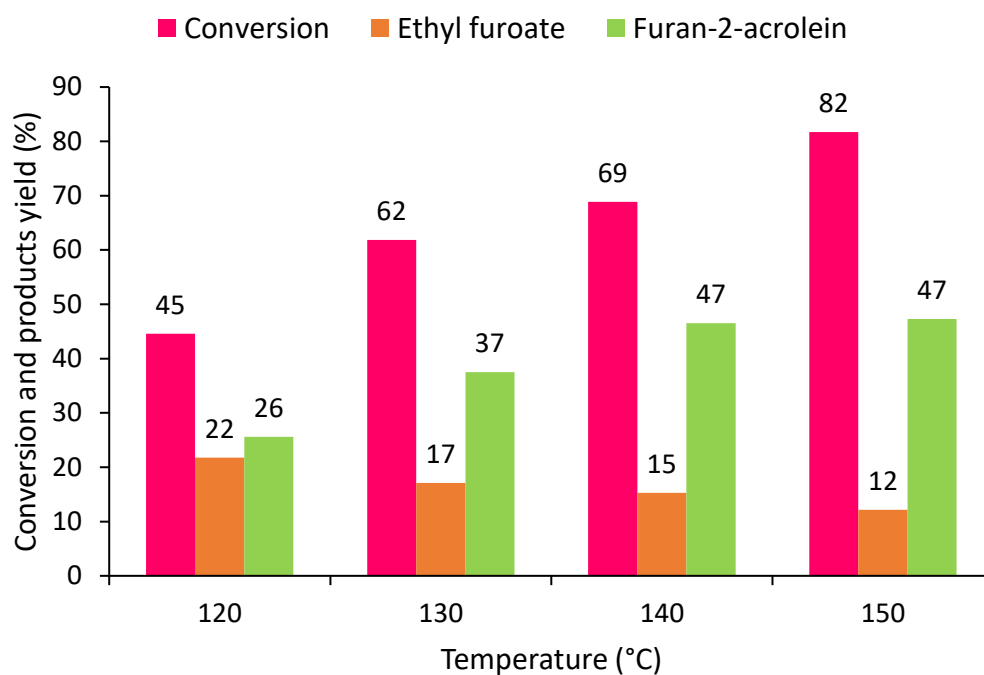


Figure 7.26: Reaction trend in function of temperature. Condition: Furfural 86 μ L, EtOH 6mL, 0.025mg catalyst, 0.1g Na_2CO_3 , t=6hours, stirrer speed =350rpm. Catalyst used: Au/AC HT120

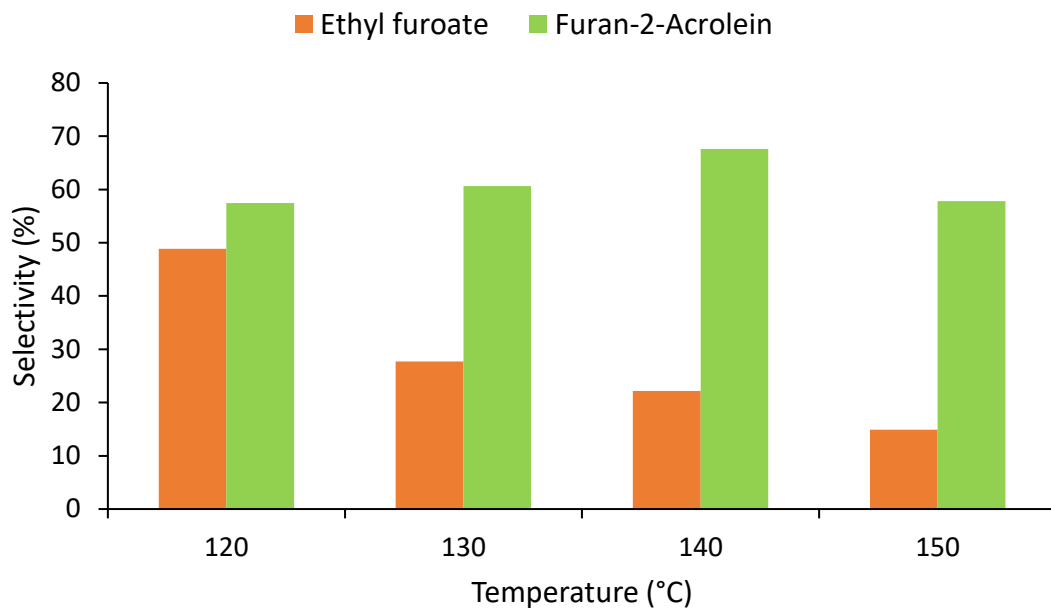


Figure 7.27: Reaction trend in function of temperature. Condition: Furfural 86 μ L, EtOH 6mL, 0.025mg catalyst, 0.1g Na_2CO_3 , t=6hours, stirrer speed =350rpm. Catalyst used: Au/AC HT120

A trend similar to the one obtained for Au/AC PVA2.4 was obtained. In particular, from Figure 7.26 it could be seen that the increase of temperature helps the conversion of furfural, which starts from 45% and reach 82% at 150°C. Moreover, higher temperature decreases the yield of Etfur that drop from 22% to 12% and increase the furan 2 acrolein yield from 26% to 47%. Also here the Fur2acr selectivity enhances and 140°C is the best temperature to obtain a higher oxidative condensation product. As it has already been seen, 150°C causes a higher carbon loss (22% vs 10% at 140°C), probably due to the formation of furfural polymerization products.

-
- ¹³⁰ M. Besson, P. Gallezot, Fine Chemicals through Heterogeneous Catalysis, *Wiley-VCH*, **2001**, 491–518.
- ¹³¹ S. E. Davis, B. N. Zope, R. J. Davis, On the mechanism of selective oxidation of 5-hydroxymethylfurfural to 2,5-furandicarboxylic acid over supported Pt and Au catalysts, *Green Chem.*, **2012**, *14*, 143–147
- ¹³² L.H.S. Guimarães, Carbohydrates from Biomass: Sources and Transformation by Microbial Enzymes. In Carbohydrates-Comprehensive Studies on Glycobiology and Glycotechnology, *Intech*, **2012**, *20*, 441–456
- ¹³³ X. Tong, Z. Liu, L. Yu, Y. Li, A tunable process: catalytic transformation of renewable furfural with aliphatic alcohols in the presence of molecular oxygen, *Chem. Commun.*, **2015**, *51*, 3674-3677.
- ¹³⁴ Y. Gao, X. Tong, H. Zhang, Selective carbon-chain increasing of renewable furfural utilizing oxidative condensation reaction catalyzed by mono-dispersed palladium oxide, *Molecular Catalysis*, **2019**, *477*, 110545
- ¹³⁵ X. Tong, Z. Liu, J. Hu, S. Liao, Au-Catalyzed Oxidative Condensation of Renewable Furfural and Ethanol to Produce Furan-2-acrolein in the Presence of Molecular Oxygen, *Applied Catalysis A, General*, **2016**, *510*, 196-203.

8 Chapter 8-Conclusions and Future work

The use of sol-immobilization method for the synthesis of supported gold nanoparticles has permitted us to investigate how the stabilizing agent affects the catalyst properties and the catalytic performance for a range of important model catalytic reactions. In particular, with this preparation method, it was possible to compare the stabilizing effect of different polymers, like the polyvinyl alcohol, the polyvinylpyrrolidone and the polyethylene glycol, and to study the effect of polymer: Au weight ratio in terms of controlling the final morphology of the catalyst and the effect in terms of catalytic performance.

In particular, from TEM analysis of fresh and spent catalysts, it can be shown that in the absence of the polymer that acts as stabilizing agent gives worst dispersion of the Au nanoparticles on the support and affects thermal stability of the supported Au nanoparticles. The absence of polymer can enhance the agglomeration of the Au nanoparticles for reactions at high reaction temperature and decrease the number of active sites. Indeed, the case of the furfural oxidation reaction has shown how the stabilizing agent could influence the mean particle size of the supported metal nanoparticles; without the polymer, a large agglomeration of the nanoparticles was observed (mean particle size of Au/AC PVA0 fresh was 7.8 nm, after reaction it was 14 nm).

However, from XPS analysis it was observed that at high polymer: Au weight ratio (more than 1.2) may increase the coverage of the gold nanoparticles on the surface, causing a decrease in the value of Au available on the catalyst surface. For example, the sample with the lowest polymer amount Au/AC PVP0.3 has a surface atomic ratio Au/C equal to 0.016, instead Au/AC PVP2.4 has 0.0013.

Therefore it is important the weight ratio of polymer: Au to be tuned in order to have the following requirements for an active and stable catalyst: (i) a minimum amount of polymer in order to obtain higher surface atomic ratio Au/C, (ii) a good dispersion of the gold nanoparticles on the surface of the support, (iii) a higher number of Au available active sites to facilitate the maximum activity, and finally (iv) a catalyst with good stability. By choosing the proper polymer and by controlling the polymer: Au weight ratio, it can be found an optimum ratio for satisfying the previous parameters. A series of catalysts were synthesized and the catalytic performance was investigated for each reaction: Glucose oxidation to glucaric acid, HMF oxidation to 2,5-furandicarboxylic acid, oxidation of 1,6 Hexanediol to Adipic acid, furfural oxidative condensation and oxidative esterification, 4-Nitrophenol reduction to 4-aminophenol.

Reaction	Best catalyst	Mean particle size (nm)	Surface atomic ratio Au/C
Glucose oxidation	Au/AC PVA0.6	2.7 ^b	0.013
HMF oxidation	Au/AC PVA 0.6	2.7 ^b	0.013
Furfural oxidative condensation	Au/AC PVA 2.4	2.4 ^b	0.0013
4-Nitrophenol reduction	Au/AC PEG 1.2	6.2 ^a	-

Table 8.1: List of catalytic reactions studied with the catalyst that show the best performance in terms of product yield. Mean particle size and surface atomic ratio Au/C of each catalyst reported. ^aMean crystallite size by XRD analysis. ^bMean particle size by TEM analysis

Table 8.1 shows that the optimum polymer:Au weight ratio in terms of catalytic performance for each reaction is not the same. An explanation could be attributed to the different reaction conditions used: for example, reaction carried out at higher temperature (for example for furfural oxidative condensation), could favour the polymer solubilization and therefore the accessibility of a higher number of active sites of Au during the reaction. Meanwhile, the blocking behavior of the polymer is higher for reaction carried on at lower temperature (for example of glucose oxidation). Moreover, the polymer may be restructured during the reaction and depending on the reaction conditions, changing the availability of the active sites. By using a lower amount of polymer, the restructuring is stronger (sintering of particle size after the reaction), instead higher amount of stabilizing agent leads to the formation of a catalyst with higher stability. To understand the real nature of the active site, it is necessary to perform in situ/operando studies using synchrotron facilities or carrying out in situ IR/operando studies and by changing the type of support (for example, TiO₂, ZrO₂) to investigate the structure-activity relationships. Moreover, to study how the amount of polymer affects the catalyst stability in reaction, further extensive investigation could be done on the reusability of the catalysts.

The research of a practical methodology to remove the excess of stabilizing agent from the surface of metal nanoparticles and the support was carried out. Two different experimental approaches to remove the PVA stabilizer from the active sites of gold nanoparticles and the catalyst surface was

carried out: the addition of a washing step at 60°C or by using heat treatment protocols on the final catalyst at different temperatures (120°C, 200°C and 250°C). Mild conditions (the washing and the heat treatment at 120°C) permit to remove partially the stabilizing agent and increase the amount of active sites available, without a significant increase on the mean particle size of Au.

Finally, we have observed that for the glucose oxidation reaction, a strong absorption on the catalytic surface of the glucaric acid causes a plateau in the glucaric acid yield even in presence of NaOH. However, this phenomena was not observed for the FDCA yield in the HMF oxidation reaction. To understand and evaluate the nature and strength of adsorption for the reactants, intermediates and products at this moment a computational studies are carried out to understand and explain the deactivation phenomena.

The series of catalysts prepared could be investigated for other types of reactions (hydrogenations or oxidations); in the following part, it is reported an initial catalytic screening of the Au/AC PVA series for the 1,6-hexanediol oxidation to adipic acid (the catalytic tests are carried out from the research group of the University of Lille, France), as an important alternative reaction for the production of adipic acid, which is an important chemical product in industrial chemistry.

8.1 Catalytic oxidation of 1,6-hexanediol

The reaction of 1,6-hexanediol (HDO) oxidation to Adipic acid (AA) has significant importance in the industrial field: as it was seen in Chapter 1, the possibility to produce HDO from renewable resources makes this molecule a potential bio-starting material and the adipic acid is the main monomer for the production of nylon 6,6. Furthermore, the study of this reaction could be useful for an ulterior comparison with the glucose oxidation because it is a linear C6 molecule like glucose, but HDO has only two terminal OH groups; the absence of any other functional group could help to limit side reactions and focus the research only on the desired pathway.

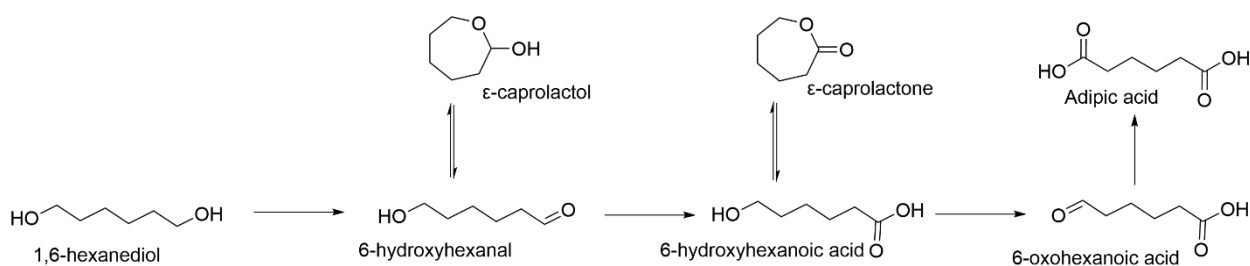


Figure 8.1: Reaction pathways for the oxidation of 1,6-hexanediol to adipic acid

Figure 8.1 reports the reaction pathways of the reaction: at first, HDO is oxidized to an intermediate 6-hydroxyhexanal (HH). The presence of an OH and an aldehyde group can lead to the cyclization of HH and the formation of the structural isomer ε-caprolactol or it could be subsequently oxidized to 6-hydroxyhexanoic acid (HHC), in equilibrium with the isomer ε-caprolactone. Finally, AA was obtained by subsequent oxidation of HHC via 6-oxohexanoic acid (OH).

8.1.1 Oxidation of 1,6-hexanediol: Effect of reaction time

As it was done for the previous reactions, time on stream analysis as a function of reaction time was carried out to determine the catalytic performance of the studied catalysts.

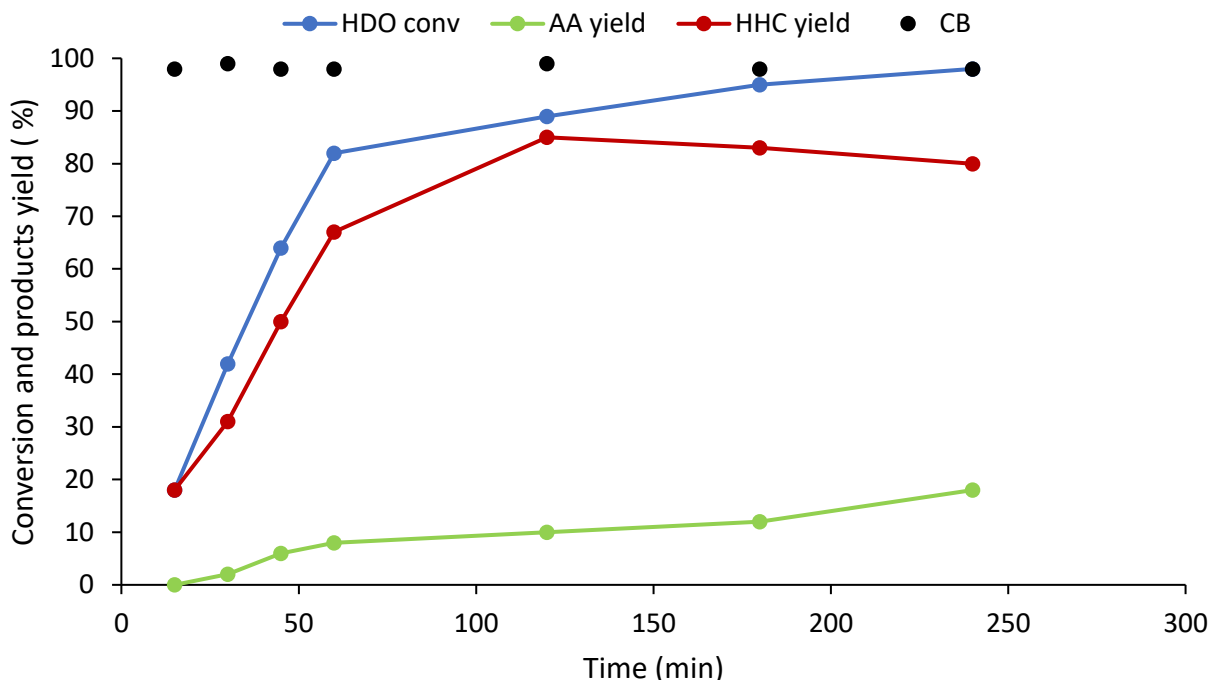


Figure 8.2: Conversion and yield of products as a function of reaction time. Experimental conditions: HDO aqueous solution 20mL, 2 eq of NaOH, HDO/metal molar ratio, $P_{air}=15\text{bar}$, $T=110\text{ }^{\circ}\text{C}$, stirrer speed =600 rpm. Catalyst used=Au/AC PVA1.2

The chosen catalyst that it is presented in this figure is Au/AC PVA 1.2 as a model example. From *Figure 8.2* it can be noticed that the carbon balance during the reaction was around 98%. After 15 minutes of reaction, it is notable that the conversion of 1,6-hexanediol (HDO) was around 20% and the primary product reported was 6-hydroxyhexanoic acid (HCC). The Increase of reaction time has led to an increase of HDO conversion, which reached 98% for 4h of reaction. The main products reported during the reaction were the 6-hydroxyhexanoic acid, the molecule obtained from the oxidation of one terminal -OH group. The presence of 6-hydroxyhexanal was not detected, probably because of the high reactivity of the aldehyde group. In particular, after 15minutes the primary product detected was HHC, then, as the reaction time increased it continued to increase, reaching a yield of 83% after 2 hours. However, with a further increase of reaction time, a slow decrease in the amount detected, showing a yield of 80% after 4 hours. In the case of adipic acid the yield was very low at low HDO conversion. Increasing the reaction time an increase in the amount of AA product was detected (19% after 4 hours). The comparison of these trends suggests the role of HHC as intermediate and, as it has suggested from the article of Capece et al, the second oxidation step from HHC to AA is the slow step of the reaction.¹³⁶

8.1.2 Oxidation of 1,6-hexanediol: Screening of the catalysts

Once the reaction pathway of the reaction was identified, the catalytic evaluation of the catalysts prepared by varying the amount of PVA (PVA: Au weigh ratio) was investigated.

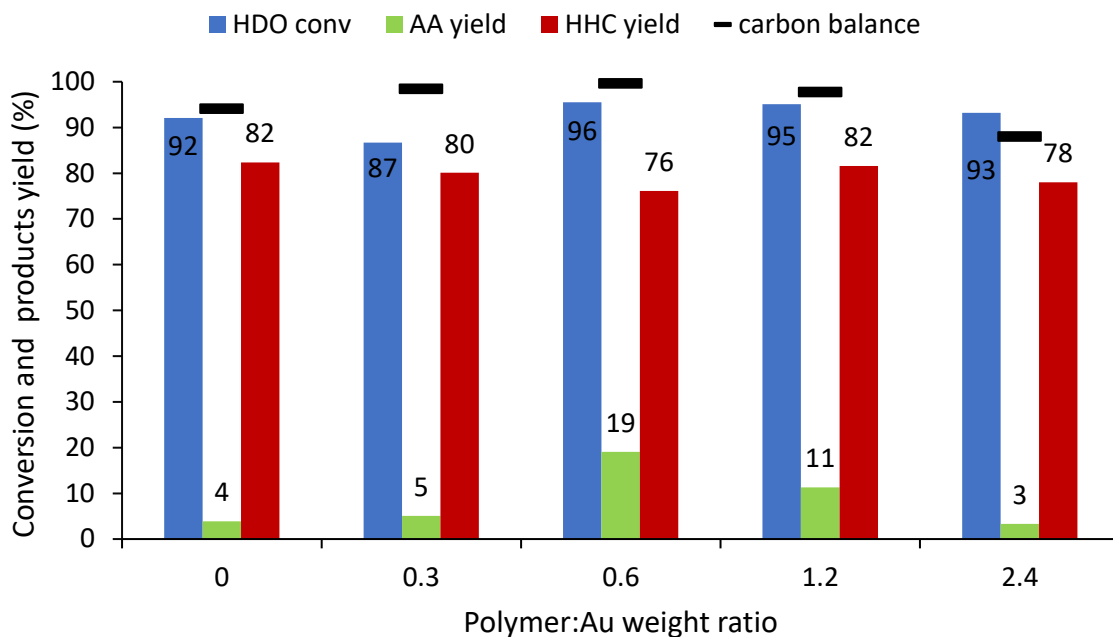


Figure 8.3: Conversion and yield of products for Au/AC PVA series. Experimental Conditions: HDO aqueous solution (2 mL, 14 mmol/L⁻¹), 2 eq of NaOH, m catalyst =5-10 mg, Pair=15bar, T=110 °C, t=4h, stirrer speed=600 rpm.

From the data obtained in Figure 8.3, it is possible to see that for all the catalysts the carbon balance was above 98%, as in the previous data presented. Moreover, the conversion of HDO did not change drastically with different amounts of PVA, and was constant around 90% for all the catalysts (the lowest was 87% for Au/AC PVA0.3 and the higher was 96% for Au/AC PVA0.6). However, further catalytic tests performed at lower and initial reaction time could help to determine the initial kinetics of the catalysts and to compare the catalytic activity. The same consideration could be done for the HHC yield; the yield for the intermediate remained high for all the samples tested: Au/AC PVA0 showed a yield of 82%, then the HHC yield slightly decreased reaching a value of 76% for Au/AC PVA0.6 and, finally, it stayed constant around 80% for the catalyst with a higher amount of PVA (Au/ACPVA1.2 and Au/AC PVA2.4). AA instead seems to be affected by the stabilizing agent amount: the catalysts Au/AC PVA0 and Au/AC PVA0.3 gave a low yield of AA (4% and 5%), then Au/ACPVA0.6 showed a 19% yield and finally decreased (11% for Au/ACPVA1.2 and 3% for Au/AC PVA2.4) when the amount of PVA was increased for the synthesized catalysts, showing that at higher amount of PVA and PVA coverage on the surface the productivity to AA was lower.

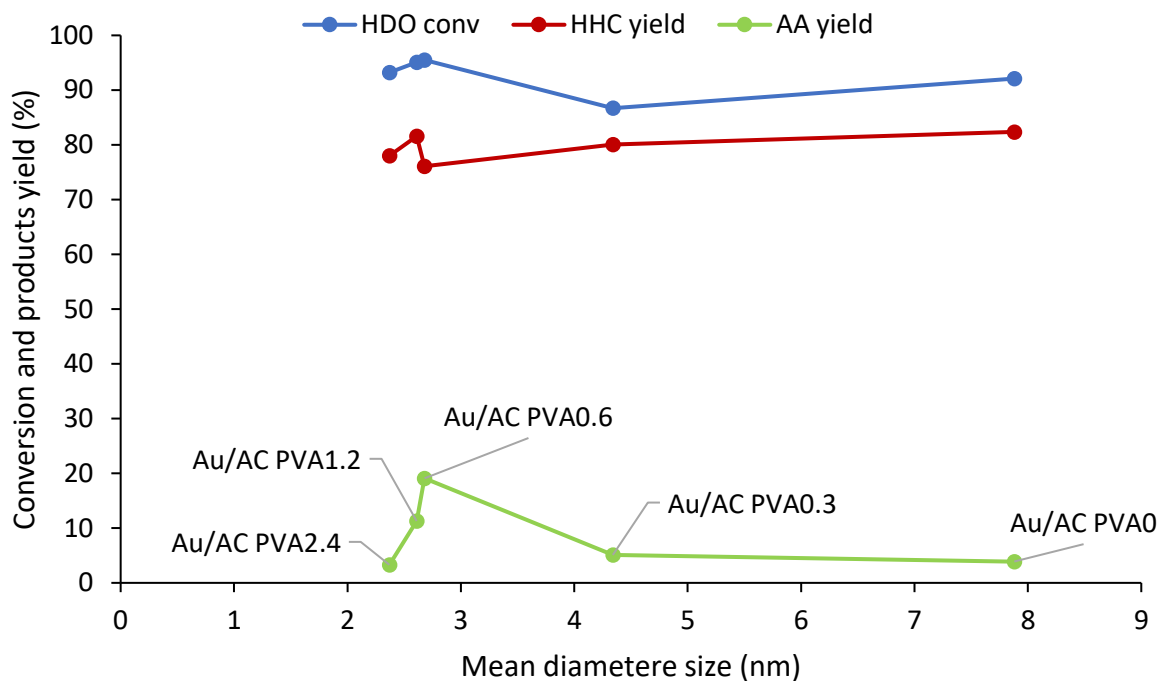


Figure 8.4: Conversion and products yield in function of mean diameter size

Conversion and yield obtained were plotted as a function of the mean particle size of Au and Figure 8.4 shows the results obtained. For the HDO conversion and HCC yield, the catalytic trends obtained are here described: the HDO conversion was higher in the presence of Au nanoparticles with mean particle size of 2.6 nm (96%), then slightly it was decreased when the mean particle size is bigger than 4 nm; the HHC yield was varied between 76% and 82%. The AA yield trend instead has a volcano shape: the catalyst with the highest amount of PVA (Au/AC PVA 2.4) showed a low amount of diacid product (3%). By keeping the dimension of the Au nanoparticles in a similar range, but decreasing the amount of stabilizer (PVA), the AA yield increased up to 19% for Au/AC PVA0.6 and after that, the yield decreased to 5% and 4%, respectively for Au/AC PVA0.3 and Au/AC PVA0. Moreover, in this case, it seems that the NPs size is not the main factor that rules the activity of the catalyst. This is why the surface atomic ratio could give to us some possible further explanations for the observed catalytic trend.

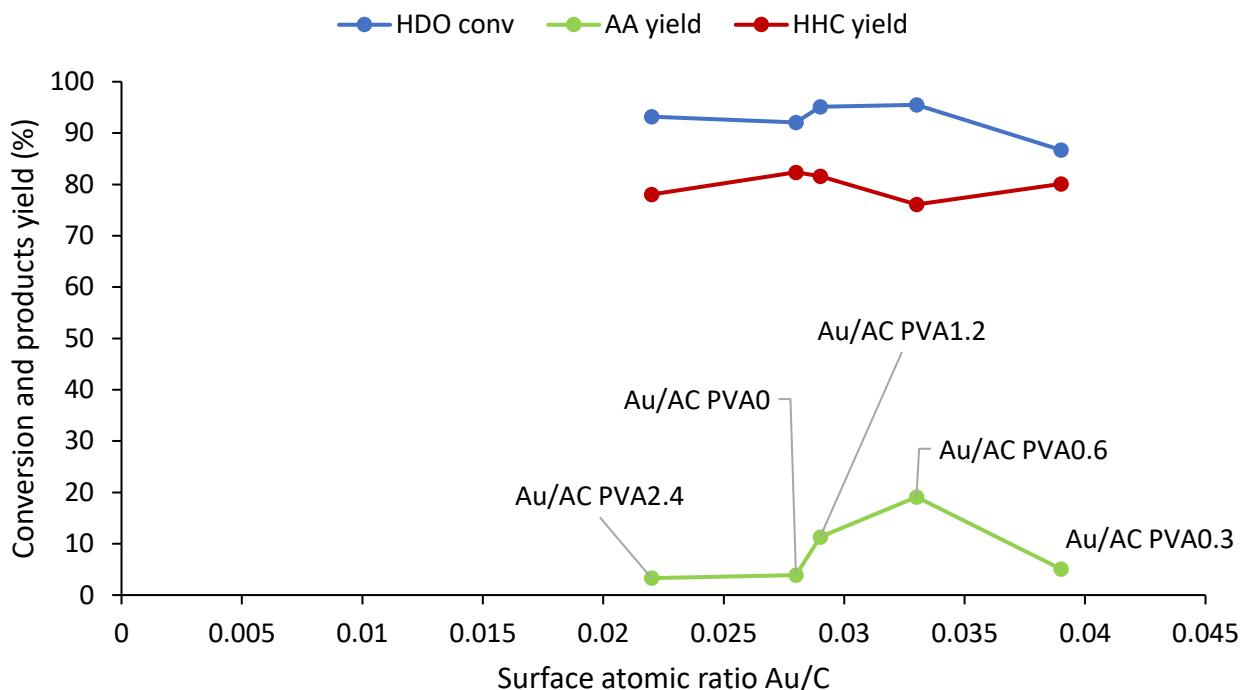


Figure 8.5: Conversion and products yield in function of surface atomic ratio Au/C

Figure 8.5 shows the results obtained in terms of XPS analysis. As it was already seen for the mean diameter size of Au, the surface atomic ratio of Au/C seems not to affect considerably the final HDO conversion and HHC yield, meanwhile, AA yield has a particular trend: low surface atomic ratio of Au/C for Au/ACPVA2.4 showed 3% of the yield to HHC and the value remained constant up to 0.028 of increase of surface atomic ratio of Au/C. However, a further increase enhanced the yield reaching a value of 19% of HHC yield for a value of 0.033 surface atomic ratio of Au/C, and this could indicate that the increased availability of gold surface sites could influence the yield to HHC. However, the sample with a higher surface atomic ratio of Au/C (Au/ACPVA0.3 with 0.039) gave a yield of 3%.

8.1.3 Oxidation of 1,6-hexanediol: Effect of base for Au/AC PVA series

As it was already presented in Chapter 1, the main disadvantage and main challenge to resolve in the use of monometallic Au catalysts is the use of strong alkaline conditions for the oxidation reactions. In particular, the use of base leads to the production of the salt of the acid required, thus further purification steps are required to obtain the acid in the pure form. It is interesting to see how the catalytic behavior varies in the absence of NaOH for the presented reactions and Figure 8.6 reports the catalytic results obtained.

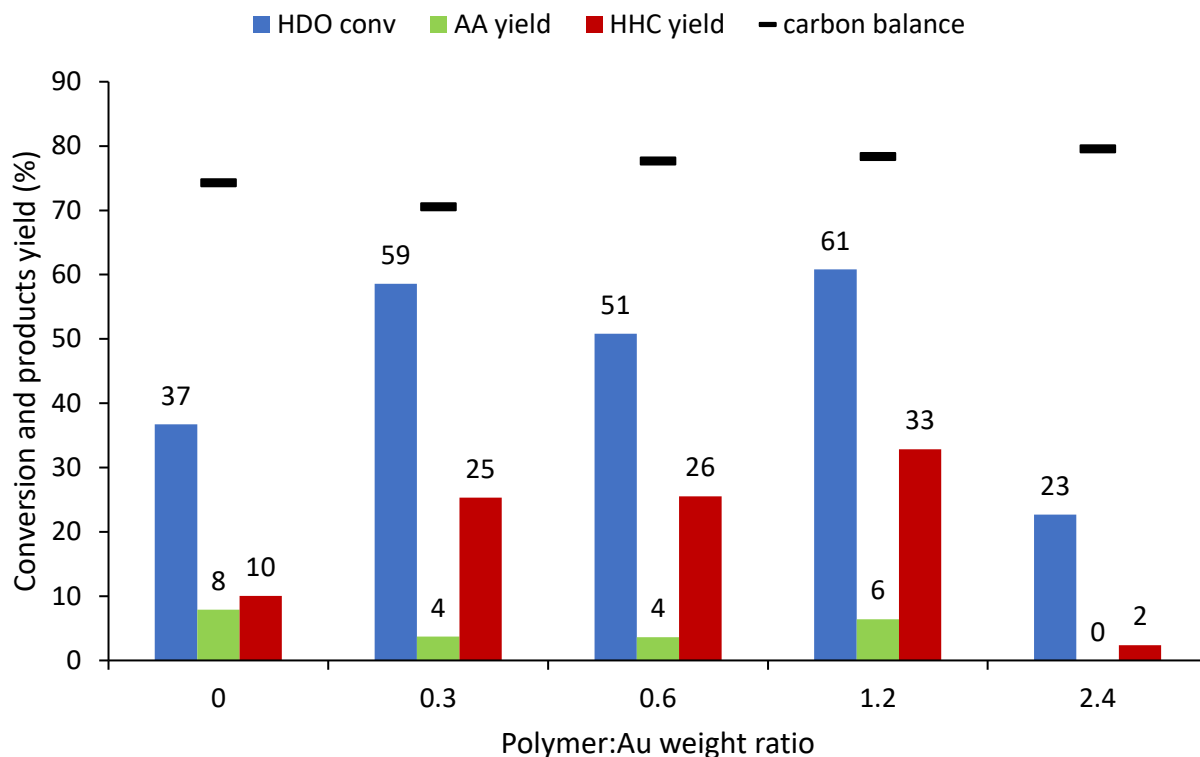


Figure 8.6: Conversion and products yield for Au/AC PVA series in absence of NaOH. Experimental Conditions: HDO aqueous solution (2 mL, 14 mmol/L⁻¹), m catalyst =5-10 mg, Pair=15bar, T=110 °C, t=4h, stirrer speed =600 rpm.

The catalytic results obtained (Figure 8.6) are quite different from the one obtained in the presence of base (NaOH). The carbon balance obtained was around 75%, lower than the 95% found in the presence of NaOH. One of the possible reasons is that in a base free condition, some reaction products remain absorbed on the catalyst surface. Moreover, the mechanism reported¹³⁷ shows the possible formation of other intermediate products like the 6-hydroxyhexanal or the 6-oxohexanoic acid that are not reported in the carbon balance and can be present in base free conditions. It can be seen other effects of the absence of NaOH. In the absence of base, the HDO conversion generally decreased: in the presence of base the final conversion was in the range of 84% to 95%, but in the absence of base was in the range between 23% and 61%. It can be noticed that Au/AC PVA0 catalyst reached 37% of conversion, then by increasing the PVA to Au weight ratio, led to an increase in the range of 51-61%. However, when the PVA to Au weight ratio was 2.4 the conversion decreased to 23%. The HHC yield follows the same trend. In the absence of PVA only 10% of HHC yield was found, then increased to 26% for Au/AC PVA1.2 and followed a decrease to 2%. The AA instead seems not to vary drastically: an average of 6% remained when the PVA to Au weight ratio varied from 0-1.2.

At higher value, no formation of AA was detected showing the influence of the polymer in affecting the productivity of AA. Despite the results obtained in the presence of a base (where the catalyst with the best performance was Au/AC PVA0.6), the sample that achieves the highest conversion and highest product yield is Au/AC PVA 1.2.

For the 1,6 hexanediol oxidation reaction, an initial study was carried out on the Au/AC PVA series; however, further studies could be done in order to optimize the reaction parameters (stirring rate, amount of catalyst, temperature). In addition, the performance of catalytic tests at initial reaction time, can permit us to determine and compare in a better way catalytic activity.

Moreover, the Au/ACPVP and Au/ACPEG series could be tested and compared with the other reaction trends obtained.

Another possible future investigation could be the preparation of bimetallic catalysts, mixing Au with other noble metal like Pd and Pt, in order to improve the catalysts stability and catalytic performance.

¹³⁶ N. Capece, A. Sadier, C. Palombo Ferraz, J. Thuriot-Roukos, M. Pietrowski, M. Zieliński, S. Paul, F. Cavani, R. Wojcieszak, Aerobic oxidation of 1,6-hexanediol to adipic acid over Au-based catalysts: the role of basic supports, *Catal. Sci. Technol.*, **2020**, 10, 2644–2651

¹³⁷ N. Capece, A. Sadier, C. Palombo Ferraz, J. Thuriot-Roukos, M. Pietrowski, M. Zieliński, S. Paul, F. Cavani, R. Wojcieszak, Aerobic oxidation of 1,6-hexanediol to adipic acid over Au-based catalysts: the role of basic supports, *Catal. Sci. Technol.*, **2020**, 10, 2644–2651

Ringraziamenti



Non sono mai stata brava a dire a parole ciò che penso o provo, e il disegno è sempre stato il mezzo con cui riesco esprimermi meglio; questa volta ho pensato bene di reinterpretare a modo mio una delle immagini più significative del mio dottorato: immagini TEM di nanoparticelle di oro. La loro distribuzione sul supporto è un po' disomogenea, lo ammetto, ma ciascuna zona rappresenta una fase del mio percorso...Cominciamo dal basso a destra! La zona verde raffigura le piccole gioie scientifiche e umane che nel mio percorso si sono susseguite: uno strumento che dopo tanto impegno funziona di nuovo, il momento in cui trovi un'ipotesi che spiega i tuoi dati, un oral ad un congresso che va meglio del previsto, il prof soddisfatto del lavoro svolto, uno studente contento del progetto che gli proponi. Piccoli o grandi, (anche le dimensioni delle nanoparticelle sono più o meno grandi), sono momenti che ti aiutano a capire i passi di crescita fatti e ad andare avanti con po' più di speranza, con un po' più di verde. Ci sono però stati momenti grigi: la paura di non farcela, nulla che funziona, il non essere all'altezza, i dati che non tornano...ti sembra di non riuscire ad andare avanti (le particelle sono barrate), in quei momenti la tentazione di mollare tutto è grande e la domanda "perché lo faccio?" diventa urgente. Un altro periodo per me importante è stato il periodo all'estero svolto in Spagna. È stata un'occasione di mettermi in gioco da sola in un ambiente totalmente differente, e diverse sono le cose che ho imparato sia accademicamente sia umanamente... di sicuro più giallo-rossa sono diventata.

Un'altra caratteristica delle nanoparticelle mi ha sempre colpito (anche se a livello di ricerca, è visto come un difetto): mentre si formano, esse tendono a stare vicine e a formare agglomerati. Nello studiarle, ho capito che il loro è un comportamento sensatissimo e ragionevole: senza persone che stessero vicino a me, che condividessero più o meno tutti i momenti di questo periodo, sicuramente questo TEM sarebbe decisamente più nero. Ed è per questo che tra le nanoparticelle volevo ringraziare la mia famiglia (in particolare mamma e papà, mia sorella Anna, la nonna Angelina) che mi ha sempre supportato e sostenuto nelle mie scelte; i professori che hanno avuto fiducia in me e mi hanno stimolato sempre con nuove idee (in particolare Cavani, Nikos e Maireles), compagni di laboratorio con cui ho condiviso questo grigio verde (vabbè, qui mi tocca mettervi tutti: Tommy, Paola, Ciccio, Dani, Marti, Chiara, Matti, Laura, Gianco, Giulia, Ale, Nico, Lisa, Jaco, Faso, Alice, Pio, Bacchio, Monica, Anna, Gabri, Giada, Stefi, Erica, Vale, Aisha, Claudia, Grace), tutti i tesisti che hanno avuto la sfortuna di avermi come dottoranda: il confronto con loro mi ha dato la forza di continuare (Carolina, Francesca, Alessia, Stefano, Beatsam). Tutti i miei amici non sono da dimenticare, che sempre mi hanno accompagnato nella vita anche al di fuori del laboratorio... sia quelli italiani (Andre, Mary, Palla, Barba, Ele, Linda) che i nuovi spagnoli (Rocio, Sheyla, Carmen, Isa, Elena, Federica, Ruth,

Marine). Una voce anche a Ville, una persona che, in maniera singolare e affettuosa, mi sta accompagnando quotidianamente nelle sfide di ogni giorno anche a distanza. Per ultimo (ma non per importanza) tutte le persone che ho incrociato in questo percorso (degni di nota il mio ultimo appartamento: Ornella, Livia, Mattia, Dani e Agata) o che mi sto dimenticando perché sono un disastro. Grazie a voi tutti, l'ultima parte [azzurra](#), proiettata verso un futuro incognito, potrà essere guardata con più curiosità e meno paura.